



Annual progress report of the Condensed Matter Physics and Chemistry Department 1 January - 31 December 2000

Lebech, Bente

Publication date:
2001

Document Version
Publisher's PDF, also known as Version of record

[Link back to DTU Orbit](#)

Citation (APA):
Lebech, B. (Ed.) (2001). Annual progress report of the Condensed Matter Physics and Chemistry Department 1 January - 31 December 2000. (Denmark. Forskningscenter Risoe. Risoe-R; No. 1226(EN)).

DTU Library Technical Information Center of Denmark

General rights

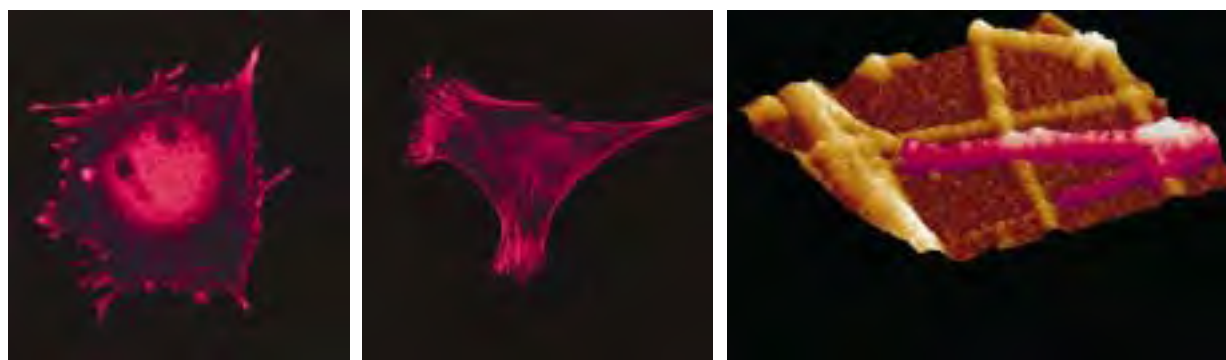
Copyright and moral rights for the publications made accessible in the public portal are retained by the authors and/or other copyright owners and it is a condition of accessing publications that users recognise and abide by the legal requirements associated with these rights.

- Users may download and print one copy of any publication from the public portal for the purpose of private study or research.
- You may not further distribute the material or use it for any profit-making activity or commercial gain
- You may freely distribute the URL identifying the publication in the public portal

If you believe that this document breaches copyright please contact us providing details, and we will remove access to the work immediately and investigate your claim.

Annual Progress Report of the Condensed Matter Physics and Chemistry Department 1 January – 31 December 2000

Edited by B. Lebech



**Risø National Laboratory, Roskilde, Denmark
March 2001**

Abstract

The Condensed Matter Physics and Chemistry Department is concerned with both fundamental and applied research into the physical and chemical properties of materials. The principal activities in the year 2000 are presented in this progress report.

The research in physics is concentrated on neutron and X-ray scattering techniques and the problems studied include two- and three-dimensional structures, magnetic ordering and spin dynamics, superconductivity, phase transitions and nano-scale structures. The research in chemistry includes chemical synthesis and physico-chemical investigation of small molecules and polymers, with emphasis on polymers with new optical properties, block copolymers, surface-modified polymers and supramolecular structures. Theoretical work related to these problems is undertaken, including Monte Carlo simulation, computer simulation of molecules and polymers and methods of data analysis.

The readers are invited to contact the department or the authors of the individual contributions for more detailed information than can be given in this report. The postal address is: Condensed Matter Physics and Chemistry Department, Risø National Laboratory. P.O. Box 49, DK-4000 Roskilde, Denmark. Web address is <http://www.risoe.dk/rispubl/FYS/fysik.htm>. E-mail addresses may be found under the titles of the contributions.

This report contains unpublished results and should not be quoted without permission from the authors.

Front cover illustration:

An example of engineering and imaging of cell adhesion to solid surfaces. Cultured cells display more outgrowths and better attachment to glass coated with fibrillar collagen (centre image) than to bare glass (left image). This is revealed by confocal microscopy of the fluorescently stained actin component of the cell skeleton. An Atomic Force Micrograph (right image) of a cell attached to fibrillar collagen shows the alignment of the initially very fine cell outgrowths (purple) with the collagen fibrils (yellow) (see section 2.5.19. of this report).

Back cover illustration:

Phase diagram of the magnetic structures in $\text{TmNi}_2\text{B}_2\text{C}$ (see section 2.3.4. of this report).

ISBN 87-550-2790-3; 87-550-2791-1 (Internet)
ISSN 0206-2840
ISSN 1397-8985

Table of contents

| | |
|--|-----------|
| 1. Introduction and post festum..... | 7 |
| 2. Research projects in the department..... | 10 |
| 2.1. Theory | 12 |
| 2.1.1. Scattering from discrete nano-scale structures - interpretation of the resulting line shape..... | 12 |
| 2.1.2. Relaxation properties of antiferromagnetic nano-particles..... | 13 |
| 2.1.3. Form factor for micellar coronas with excluded volume interactions..... | 14 |
| 2.1.4. New Monte Carlo simulation technique applied for polymer folding..... | 15 |
| 2.2. Magnetism..... | 16 |
| 2.2.1. New results on the excitations of an S=1 quantum chain..... | 16 |
| 2.2.2. Correlations and fluctuations in the 2D Heisenberg antiferromagnet..... | 18 |
| 2.2.3. Excitations around the quantum critical point in LiHoF ₄ | 19 |
| 2.2.4. A time-of-flight neutron scattering study of the dynamics of magnetic nanoparticles... .. | 20 |
| 2.2.5. Spin precession in ferrimagnetic maghemite nanoparticles..... | 21 |
| 2.2.6. Spin dynamics in Cu(DCOO) ₂ ·4D ₂ O..... | 22 |
| 2.2.7. Magnetic-field dependent excitations of the ordered quasi-1D HAF CsNiCl ₃ | 23 |
| 2.2.8. Specific heat capacity and magnetocaloric effect of Fe-doped CsNiCl ₃ | 24 |
| 2.2.9. Magnetization of solid oxygen confined into nanoporous materials..... | 25 |
| 2.2.10. A model for the change of modulation vectors observed in the magnetic structure of CeSb..... | 26 |
| 2.3. Superconducting materials and phenomena..... | 27 |
| 2.3.1. Interaction between magnetism and superconductivity in TmNi ₂ B ₂ C with H [110] studied using Small Angle Neutron Scattering..... | 27 |
| 2.3.2. Form factor analysis of flux line lattice in the magnetic superconductor TmNi ₂ B ₂ C..... | 28 |
| 2.3.3. Temperature dependence of the flux line lattice transition into square symmetry in superconducting LuNi ₂ B ₂ C..... | 29 |
| 2.3.4. Phase diagram of TmNi ₂ B ₂ C in an in-plane magnetic field..... | 30 |
| 2.3.5. Heat capacity of TmNi ₂ B ₂ C in a magnetic field applied in the a- and c-axis direction.. | 31 |
| 2.3.6. The magnetic structures in the SC state of ErNi ₂ B ₂ C in an in-plane magnetic field..... | 33 |
| 2.3.7. Coupled magnetic excitations in single crystal PrBa ₂ Cu ₃ O _{6.2} | 34 |
| 2.3.8. Phonons in single crystal PrBa ₂ Cu ₃ O _{6.2} | 35 |
| 2.3.9. Topological analysis of YBa ₂ Cu ₃ O _{6.98} : I. Critical points..... | 36 |
| 2.3.10. Topological analysis of YBa ₂ Cu ₃ O _{6.98} : II Space partitioning and determination of the charge transfer..... | 38 |
| 2.3.11. Magneto optical investigations on stripes of YBa ₂ Cu ₃ O _x thin film..... | 40 |
| 2.3.12. Magneto optical investigations of tapes with varying filament thickness..... | 41 |
| 2.3.13. Relation between texture and critical current density of textured YBa ₂ Cu ₃ O _x plates..... | 42 |
| 2.3.14. YBCO/Ag superconducting tapes..... | 44 |
| 2.3.15. Improvement of BPSCCO/Ag-sheathed tapes by manipulation of the final cooling stage..... | 45 |
| 2.3.16. Post annealing of high-T _c superconducting BSCCO-tapes in Ag-clad..... | 46 |
| 2.3.17. The effect of intermediate pressure in the opit fabrication on the current paths and the current carrying capability of Bi-2223 tapes..... | 47 |
| 2.3.18. Magneto-optical investigations as a tool to improve quality of (Pb,Bi)-2223 tapes..... | 48 |
| 2.4. Structures and defects..... | 49 |
| 2.4.1. A perdeuterated cryoprotectant for neutron studies and a demonstration of its use for neutron powder diffraction on l(-)-ephedrine hemihydrate..... | 49 |
| 2.4.2. Synthesis and crystal structure analysis of ZnAPO-35 and Zn ₂ (OH) _{0.14} F _{0.86} PO ₄ based on x-ray and neutron powder diffraction data..... | 50 |
| 2.4.3. A neutron powder diffraction study Strontium Oxalate Hydrate, SrC ₂ O ₄ ·2D ₂ O..... | 51 |

| | |
|--|------------|
| 2.5. Structures and interfaces..... | 52 |
| 2.5.1 Stabilization of the Si(111)- $\begin{pmatrix} 3 & 2 \\ -1 & 1 \end{pmatrix}$ -Pb low temperature phase at room temperature ... | 52 |
| 2.5.2 Structural investigation of Si(111)- $\sqrt{3}\times\sqrt{3}$ -Ag surface at low temperature..... | 53 |
| 2.5.3 Low-temperature structure of indium quantum chains on silicon..... | 54 |
| 2.5.4 Thin bonded Silicon wafers with penetrating strain fields..... | 56 |
| 2.5.5 Growth of Si cluster on CaF ₂ films..... | 57 |
| 2.5.6 Structure of CaF ₂ films on Si(111) examined by SXRD..... | 58 |
| 2.5.7 Subsurface dimerization in III-V compound semiconductor (001)-surfaces..... | 60 |
| 2.5.8 Ordering of regio-irregular polyalkylthiophenes by doping in solution prior to film formation..... | 62 |
| 2.5.9 Structure of poly-dodecyl-bithiophene films: polymer electronics materials with increased oxidation potential..... | 64 |
| 2.5.10 ASAXS investigations of steam reforming catalysts..... | 66 |
| 2.5.11 Different approaches to the analysis of small angle scattering experiments on porous aluminum-hydroxide..... | 67 |
| 2.5.12 Particle-particle interaction in aluminum-hydroxides..... | 68 |
| 2.5.13 Adsorption of beta-lactoglobulin on Si investigated by ellipsometry..... | 69 |
| 2.5.14 Chain length determination of grafted PEG-silanes by TOF-SIMS..... | 70 |
| 2.5.15 Poly(ethylene glycol)-silanes – a model system study..... | 71 |
| 2.5.16 TOF-SIMS investigation of single carbon fibres in a PEEK matrix..... | 72 |
| 2.5.17 Polymer tribology - the influence of surface topography on the wear behaviour of carbon fibre reinforced PEEK sliding against stainless steel..... | 73 |
| 2.5.18 Corrosion of carbon fibres in a PEEK matrix studied by atomic force microscopy..... | 74 |
| 2.5.19 High-resolution imaging of cell adhesion to fibrillar collagen-coated substrate..... | 75 |
| 2.5.20 An X-ray reflectivity study of a model biomembrane on solid support..... | 76 |
| 2.5.21 Neutron reflectivity of a model biomembrane..... | 77 |
| 2.5.22 Use of highly n-doped silicon as an electrode for in-situ neutron and X-ray reflection studies of an electrochemical system..... | 78 |
| 2.6. Langmuir films..... | 79 |
| 2.6.1 Grazing-incidence X-ray diffraction from Langmuir films of alkylthiol passivated gold nanoparticles..... | 79 |
| 2.6.2 Langmuir films of surfactant polythiophene derivatives studied by grazing angle X-ray diffraction and X-ray reflectivity..... | 80 |
| 2.6.3 Crystalline β -sheet monolayers - A new class of ordered molecular templates..... | 81 |
| 2.6.4 2D Mono- and Bi-metal ionic arrays self assembled on different subphases..... | 82 |
| 2.6.5 Self assembled 2D bimetal ionic arrays, with varied organic spacer lengths..... | 84 |
| 2.6.6 Self-assembly of interdigitated bilayers of long-chain cholesteryl esters at the air-water interface. Effect of long-chain alcohol and acid additives..... | 85 |
| 2.6.7 Specific recognition between cholesteryl glutamate and amino acids at the air-liquid interface..... | 87 |
| 2.6.8 Mixed films of cholesterol derivatives at the air-solutions interface..... | 89 |
| 2.6.9 Monitoring a polymerization reaction in a self-assembled monolayer at the air-water interface..... | 90 |
| 2.6.10 Homochiral oligo-peptides from racemic precursors..... | 91 |
| 2.6.11 Two-dimensional packing arrangement of enantiomerically pure and racemic stearyl-lysine-thioethyl esters..... | 92 |
| 2.6.12 Polystyrene sulfonate at the air-liquid interface..... | 93 |
| 2.6.13 Mixed ganglioside/phospholipid Langmuir monolayers..... | 94 |
| 2.6.14 Studies on mixed Gramicidin D - lipid monolayers at the air water interface..... | 96 |
| 2.6.15 Structure analysis of a metallosupramolecular polyelectrolyte-amphiphile complex at the air-water interface..... | 97 |
| 2.6.16 Condensation of DNA molecules at cationic lipid monolayers..... | 98 |
| 2.6.17 Langmuir monolayers with fluorinated groups in the hydrophilic head..... | 99 |
| 2.6.18 A structural study of phosphatidylinositol phosphate monolayers..... | 100 |
| 2.7. Microemulsions, surfactants and biological systems..... | 102 |

| | | |
|--------------|--|------------|
| 2.7.1. | Time evolution of the planar lamellar to the lamellar vesicle phase observed in an ionic surfactant system | 102 |
| 2.7.2. | Planar lamellar and lamellar vesicles phases in nonionic surfactant systems | 103 |
| 2.7.3. | Structural characterisation of multi-lamellar di-acyl phosphatidylcholine lipid bilayer by small-angle scattering | 104 |
| 2.7.4. | Simple structural microtubule cap | 105 |
| 2.7.5. | Simple mechanical interpretation of tip shapes observed at growing microtubule ends | 105 |
| 2.7.6. | Pulling strings at finite temperature: Another force-extension formula for the worm-like chain model | 106 |
| 2.7.7. | Calibrating an optical trap | 106 |
| 2.7.8. | Automatic differentiation of multichannel EEG signals | 106 |
| 2.8. | Polymers..... | 107 |
| 2.8.1. | Lateral quantification of spin coated polymer films on silicon by TOF-SIMS and AFM..... | 107 |
| 2.8.2. | Vertical quantification of spin coated polymer films on silicon by TOF-SIMS and AFM..... | 108 |
| 2.8.3. | The bulk dynamics of a compositionally asymmetric diblock copolymer studied using dynamic light scattering and NMR..... | 109 |
| 2.8.4. | Reversible thermal gelation in soft spheres..... | 110 |
| 2.8.5. | Ordered microphase in Pluronic type block copolymers, PEO-PPO-PEO | 111 |
| 2.8.6. | Phase behavior near the isotropic critical Lifshitz point of a ternary homopolymer/block copolymer system..... | 112 |
| 2.8.7. | Composite capable of rapid volume change..... | 113 |
| 2.8.8. | Response of a dielectric elastomer actuator..... | 114 |
| 2.8.9. | Artificial muscles from 3M VHB 4910 tape | 115 |
| 2.8.10. | Dielectric elastomer actuators | 116 |
| 2.8.11. | Properties of Polypyrrole doped with alkyl benzene sulfonate | 117 |
| 2.8.12. | Microporous polymer membranes for lithium polymer batteries..... | 118 |
| 2.9. | Organic chemistry | 119 |
| 2.9.1. | Easy access to 3,8-diaryl-difurano[2,3- α :2',3'- f]naphthalenes: A new extended aromatic system | 119 |
| 2.9.2. | On the conformational properties of [n]cyclophanes: A new application of the Ramachandran plot using crystallographic data | 120 |
| 2.9.3. | How the R -factor changes as molecules become larger | 121 |
| 2.10. | Instrumentation..... | 122 |
| 2.10.1. | Test of 8.4 Tesla Nb/Ti superconducting magnet..... | 122 |
| 2.10.2. | The facility for plastically deformed germanium single-crystal wafers | 123 |
| 2.10.3. | McStas developments at Risø..... | 125 |
| 3. | Publications, lectures, educational and organisational activities..... | 126 |
| 3.1. | International publications | 126 |
| 3.2. | Publications for a broader readership, theses and reports | 134 |
| 3.3. | Conference lectures, published and lectures, inclusive published abstracts..... | 135 |
| 3.3.1. | Conference lectures, published..... | 135 |
| 3.3.2. | Lectures, inclusive published abstracts..... | 136 |
| 3.4. | Patent applications | 144 |
| 3.5. | Meetings and Courses | 144 |
| 3.5.1. | Ph.D. Course on "Magnetism and Magnetic Materials"..... | 144 |
| 3.5.2. | Topical Meeting on Biophysics – Biological Physics | 144 |
| 3.5.3. | The Danish Physical Society's Annual Meeting..... | 144 |
| 3.5.4. | DANSSK- Dansk NeutronSpredningsSelskab Årsmøde..... | 144 |
| 3.5.5. | European meeting on "Lipid lipase interaction in the "Øresund" region"..... | 145 |
| 3.6.6. | Inauguration meeting for the ESS-Scandinavia..... | 146 |
| 3.5.7. | Thematic day on "Gluing and adhesion"..... | 146 |

| | | |
|-------------|--|------------|
| 3.5.8. | Discussion meeting on the “Interaction between Physics and Biology, in Particular in Relation to Teaching Students and Training Young Researchers at the Graduate Level” | 147 |
| 3.6. | Memberships of committees and boards..... | 148 |
| 4. | Staff, guests, students, degrees and awards | 150 |

1. Introduction and post festum

Klaus Bechgaard

e-mail: klaus.bechgaard@risoe.dk

The year 2000 Annual Report of the activities of the Department of Condensed Matter Physics and Chemistry is to be the Department's last progress report. From January 2001 the Department was closed and its research in Polymer Physics and Polymer Chemistry transferred to the new Polymer Department. The separation of Polymer Science and the formation of the new Department is a consequence of the establishment of a joint action, known as the Danish Polymer Centre (DCP) between Risø National Laboratory and the Technical University of Denmark in 1999. The DCP will present a clearer profile as a centre for research and education and as a partner in collaborations with industry when the Risø partner constitutes an independent Department. The remainder of the research in structural physics based on Neutron and X-ray scattering, and other activities in Condensed Matter Physics and Biophysics was transferred to the Department of Materials Science after some revision.

The sudden and unplanned closure of DR3 last year is at the origin of some of the reorganisational measures. In the last decade of its operation the main function of DR3 was to produce neutron beams for research in biology, chemistry, physics and materials science. The users of DR3 in this period were Risø scientists, a large and active community of international collaborators and Danish university groups. The closure of DR3 came at a particularly inopportune time. A strategy for a planned closure of DR3 sometime in the period 2006 to 2008 had been drafted. This strategy called for Risø's participation in the Spallation Neutron Source, currently being constructed at Oak Ridge National Laboratory in Tennessee. Risø's directors decided that with the closure of DR3, the future and funding of neutron scattering should be decided according to national priorities. This decision was partially vindicated by the decision of the Ministry of Research that in 2001 any monies saved by the closure of DR3 will be removed from Risø's budget, and used to start the decommissioning of DR3: it is presently unclear what will happen in 2002 and beyond. What is clear at this point is that neutron scattering is not seen as being a key element of the recently published Risø strategy, and that a national strategy for Denmark needs to be created.

On the positive side several international neutron scattering research centres have been interested in establishing scientific collaborations and in a relocation of the best instruments from DR3. It has been decided that the best scientific and logistical fit was with Paul Scherrer Institute (PSI) in Switzerland. In return for relocating three instruments from Risø, PSI offers 50% access in a period of six years, which corresponds to about 60 beam weeks per year. Likewise to strengthen structural physics on site the neutron house will be transformed into an X-ray house and instruments will be rebuilt to meet future demands.

Despite the turmoil experienced in 2000 by the Department's staff, the scientific productivity and quality remained as high as in previous years, as documented in the present annual report.

A very unhappy consequence of the closure of DR3 is the future lay off of permanent staff. Their excellent skills, friendship and personalities will be missed.

In December we were deeply saddened by the sudden passing away of Annette Liljenström. Our feelings at the tragic loss of our friend and respected colleague are expressed in the Danish obituary reprinted on the following page.

Finally, let me express my sincere personal thanks to all members of the Department: It has been a privilege to work with you during the past seven years. The quality of your work and your devotion to solving the tasks of the Department has been outstanding.

Onsdag den 13. December fik vi det ubegribelige budskab at Anette Liljenström var død. Den dag og dagene derefter var tunge, sørgmodige dage.

Anette havde kun arbejdet i Afdelingen for Materialers Fysik og Kemi i få år; men i løbet af ganske kort tid blev hun en naturlig del af afdelingen, et holdpunkt som vi ikke kunne forestille os at være foruden. Anette var en afholdt kollega - for mange af os en ven, som vi kunne dele

vores glæder og sorger med. Anette var et varmhjertet, kompetent menneske med en sjælden helstøbt personlighed. Der var en mening med og en holdning bag alt hvad hun foretog sig. Når Anette påtog sig en opgave blev den gennemført i overensstemmelse med de høje normer hun havde for kvalitet, stil og hvordan man skulle behandle andre mennesker.

Det har mange af vore udenlandske gæster nydt godt af, og det har givet afdelingen et godt ry som et sted, hvor gæster følte sig velkommen. Inden for få timer efter at nyheden om Anettes død var blevet kendt, modtog vi utallige e-mails fra samarbejdspartnere som ønskede at give udtryk for deres sorg og medfølelse.

Vi vil aldrig kunne forstå hvorfor Anette skulle tages fra os, og endnu mindre hvorfor hun ikke skulle få lov

til at se sine børn vokse op. Familien var Anettes et og alt, og det er ubegribeligt at hun ikke kunne få lov at blive ældre og være en del af dens liv og fællesskab.

Alle vores tanker og sympati går til Anettes mand, Jan og deres tre børn, Andreas, Anja og Jonathan.

På Fysikafdelingens vegne
*KURT NØRGAARD CLAUSEN, BENTE LEBECH,
ROBERT FEIDENHANS'L og
NIELS HESSEL ANDERSEN*



Til ANETTE som jeg har delt kontor med de sidste 5 år

Kære lille ven, nu er det forbi
En kølig regn isner i mit hjerte
Jeg husker de dage du var her
Som skygge og form fulgtes vi ad
Fysik havde vi ikke forstand på
Et-nul-otte var vort bedste sted
Arbejde afviste du aldrig
Glad og i godt humør var du
Frugt- og urtete bryggede vi altid
Fremmed mad med krydderier
havde du smagt med sympati
Kærlighed og omsorg var din styrke
Retfærdighed og medmenneskelighed ligeså
Tvillingetegnet havde du og jeg
Ni somre skilte os i år
Min krop skælvede da nyheden kom -
at du havde forladt denne verden
Hvorfor hastede det så meget
at rejse derop en decembemat?
Hvem vil nu høre min morgensang?
Te og mad, men uden dig
Tårene triller langsomt ned
som tåger en vintermåned

CA STUDINSKI

2. Research projects in the department

The work is divided in the following subject categories:

2.1.Theory

2.2.Magnetism

2.3.Superconducting materials and phenomena

2.4.Structures and defects

2.5.Structures and interfaces

2.6.Langmuir films

2.7.Microemulsions, surfactants and biological systems

2.8.Polymers

2.9.Organic chemistry

2.10. Instrumentation

2.1. Theory

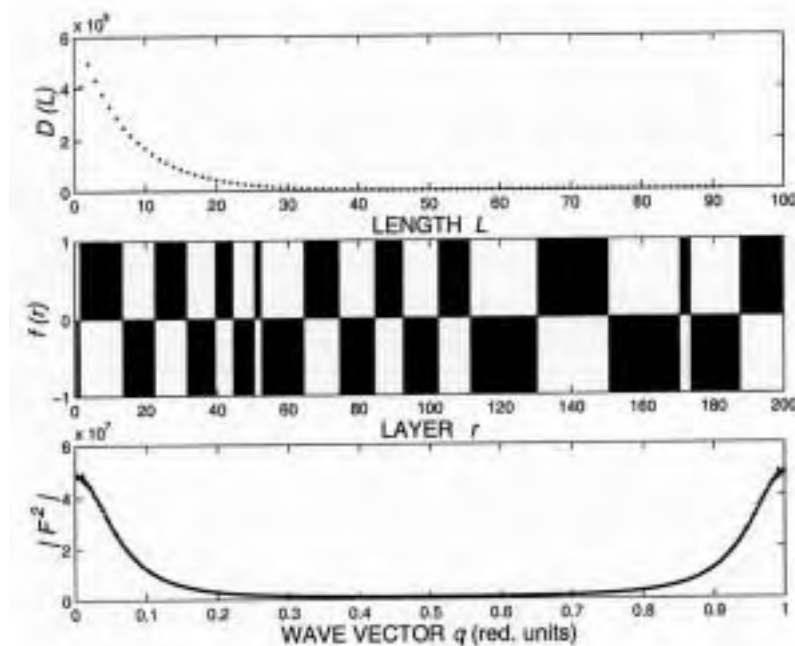
2.1.1. Scattering from discrete nano-scale structures - interpretation of the resulting line shape

P.-A. Lindgård, *Condensed Matter Physics and Chemistry Department, Risø National Laboratory, Denmark*

e-mail: p.a.lindgard@risoe.dk

The interpretation of the scattering results from samples containing small regions or domains of ordered structures are of general interest in many branches of physics and chemistry. It is well known that ramified domains, like those close to a phase transition temperature, T_c , give rise to a simple Lorentzian line shape. Further from T_c when the domain boundaries sharpen up the Lorentzian squared line shape is expected: $1/(\kappa^2 + q^2)^\phi$, where $\phi = 2$. It is often interpreted in terms of Porod's law, which for isolated, spherical particles with a sharp boundary, gives the exponent $\phi = (d + 1)/2$, where d is the dimension. However, this need not be correct; for example it is NOT for the space filling phase-antiphase case. An analysis was made of a simple $d=1$ model for a layered structure, with scattering length $f(r)=1$ for the in-phase domain at plane r , and $f(r')=-1$ for the out-of-phase domain at plane r' . They are distributed in slabs containing several consecutive similar planes, with a thickness L , distributed according to a distribution $D(L)$, see fig.1. The lower panel shows the resulting line shape of the (small angle) scattering at $q=0$ and at the first Bragg point at $q=1$. For an exponential distribution $D(L)=\exp(-L/\xi)$ the average slab thickness is $\langle L \rangle = \xi$. The corresponding scattering line shape yields a perfect fit to a Lorentzian, i.e. with $\phi = 1$, with a HWHM = κ . Remarkable, however, is that the relation between κ and ξ is $\xi = \pi / \kappa$ and NOT $\xi = 2\pi / \kappa$, as expected for isolated scatterers of mean size $\langle L \rangle$. This was discussed analytically previously¹ and is here tested by direct simulation.

Fig.1 demonstrates, that if one in $D(L)$ reduces the probability for finding single layer slabs by 75%, the line shape changes to one which can be fitted perfectly to $1/(\kappa^2 + q^2)^\phi$, where $\phi = 1.36$. If it is reduced by 50%, a perfect fit with $\phi = 1.86$ can be obtained. This shows that the interpretation of the line shape must be made carefully and in general in conjunction with a proper model for the real space structure. It has strong consequences for the interpretation of the oxygen ordering in $YBa_2Cu_3O_{6+x}$. The scattering function for more general space filling distributions with several different scattering lengths was previously derived analytically².



¹ T. Fiig, N. H. Andersen and P.-A. Lindgård, *Phys. Rev. B* **54**, 556 (1996).

² G. Uimin and P.-A. Lindgård, *Acta. Cryst.*, **A53**, 15 (1997).

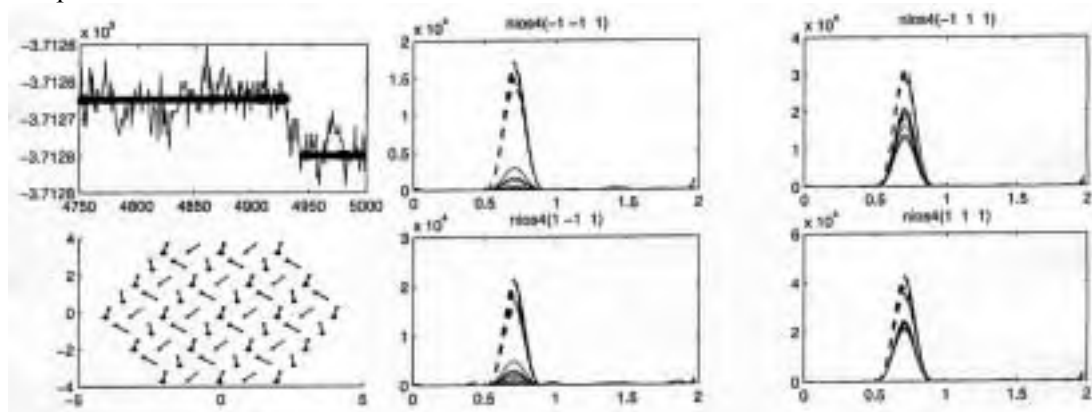
2.1.2. Relaxation properties of antiferromagnetic nano-particles

P.-A. Lindgård, *Condensed Matter Physics and Chemistry Department, Risø National Laboratory, Denmark*

e-mail: p.a.lindgard@risoe.dk

Nano-sized magnetic particles are interesting for several reasons. Perhaps foremost because of their great use as information storage material and the constant pressure to increase the information density. However, there are also several remarkable features in which they internally or in assembly behave quite different from their bulk counter parts. For example they may be used to create various self assembled surface nano-structures¹. The super-paramagnetic relaxation in which the magnetic moment of a particle switches from one direction or energy minimum to another is of interest for the storage applications. It can occur both thermally activated, resulting in an Arrhenius relaxation - and by quantum tunnelling. In principle the particles can at low temperatures be in a coherent, mixed quantum state - and hence might be candidates for quantum computers².

The antiferromagnetic particles are particularly interesting because they possess even classically, a very complex ground state. This make them model systems for a whole range of problems, where finding the global minimum in a rugged energy landscape is on the agenda. The foremost example is that of protein folding, but also for metallurgical texture problems. Spherical NiO particles with 381 spins have been studied assuming the bulk *fcc* structure. The interaction constants are known from bulk measurements, $J_1 = 16\text{K}$ and $J_2 = -221\text{K}$. Because of the *fcc* structure there is considerable frustration of the magnetic structure, yet giving a simple type-II AFM bulk structure. However, for the small particle it is a 4-*q* structure with about equal population of the three equivalent antiferromagnetic vectors $\mathbf{Q} = (1,1,1)$, $(-1,1,1)$, $(1,1,-1)$ and $(-1,-1,1)$. In Fig.1. is shown a simulation of the approach towards equilibrium at $T=300\text{K}$. The energy as a function of number of Monte Carlo steps (MCS) is shown in the upper left panel. It shows that a plateau is reached at which the total energy fluctuates around $\langle E_{\text{tot}} \rangle = -371265 \text{ K}$ for actually more than a thousand MCS's up to 4925 MCS. Then, abruptly, the system finds a different state with the energy fluctuating around $\langle E_{\text{tot}} \rangle = -371280\text{K}$. This is only 15K lower, corresponding to the energy of just one nearest neighbour bond. To the lower left is shown a projection of the corresponding structures, indicating that the restructuring is occurring only on one sublattice (giving rise to an apparent doubling of the spins). The changes in the corresponding Bragg peaks are shown in the right panels. The structure is approaching one with equal population of the 4 possible \mathbf{Q} vectors. However, the lowest energy state found, $\langle E_{\text{tot}} \rangle = -371346\text{K}$, is still 74K lower. This can be reached in similar steps only after many thousands of MCS. One notices the very small energy changes relative to the total energy and to the involved interaction constants. Such intricate relaxation phenomena are also found in the protein-folding problem. The stepwise relaxation is very different from the power-law relaxation found in bulk AFM³.



¹ W. Wen, L. Zhang and P. Sheng, *Phys. Rev. Lett.* **85**, 5464 (2000).

² E. M. Chudnovsky and J.R. Friedman, *Phys. Rev. Lett.* **85**, 5206 (2000).

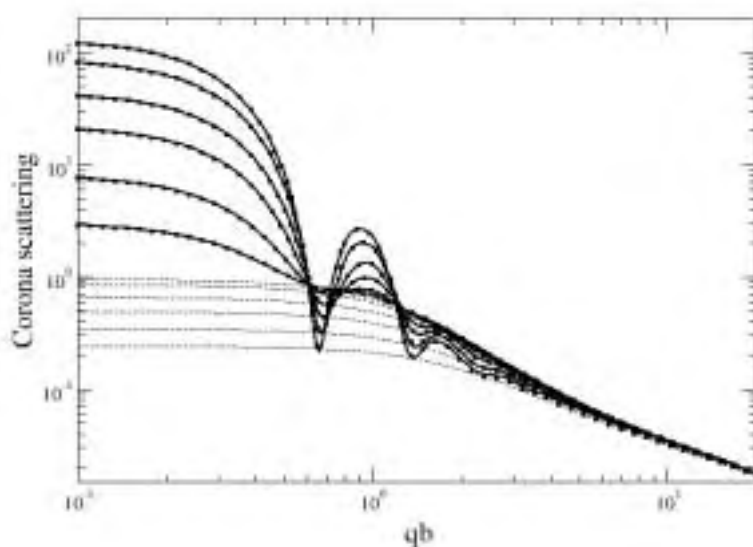
³ T. Castán and P.-A. Lindgård, *Phys. Rev.* **40**, 5069 (1989).

2.1.3. Form factor for micellar coronas with excluded volume interactions

C. Svaneborg, *Condensed Matter Physics and Chemistry Department, Risø National Laboratory, Denmark* and J. S. Pedersen, *Department of Chemistry, University of Aarhus, Denmark*
e-mail carsten.svaneborg@risoe.dk

The corona scattering of a micelle contains information about single chain properties as well global properties such as the radial monomer profile. The corona scattering can be separated into two contributions: a contribution due to single-chain scattering, and an inter-chain contribution, however, the corona scattering can also be regarded as being caused by an average radial profile (a core-shell model), and density fluctuations about that average profile that are caused by chain connectivity and the “correlation hole” between chains. We have demonstrated that the fluctuation scattering contribution can be modelled by a Random-Phase Approximation expression using self-consistent analysis of Monte Carlo simulation data for the corona scattering. The corona was represented as a number of chains interacting through excluded volume interactions and tethered to a spherical core in the simulations. The resulting model expression has the interpretation of being the scattering from a layer of dilute/semi-dilute polymer solution with a radial density profile, based on this expression we are able obtain the apparent second virial coefficient as well as the osmotic compressibility of the micellar corona as for an ordinary polymer solution. The compressibility obtained shows an universal dependence on the reduced surface coverage for simulations varying number of chains. chain length, or core radius, while the apparent second virial coefficient follows an approximate power law as function of reduced surface coverage.

This model has also been used for fitting Monte Carlo simulation data. The model depends on the single chain radius of gyration, an excluded volume coefficient and a radial profile of the corona. We have obtained excellent fits using a Maximum Entropy estimate for the corona profile for a wide range of experimentally realistic corona parameters, and the corona profile and radius of gyration obtained from fits are in very good agreement with results obtained directly from the Monte Carlo simulation.



Corona scattering from simulation varying number of chains $N=3, 8, 22, 44, 87, 131$ (from bottom to top) data are normalized to coincide at high q .

Corona scattering (thick lines), model using RPA expression and core-shell scattering (boxes). Fluctuation scattering contribution (thin lines)

2.1.4. New Monte Carlo simulation technique applied for polymer folding

J. Borg, M. H. Jensen, K. Sneppen, G. Tiana, *Niels Bohr Institute and Nordita, Denmark* and P.-A. Lindgård, *Condensed Matter Physics and Chemistry Department, Risø National Laboratory, Denmark*
e-mail: borg@alf.nbi.dk

The mechanisms behind protein folding are intensively discussed. Their native structure consists of two dominant kind of building blocks, the alpha-helices and beta-sheets, both stabilised by hydrogen bonds. The driving force for the folding process is widely believed to be the hydrophobic interactions between the amino-acids, but the interplay between the hydrophobicity and the hydrogen bonding is not well understood.

We have studied the thermodynamics of these two forces in a simplified homopolymer model using a newly develop Monte Carlo (MC) simulation technique. Indeed, the effect of the hydrogen bonds is to reduce the entropy of the low-lying states dramatically, leading to conformations displaying secondary structures. For compact polymers a spin-glass type of transition is found between helix-rich states and low-entropy sheet-dominated states.

Complex systems, such as spin-glasses or proteins, are very difficult to study numerically. New MC-type of simulation techniques commonly referred to as general ensemble sampling methods, have been developed during the past decade to improve phase space sampling for such systems. They are all based on an iterative calculation scheme, which unfortunately has poor convergence properties. We have found an iteration scheme for the generalized ensemble methods with order(s) of magnitude faster convergence. It consists of two elements: (1) An algorithm to distinguish between distributions arising from respectively equilibrium- and non-equilibrium processes. (2) A maximum-likelihood estimation of the unknown thermodynamic quantities. This estimation is constituted by a generalization of the multi-histogram equations, originally derived by A. M. Ferrenberg and R. H. Swendsen¹. We are currently testing the method on long homopolymers ($N \sim 4000-10000$, see Fig. 1) and spin-glasses.

Two other lines of research are in progress using this simulation technique. The first is to calculate the free energy landscape for a newly suggested minimal model for proteins, which focuses on the local shuffling into tertiary structures². The second line is to do the same type of calculation for more realistic off-lattice models.

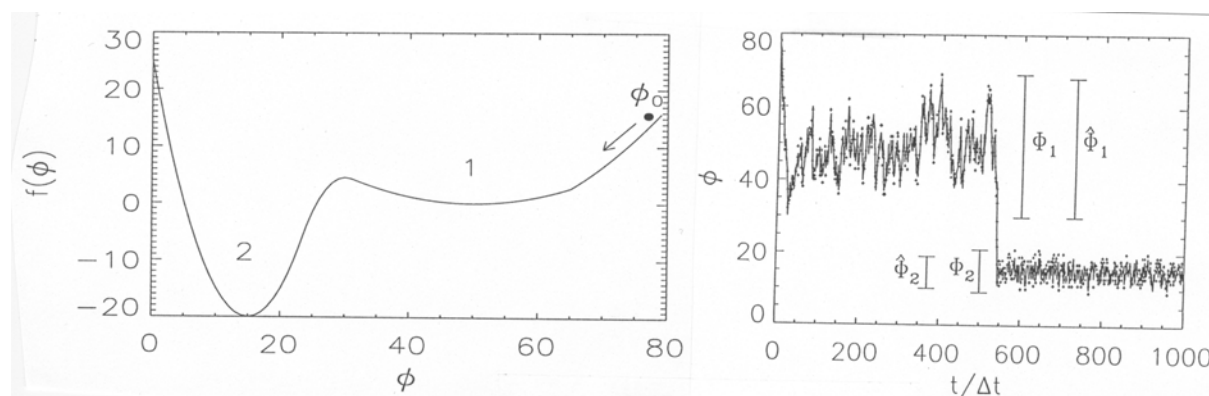


Fig. 1. Left, the free energy landscape $f(\phi)$ with two minima as function of the state variable ϕ for some system, which is initialised in state ϕ_0 . Right, shows a possible time evolution of the system in a MC-simulation. The full line is the actual history, whereas the marks (+) show the test states of the Markov chain. Two non-equilibrium transitions are observed, $\phi_0 \rightarrow \phi_1$ and $\phi_1 \rightarrow \phi_2$. The figure also shows the extended regions $\hat{\phi}_1$ and $\hat{\phi}_2$ obtained by the inclusion of the test states within each basin.

¹ A. M. Ferrenberg and R. H. Swendsen, Phys. Rev. Lett. **63**, 1195 (1989).

² P.-A. Lindgård and H. Bohr, Phys. Rev. Lett. **77**, 779 (1996).

2.2. Magnetism

2.2.1. New results on the excitations of an $S=1$ quantum chain

M. Kenzelmann, R. A. Cowley, *Oxford Physics, Clarendon Laboratory, P, W. J. L. Buyers, National Research Council of Canada, Canada*, and D. F. McMorrow, *Condensed Matter Physics and Chemistry Department, Risø National, Denmark*
e-mail: r.cowley@physics.ox.ac.uk

The excitations of one-dimensional Heisenberg antiferromagnets have attracted considerable attention ever since Haldane predicted that the excitations of integer and half-integer spin chains are different. Integer spin chains have an energy gap at low temperatures while half-integer chains have a continuous spectrum extending to zero energy. We have used neutron scattering techniques to re-examine the excitations of the integer spin chain material, CsNiCl_3 , and have determined the temperature dependence of the excitations and found a continuous spectrum extending up in energy above the gap for wave vectors near the antiferromagnetic point, $Q = \pi$.

CsNiCl_3 was chosen for study because its properties are well known. The exchange interaction along the chains is $J = 2.28 \text{ meV}$ ¹ and there is a weaker inter-chain interaction of $J' = 0.044 \text{ meV}$ while the single ion anisotropy is much smaller. Three dimensional, $3D$, long-range antiferromagnetic ordering occurs below 4.85 K but sufficiently far above this temperature the excitations are expected to be largely characteristic of an $S = 1$ Heisenberg quantum chain.

The neutron scattering experiments were performed using the RITA spectrometer at the DR3 reactor. The incident neutrons were thermalised in the cold source and a pyrolytic graphite monochromator used to select the required incident neutron energy. The rotating velocity selector was used to suppress unwanted neutrons that were Bragg reflected by the higher order planes of the monochromator. The scattered neutron beam was analysed by using a cooled Be filter and reflection from a seven component pyrolytic graphite analyser aligned so that all of the analysers reflected 5 meV neutrons and reflected them on to different parts of the position sensitive detector. With this arrangement the energy resolution was typically 0.18 meV (FWHM). The single crystal was mounted in a variable temperature cryostat and the scattering measured to determine the properties of the excitations particularly for $Q = \pi$, the antiferromagnetic wave vector.

Figure 1 shows the scattering observed after subtracting the background with the sample at three different temperatures, above the $3D$ antiferromagnetically ordered phase. The scattering shows an excitation as predicted by Haldane with an energy at low temperatures in agreement with previous measurements and in addition a long high energy tail extending up to 12 meV in energy transfer. The experiments were repeated at temperatures between 2 K and 70 K to determine the temperature dependence of the scattering.

The scattering from the well-defined mode was best fitted by a Voigt function with the Gaussian representing the resolution function and the Lorentzian the temperature broadening of the excitation and the results of the fits are shown in Fig. 1. The results for the energies and widths of the excitations are plotted in Fig. 2. An unexpected feature of the results is that the energy of the excitation increases by more than a factor of three while the Lorentzian half-width is always less than the energy. This behaviour is very different from that of $3D$ antiferromagnets where the $Q = \pi$ excitation decreases in energy and rapidly becomes over-damped with increasing temperature. In Fig. 2 we also show the theoretical predictions for the energy² and line-width³ that have been obtained with the non-linear sigma model (NL σ M). The model is expected to be most satisfactory at low temperatures where our results may be influenced by inter-chain coupling. Nevertheless the theories underestimate the temperature dependence near 20 K and then fail to reproduce the flattening off beyond 35 K . The latter is probably because the NL σ M is a continuum approximation and so does not include a lattice cut-off at high temperatures.

¹ R. Morra, W. J. L. Buyers, R. L. Armstrong, and K. Hirakawa, *Phys. Rev. B* **38** 543 (1988), H. A. Katori, Y. Ajiro, T. Asano and T. Goto, *J. Phys. Soc. Jpn.* **64**, 3038 (1995).

² Th. Jolicoeur and O. Golinelli, *Phys. Rev.* **B50**, 9265 (1994).

³ D. Damle and S. Sachdev, *Phys. Rev.* **B57**, 8307 (1998).

Even more surprising was the observation of a continuum component at low temperatures. These experiments after correction for neutron absorption show that the continuum component is about $12 \pm 2\%$ of the total scattering for $Q = \pi$. In contrast, calculations based on numerical diagonalisation of spinchains¹ or by three-particle scattering in the NL σ M predict an intensity of only 2%. The reason for this discrepancy is currently unknown. The continuum scattering is qualitatively very similar to the spinon-pair continuum observed for $S = 1/2$ systems in that the peak energy is approximately twice the maximum energy of the excitations and the scattering is observed near $Q = \pi$ and not near $Q = 0$. This suggests that there is a spinon-like character to the excitations in CsNiCl₃. Possibly this arises from the frustrated nature of the inter-chain interactions.

Because of the unexpected nature of these results similar experiments on CsNiCl₃ have been performed using the MARI spectrometer at ISIS and the DUALSPEC spectrometer at Chalk River. The results of these experiments are consistent with the results described above. Financial support for the work was provided by the EPSRC, by the EU through the LIP programme, by the British Council-Nation Research Council of Canada programme and by a TMR Fellowship from the Swiss National Science Foundation, 83EU-053223.

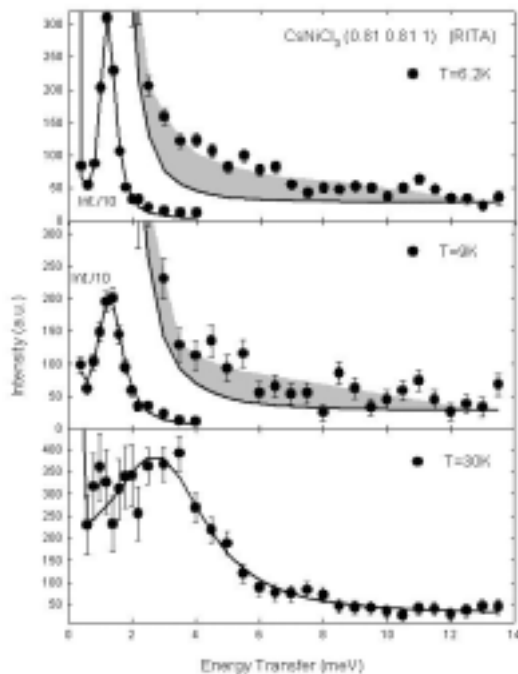


Fig. 1. The scattering observed at the antiferromagnetic point, $Q = \pi$, at three different temperatures from the magnetic chains in CsNiCl₃. The solid line is a fit to the Haldane excitation and the hatched area is the continuum scattering.

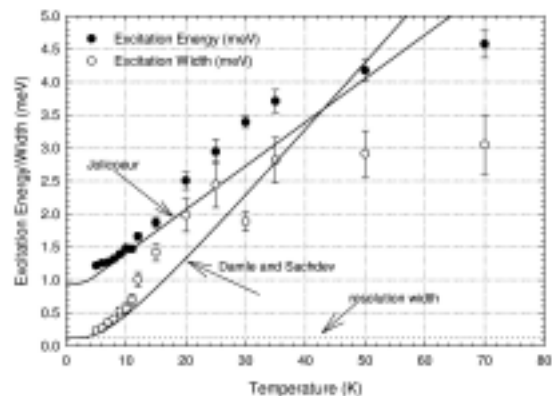


Fig. 2. The energy and width of the excitation for $Q = \pi$ as a function of temperature for CsNiCl₃ as compared with theories^{2,3}.

¹ M. D. P. Horton and I. Affleck, Phys. Rev. **B17**, 11891 (1999).

2.2.2. Correlations and fluctuations in the 2D Heisenberg antiferromagnet

H. M. Rønnow, D. F. McMorrow and N. B. Christensen, *Condensed Matter Physics and Chemistry Department, Risø National Laboratory, Denmark*, R. Coldea, *Solid State Division, Oak Ridge National Laboratory, USA*, A. Harrison, I. D. Youngson, *Department of chemistry, University of Edinburgh, UK*, and O. Syljuåsen, *NORDITA, Copenhagen, Denmark*
e-mail: hmr@ill.fr

The last decade witnessed considerable efforts and achievements in the understanding of the 2D Heisenberg antiferromagnet. In particular the quantum ($S=1/2$) system on a square lattice was elected to one of the primary archetype spin model systems. Through neutron scattering studies on the excellent physical realisation, $\text{Cu}(\text{DCOO})_2 \cdot 4\text{D}_2\text{O}$ with exchange interaction $J=6.31 \text{ meV}=73 \text{ K}$, we have obtained the most complete characterisation of the finite temperature properties of this spin model^{1, 2, 3}. At $T=0$ the system is long range ordered with sharp spin wave excitations. The order is destroyed by thermal fluctuations for $T>0$, but the system is still strongly correlated and looks ordered with propagating excitations on short length and time scales. This behaviour is contained in the structure factors, which are Fourier transforms to the spin-spin correlation functions as summarised in figure 1. The instantaneous structure factor, $S(q)$, was measured using the RITA spectrometer at Risø in an energy integrating configuration. The data covering $0.2 < T/J < 1.4$ are in good agreement with the combined predictions based on the low temperature renormalised classical non-linear- σ -model (NL σ M), Quantum Monte Carlo (QMC) and high-temperature expansion (HTE). The dynamic structure factor, $S(q, \omega)$ was measured up to $T/J=0.6$ at the time-of-flight spectrometer HET at ISIS. The excitation spectrum displays well defined spin waves although damped and softened due to the finite correlation length. The data enabled us to detect a problem with previous dynamic QMC calculations, which could have impact on the widely used maximum entropy method (MEM). Avoiding this problem, new QMC calculations are in excellent agreement with the data. But more remarkable is the consistency with a renormalised classical prediction for the softening $Z_c(T)$ and the simple estimate that the lifetime $J/\Gamma(T)$ equals the correlation length $\xi(T)$ divided by the spin wave velocity $v_s(T)$.

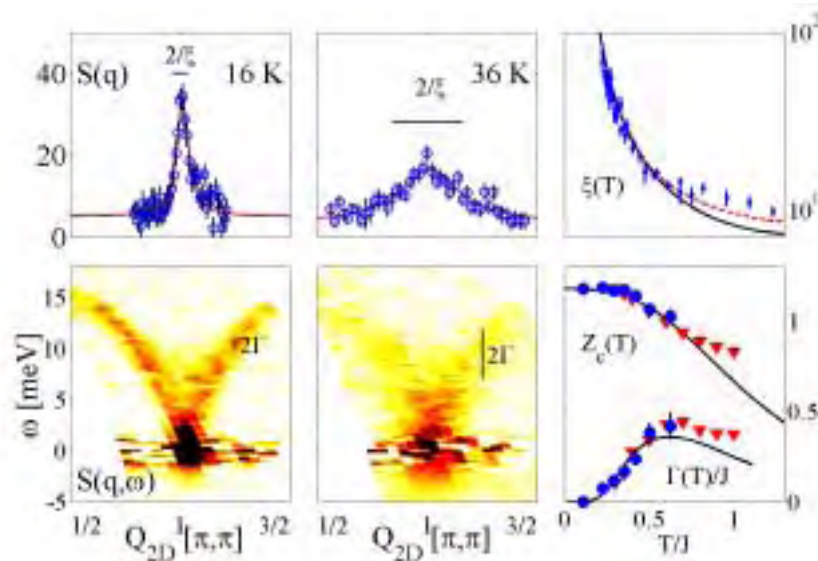


Fig. 2. $S(q)$ (top) and $S(q, \omega)$ (bottom) at , respectively, 16 K (left) and 36 K (middle). For $S(q)$, the lines shows resolution convoluted fits to Lorentzians, and the corresponding values of ξ and Γ are indicated. Right top: $\xi(T)$ extracted from energy integrating neutron scattering, compared to the NL σ M (solid) and HTE (dashed) predictions. Bottom: temperature dependence of $\Gamma(T)/J$ and $Z_c(T)$ for the data (circles), QMC (triangles) and theory (solid line).

¹ H. M. Rønnow, D. F. McMorrow and A. Harrison, Phys. Rev. Lett. **82**, 3152 (1999).

² H. M. Rønnow, D. F. McMorrow, A. Harrison, I. D. Youngson, R. Coldea, T. G. Perring, G. Aeppli and O. Syljuåsen, Correlations and fluctuations in the 2D Heisenberg antiferromagnet, J. Mag. Mag. Mater., in press.

³ H. M. Rønnow, D. F. McMorrow, R. Coldea, A. Harrison, I.D. Youngson, T. G. Perring, G. Aeppli, O. Syljuåsen, K. Lefmann and C. Rischel, Spin dynamics of the model 2D antiferromagnet CFD, Phys. Rev. Lett. submitted.

2.2.3. Excitations around the quantum critical point in LiHoF₄

H. M. Rønnow, D. F. McMorrow, *Condensed Matter Physics and Chemistry Department, Risø National Laboratory, Denmark*, R. Parthasarathy, T. F. Rosenbaum, *University of Chicago, USA*, G. Aeppli, *NEC Research, New Jersey, USA*, J. Jensen, *Ørsted Laboratoriet, University of Copenhagen*
 e-mail: hmr@ill.fr

LiHoF₄ is a dipole coupled Ising ferromagnet¹. Subjected to a magnetic field perpendicular to the Ising axis, the system undergoes a quantum phase transition (QPT) from ordered ferromagnet to polarised paramagnet (Fig.1, top right). There is much current interest in the behaviour of fluctuations around such QPTs, and LiHoF₄ is one of the few physical realisations for which the Hamiltonian is well understood and the transition is easily controlled (by changing the field). LiHoF₄ can furthermore be diamagnetically diluted to give information on percolation and annealing in the quantum regime. However, one complication is that there is a sizeable hyperfine coupling to the nuclear magnetic moments, which is responsible for the small upturn in the critical field at lowest temperatures. Using the TAS7 spectrometer at Risø, we have characterised the magnetic excitation spectrum around the QPT (see Fig. 1, left)². At all fields, there is a finite gap at $Q=(2,0,0)$, with a field dependence as shown in Fig. 1, bottom right. According to the simple transverse field Ising model, the gap should soften completely at the critical field. But the hyperfine coupling leaves a finite gap even at the quantum critical point, which will have important implications on the scaling behaviour in the entire critical regime.

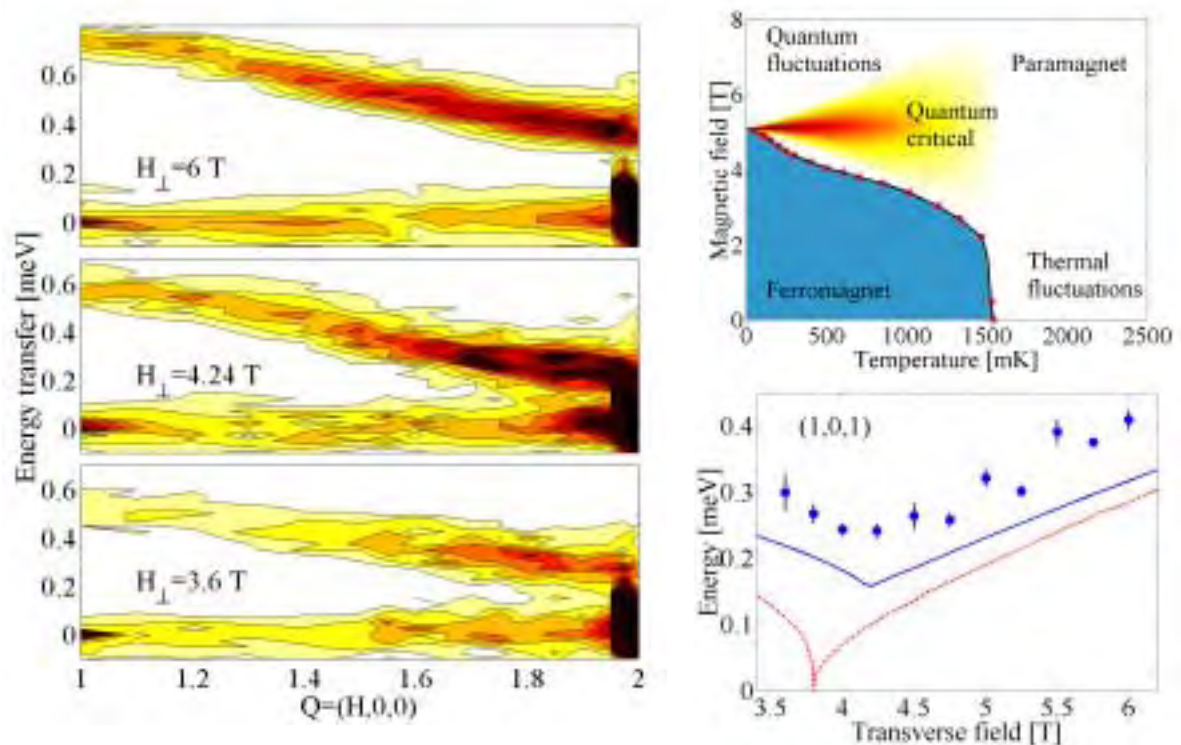


Fig. 1. Top right: Phase diagram of LiHoF₄ with a magnetic field applied perpendicular to the Ising axis. Left: Longitudinal excitation spectrum at three fields relatively below, at and above the quantum critical point. The resolution can be inferred from the dark ellipsoid around the (2,0,0) Bragg peak. Bottom right: Field dependence of the energy gap compared to a random-phase-approximation (RPA) calculation respectively with (solid) and without hyperfine interactions included. The 28% discrepancy with our data witness additional fluctuations not included in the RPA calculation.

¹ D. Bitko, T. F. Rosenbaum and G. Aeppli, *Phys. Rev. Lett.* **77**, 940 (1996).

² H. M. Rønnow, *Aspects of Quantum Magnetism*, Thesis 2000, University of Copenhagen.

2.2.4. A time-of-flight neutron scattering study of the dynamics of magnetic nanoparticles

S. N. Klausen, K. Lefmann, K. N. Clausen and P.-A. Lindgård, *Condensed Matter Physics and Chemistry Department, Risø National Laboratory, Denmark*, F. Bødker, M. F. Hansen and S. Mørup, *Department of Physics, Technical University of Denmark, Denmark*, M. Telling, *ISIS Department, Rutherford Appleton Laboratory, UK*
e-mail stine.nyborg.klausen@risoe.dk

The fluctuations of magnetization direction in nanoparticles are currently subject of much attention. Studies of these phenomena are motivated not only by interest in the fundamental properties of ultrafine particles but also by the applications of such particles in *e.g.* magnetic recording media, ferrofluids and catalysts. Recently the first triple-axis neutron scattering measurements of magnetic fluctuations in nanoparticles was performed using an antiferromagnetic reflection¹. Here we present time-of-flight measurements of magnetic fluctuations in hematite (α -Fe₂O₃) nanoparticles performed at the IRIS spectrometer at the ISIS spallation source at Rutherford Appleton Laboratory, UK. The sample is the same as in ref. 1 but the time-of-flight resolution is remarkably better. A time-of-flight spectrum is shown in Fig. 1. The two broadenings of the elastic component at about 1.4 Å⁻¹ are due to the magnetic dynamics of the hematite particles. Fig. 2 shows the logarithm of the normalised measured intensity versus energy transfer ε of the neutrons for various temperatures. Fits to the data are also shown. Superparamagnetic relaxation and collective magnetic excitations are clearly visible, see *e.g.* ref. 1. A complete data analysis is not completed yet. Further work on the analysis of the data is in progress.

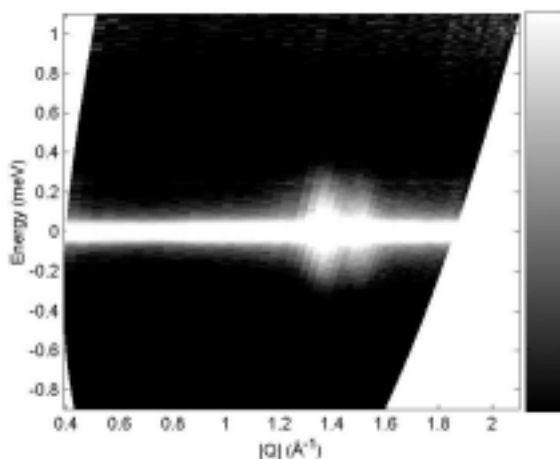
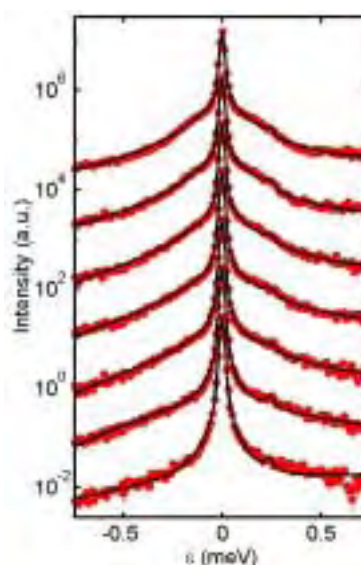


Fig. 1. Time-of-flight spectrum of hematite nanoparticles measured at 325 K. The measured intensity is shown as a function of momentum transfer Q and energy transfer of the neutrons.

Fig. 2. Cuts in the time-of-flight spectra obtained at $Q = 1.37$ Å⁻¹. The spectra are measured at temperatures $T = 5, 50, 100, 150, 200, 265$ and 325 K (from below). Data are shown with offsets. The solid lines are fits to the experimental data. The peaks at about 0.24 meV are a feature of the instrument and a consequence of fast neutrons from the proton excitation process.



¹ M. F. Hansen, F. Bødker, S. Mørup, K. Lefmann, K. N. Clausen and P.-A., Lindgård, *Phys. Rev. Lett.* **79**, 4910 (1997).

2.2.5. Spin precession in ferrimagnetic maghemite nanoparticles

S. N. Klausen, K. Lefmann, K. N. Clausen and P.-A. Lindgård, *Condensed Matter Physics and Chemistry Department, Risø National Laboratory, Denmark*, F. Bødker, M. F. Hansen and S. Mørup, *Department of Physics, Technical University of Denmark, Denmark*
 e-mail: stine.nyborg.klausen@risoe.dk

Most studies of magnetic fluctuations in nanoparticles have been performed using ac and dc magnetisation measurements and/or Mössbauer spectroscopy. These techniques allow studies of fluctuations in the range 10^{-10} - 10^{-4} s while neutron scattering can be applied for fluctuations in the range 10^{-12} - 10^{-7} s. The applied neutron scattering technique is particularly useful for studies of transverse

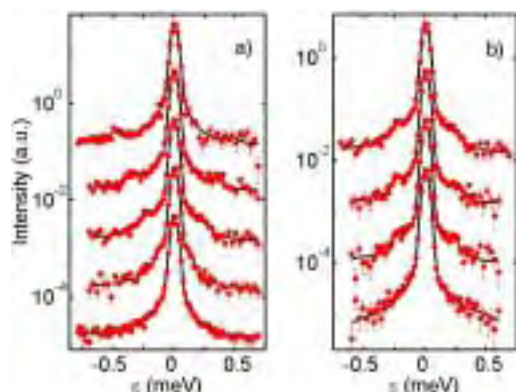


Fig. 1. Inelastic neutron data for a) applied fields of 1, 2, 3 and 4 T (from below) at 300 K and b) in an applied field of 2 T at 6, 100, 210 and 300 K (from below) with fits. Data are shown with offsets.

fluctuations near an easy direction of magnetisation (collective magnetic oscillations) and reversal of the magnetisation direction along an easy axis (superparamagnetic relaxation). Both phenomena are interesting from a fundamental as well as from a technological point of view.

We present inelastic neutron scattering studies of 4 nm maghemite (γ - Fe_2O_3) nanoparticles.¹ The data consists of a series of scans of the neutron energy transfer, ε , at fixed momentum transfer, $\kappa = 1.305(5) \text{ \AA}^{-1}$. This value equals the first antiferromagnetic reflection arising from ferrimagnetic order in bulk maghemite:

$Q = 1.31 \text{ \AA}^{-1}$. The data are fitted to an elastic signal from incoherent scattering, a quasielastic Lorentzian line and a damped harmonic oscillator line for the dynamics of the precession states. In the fitting procedure the signal is multiplied by the detailed balance factor and the intensity is multiplied by correction factors for change in resolution function volume and powder scattering angle

dependence. Figure 1 shows the intensity as a function of ε for various fields and temperatures. The inelastic peak from the precession modes are clearly visible and are seen to move out from $\varepsilon = 0$ with increasing field as expected. The position of the inelastic peak is seen to be constant and the intensity increases with temperature as expected. This shows that the inelastic signals stem from coherent precession of the particle moments. In fig 2a we show the dependence of the inelastic peak position on the applied field. The full line is a fit to the so-called ferromagnetic mode, described in the literature, averaged over applied field. This yields the anisotropy field $B_A = 0.3(1) \text{ T}$ and a g -value of $2.03(2)$.

Figs. 2b and 2c show $R_{in} = A_{in}/(A_{in}+A_q)$ as a function of applied field and temperature. Here A_{in} and A_q are the areas of the inelastic signal and the quasielastic component. It is seen that the field dependence is in agreement with the predicted behaviour. The only free parameter of the fit is the (mean) saturation particle moment (at $T = 300 \text{ K}$) which was found to be $1840 \pm 170 \mu_B$. The temperature dependence of R_{in} is consistent with what expected and yields $\mu = 1470 \pm 290 \mu_B$. Spherical maghemite particles with $d = 4 \text{ nm}$ would have a moment of about $1440 \mu_B$, which is in good agreement with our data.

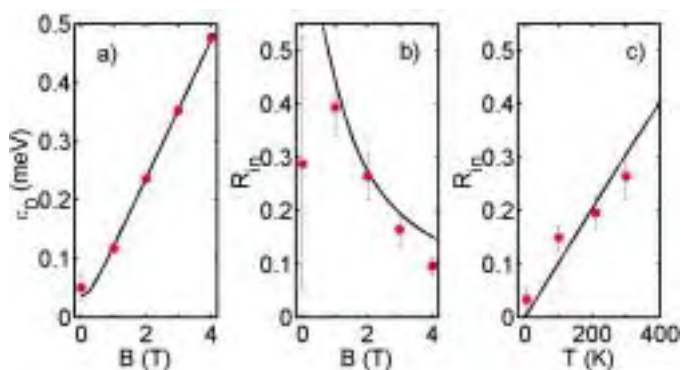


Fig. 2. a) Centre of inelastic peaks as a function of magnetic field at $T = 300 \text{ K}$, experimental value of R_{in} as a function of b) magnetic field at $T = 300 \text{ K}$ and c) temperature at $B = 2 \text{ T}$.

¹ K. Lefmann, F. Bødker, S. N. Klausen, M. F. Hansen, K. N. Clausen, P.-A. Lindgård and S. Mørup, A neutron scattering study of spin precession in ferrimagnetic nanoparticles, submitted to Europhys. Lett.

2.2.6. Spin dynamics in $\text{Cu}(\text{DCOO})_2 \cdot 4\text{D}_2\text{O}$

N. B. Christensen, D. F. McMorrow, *Condensed Matter Physics and Chemistry Department, Risø National Laboratory, Denmark*, H. M. Rønnow, *CEA-Grenoble*, R. Coldea, T. G. Perring, *ISIS facility, Rutherford Appleton Laboratory, UK*, A. Harrison, *Department of Chemistry, University of Edinburgh*, G. Aeppli, *NEC Research Institute, USA*
e-mail: niels.b.christensen@risoe.dk

The magnetic properties of CuO_2 layers is a matter of great interest, both from the point of view of fundamental 2D magnetism, and in particular because of the central role they play in the cuprate high- T_c superconductors. $\text{Cu}(\text{DCOO})_2 \cdot 4\text{D}_2\text{O}$ (CFTD) consists of nearly isolated CuO_2 sheets and is known to be an excellent realisation of the two-dimensional quantum Heisenberg antiferromagnet on a square lattice (2DQHAFSL). Furthermore, the low nearest neighbour coupling constant $J \sim 70$ K (compared to another 2DQHAFSL, the cuprate parent compound LaCuO_4 where $J \sim 1500$ K) makes neutron scattering studies of the spin dynamics on a temperature scale of J feasible. As a continuation of an ongoing project to investigate unresolved questions about the 2DQHAFSL¹ we have used the MAPS spectrometer at ISIS, Rutherford Appleton Laboratory to investigate several outstanding questions:

1) Measurements of the spin wave softening and damping to a higher temperature than previously obtained. 2) Determination of the q -scaling of the spin wave scattering. This carries important information on the interplay of quantum and thermal fluctuations. 3) Search for the multimagnon continuum, which has never previously been observed in 2D systems. 4) Resolve the puzzle of the zone-boundary dispersion: In LaCuO_4 the spin wave energy at $(\pi, 0)$ is 13 % higher than at $(\pi/2, \pi/2)$ ² whereas previous experiments on CFTD indicated a 7 % dispersion in the other direction, a result that is further supported by Monte Carlo simulations and exact diagonalisation¹.

The full data analysis has not been performed yet, but preliminary analysis indicates that at least the first three goals have been reached. In the figure we show an example of the excellent data quality obtained with the 16 m^2 position sensitive detectors at MAPS, which allow us to resolve spin wave branches in eleven zones of the reciprocal lattice, their intensity being highest at the five antiferromagnetic zone centers.

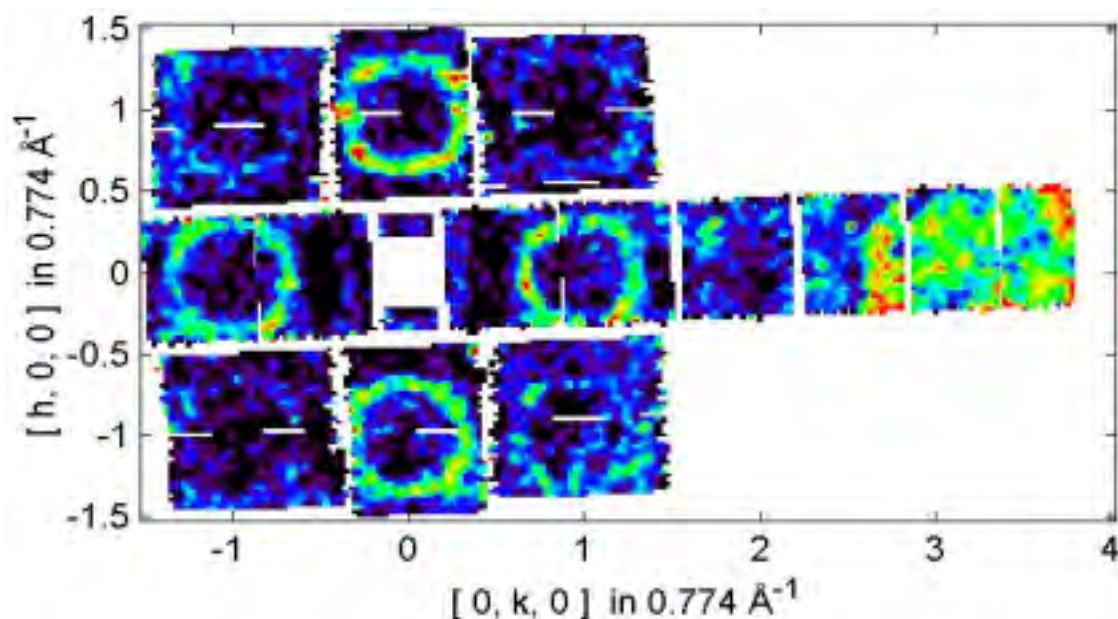


Fig. 1. Spin waves at energy transfers between 12 and 13 meV measured at 7 K using the 16 m^2 position sensitive detector banks of the MAPS spectrometer at ISIS, Rutherford Appleton Laboratory.

¹ H. M. Rønnow, Aspects of quantum magnetism, Thesis 2000, University of Copenhagen.

² R. Coldea, S. M. Hayden, G. Aeppli, T. G. Perring, C. D. Frost, T. E. Mason, S.-W. Cheong and Z. Fisk, Spin waves and electronic interactions in La_2CuO_4 , *J. Phys. C: Condens. Matter*, in print.

2.2.7. Magnetic-field dependent excitations of the ordered quasi-1D HAF CsNiCl₃

M. Enderle, *Condensed Matter Physics and Chemistry Department, Risø National Laboratory, Denmark/Institute Laue-Langevin, Grenoble, France*, W.J.L. Buyers, *Neutron Program for Materials Research, Canada*, P. Vorderwisch, M. Meißner, P. Smeibidl, *Hahn-Meitner-Institut, Berlin, Germany*
 e-mail: enderle@ill.fr

CsNiCl₃ has strong antiferromagnetic superexchange along its hexagonal c-axis (leading to a saturation field of about 65T), and small antiferromagnetic interactions perpendicular to c. The Ni²⁺ ion carries spin 1, the tiny Ising anisotropy is negligible. At lowest temperatures, the small interchain interactions just prevent a macroscopic quantum ground state, the Haldane ground state. Instead an antiferromagnetically ordered phase develops below 4.4K. However, the spin dynamics in the ordered phase is unusual. The magnetic excitations display a strong field dependence, which is not explained by spin-wave theory not even if higher order terms are taken into account¹. This strong field dependence in the ordered phase was explained by a theory (A&W)² which allows for longitudinal fluctuations of the staggered magnetization density and thus takes into account the quantum fluctuations.

We attempted a more detailed test of the A&W theory at the cold triple axis spectrometer V2 in Berlin, equipped with a vertical 14.5T cryomagnet. The 3D dispersion was investigated at 0.84T, 4T, 8T and 14T (fig.1). Up to 4T, the observed dispersion is qualitatively described by A&W calculations. Above 4T, the predicted field dependence is stronger than actually observed and the dispersion perpendicular to the chains is much flatter than expected. Even the out-of-plane mode, which is expected to behave like a standard spin-wave mode displays a significantly flattened dispersion at 14T. In the A&W theory, the band width of the excitations is not affected by the magnetic field. The field dependence of the antiferromagnetic Bragg peak intensity at (1/3 1/3 1) (fig.2) seems to be a key to understand this behaviour. Up to about 4T, the intensity increases as predicted by A&W. Note that a classical antiferromagnet would display a decreasing staggered magnetization, not an increase as is clearly the case for CsNiCl₃. However, the observed field dependence flattens w.r.t. the A&W calculation beyond 4T. Of course, the staggered magnetization must vanish at the saturation field (about 65T) and therefore may exhibit a maximum at some intermediate field strength. The increasing ferromagnetic component of the ordered moment is neglected in the A&W calculation and may be the reason for its failure at higher field strengths.

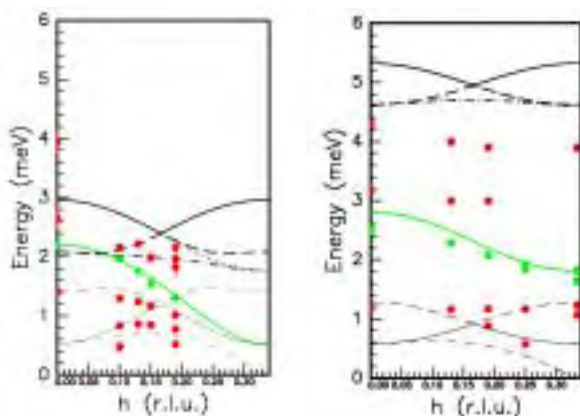


Fig. 1. (*hh1*)-Dispersion of the magnetic excitations at 4T (left) and 14T (right) at T=2K. Lines are A&W theory, the “classical” out-of-plane mode is indicated green.

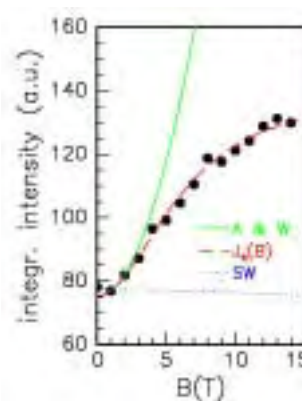


Fig. 2. Magnetic field dependence of the magnetic Bragg peak intensity at (1/3 1/3 1), integrated intensity of rocking scans vs. field at 2K, SW: spin wave theory, Js(B): guide for the eye.

¹ M. Enderle, Z. Tun, W. J. L. Buyers and M. Steiner Phys. Rev. **B59**, 4235 (1999).

² I. Affleck and G. Wellman, Phys.Rev. **B46**, 8934 (1992).

2.2.8. Specific heat capacity and magnetocaloric effect of Fe-doped CsNiCl₃

M. Enderle, *Condensed Matter Physics and Chemistry Department, Risø National Laboratory, Denmark/Institute Laue-Langevin, Grenoble, France*, J. Wolf, K. Kiefer, M. Rheinstädter, *Technische Physik, Universität des Saarlandes, Saarbrücken, Germany*
 e-mail: enderle@ill.fr

Fe²⁺ in CsFeCl₃ has a large single-ion anisotropy of easy-plane type. If CsNiCl₃ is doped with Fe²⁺, its weak Ising anisotropy is believed to be modified towards an easy-plane type anisotropy. Indeed the quasi-one-dimensional Heisenberg exchange along the hexagonal c-axis may lead to an average anisotropy at the Ni-site, which is effectively easy-plane like. A phase diagram characteristic for weak easy plane anisotropy with two ordered magnetic phases at high fields had been suggested by neutron diffraction on the 2% Fe-compound¹. Specific heat experiments had displayed only one anomaly at high magnetic fields². Our recent sensitive specific heat experiments clearly reveal two transitions above the spin-flop field of about 2.4T (Fig.1)³. These results show unambiguously that the phase diagram of the doped compound has the topology of the weak easy-plane case and hence that the anisotropy can be modelled from weak Ising to weak easy-plane type by doping with Fe²⁺.

With 10% Fe²⁺, we still observe the weak easy-plane type phase diagram as with 2% Fe (Figs.2 and 3). Compared to the strong easy-plane case (e.g. CsMnBr₃) a second high-field phase is observed, the umbrella phase. For a wide range of fields the umbrella phase and not the fan phase is the low-temperature phase. In this umbrella phase 2/3 of the spins are canted out of the easy plane in order to allow an orientation of all spins almost perpendicular to the magnetic field. For more details on the structures in the different phases see¹.

Apart from a higher value of the effective anisotropy in the 10% compound, we observe an immense broadening of the phase transition between fan and umbrella phase, while the paramagnetic-fan phase transition appears still rather “sharp”. We attribute this broadening to Fe-pairs along the c-axis, which act as a random field type defect in the umbrella phase but not in the fan phase².

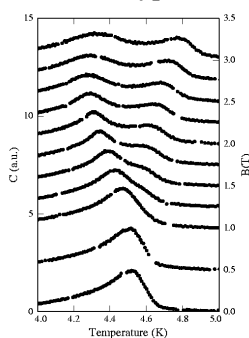


Fig. 1. CsNi_{0.98}Fe_{0.02}Cl₃: heat capacity with B perpendicular to c.

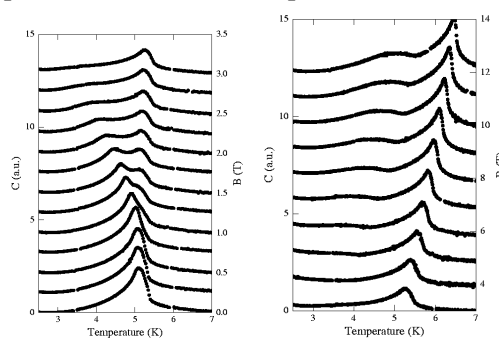


Fig. 2. CsNi_{0.9}Fe_{0.1}Cl₃: heat capacity with B perpendicular to c.

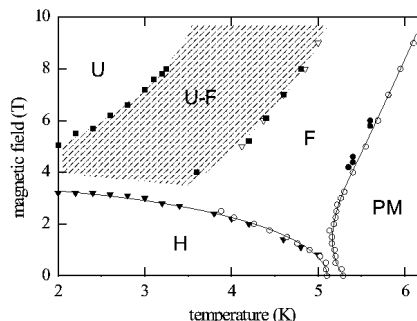


Fig. 3. Phase diagram of CsNi_{0.9}Fe_{0.1}Cl₃ as obtained by heat capacity (circles) and magnetocaloric effect (triangles). U: umbrella phase, F: fan phase, PM: paramagnetic phase, H: helix phase.

¹ M. Winkelmann, R. Schneider, M. Enderle, T. Asano, Y. Ajiro and M. Steiner, *J. Phys. Condens. Matter* **9**, 703 (1997).

² T. Asano, Y. Ajiro, M. Mekata, K. Kamishima, T. Goto, H. A. Katori and K. Katsumata, *J. Magn. Magn. Mater.* **177-181**, 640 (1998).

³ J. Wolf, K. Kiefer, M. C. Rheinstädter and M. Enderle, Tuning anisotropy by impurities; magnetocaloric experiments on CsNi_{0.9}Fe, to be published; K. Kiefer, J. Wolf and M. Enderle, Anisotropy-tuning by doping: Phase diagram of CsNi_{0.98}Fe_{0.02}Cl₃ measured by specific heat capacity and magnetocaloric effects, submitted to *J. Low. Temp. Phys.*

2.2.9. Magnetization of solid oxygen confined into nanoporous materials

M. Enderle, *Condensed Matter Physics and Chemistry Department, Risø National Laboratory, Denmark/Institute Laue-Langevin, Grenoble, France*, R. Ackermann, T. Knoblauch, D. Wallacher and K. Knorr, *Technische Physik, Universität des Saarlandes, Saarbrücken, Germany*
e-mail: enderle@ill.fr

Molecular oxygen carries spin 1 and interacts antiferromagnetically via direct exchange. Three solid phases are known, the cubic γ -phase with only partial order of the oxygen symmetry axes, the rhombohedral β -phase with complete orientational order and short-range antiferromagnetic order in the basal planes, and the monoclinic α -phase, which can be regarded as a distorted β -structure with collinear antiferromagnetic long-range order. Bulk oxygen displays a magnetization step at the $\gamma\beta$ - as well as the $\beta\alpha$ - transition. These are related to steps in the cell volume and the sensitive dependence of the antiferromagnetic direct exchange on the distance.

The confinement into pores with nanometer-sized diameters is known to suppress all structural phase transitions of solid nitrogen. We investigated oxygen by magnetization measurements¹. The static susceptibility (M/H) of completely filled pores is shown in figure 1 for substrates with different pore diameter. With a confinement to 6.7nm and 13.2nm pore diameters both phase transitions are still visible and only appear smeared out. At lowest temperatures, a paramagnetic contribution is observed which corresponds to a few percent uncorrelated oxygen molecules in corners or edges of the substrate. (The Curie-Weiß temperature of this contribution is below 3K and indicates almost free magnetic moments.) At 4.1nm and 3.3nm pore diameter the behaviour appears quite different. Apart from the Curie-component, which is explained by less than 5%, uncorrelated spins there is barely any change of the magnetization.

After subtraction of the Curie-component a broad maximum remains at pore sizes of 4.1nm and 3.3nm. The total change of the magnetization is only a fraction of the step at the $\gamma\beta$ -transition. A possible explanation is quasi-one dimensional behaviour – indeed a broad magnetization maximum is a typical feature of a one-dimensional antiferromagnet. X-ray data point to an extremely broadened $\gamma\beta$ - coexistence region – nevertheless, even a pure γ -phase should eventually order magnetically, unless it is quasi-one-dimensional.

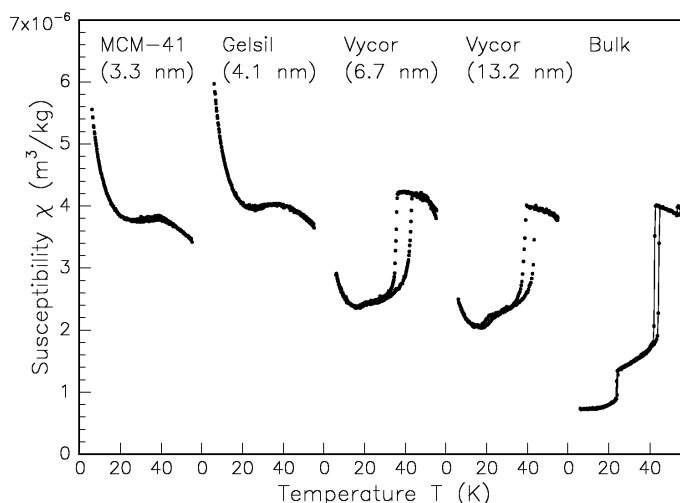


Fig. 1. Static susceptibility M/H of oxygen condensed into nanoporous substrates in comparison with bulk oxygen. The step-like anomalies of bulk oxygen indicate the magneto-structural phase transitions, which seem to be suppressed at the lowest pore sizes.

¹ R. Ackermann, T. Knoblauch, K. Knorr, D. Kumar, K. Unger and M. Enderle, Magnetic behaviour of O₂ confined in nanopores, submitted to J. Low Temp. Phys.

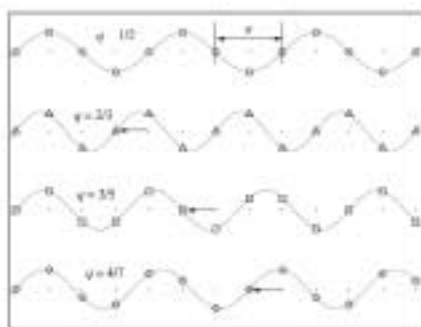
2.2.10. A model for the change of modulation vectors observed in the magnetic structure of CeSb

J. Wolny, A. Wnęk, *Faculty of Physics and Nuclear Techniques, University of Mining and Metallurgy, Krakow, Poland*, Hae Seop Shim, *Korean Atomic Energy Research Institute, Taejon, South Korea* and B. Lebech, *Condensed Matter Physics and Chemistry Department, Risø National Laboratory, Denmark*

e-mail: bente.lebech@risoe.dk

The model for the modulation vectors describing the magnetic structure in CeSb is based on the assumption that whenever the propagation vector of the modulation is parallel to the symmetry direction, the modulation must be commensurate with the basic crystal structure, and vice versa.. We assume two components of the modulation vector – one parallel to the symmetry direction (q_x) and one perpendicular (q_y) to it. Hence, $q_y = 0$ requires that q_x has a commensurate value. If the length of the modulation vector changes continuously, passing through consecutive commensurate and incommensurate values, the modulation vector $\mathbf{q} = (q_x, q_y, 0)$ must rotate with respect to the symmetry direction. Such behaviour is as it is indeed observed for the modulated magnetic structures in Nd and Nd-Pr alloys¹.

The light rare earth metals Nd and Pr crystallise in a double hexagonal close packed structure. It has been shown experimentally that the fundamental commensurate values can be expressed by the relations: $q_x = 1/n$ and $q_y = 0$, where n is an integer. One-dimensional commensurate-incommensurate phase transitions for the modulation vectors associated with magnetic order, for instance at the hexagonal sites, is given by deviations from the equation, i.e. for $q_y \neq 0$. The modulation vectors change with the temperature and their q_y component goes zero for all commensurate values of the modulation vector¹. For CeSb with the sodium chloride crystal structure no component of magnetic modulation vector perpendicular to the symmetry direction has been observed², i.e. a model for CeSb will be simpler and should allow all possible modulation vectors to be commensurate. Experiments tell that the lower and upper limits for the length of modulation vector are $1/2$ and $2/3$, respectively. There are infinitely many commensurate values in this region, which has led to the well-known devil's staircase type of modulated structure³, but only the magnetic satellite peaks are only significant for particular values of the length of the modulation vector and therefore these are most essential values to model. In the present model it is supposed that the magnetic commensurate structure is pinned on atomic layers. This is illustrated in the figure. Here the modulation is shown as atomic displacements, rather than magnetic modulation vectors, because only the repeat distance and the orientation of it are important in this model picture. For the centred tetragonal structures the natural distance between the layers of atoms in symmetry direction is half of the basic period for atomic structure for any integer multiple of the half wavelength. The jumps between different nodes of modulation vector are accompanied with the change of the corresponding wavelengths by $1/2$ r. l. u., and this leads to the following recursive



equation: $1/2 \cdot \lambda_m \cdot n = 1/2 \cdot \lambda_{m-1} \cdot n \pm 1/2$, where λ_{m-1} and λ_m are the former and the next wavelengths, and $n = 1, 2, 3, \dots$. The minus sign describes the sequence of decreasing of wavelengths observed in CeSb for heating and the plus sign corresponds to the increasing sequence of wavelengths observed for CeSb when cooling. Further details will be published in the Proceedings of "The 1st International Symposium of Advance Science Research", Japan Atomic Energy Research Institute, Tokai, Ibaraki, Japan, October 31-November2, 2000.

¹ B. Lebech, J. Wolny and R.M. Moon, *J. Phys.: Condens. Matter* **6**, 5201 (1994), J. Wolny and B. Lebech, *J. Magn. Magn. Mater.* **140-144**, 741 (1995).

² J. Rossat-Mignod, P. Burel, J. Villain, H. Bartholin, Wang Tcheng Si, D. Florence, O. Vogt, *Phys. Rev.* **B16**, 444 (1977), P. Fischer, B. Lebech, G. Meier, B.D. Rainford and O. Vogt, *J. Phys. C: Solid State Phys.* **11**, 345 (1978).

³ J. von Boehm and P. Bak, *Phys. Rev. Lett.* **42**, 122 (1979), J. Bohr and F. Grey, *Condens. Matter News* **1**, 12 (1992).

2.3. Superconducting materials and phenomena

2.3.1. Interaction between magnetism and superconductivity in $\text{TmNi}_2\text{B}_2\text{C}$ with $\mathbf{H} \parallel [110]$ studied using Small Angle Neutron Scattering

A. B. Abrahamsen, K. Mortensen, N. H. Andersen, *Condensed Matter Physics and Chemistry Department, Risø National Laboratory, Denmark*, D. Lopez, P. L. Gammel, *Bell Laboratories, USA*, P. C. Canfield, *Ames Laboratory and Iowa State University, USA*
 e-mail: asger.abrahamsen@risoe.dk

Small Angle Neutron Scattering (SANS) was used to study the reflectivity of the Flux Line Lattice (FLL) induced by an applied field along the crystalline [110] direction of $\text{TmNi}_2\text{B}_2\text{C}$. An increase of the scattered intensity is observed as a field induced magnetic phase is approached.

Recent neutron scattering experiments on $\text{TmNi}_2\text{B}_2\text{C}$ with the applied field along the a -axis have revealed the existence of a field induced magnetic phase with an ordering vector $\mathbf{Q}_A = [0.48, 0, 0]$ in contrast to the zero field magnetic phase having $\mathbf{Q}_F = [0.094, 0.094, 0]$ below $T_N = 1.5 \text{ K}$ ¹. The \mathbf{Q}_A phase exists above fields of 5 kOe and it has a Néel temperature increasing from 1.5 K to 2.0 K at 5 kOe and 12 kOe.

A slightly distorted hexagonal FLL was observed at fields between 0-15 kOe and temperatures ranging from 1.7-4 K, and no symmetry changes were seen as the \mathbf{Q}_A phase was entered. Figure 1 shows the logarithm to the FLL reflectivity, which should decrease linearly with the magnetic field B according to Ginzburg-Landau theory²

$$\ln|h(q)|^2 = \ln\left(\frac{\Phi_0^2}{(2\pi\lambda)^4}\right) - \frac{4\pi^2\xi^2}{\Phi_0} B \quad (1)$$

where $h(q)$ is the FLL form factor, Φ_0 the flux quantum, λ the penetration depth and ξ the coherence length. The linear field dependence is found at temperatures $T = 3 \text{ K}$ and 4 K well above the magnetic transition and the coherence length can be determined from the slope of the curve giving $\xi = 59 \text{ \AA}$ and 81 \AA respectively. At lower temperatures $\ln|h(q)|^2$ increases above 4 kOe indicating that the superconducting length scales λ and ξ are changing as the magnetic phase is approached. A similar increase of the scattered intensity upon approaching the \mathbf{Q}_F phase has been observed with the applied field along the c -axis².

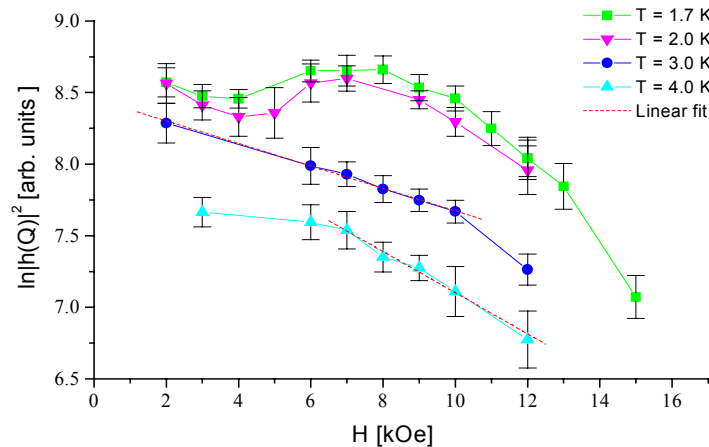


Fig. 1. Field dependence of the logarithm of the flux line lattice reflectivity of $\text{TmNi}_2\text{B}_2\text{C}$ in an applied field along the [110] direction. The deviation from a linear decrease as described by eq. (1) at low temperatures is caused by the onset of a field induced magnetic phase.

¹ K. Nørgaard, M. R. Eskildsen, N. H. Andersen, J. Jensen, P. Hedegaard, S. N. Clausen and P. C. Canfield, *Phys. Rev. Lett.* **84**, 4982 (2000).

² M. R. Eskildsen, Ph.d. thesis, Risø-R-1084(EN) (1998).

2.3.2. Form factor analysis of flux line lattice in the magnetic superconductor TmNi₂B₂C

A. B. Abrahamsen, M. R. Eskildsen, K. Mortensen, N. H. Andersen, *Condensed Matter Physics and Chemistry Department, Risø National Laboratory, Denmark*, P. L. Gammel, *Bell Laboratories, Lucent Technologies, New jersey 07974, USA*, P.C. Canfield, *Ames Laboratory and Iowa State University, Ames, Iowa 50011, USA*
e-mail: asger.abrahamsen@risoe.dk

The coexistence of superconductivity ($T_c = 11$ K) and antiferromagnetic ordering ($T_N = 1.5$ K) in TmNi₂B₂C leads to complicated phase diagrams of the magnetic ordering and flux line lattice (FLL) structures observed with neutron scattering¹. A quantitative determination of the superconducting coherence length, ξ , and penetration depth, λ , is often extracted from the field dependence of the intensity of the first order FLL reflections. However, the presence of magnetic phases and metamagnetic transitions affects the superconducting length scales complicating this method. In stead we analyse several FLL reflections at each temperature and field, to attempt a determination of λ and ξ .

Figure 1 shows a diffraction pattern of the square FLL in TmNi₂B₂C when the field is applied along the c -axis. The intensities of the diffraction spots are proportional with the square of the FLL form factor $h(q)$, which can be found from Ginzburg-Landau theory²:

$$h(q) = \frac{\Phi_0}{(2\pi)^2} \frac{q_{10}^2}{1 + \lambda^2 q^2} \text{Exp}(-\sqrt{2}\xi q) \quad (1)$$

where Φ_0 is the flux quantum, q is the scattering vector, q_{10} is the vector indexed (10) in Fig. 1. This describes how the intensity decreases with increasing scattering vectors, as seen on Fig.1. We have examined the ratio between reflections with index (n_x, n_y) and (10) measured by small angle neutron scattering¹. According to Eq. 1 this ratio should only depend on the coherence length since the denominator can be approximated, $1 + \lambda^2 q^2 \approx \lambda^2 q^2$, whereby the penetration depth dependence is removed. Fig. 2 shows the experimental values obtained in the magnetic phase, but the ratio between the (11) and the (10) reflection is much higher than predicted values of respectively 0.25, 0.031 and 0.04 from Eq. 1 (neglecting the exponential factor but including Lorentz factor corrections). Further investigations are needed to determine the origin for the discrepancy.

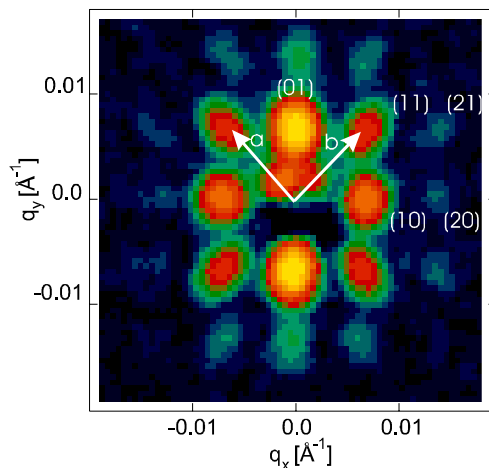


Fig. 1. Neutron diffraction pattern from the flux line lattice in TmNi₂B₂C at $H = 2$ kOe and $T = 1.5$ K. The basal plane orientation of the tetragonal crystalline unit cell is shown by arrows and the FLL reflection are indexed by (n_x, n_y) .

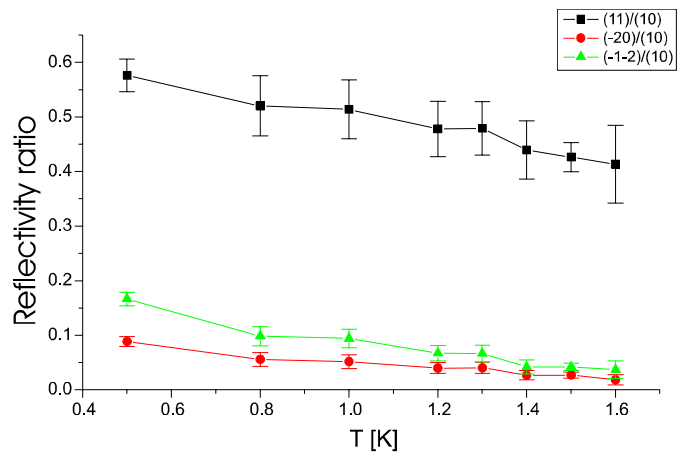


Fig. 2. Ratio between intensities of the flux line lattice diffraction spots shown in Fig. 1. This ratio should only depend on the coherence length, but the (11)/(10) ratio is much higher than predicted from Eq. 1 which gives 0.25(□), 0.04(Δ) and 0.031(●) when the Lorentz factor is included and the exponential factor is neglected.

¹ M. R. Eskildsen, K. Harada, P. L. Gammel, A. B. Abrahamsen, N. H. Andersen, G. Ernst, A. P. Ramirez, D. J. Bishop, K. Mortensen, D. G. Naugles, K. D. D. Rathnayaka and P. C. Canfield, *Nature* **393**, 242 (1998); K. Nørgaard, M. R. Eskildsen, N. H. Andersen, J. Jensen, P. Hedegård, S. N. Klausen and P. C. Canfield, *Phys. Rev. Lett.* **84**, 4982 (2000).

² A. Yaouanc, P. D. deReotier and E. H. Brandt, *Phys. Rev.* **B55**, 11107 (1997).

2.3.3. Temperature dependence of the flux line lattice transition into square symmetry in superconducting LuNi₂B₂C

M. R. Eskildsen, A. B. Abrahamsen, K. Mortensen, N. H. Andersen, *Condensed Matter Physics and Chemistry Dept., Risø National Laboratory, Denmark*, V. G. Kogan, P. C. Canfield, *Ames Laboratory and Dept. of Physics and Astronomy, Iowa State University, USA*, P. L. Gammel, *Bell Laboratories, Lucent Technologies, USA*

e-mail: morten.eskildsen@physics.unige.ch

We have investigated the temperature dependence of the flux line lattice (FLL) structural phase transition in the tetragonal superconductor LuNi₂B₂C ($T_c = 16.6$ K) into a square symmetry.

The FLL was studied using the small angle neutron scattering (SANS) spectrometer on the cold neutron beam line at the Risø National Laboratory DR3 research reactor. We used a 1 gram single crystal sample, grown from a high temperature flux using isotopically enriched ¹¹B to enhance the neutron transmission. Incident neutrons with wavelengths, λ_n , between 6 and 15.6 Å, and spread $\Delta\lambda_n/\lambda_n = 24\%$ were used. Magnetic fields in the range 1.5 to 10 kOe were applied parallel to the crystalline c -axis and to the incoming neutrons. To avoid a change in the experimental resolution as the applied field was varied, the neutron wavelength and the field was changed in concert to keep the scattering angle $2\theta = q \lambda_n/2\pi$ constant. Here $q = 2\pi \sqrt{H/\phi_0}$ with $\phi_0 = hc/2e$ is the FLL scattering vector. This approach allows a direct comparison of the results obtained at different fields. The measurements were performed at temperatures between 2 and 20 K, following a constant field cooling procedure. A background signal obtained above T_c was subtracted from the data.

The onset of the square to hexagonal symmetry transition is signalled by an azimuthal broadening of the FLL (1,0)-reflections¹, which later evolves into an azimuthal split. In general, the azimuthal splitting was only directly observable when it was above $\sim 10^\circ$, comparable to experimental resolution which was slightly less than 14° . To determine the transition onset field, H_2 , we analyzed the azimuthal intensity distribution in each diffraction pattern, fitting the azimuthal intensity distribution to a Gaussian to extract the width.

In the (H, T) -phase diagram in the figure we show equi-width contours, which directly gives a picture of $H_2(T)$. Here we have used the 14.2° contour line which is just above the experimental resolution, as the threshold for the transition onset. At temperatures below 10 K the onset field of the transition is only weakly temperature dependent. Above 10 K $H_2(T)$ rises sharply, bending away from the upper critical field. This suggests that in fields just below H_{c2} , the flux line lattice is hexagonal.

The square FLL is stabilised by non-local flux line interactions, which in general gets stronger as the flux line spacing decreases, i.e. with increasing applied field. The fact that the FLL seems to be (distorted) hexagonal just below H_{c2} , indicates the presence of an additional isotropic flux line repulsion in this region.

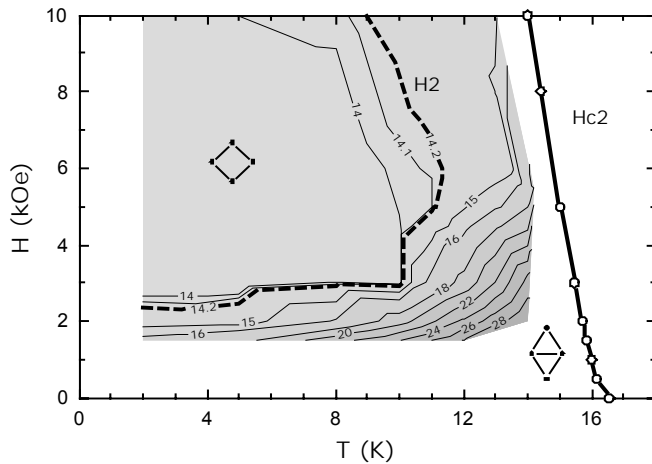


Fig. 1. (H, T) -phase diagram showing $H_2(T)$, defined by the 14.2° contour as described in the text. The shaded area indicates the portion of the phase diagram where measurements were performed. At high fields and low temperatures the FLL is square symmetric. As the temperature is raised or the field lower the FLL gradually transforms into a hexagonal symmetry. The onset of the square to hexagonal symmetry transition, $H_2(T)$, is indicated by the dashed line.

¹ P. L. Gammel, D. J. Bishop, M. R. Eskildsen, K. Mortensen, N. H. Andersen, I. R. Fisher, K. O. Cheon, P. C. Canfield and V. G. Kogan, *Phys. Rev. Lett.* **82**, 4082 (1999).

2.3.4. Phase diagram of TmNi₂B₂C in an in-plane magnetic field

K. Nørgaard, M. R. Eskildsen, N. H. Andersen, A. Abrahamsen, *Condensed Matter Physics and Chemistry Department, Risø National Laboratory, Denmark* and P. C. Canfield, *Ames National Laboratory & Iowa State University, USA*
 e-mail: katrine.noergaard@risoe.dk

This experiment was performed in order to establish the high field part of the magnetic phase diagram of TmNi₂B₂C, when applying the field in the a-direction. As a result of these experiments, the experimental phase diagram is shown in Fig. 1, showing the \mathbf{Q}_F and \mathbf{Q}_A phases, and the superconducting upper critical field¹. The magnetic ordering vectors are: $\mathbf{Q}_F = (0.094, 0.094, 0)$ and $\mathbf{Q}_A = (0.482, 0, 0)$. The \mathbf{Q}_F phase is a unique long wavelength phase, which exists at zero field, and extends up to fields of 14 kOe. The \mathbf{Q}_A phase is an almost perfect antiferromagnetic phase. We believe that the origin of these magnetic states lies in two effects: A suppression of the ferromagnetic component of the RKKY exchange interaction in the SC phase, and a reduction of the SC condensation energy due to the periodic modulation of the moments at \mathbf{Q}_A . The purpose of this experiment was to examine whether SC influences the properties of the \mathbf{Q}_A phase.

A single crystal of TmNi₂B₂C was mounted with a magnetic field in the a-direction, and (100) and (010) in the scattering plane. Measurements were performed up to 6 T and between 100 mK and 15 K. The intensity of the \mathbf{Q}_A phase at 24 kOe vs temperature is shown in Fig 2. When increasing the temperature, a normal phase changes into a SC phase at ~ 1.5 K and at ~ 5 K we re-enter the normal phase. No signs of change in the magnetic intensity were observed at the SC transitions, at 22, 24 and 26 kOe.

Fig. 3 and 4 shows [h00]-scans through the \mathbf{Q}_A peak at different fields and temperatures. Increasing the field causes the growth of a peak at $\mathbf{Q}_L = (0.495, 0, 0)$. The accuracy of the alignment of the spectrometer is ~ 0.001 - 0.002 rlu, so we must conclude that it is an incommensurate structure. Contrary to the \mathbf{Q}_A phase, the \mathbf{Q}_L phase shows strong hysteresis in both field and temperature. The origin of the phase is still unknown. Two unique properties characterise the \mathbf{Q}_L and \mathbf{Q}_A phases. First of all they persist to a field of 60 kOe applied perpendicular to the magnetic moments in an Ising-like system. The Zeeman energy of the magnetic moments in a 60 kOe field would amount to 16 Kelvin, which questions whether or not the \mathbf{Q}_A or \mathbf{Q}_L phases are indeed magnetic phases. Second of all the phases stabilise in increasing field, instead of suppressing them as would be expected.

A first hand conclusion, is that it may be that the \mathbf{Q}_A phase is supported by a Tm quadrupol ordering resulting in a lattice distortion at \mathbf{Q}_A , and that the low intensity tail has its origin in a magnetic moment arising on the Ni-site, giving rise to scattering at the maximum of the susceptibility which is at \mathbf{Q}_A .

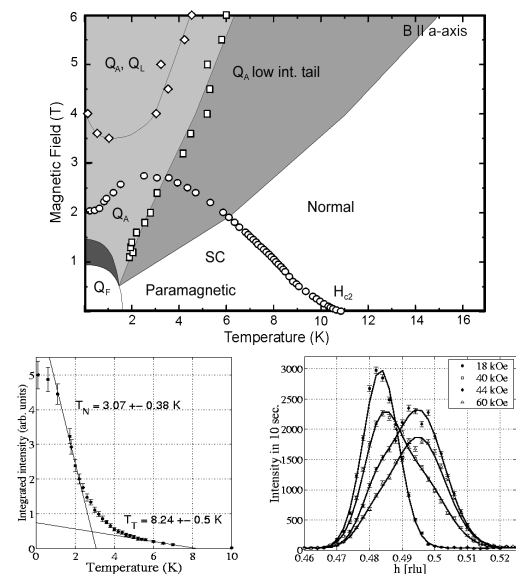


Fig. 1. Magnetic field versus temperature phase diagram of TmNi₂B₂C. Experimental phase diagram. The dark grey area is coexistence of \mathbf{Q}_F and \mathbf{Q}_A , the light grey area is the \mathbf{Q}_A and/or \mathbf{Q}_L phases, and the medium grey area is the low intensity part of the \mathbf{Q}_A phase. Squares indicate T_N , and circles are the superconducting upper critical field from Naugle *et al.* The linear fit to the steep part of Fig. 2 gives $T_N(B)$, and T_T is determined from a linear fit to the last three data points.

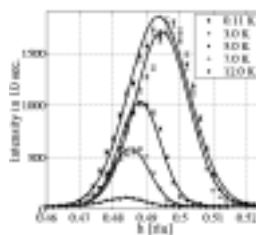


Fig. 2. Left: Int. intensity of the \mathbf{Q}_A peak at 2.4 tesla.

Center and right: [h00] scans of the \mathbf{Q}_A peak. At 0.1 K, increasing field from 18 kOe to 60 kOe. At 60 kOe, increasing temperatures from 0.1 to 12 K.

¹ D. G. Naugles, K. D. D. Rathnayaka, K. Clark and P. C. Canfield, *Int. J. Mod. Phys.* **13**, 3715 (1997).

2.3.5. Heat capacity of TmNi₂B₂C in a magnetic field applied in the a- and c-axis direction

K. Nørgaard, M. R. Eskildsen, N. H. Andersen, A. Abrahamsen, *Condensed Matter Physics and Chemistry Department, Risø National Laboratory, Denmark*, M. Meissner, *BENSC, Hahn-Meitner-Institut, Germany* and P. C. Canfield, *Ames National Laboratory & Iowa State University, USA*
 e-mail: katrine.noergaard@risoe.dk

TmNi₂B₂C is a superconductor, with $T_c = 11$ K. Tm³⁺ is magnetically ordered, with a long wavelength antiferromagnetic spin density wave, $\mathbf{Q}_F = (0.094, 0.094, 0)$ below $T_N = 1.5$ K. This long wavelength structure is unique among the borocarbides. Generally the magnetic moments in TmNi₂B₂C are Ising-like the easy axis along the *c*-direction.

When a magnetic field is applied perpendicular to the magnetic moments, superconductivity should be suppressed, whereas the magnetic structure should remain essentially unaffected up to a critical field where the moments collapse. Neutron diffraction studies have shown that a magnetic field of approximately 1 T develops a new magnetic structure with an ordering vector of $\mathbf{Q}_A = (0.482, 0, 0)$ ¹. The scattering intensity of \mathbf{Q}_A versus temperature has a peculiar behaviour. It saturates at low temperatures, decreases linearly for a while, rounds off at approx. 2.5 K and maintains a low intensity until 8-12 K. This low intensity tail is not yet understood. When a magnetic field is applied along the *c*-direction, the zero field structure coexists along with a slightly different magnetic structure, which appears at 0.2 T. The ordering vector of this structure is $\mathbf{Q}_{F2} = (0.12, 0, 0)$. At 1 T the magnetic structures cease to exist because all the magnetic moments line up in the magnetic field direction.

In a recent model study¹ it was suggested that the origin of these magnetic states lies in two effects: A suppression of the ferromagnetic component of the RKKY exchange interaction in the superconducting phase, and a reduction of the superconducting condensation energy due to the periodic modulation of the electronic structure with wave vector \mathbf{Q}_A . The model accounts well for the experimental phase diagram for the field in the *c*-direction. For the *a*-direction it fits at low fields, but at high fields there is no understanding of the experiments.

The heat capacity measurements were performed in order to study the thermodynamics of the phase transitions arising in a magnetic field, hoping to supplement the information obtained by neutron scattering¹. The heat capacity measurements have been performed at BENSC, HMI Berlin with a relaxation type calorimeter using the constant heat flow technique. The TmNi₂B₂C-crystal (dimensions = 0.45 x 0.90 x 0.55 mm³) was mounted onto the sapphire calorimeter chip and orientated with respect to the magnetic field direction using a small amount (~100 μg) of thermal contact grease.

Magnetic field in the *a*-axis direction:

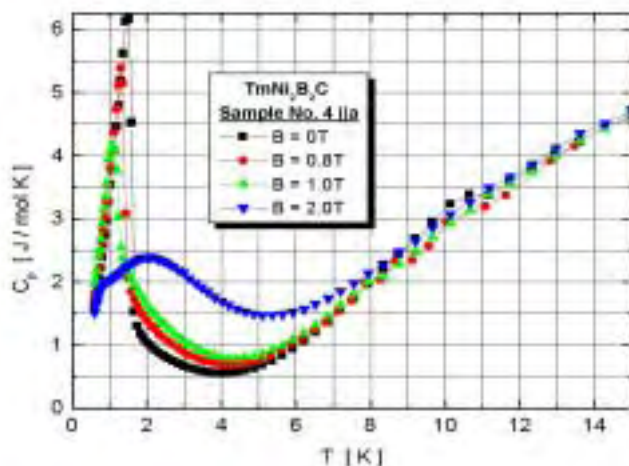


Fig. 1. Heat capacity of TmNi₂B₂C with an applied magnetic field along the *a*-direction.

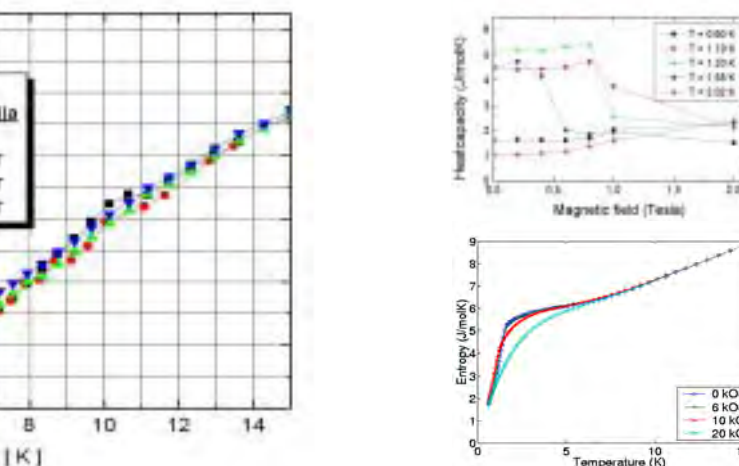


Fig. 2. Upper right: Field dependence of the heat capacity. Temperatures are determined with an accuracy of 10 mK.

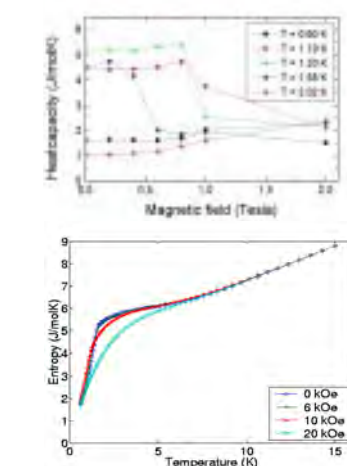


Fig. 3. Lower right: The entropy of TmNi₂B₂C, calculated using the data in Fig. 1.

¹ K. Nørgaard, M. R. Eskildsen, N. H. Andersen, J. Jensen, P. Hedegaard, S. N. Clausen and P. C. Canfield, *Phys. Rev. Lett.* **84**, 4982 (2000), and this Annual Report.

Figure 1 shows the heat capacity of $\text{TmNi}_2\text{B}_2\text{C}$ with the field in the a -direction. Notice the antiferromagnetic Néel transition at 1.5 K in zero field. The superconducting transition at 11 K in zero field is only a small bump on the graph, and it moves down in temperature as the field is increased.

The field dependence of the heat capacity in Fig. 2, confirms an interesting feature of the phase diagram determined by neutron scattering, namely that the phase transition from Q_F to Q_A moves to lower fields as the temperature increases towards 1.6 K.

In Fig. 3, the entropy is plotted. The integration from 0 to 0.6 K is determined by setting the value of the entropy at 15 K equal to the zero field value. Extrapolating the specific heat data to zero temperature gives the same result within the estimated uncertainty

Magnetic field in the c -direction:

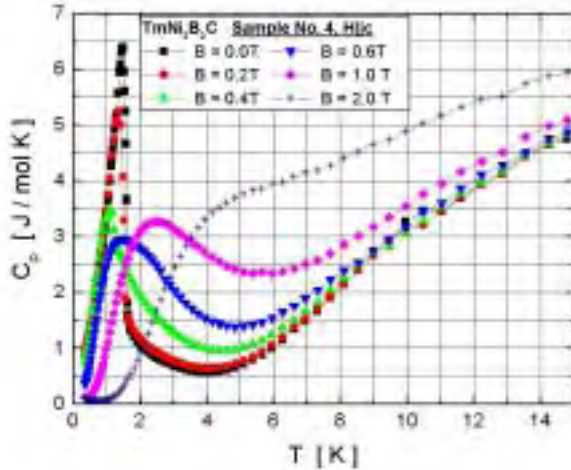


Fig. 4. Left: Heat capacity of $\text{TmNi}_2\text{B}_2\text{C}$ with an applied magnetic field along the c -direction.

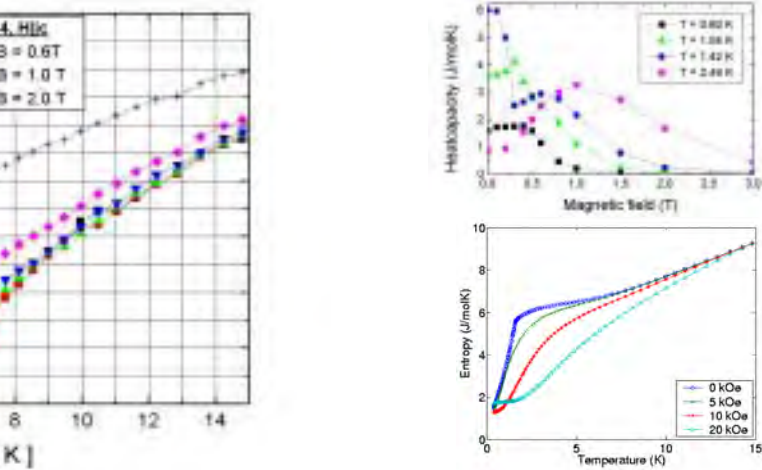


Fig. 5. Upper right: Field dependence of the heat capacity. Temperatures are determined with an accuracy of 10 mK.

Fig. 6. Lower right: The entropy of $\text{TmNi}_2\text{B}_2\text{C}$, calculated using the data in Fig. 4.

The heat capacity, field dependence and entropy (figures 4, 5, and 6) for the c -axis direction are comparable to the data for the a -axis direction, and the field induced changes are similar: The magnetic transition at T_N moves to lower temperatures where after a broad maximum occurs as a result of the field-induced Schottky contribution.

An important question, which has not yet been answered, is whether the observed transitions are magnetic, and result exclusively from the Tm^{3+} ions. Since the crystal field ground state of the Tm^{3+} ion is a doublet the entropy should approach a value close to $R\ln 2 = 5.76 \text{ J/molK}$ for small magnetic fields, and when the higher lying levels are insignificantly populated. Figs. 3 and 6 show that this is indeed the case for temperatures approaching 5 K. Thus, at low fields the phase transitions appear to be governed by the Tm^{3+} ions. Above 5 K an increase due to the higher lying levels are expected.

Movshovich *et al.*¹ have measured zero field specific heat data, that are consistent with our results, and estimated the electronic (of the order 0.035 J/molK) and phonon (Debye temperature $\sim 320 \text{ K}$) contributions. Despite that the Debye temperature is determined with rather large uncertainty it is concluded that the electron and phonon contributions are relatively small up to 15 K.

However, although the low field specific heat data are consistent with the magnetic properties expected for the Tm^{3+} ions, it remains to be analysed if the same holds true for the high field data. Model calculations aiming to elucidate this are in progress². Alternatively we speculate if the Q_A phase may be supported by a Tm quadrupol ordering resulting in a lattice distortion at Q_A , and/or that a magnetic moment on the Ni-site may interacts antiferromagnetically with the Tm moments and stabilise the Q_F structure.

¹ R. Movshovich, M. F. Hundley, J. D. Thompson, P. C. Canfield, B. K. Cho and A. V. Chubnikov, *Physica C* **227**, 381 (1994).

² J. Jensen, private communication.

2.3.6. The magnetic structures in the SC state of $\text{ErNi}_2\text{B}_2\text{C}$ in an in-plane magnetic field

K. Nørgaard, M. R. Eskildsen, N. H. Andersen, *Condensed Matter Physics and Chemistry Department, Risø National Laboratory, Denmark*, and P. C. Canfield, *Ames National Laboratory & Iowa State University, USA*

e-mail: katrine.noergaard@risoe.dk

$\text{ErNi}_2\text{B}_2\text{C}$ is a magnetic superconductor, with $T_c = 11$ K and $T_N = 6$ K. Magnetic ordering and superconductivity are generally mutually exclusive, as they represent two different ground states of correlated electron systems. There exists however a small group of materials where these two phenomena coexist, as they do in the rare-earth nickel borocarbides. This offers a unique possibility to test our understanding of both of these phenomena and in particular of the interplay between them. In many of these compounds the magnetic structure is stabilised by a peak in the susceptibility produced by Fermi surface nesting¹. This should lead to a so-called superzone gap formation, reducing the DOS at the Fermi level and thus suppressing T_c . On the other hand, only small changes in the magnetic structure away from the nesting vector can then lead to changes in the superconducting transition temperature.

In $\text{ErNi}_2\text{B}_2\text{C}$ superconductivity ($T_c = 11$ K) coexists with magnetic ordering ($T_N = 6$ K), a magnetic ordering determined by the propagation vector $\mathbf{Q}_A = (0.553, 0, 0)$. In Fig. 1 is shown the (H, T) phase diagrams for fields in [001], [110], and [100] determined by Bud'ko et al.². Notice the decrease in H_{c2} just below T_N , which is caused by the \mathbf{Q}_A phase. Bud'ko et al. ascribes the sharp jump in H_{c2} at T_N for the field in [001] to the competition between superconductivity and the \mathbf{Q}_A phase, and suggests that the flat H_{c2} curves at T_N for fields along [110] and [100] may be due to magnetic phases with ordering vectors different from \mathbf{Q}_A .

This experiment indicates that the magnetic \mathbf{Q}_A structure remains up to fields of 1.75 T, contradicting the interpretation of the Bud'ko results presented above. However, looking at the relative intensities of the higher order peaks of \mathbf{Q}_A in a magnetic field in the [100] direction at 4 Kelvin shown in figure 2, one notice several jumps in second order intensity compared to first order intensity at 7–9 and 11–12 kOe. The first jump coincides with the magnetisation measurements by Budko et al., and with a shift in the magnetisation vector from 0.553 to 0.580. The second jump appears at H_{c2} . Unfortunately, the data are insufficient for determining the properties of the magnetic phase. Usually only odd order magnetic peaks exist, but in this case the magnetic field is applied parallel to the magnetic moments, thereby inducing a “ferrimagnetic” structure with a period of $2\mathbf{Q}_A$.

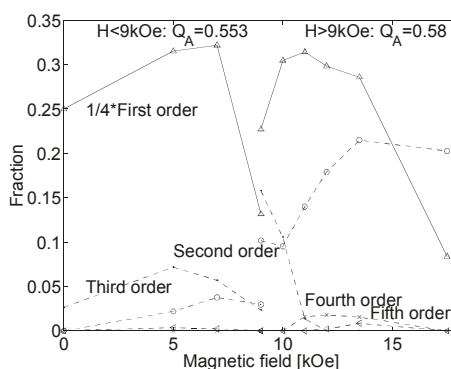
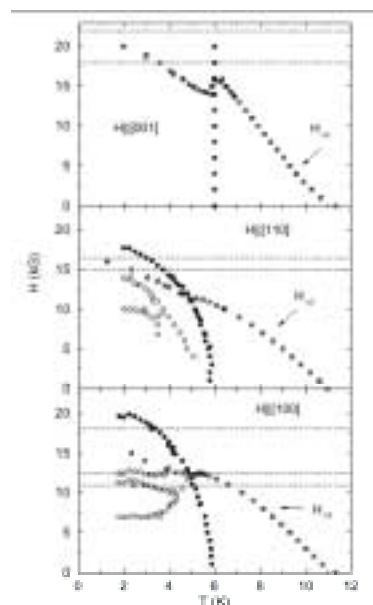


Fig. 2. Relative intensities of the higher order peaks in $\text{ErNi}_2\text{B}_2\text{C}$ compared to first order intensities, at $T = 4$ K. Notice the jump in second and third order intensity at 9 kOe, and the rise in second order intensity at 11–13 kOe, coexisting with a sudden drop in third order intensity.

Fig. 1. Left: (H, T) phase diagrams for $\text{ErNi}_2\text{B}_2\text{C}$. Symbols: Stars: H_{c2} , closed circles: T_N , open circles: phase lines separating different types of local magnetic order.

¹ S. B. Dugdale, M. A. Alam, I. Wilkinson, R. J. Hughes, I. R. Fischer, P. C. Canfield, T. Jarlborg and G. Santi., *Phys. Rev. Lett.* **83**, 4824 (1999).

² S. L. Bud'ko and P. C. Canfield., *Phys. Rev.* **B61**, R14932 (2000).

2.3.7. Coupled magnetic excitations in single crystal PrBa₂Cu₃O_{6.2}

S. J. S. Lister, A. T. Boothroyd, *Department of Physics, Clarendon Laboratory, Oxford University, UK*, N. H. Andersen, B. H. Larsen, *Risoe National Laboratory, Denmark* A. A. Zhokhov, *Russian Academy of Sciences, Institute of Solid State Physics, Russia* A. R. Wildes, *Institut Laue-Langevin, Grenoble, France*
 email: s.lister1@physics.ox.ac.uk

It is now generally believed that the anomalous properties of non-superconducting PrBa₂Cu₃O_{6+x} (PrBCO) are caused by a hybridisation of the Pr 4*f* and O 2*p* orbitals. Given the likelihood that the electronic and magnetic properties both depend on this hybridisation, including the occurrence or otherwise of superconductivity in PrBCO, detailed information on the strengths and symmetries of the magnetic interactions is desirable. We have previously reported inelastic neutron scattering measurements on a single crystal of PrBa₂Cu₃O_{6.2} performed with the RITA spectrometer^{1,2}. Using this data and a spin wave model of the coupled Cu-Pr system we have independently determined the strength of the Pr-Pr, Cu-Pr and Cu-Cu interactions.

Two peaks are observed at low energies consistent with previous data from polycrystalline samples³. We interpret these in terms of the low-lying energy levels of Pr³⁺ in a tetragonal crystal field. The lowest energy peak exhibits a significant dispersion as shown in Fig. 1. We identify this peak with a transition within the ground state doublet of Pr³⁺ whose degeneracy is lifted by the magnetic ordering. The Pr-Pr exchange interaction produces a dispersion of this excitation, which is indicated by the dotted line in Fig. 1. The discrepancies near the magnetic zone centres suggest that the effect of the Cu spin waves needs to be included. Guided by studies of the non-collinear magnetic structure of PBCO⁴, we introduce a pseudo-dipolar Cu-Pr interaction. This gives a much better fit to the dispersion (solid line in Fig. 1) by varying both the Pr-Pr exchange interaction and the dominant component of the Cu-Pr coupling tensor. In addition, the Cu-Pr coupling also produces a gap in the lowest energy Cu spin wave branch that has also been measured. The strength of the Cu-Pr coupling obtained from the fit is consistent with observed magnetic structure. The Pr-Pr interaction is also found to be surprisingly strong, and both interactions make similar sized contributions to the molecular field at the Pr site.

Measurements of the optic Cu spin-wave mode are shown in Fig. 2. The gap at the magnetic zone centre of 53 meV implies a Cu-Cu inter-plane coupling about half that in YBCO, assuming that the in-plane exchange is the same (this seems to be confirmed by preliminary measurements using the MAPS spectrometer at ISIS).

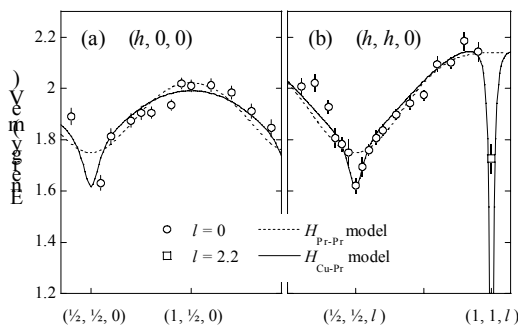


Fig. 1. Measured (open symbols) and calculated (lines) dispersion of lowest energy Pr excitation. Magnetic zone centres at $(\frac{1}{2}, \frac{1}{2}, 0)$ and $(1, 1, 0)$.

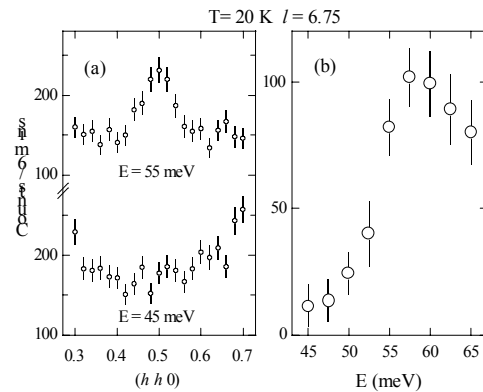


Fig. 2. (a) Optic Cu spin wave measured with constant energy scans through $(0.5, 0.5, 6.75)$. (b) Amplitude of peak as a function of energy.

¹ S. J. S. Lister, A. T. Boothroyd, B. H. Larsen, N. H. Andersen, A. A. Zhokov, A. N. Christensen and A. Wildes, *Risø-R-1156(EN)*, 34 (2000).

² S. J. S. Lister, A. T. Boothroyd, N. H. Andersen, A. A. Zhokhov, A. N. Christensen and T. Wolf, *Physica C* **317-318**, 572 (1999).

³ H.-D. Jostarndt, U. Walter, J. Harnischmacher, A. Severing and E. Holland-Moritz, *Phys. Rev. B* **46**, 14872 (1992).

⁴ A. T. Boothroyd, N. H. Andersen, E. Brecht and Th. Wolf *Phys. Rev. Lett.* **78**, 130 (1997).

2.3.8. Phonons in single crystal PrBa₂Cu₃O_{6.2}

B. H. Larsen, *Condensed Matter Physics and Chemistry Department, Risø National Laboratory, Denmark*, A. T. Boothroyd, S. J. S. Lister *Department of physics, Clarendon Laboratory, Oxford University, United Kingdom*, N. H. Andersen, *Condensed Matter Physics and Chemistry Department, Risø National Laboratory, Denmark*, A. R. Wildes, *Institut Laue-Langevin, Grenoble, France*, A. A. Zhokhov, *Russian Academy of Sciences, Institute of Solid State Physics, Chernogolovka, Russia*, A. N. Christensen, *Department of Chemistry, University of Aarhus, Denmark*
 e-mail: britt.h.larsen@risoe.dk

One of the outstanding problems of layered cuprate superconductors is to explain the absence of superconductivity in PrBa₂Cu₃O_{6.2}. YBa₂Cu₃O_{6+x} and RBa₂Cu₃O_{6+x} (where R are the lanthanoids) are isostructural and are all superconducting with T_c around 90K (for $x \approx 1$) except PrBa₂Cu₃O_{6+x}. Both YBa₂Cu₃O_{6+x} and PrBa₂Cu₃O_{6+x} change from tetragonal to orthorhombic with increased oxygen content and both form CuO linear chains in the basal plane for large doping, x .

An influential model¹ explains the absence of superconductivity in PrBa₂Cu₃O_{6+x} by a localization of the holes in hybridized Pr-O bonds. This would suggest a significantly different electronic configuration around the Pr atom and a change of the phonon frequencies associated with the Pr-O bond.

Measurements are performed on a large single crystal of PrBa₂Cu₃O_{6.2} with a volume of about 1cm³. The crystal is underdoped with $x=0.2$, and is of high purity with only marginal Ba on the Pr site. The phonons are measured by inelastic neutron scattering at IN22 at ILL in Grenoble. Scans are performed in Brillouin zones with high Q to minimize the intensity of magnetic excitations.

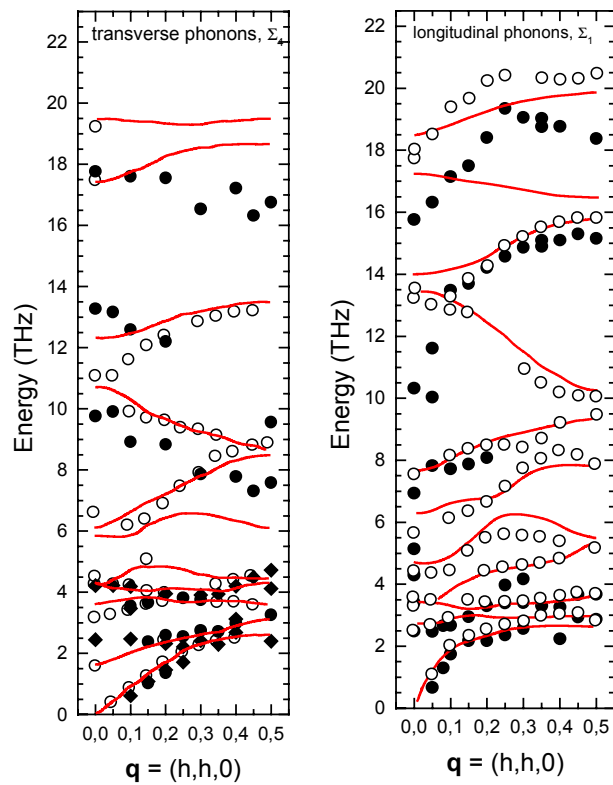


Fig. 1. Measurements of the phonons in YBa₂Cu₃O_{6.2} are shown as open points². The lines indicates numerical simulations of the YBa₂Cu₃O_{6.2} phonons³. The filled points are measurement of phonons in PrBa₂Cu₃O_{6.2}.

The phonon branches measured along $(h,h,0)$ direction are shown in Fig 1. The open point and solid lines are data and numerical calculations of phonons in YBa₂Cu₃O_{6.2} respectively. The filled points are the measured phonons on PrBa₂Cu₃O_{6.2}. Depending on whether the q vector of the excitation is along or perpendicular to the Bragg point Q of the Brillouin zone in which the phonon is measured the phonon is labelled either longitudinal or transverse.

From Fig. 1 it is seen, that at low energies the phonons in PrBa₂Cu₃O_{6.2} coincides with the phonons of YBa₂Cu₃O_{6.2}. At energies above 6 THz there is an overlap of some of the branches whereas other phonon branches seem displaced by several THz.

A tentative explanation is that the low frequency phonons reflect the collective displacement modes in the unit cell. A difference in weight of Pr and a difference in the bonds to Pr will not influence the displacement modes significantly. The high energy modes reflect more local bonds. The fact that some of these are identical to YBa₂Cu₃O_{6+x} and some are significantly different agrees with the hypothesis. A detailed identification of the different phonon modes using numerical simulations is in progress.

¹ R. Fehrenbacher and T. M. Rice, Phys. Rev. Lett. **70**, 3471 (1993).

² L. Pintschovius and W. Reichardt, Chapter 6 in Neutron scattering in Layered Copper-Oxide Superconductors, eds. A. Furrer, Kluwer Academic Publishers, (1998).

³ S. L. Chaplot, W. Reichardt, L. Pintschovius and N. Pyka, Phys. Rev. Lett. **B52**, 7230 (1995).

2.3.9. Topological analysis of YBa₂Cu₃O_{6.98}: I. Critical points

T. Lippmann, *GKSS, Geesthacht, Germany*, N. H. Andersen, *Condensed Matter Physics and Chemistry Department, Risø National Laboratory, Denmark*, Th. Wolf, *Forswchungszentrum Karlsruhe, ITP, Germany*, J. R. Schneider, *DESY/HASYLAB, Hamburg, Germany*
e-mail: niels.hessel@risoe.dk

Investigations of chemical bonding via the analysis of the charge density distribution of a crystal structure is an important part for the understanding of the physical and chemical properties of condensed matter. Reliable results of high- T_c superconductor structures were missing up to now because of poor crystal quality (poly-domains, twinning) and data quality (large systematic errors due to high absorption and extinction). Recently, we have shown that high-energy synchrotron radiation is an excellent tool to measure high quality data on small samples of irregular shape, which contain both light and heavy elements^{1,2,3}. Reasons are negligible absorption, small extinction and good beam conditions (stability) at the high-energy beamline BW5. Together with the availability of mono-domain single crystals, the investigation of bonding in high- T_c superconductor structures via charge density analyses becomes possible now.

The data have been measured at beamline BW5 (E = 100 kV) and the data refinement results and density maps have already been presented³. Both refinements of the data and topological analyses of the charge density distribution have been carried out using VALRAY⁴. So-called 'critical points' are local maxima, minima and saddle points of a charge density distribution. They are obtained by analysing the gradient vector field of the density and are characterised via their second derivatives. Most interesting for a characterisation of the bonds are the saddle points, where the charge density

Table 1. Locations and properties of the bond critical points. x, y, z : fractional co-ordinates, ρ : charge density [$\text{e}\text{\AA}^{-3}$], $\nabla^2\rho$: Laplacian [$\text{e}\text{\AA}^{-5}$], α : bond angle at the critical point.

| Atoms | x | y | z | ρ | $\nabla^2\rho$ | α |
|---------------------|------------|------------|-----------|-----------|----------------|----------|
| Cu(1), O(1) | 0.0 | 0.2477(9) | 0.0 | 0.499(11) | 11.34(19) | 180° |
| Cu(1), O(4) | 0.0 | 0.0 | 0.0754(4) | 0.633(24) | 16.77(57) | 180° |
| Cu(2), O(2) | 0.2433(5) | 0.0 | 0.3683(6) | 0.582(8) | 11.57(9) | 177.4° |
| Cu(2), O(3) | 0.0 | 0.2415(5) | 0.3677(5) | 0.551(7) | 10.51(7) | 177.9° |
| Cu(2), O(4) | 0.0 | 0.0 | 0.2579(6) | 0.279(9) | 2.99(9) | 180° |
| Y, O(2) | 0.5 | 0.2444(10) | 0.4370(6) | 0.321(3) | 4.62(3) | 176.8° |
| Y, O(3) | 0.2407(11) | 0.5 | 0.4368(5) | 0.342(2) | 4.86(2) | 180° |
| Ba, O(1) | 0.2164(33) | 0.5 | 0.0855(1) | 0.187(1) | 1.95(2) | 176.3° |
| Ba, O(2) | 0.5 | 0.2368(19) | 0.2889(5) | 0.162(1) | 1.69(1) | 178.5° |
| Ba, O(3) | 0.2391(7) | 0.5 | 0.2889(5) | 0.167(1) | 0.167(1) | 177.9° |
| Ba, O(4) | 0.2158(7) | 0.2428(8) | 0.1703(4) | 0.248(2) | 2.41(1) | 173.8° |
| O(2), O(2) | 0.5 | 0.0 | 0.5 | 0.180(3) | 1.26(3) | 180° |
| O(3), O(3) | 0.0 | 0.5 | 0.5 | 0.185(1) | 1.16(1) | 180° |
| Cu(1), Cu(1) | 0.5 | 0.0 | 0.0 | 0.065(1) | 0.22(1) | 180° |

¹ T. Lippmann and J. R. Schneider, *J. Appl. Cryst.* **33**, 156 (2000).

² T. Lippmann, and J. R. Schneider, *Acta Cryst.* **A56**, 575 (2000).

³ T. Lippmann, N. H. Andersen, Th. Wolf, J.R. Schneider, *HASYLAB Annual Report 1999*, 497.

⁴ R. F. Stewart, M. A. Spackman and C. Flensburg: *VALRAY Users Manual*, Carnegie Mellon, University, Pittsburgh, USA, and University of Copenhagen, Denmark (2000).

has a minimum in one dimension and maxima in the two remaining dimensions. Conclusively, these points are always found between two bonded atoms, and the bonds can therefore be quantitatively characterised by the density ρ and the Laplacian $\nabla^2\rho$ at the critical points. The latter is always strongly positive for ionic bonding and negative in the case of covalency¹.

In the unit cell, 100 critical points have been found: 45 bond points (b), 37 ring points (r), where the density has a maximum in one dimension and minima in the second and third, and 5 local minima, i.e. cage points (c). No non-nuclear maximum was found. Adding the 13 nuclear maxima (n), the set of points obeys well the Morse equation

$$n - b + r - c = 0$$

Table 1 shows the locations and properties of the unique bond saddle points in the $\text{YBa}_2\text{Cu}_3\text{O}_{6.98}$ structure, which have been derived from the set of 45 bond points after elimination of symmetry-equivalents.

According to these results there are no covalent parts of bonding in the structure, i.e. the bonding is completely ionic. The strongest bonds are obviously those between Cu(1) and O(1) and O(4) on the one hand and Cu(2) and O(2) and O(3) on the other hand. Compared to these, the Cu(2)-O(4) bond differs considerably both in the density at the critical point and the Laplacian. These results agree well with the bond lengths, which are about 2.3 Å for Cu(2)-O(4) and ≈ 1.9 Å for the other Cu-O bonds, respectively. The reason for the bond length differences might be found in the presence of the large Ba ion at fractional coordinate 0.5,0.5,0.184, which enlarges the Cu(2)-O(4) bond length by repulsion of the neighbouring copper ions in the $(x,y,0)$ and $(x,y,0.355)$ planes via ionic forces.

Conclusively, the densities and Laplacians at the critical points in the Y- and Ba-O bonds should be smaller than in the Cu-O bonds, which was impressively underlined by our results. For Y-O the distances are 2.4 Å, the densities are about $0.33 e\text{Å}^{-3}$ and the Laplacians $4.7 e\text{Å}^{-5}$ and for Ba distances of about 2.9 Å correspond to densities of about $0.175 e\text{Å}^{-3}$ and Laplacians of about $1.8 e\text{Å}^{-5}$. An exception is found for the Ba-O(4) bond, where the smaller distance of 2.7 Å is reflected by a density of $2.5 e\text{Å}^{-3}$ and a Laplacian of $2.4 e\text{Å}^{-5}$.

Additionally, bond points have been found between O(2)-O(2), O(3)-O(3) and Cu(1)-Cu(1), respectively. Since ionic bonding can be excluded here and the densities at the critical points are too small for covalency, these findings are obviously artefacts due to the model functions that have been used for modelling of the valence charge densities.

Since, if symmetry constraints are absent, a bond critical point need not to be on the direct connection line between two atoms, the bond angle at the critical points were additionally calculated and shown in the table. Compared to straight bonds (180°), deviations up to about 6° occur, which can be regarded as a consequence of repulsion of valence electrons or 'holes'.

We thank C. Flensburg, University of Copenhagen, for providing the functions for the heavy ions and for help with VALRAY.

¹ F. W. Bader: Atoms and Molecules, Clarendon Press, Oxford (1994).

2.3.10. Topological analysis of $\text{YBa}_2\text{Cu}_3\text{O}_{6.98}$: II Space partitioning and determination of the charge transfer

T. Lippmann, *GKSS, Geesthacht, Germany*, N. H. Andersen, *Condensed Matter Physics and Chemistry Department, Risø National Laboratory, Denmark*, Th. Wolf, *Forschungszentrum Karlsruhe, ITP, Germany*, J. R. Schneider, *DESY/HASYLAB, Hamburg, Germany*
e-mail: niels.hessel@risoe.dk

One of the most interesting open questions of the study of high- T_c superconducting structures deals with the electronic charge transfer, i.e. the rearrangement of valence electrons caused by the chemical bonding of the atoms. Preceding investigations of these structures have been carried out e.g. using Auger electron spectroscopy¹ or electron diffraction². In the first study, however, only vague statements concerning the charge transfer from copper to oxygen were made, because the valences of elements other than Cu were assigned. The second investigation gives more precise values for the charge transfer, but since it was based on only a few $00l$ reflections, only the transfer between the planes perpendicular to the c -axis could be determined.

Additionally, both methods suffer from the high sensitivity on the sample surfaces, i.e. no bulk investigations are possible. Since the high- T_c materials are known to show oxygen loss effects, corruption of the results may occur using these methods.

Topological analyses of high-energy synchrotron radiation data now allow for the determination of charge transfer from accurate X-ray structure factors³. The method is based on the examination of gradient vector field of an electronic charge density distribution. The gradient vectors end at points, where the density has a local maximum (normally the atomic nuclei). The region containing all gradients, which terminate at the same nucleus, defines an atomic basin, and the boundaries of the basins are not crossed by gradient vectors⁴. Conclusively, the boundaries are defined via their normal vectors $\mathbf{n}(\mathbf{r})$ such that

$$\nabla\rho(\mathbf{r}) \cdot \mathbf{n}(\mathbf{r}) = 0$$

and are called surfaces of zero flux. By integration of the density inside the atomic basins, the total charge of a unit cell can be ascribed to the atoms in the cell. Thus, precise evaluations of the charge transfer are possible.

Tab. 1 shows the integration results of our $\text{YBa}_2\text{Cu}_3\text{O}_{6.98}$ data and the corresponding valence states. In the case of the heavy ions, the results underline the presence of Y^{3+} and Ba^{2+} in this structure. Concerning the Cu and O ions, however, the charge transfer is not complete. This observation is in good agreement with an earlier investigation on Cu(I) in Cuprite, where a formal notation of $\text{Cu}_2^{0.6}\text{O}^{1.2}$ was found. The chemical difference between Cu(1) and Cu(2), however, is significantly underlined by a charge transfer difference of about $0.44 e$. On the other hand, the oxygen valences are less than 2-, but the table also shows differences between the ions in the CuO chain (O(1), in the superconducting plane (O(2), O(3)) and the O(4) ion.

¹ K. Ogawa, S. Noro and K. Maki, *J. Appl. Phys.* **82**, 1640 (1997).

² L. Wu, Y. Zhu and J. Taftø, *Phys. Rev. B* **59**, 6035 (1999).

³ T. Lippmann and J.R. Schneider, *Acta Cryst.* **A56**, 575 (2000).

⁴ F. W. Bader, *Atoms in Molecules*, Clarendon Press, Oxford (1994).

Table 1. Total charge inside the atomic basins and corresponding valence states, volumes of the atomic basins and average radii, ionic radii for various valence states and coordinations for comparison purposes.

| Atom | Charge [electrons] | Valence state | Volume [Å ³] | <i>r</i> [Å] | Ionic radii taken from ¹ [Å] |
|--------------|-----------------------|------------------|-----------------------------|-----------------|--|
| Y | 36.34 | 2.66+ | 11.933 | 1.417 | 1.156 (Y(III), 8 coordinate) |
| Ba | 53.86 | 2.14+ | 21.520 | 1.725 | 1.56 (Ba(II), 8 coordinate) |
| Cu(1) | 27.90 | 1.10+ | 12.951 | 1.457 | 0.87 (Cu(II), 6 coordinate) |
| Cu(2) | 27.46 | 1.54+ | 9.048 | 1.293 | 0.68 (O(-II), 4 coordinate) |
| O(1) | 9.54 | 1.54- | 13.598 | 1.481 | 1.28 (O(-II), 8 coordinate) |
| O(2) | 9.71 | 1.71- | 12.246 | 1.430 | |
| O(3) | 9.71 | 1.71- | 12.394 | 1.436 | |
| O(4) | 9.29 | 1.29- | 12.446 | 1.438 | |

Using the charge transfer results above the charge within the planes \perp to the *c*-axis were calculated for comparison with results presented by² and shown in Table 2. Good agreements were found in the superconducting CuO₂ plane and for Y, but in the other planes differences up to 0.4 electrons occur. It is interesting to note that the charge transfer of holes to the CuO₂ planes is 0.12, which is close to the generally accepted value of 0.16 for optimally doped high-*T_c* superconductors.

Table 2. Charge excess of planes \perp to the *c*-axis in YBa₂Cu₃O_{6.98}. Comparison with results from Ref. 2.

| Plane | Charge differences from: | |
|------------------------|-------------------------------|------------|
| | <i>Wu et al.</i> ² | This study |
| CuO | -0.15 | -0.44 |
| BaO | 0.45 | 0.85 |
| CuO₂ | -1.7 | -1.88 |
| Y | 2.7 | 2.66 |

Additionally, Tab.1 presents the atomic volumes and mean atomic radii compared to ionic radii taken from⁵. Generally, all calculated radii are larger than the literature values, which is obviously a consequence of the fact that the whole space in the unit cell was covered by the evaluation procedure.

A calculation of the ‘surfaces of zero flux’ via a topological analysis of the charge density distribution allows for the determination² and visualisation³ of the boundaries of atomic basins, *i.e.* the interatomic surfaces in condensed matter. Visualisation and a detailed analysis of the atomic shapes with respect to their coordination and valence states are currently under progress. Further evaluations deal with the integrated properties inside the atomic basins.

We thank C. Flensburg, University of Copenhagen, for providing the functions for the heavy ions and for help with VALRAY.

¹ www.webelement.com

² C. Flensburg and D. Madsen, Acta Cryst. **A56**, 24 (2000).

³ E. A. Merritt and D. J. Bacon, Methods Enzymol. **B277**, 505 (1997).

2.3.11. Magneto optical investigations on stripes of $\text{YBa}_2\text{Cu}_3\text{O}_x$ thin film

B. H. Larsen, B. A. Jacobsen, N. H. Andersen *Condensed Matter Physics and Chemistry Department, Risø National Laboratory, Denmark*, P. Paturi, *Wihuri Physical Laboratory, Department of Physics, University of Turku, Finland*. Y. Q. Shen, *NKT Research, Brøndby, Denmark*
 e-mail: britt.h.larsen@risoe.dk

For investigations of e.g. superconducting $\text{Bi}_2\text{Sr}_2\text{Ca}_2\text{Cu}_3\text{O}_x$ tapes or $\text{YBa}_2\text{Cu}_3\text{O}_x$ coated conductors, the local current density can be extracted from a magneto optical (MO) measurement. To test this method on a geometrically well-defined system, stripes of $\text{YBa}_2\text{Cu}_3\text{O}_x$ thin films with T_c close to 92K was fabricated as a test system. The stripes consist of 200nm thick laser ablated $\text{YBa}_2\text{Cu}_3\text{O}_x$ film on a substrate of MgO. Several geometries were made in order to investigate the coupling between neighbouring stripes. Here are shown results for stripes that are 220 μm wide and spaced 200 μm apart. The chips were fabricated at NKT Research A/S.

The magneto optical imaging technique records the magnetic field in a plane over the sample surface using the Faraday rotation in a MO-film consisting of Bi-doped yttrium ion garnets. To make the inversion from the measured magnetic field to current density we use a method described by Wijngaarden et al.¹.

To correct for uneven distribution of the light in the microscope, local defects in the MO films and offset in the signal from the CCD camera, a background picture at the same magnetic field but with a temperature above T_c is used. After subtracting the CCD bias found in a picture with no applied field, the measured picture is divided with the background picture. Fig. 1 shows a corrected picture for $T=50\text{K}$ and $B_{\text{applied}}=48\text{mT}$. The shielding of the field by the superconductor is clearly seen. In Fig. 2 the average intensity along a line perpendicular to the strips are shown for different temperatures.

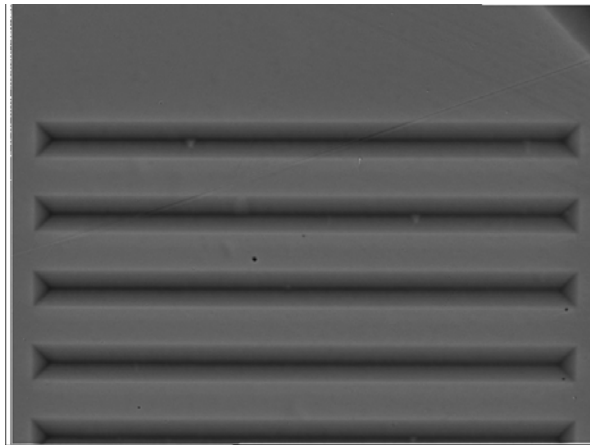


Fig.1. MO picture at $T=50\text{K}$ and $B_{\text{applied}}=48\text{mT}$.

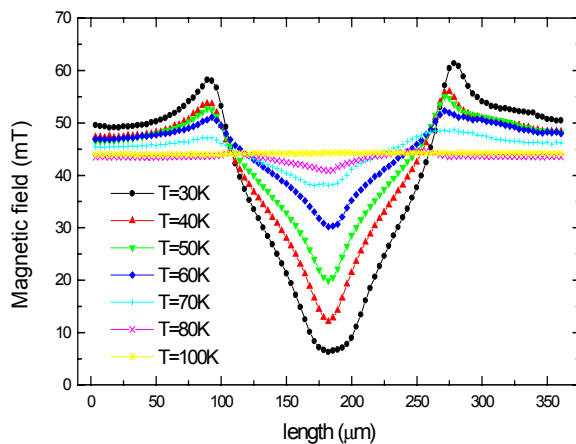


Fig. 2. Magnetic field profiles for different T .

The focusing of the field just outside the superconductor is clearly seen. A slight discrepancy from the triangular shape predicted by the Bean model is observed. This could be due to the dependence of j_c on the magnetic field.

Using the Wijngaarden method, the MO picture is converted to a map of the current density. Fig. 3 shows the average current density in the directions of the stripes measured along a line perpendicular to the stripes. The average j_c is found to be around $7 \cdot 10^{11} \text{ A/m}^2$.

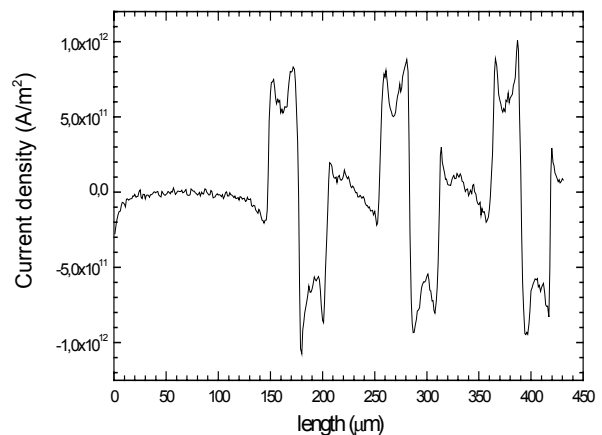


Fig. 3. Calculated j_c profile for $T=50\text{K}$.

¹ R. J. Wijngaarden, H. J. W. Spoelder, R. Surdeanu and R. Griessen, *Phys. Rev* **B54**, 6742 (1996).

2.3.12. Magneto optical investigations of tapes with varying filament thickness

B. H. Larsen, N. H. Andersen *Condensed Matter Physics and Chemistry Department, Risø National Laboratory, Denmark*, M. Eriksen, *Department of Manufacturing Engineering, DTU, Denmark*, B. Seifi, *Nordic Superconducting Technology A/S, Denmark*
e-mail: britt.h.larsen@risoe.dk

In a collaboration between the Department of Manufacturing Engineering from DTU, Nordic Superconducting Technology A/S and Risø to improve the current carrying capability of $\text{Bi}_2\text{Sr}_2\text{Ca}_2\text{Cu}_3\text{O}_x$ powder-in tube tapes we have investigated tapes with different number of filaments and two different flat rolling techniques. The 6 different tapes had 37, 55 or 85 filament and were either rolled from round (the standard procedure) or rolled from a square tube, which was made in the last drawing step.

One aim of this was to make tapes with different thickness of the individual filaments. The heat treatment of each type of tape was individually optimized. The average thickness of the individual filaments was $13\mu\text{m}$, $11\mu\text{m}$ and $8\mu\text{m}$ for 37, 55 and 85 filament respectively. The thinner the filaments the shorter were the sintering times needed to optimize the tapes. Furthermore, the spread in the thickness of the filaments and the overall filament homogeneity were better for the square rolled tapes than for the standard round rolled tapes. This effect is more pronounced the fewer the filaments.

Below are shown magneto optical (MO) pictures of the two types of tapes with 55 filament. The intensity is proportional to the local magnetic field in any given point. The shielding from the individual filaments in the tapes are clearly seen. Below each MO picture is shown the average intensity along a line perpendicular to the filaments. The square rolled tape shields the field homogenously across the tape whereas the round rolled tape has a much weaker shielding at the edges. This and the fact that the slopes of the curves near the edges are smaller, indicates that j_c is lower at the edges of the round rolled tape. For the square rolled tape, the filaments have more uniform j_c .

Both pictures have a certain granularity in the filaments. This could indicate that there are microcracks in the filaments. This is not seen in similar 37 filament tapes.

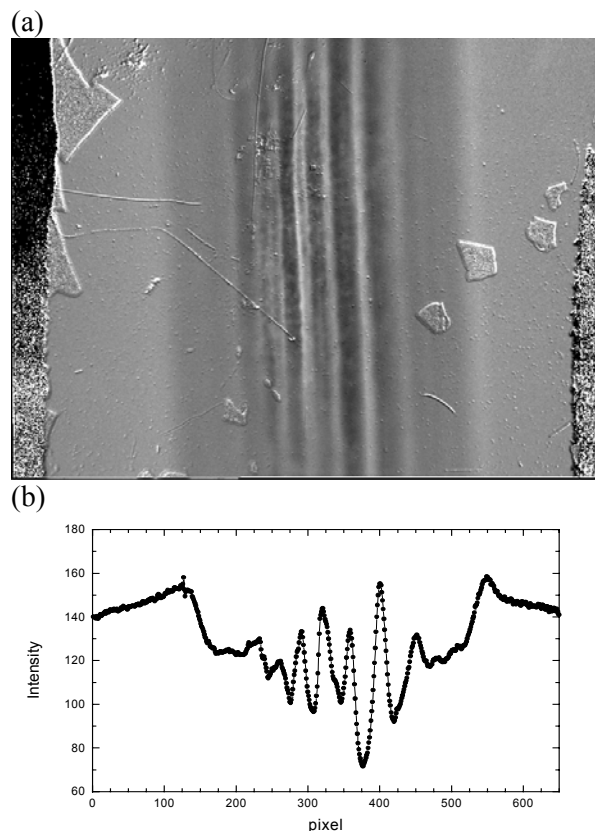


Fig. 1. Measurements for round rolled tape.

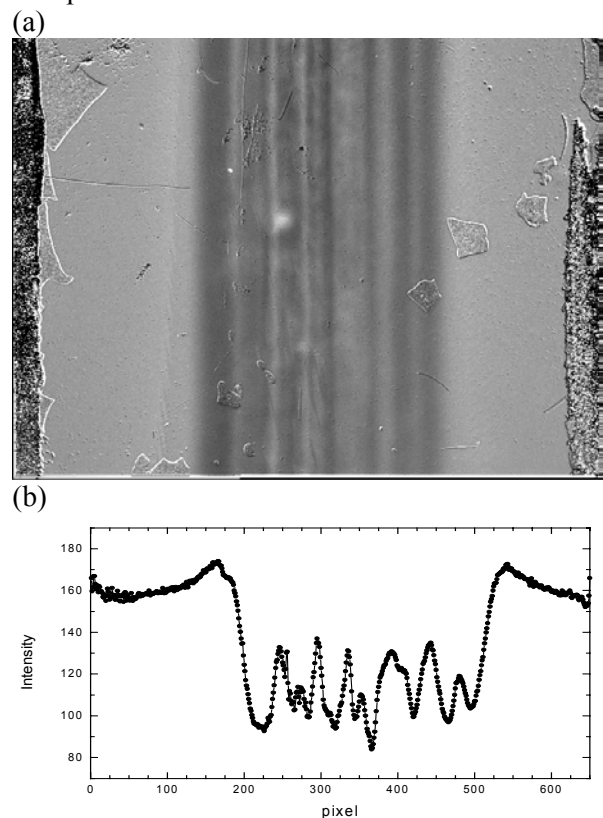


Fig. 2. Measurements for square rolled tape.

2.3.13. Relation between texture and critical current density of textured $\text{YBa}_2\text{Cu}_3\text{O}_x$ plates

B. H. Larsen, A. B. Abrahamsen, N. H. Andersen *Condensed Matter Physics and Chemistry Department, Risø National Laboratory, Denmark*, J. G. Larsen, J. K. S. Christiansen, *Haldor Topsøe A/S, Denmark*, H. F. Poulsen, *Materials Research Department Risø National Laboratory, Denmark* and T. Tschentscher, *HASYLAB, Hamburg, Germany*
e-mail: britt.h.larsen@risoe.dk

$\text{YBa}_2\text{Cu}_3\text{O}_x$ has the potential of carrying high currents in an applied magnetic field at 77 K if the material is sufficiently well textured and pinning centers for the magnetic flux are present. We have studied the relation between critical current and texture in this material. At Haldor Topsøe A/S large textured plates of $\text{YBa}_2\text{Cu}_3\text{O}_x$ with dimensions around $50 \times 3 \times 400 \text{ mm}^3$ and with a critical current above 13 kA has been developed for current leads¹. From a large plate of $\text{YBa}_2\text{Cu}_3\text{O}_x$ a rod with dimensions $5.7 \times 2.3 \times 40 \text{ mm}^3$ was cut. The critical current measured along the rod was 258 A corresponding to a transport critical current density of 1970 A/cm^2 .

The crystalline structure of the textured rod of $\text{YBa}_2\text{Cu}_3\text{O}_x$ was investigated quantitatively using x-ray diffraction. Diffraction images were taken on its largest face at 6 points spaced 5 mm apart along the rod ($z = 5 - 30 \text{ mm}$). Measurements were made at the BW5 synchrotron beamline at HASYLAB, Hamburg. The experimental set-up is described in ref 2. The beam is monochromatic with energy of 100 keV and has a penetration depth of $\sim 1 \text{ mm}$. The spot size on the sample is 1 mm in diameter and the exposure time is 2-3 s. The diffraction images were recorded on an image plate placed 1245 mm from the sample. Results from two different points are seen in Figs. 2(a) and 2(b). The two-dimensional images are analyzed by means of the program package FIT2D³.

The large in-plane face of the rod was polished and the microstructure of the sample was studied by optical microscopy using crossed polarizers (see Figs. 2(c) and 2(d)). The small black crystals are identified as Y_2BaCuO_5 (211-phase) introduced as magnetic flux pinning centers. The larger round features are void pores. The light and dark grey stripes are twins. Most informative are the regularly spaced microcracks seen as narrow black lines. These microcracks are along the (001) cleavage planes⁴. The orientation and texture agrees with the x-ray measurements.

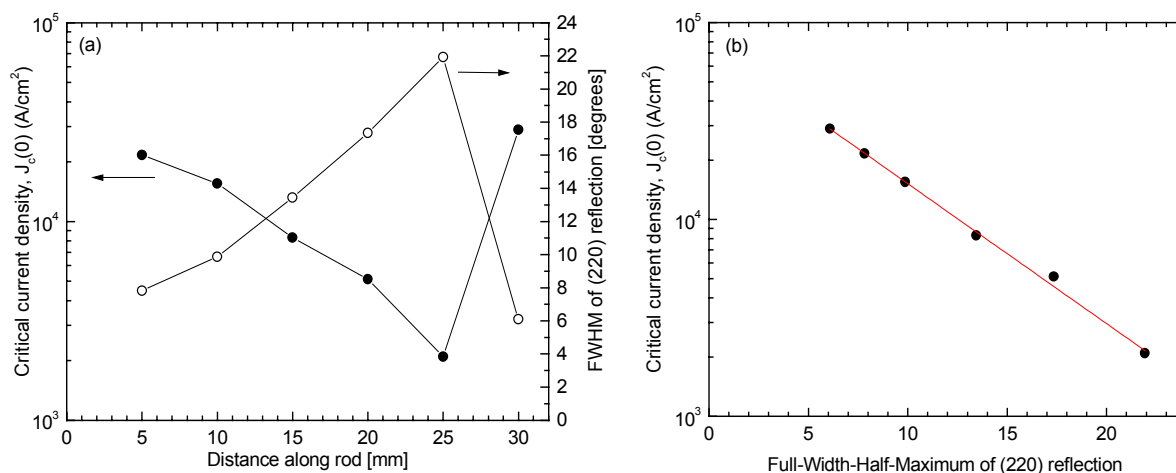


Fig. 1. (a) The magnetization critical current density in zero field is plotted as a function of position along the rod. Using the texture profiles the (220)-peak is fitted with a Gaussian and the FWHM is plotted as a function of position along the rod on the right axis. (b) The critical current as a function of FWHM of the (220) reflection shows a clear exponential dependence.

¹ J. G. Larsen, B. Kristensen, J. G. Sommerschild and E. Frost, *IEEE Trans. Appl. Supercond.* **9**, 487 (1999).

² H. F. Poulsen, T. Frello, N. H. Andersen, M. D. Bentzon and M. von Zimmermann, *Physica C* **298**, 265 (1998).

³ A. P. Hammersley, S. O. Svensson, M. Hanfland, A. N. Fitch and D. Häusermann, *High Pressure Res.* **14**, 235 (1996).

⁴ P. Diko, N. Pelerin and P. Odier, *Physica C* **247**, 169 (1995).

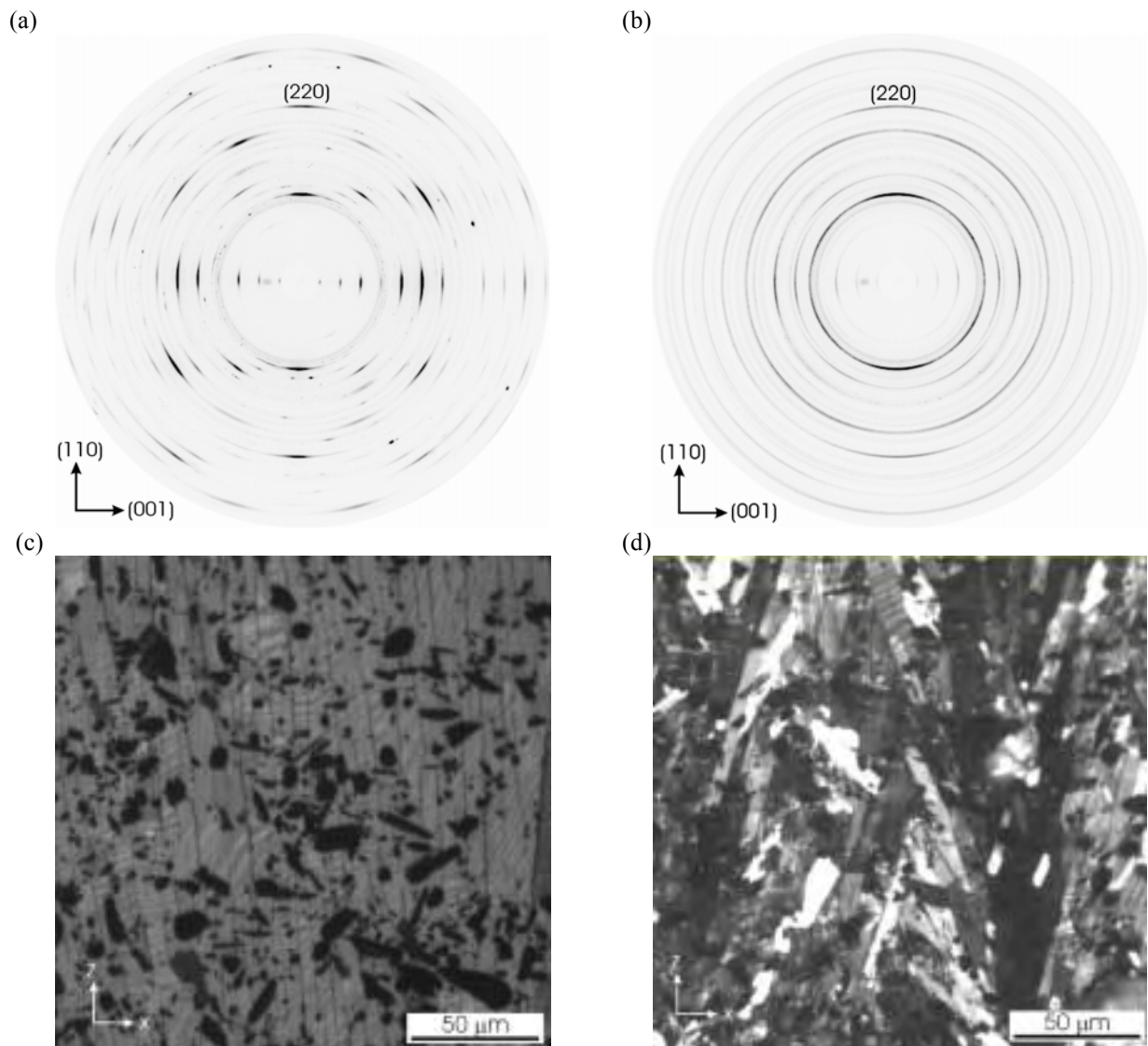


Fig 2. Synchrotron diffraction image at (a) $z=5\text{mm}$ and (b) $z=25\text{mm}$. The $(00l)$ -reflections are seen horizontally and closely spaced. Vertically are seen the $(hh0)$ -reflections. Optical images at (c) $z=5\text{mm}$ and at (d) $z=25\text{mm}$ with crossed polarizers. The black lines are microcracks along the ab -plane¹.

The rod was then cut into rectangular cubes each centred on the points where the x-ray diffraction was performed. The magnetic moment of these was measured as a function of applied magnetic field using a Moving Sample Magnetometer (MSM). From the full hysteresis curve, the magnetization critical current densities of each of the cubes were found.

Figure 1(a) shows the full-width-half-maximum (FWHM) of the (220) -reflection and the critical current density as a function of position along the rod. Fig 1(b) clearly shows the exponential dependence of the local critical current density of the texture of the material. With a (220) -texture of 7.8° the critical current density is $21.600\text{A}/\text{cm}^2$ whereas it drops to $2090\text{A}/\text{cm}^2$ at a texture of 21.9° .

The transport critical current density corresponds to the lowest of the magnetization critical current densities determined at points along the rod, i.e. at $z=25\text{mm}$. This confirms that it is the weakest position along the rod, which determines the transport critical current density and that significant improvements of the critical current can be obtained by controlling the texture better.

¹ W. W. Moorehouse, "The study of rocks in thin section" Harper & Row Publishers (1959).

2.3.14. YBCO/Ag superconducting tapes

P. Paturi, J. Raittila, H. Huhtinen, R. Laiho, *Wihuri Physical Laboratory, Department of Physics, University of Turku, Finland*, J.-C. Grivel, B. H. Larsen, N. H. Andersen, *Condensed Matter Physics and Chemistry Department, Risø National Laboratory, Denmark*, B. Seifi, *Nordic Superconductor Technologies A/S, Brøndby, Denmark*
e-mail: peetu@utu.fi

Most of high-temperature superconducting tapes are nowadays made of $\text{Bi}_2\text{Sr}_2\text{Ca}_2\text{Cu}_3\text{O}_x$ (BSCCO) powders rolled in a silver tube. However, BSCCO is not a good superconductor in a magnetic field. This is why Risø in collaboration with University of Turku and Nordic Superconducting Technologies A/S (NST) is developing similar tapes with $\text{YBa}_2\text{Cu}_3\text{O}_{6+x}$ (YBCO). YBCO single crystals and thin films are well known to have very good properties in magnetic fields, but unfortunately making good tapes of it has proven to be very hard, due to lack of alignment of the grains in the rolled tapes. Most of the YBCO tapes developed today use a different kind of method called coated conductors. This is a more complicated and still not industrialised method of making tapes compared to the 'powder-in-tube' method used with BSCCO and also here. In this project YBCO nanopowder is used. Since the grain shape in nanopowder is flatter than in micron sized powder, it is hoped that it would be possible to get the grains to align better during rolling and therefore also get texture inside the tapes, which would lead to higher critical currents also in magnetic fields.

The nanopowder was made in University of Turku using the sol-gel method¹. This produces powder which has average width of 40 nm and average height of 1-3 nm. The powder was rolled to a single filament tape in NST. This tape was then annealed in different conditions to optimise the superconducting properties of the tape. The annealing and experiments were done at Risø during the stay of P. Paturi in the fall 2000. It was found that critical currents, I_c , up to 5 A (3300 A/cm²) can be achieved by annealing for 10 h at 940°C in nitrogen atmosphere and cooling with 150°C/h and annealing with oxygen. The maximum critical temperature, T_c , of samples made by annealing in nitrogen is 89 K. These samples however, do not have any kind of textures inside as measured by synchrotron x-ray diffraction. Optical microscope images of the opened tapes show that the grains are fairly small, ca. 5 μm in diameter.

Annealing in mixed atmosphere of nitrogen and oxygen was also used, and this was found to produce some texture inside the tape, but hardly any I_c . The optimal oxygen pressure depends on the annealing temperature² and time. If the oxygen pressure is low or the time at high temperature is long so that the superconductor melts, Y_2BaCuO_5 is observed in the samples, while the I_c values get worse. These samples had typically two different superconducting phases, which had different T_c values as seen from the AC susceptibility curves. The higher T_c was always 92 K, but the lower was typically below 80 K. One of these phases is probably the weak links in grain boundaries, which haven't grown together well. Re-annealing these samples using nitrogen atmosphere and 935°C temperature produced I_c of 2.8 A. Since these samples probably have some kind of texture, the magnetic field properties of these samples are expected to be better than the ones done in only nitrogen atmosphere. This will be measured in January in University of Turku.

¹ E. Blinov, V. G. Fleisher, H. Huhtinen, R. Laiho, E. Lähderanta, P. Paturi, Yu. P. Stepanov and L. Vlasenko, *Superconducting Science and Technologies* **11**, 818 (1997).

² N.-H. Wu, H. H. Zern and C.-L. Chen, *Physica C* **241**, 198 (1995).

2.3.15. Improvement of BPSCCO/Ag-sheathed tapes by manipulation of the final cooling stage

J.-C. Grivel, K. Stahl, and N.H. Andersen, *Condensed Matter Physics and Chemistry Department, Risø National Laboratory, Denmark*; B. Seifi, *Nordic Superconductor Technologies A/S, Denmark*
e-mail: jean-claude.grivel@risoe.dk

After 10 years of development, $(\text{Bi,Pb})_2\text{Sr}_2\text{Ca}_2\text{Cu}_3\text{O}_{10+\delta}$ / Ag-sheathed superconducting tapes are emerging on the market. While their performances are now high enough in order to fulfil the requirements of a range of applications including dc cables, there is still a need for improvement in order to realise all the promises of these composites. Furthermore, the fabrication process of these tapes is still not optimised. Besides the need for an improvement of the overall performances, the reproducibility of the manufacturing process is not good enough for a real large-scale market. These points can in principle be tackled by means of a more detailed understanding of the processes related to the superconducting ceramic development from the precursor stage and through the high temperature heat treatments necessary for obtaining the final product. The superconductivity group in the department is performing studies in this view.

One of the key parameters controlling the tape performances is the final cooling stage. This is due to the fact that a small but non-negligible amount of a liquid phase is present in the ceramic core during the heat treatment at high temperature. Solidification of this liquid in a non-suitable form at grain boundaries during the final cooling stage prevents the transfer of the superconducting current from grain to grain along the length of the tape. Furthermore, low quality grain boundaries are quite sensitive to the presence of a magnetic field preventing the use of the tapes for magnet applications at 77K.

A systematic investigation of the final cooling stage was performed during year 2000. The parameters that were varied included the sintering temperature from which the cooling was started; the cooling rate; the interval the temperature over which a slow cooling was performed and the duration of the sintering step preceding the final cooling stage. DTA measurements showed that the crystallisation of the high temperature liquid phase takes place over a large temperature interval (ΔT). This explains the drastic improvement of the critical current density of tape samples when these are slowly cooled over a larger ΔT (Fig. 1).

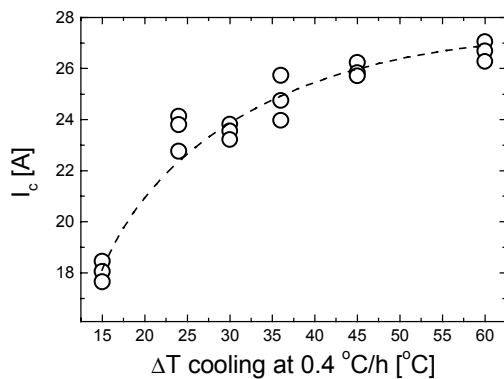


Fig. 1. Critical current density measured at 77K versus slow cooling temperature interval.

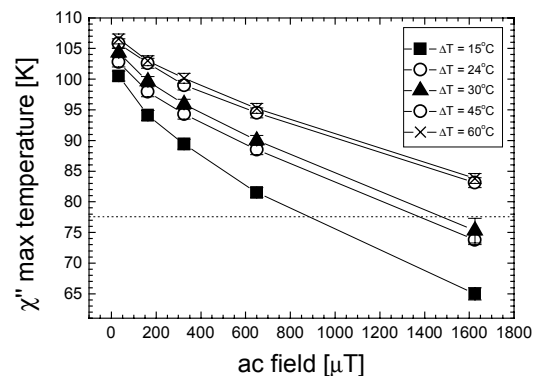


Fig. 2. ac-field dependence of the maximum of χ'' , which reflects the magnetic field penetration in the material.

Magnetisation measurements performed with various ac excitation fields were used to investigate the sensitivity of the grain boundaries to an external magnetic field. As illustrated in Fig. 2, the tapes, in which the liquid was allowed to crystallise to a larger extent (larger ΔT), are much less sensitive to a magnetic field. The parallel between I_c and the behaviour under the ac-field enables to relate the improvement of the tape performances to the higher quality of the grain boundaries.

2.3.16. Post annealing of high- T_c superconducting BSCCO-tapes in Ag-clad

B. A. Jacobsen, B. H. Larsen, N. H. Andersen, *Condensed Matter Physics and Chemistry Department, Risø National Laboratory, Denmark*, W. G. Wang, *Nordic Superconductor Technologies A/S, Brøndby, Denmark*

e-mail: birgitte.abery.jacobsen@risoe.dk

Investigations of high- T_c superconductors are often focused on how to optimize the critical temperature but for practical applications improvement of the critical current, I_c , is important as well. The Danish company Nordic Superconductor Technologies A/S (NST) is producing superconducting $\text{Bi}_2\text{Sr}_2\text{Ca}_2\text{Cu}_3\text{O}_{10}$ (BSCCO) tapes and want to use these tapes for production of superconducting cables. The tapes are made by the powder in tube technique: BSCCO powder is put into a silver tube and several mechanical processes and heat treatments are applied to get the thin superconducting tapes. Since T_c is dependent on the oxygen content it is natural to believe that the same would be the case for the critical current. In tapes of the anisotropic ceramic high- T_c materials the critical current is determined by the texture, the current density across grain boundaries (intergrain J_c) and the current density within a single grain (intragrain J_c). At present the texturing appears to be sufficiently optimized but uncertainty about the role of intra- and intergrain contributions and how they are optimized remain.

Fully processed multi filament BSCCO tapes in Ag-clad have been heat treated with a flow of different percentage of oxygen. The critical current dependence of the oxygen partial pressure, i.e. the doping level, has been investigated. In Fig. 1 is shown that the critical transport current at 77 K is reduced in any oxygen partial pressure for post annealing at or above 600°C. Fig. 2 shows a hard X-ray diffraction image of one of the heat treated tapes. The inner ring is Ca_2PbO_4 that has been decomposed from BSCCO. The Ca_2PbO_4 is an impurity phase and is also present before the heat treatment but in a much smaller amount. Some of the Ca_2PbO_4 are situated at the grain boundaries with a detrimental effect on the critical current. The decomposition happens when the temperature is 600°C or above. For fast oxygen diffusion through the silver around the BSCCO material it is necessary to make the heat treatment at or above 600°C. The conclusion is therefore that in this temperature range the critical current of the BSCCO-tapes in Ag-clad can not be improved by post annealing any oxygen partial pressure.

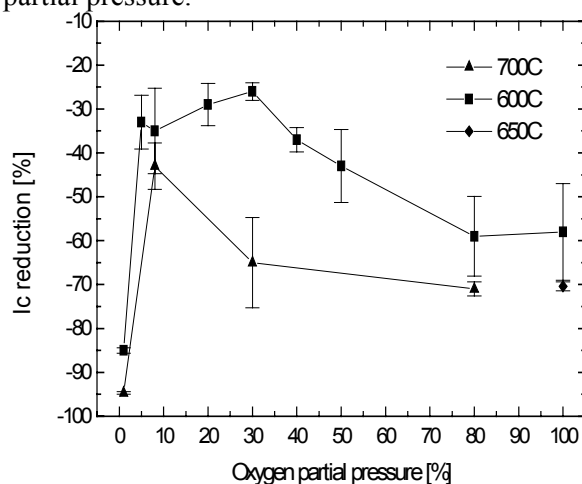


Fig. 1. The reduction in the critical current at different heat treatments and oxygen partial pressure.

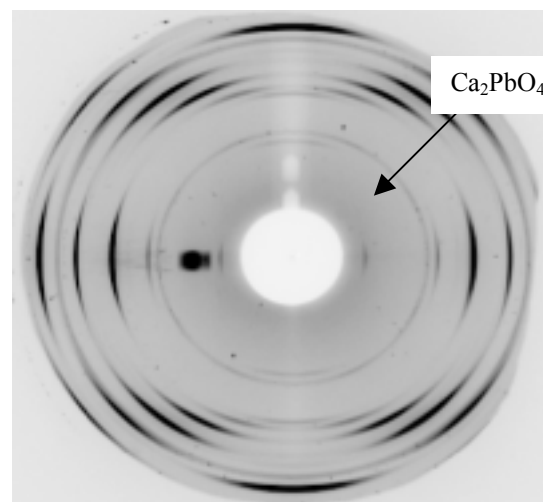


Fig. 2. X-ray diffraction image of a BSCCO tape which has been heated at 700°C with 8% oxygen flow. The intensity of the Ca_2PbO_4 powder ring increases by post annealing at temperatures at or above 600°C.

2.3.17. The effect of intermediate pressure in the OPIT fabrication on the current paths and the current carrying capability of Bi-2223 tapes

P. Skov-Hansen, *Nordic Superconductor Technologies A/S, Brøndby, Denmark*, M. R. Koblischka, *Nordic Superconductor Technologies A/S, Brøndby, Denmark* and *Condensed Matter Physics and Chemistry Department, Risø National Laboratory, Denmark*, N. H. Andersen, *Condensed Matter Physics and Chemistry Department, Risø National Laboratory, Denmark*, P. Vase, *Nordic Superconductor Technologies A/S, Brøndby, Denmark*, P. Kovac, *Institute of Electrical Engineering, Slovak Academy of Sciences, Bratislava, Slovakia* and F. Marti, *Department of Condensed Matter Physics, University of Geneva, Switzerland*
e-mail: michael.koblischka@risoe.dk

In the production of Bi-2223/Ag tapes by the Powder-in-tube method (OPIT), an important limiting mechanism in the intermediate pressing (IP) technique is the number of cracks that can not be healed in the following heat treatment. In this study it is investigated how many of the unhealed cracks can be found in the finished HTS tape. Low to high loads have been used in the IP, and the unhealed crack densities have been estimated using magneto-optical imaging, ultrasonic vibration and pure bending tests. In the magneto-optical imaging, the full field cycle up to 110 mT and downwards was measured. Fig. 1 shows the flux patterns during ramp-up field at 90 mT after zero field cooling. At 0 kN load there is very little flux shielding. The image for 3 kN load shows more shielding, but there are no large contrasts, which would indicate good superconducting properties. At 17 kN intermediate load, some of the middle filaments seem to increase in shielding capability, but only at 29 kN there is a clear contrast between filaments and spaces in-between. The magneto-optical images in Fig. 1 show that increasing the IP used improves the superconducting flux shielding, at least for the surface filaments that are visible on the images.

Recent studies has shown how ultrasonic vibrations can give an indication of how well the tape filaments are connected (Fig.2). The idea is that the strength of each individual filament is estimated using the vibrations: implosions of small bubbles on the filament surface and the vibrating pressure create a fatigue stress, which is responsible for the propagation of cracks. The more cracks that are present, the smaller pieces. Since the fracture strength of Bi-2223 is quite low, it will not take long before the first pieces fall apart, even if cracks initially are not propagating all the way through the filament. The filaments will fracture at the mechanical weakest locations: cracks, notches and weak grain boundaries. The ultrasonic vibration process will therefore reveal the number of these types of defects. After etching all filaments were intact. This indicates that there are no severe cracks in any of the filaments. After ultrasonic vibration some filaments shattered into very tiny pieces. Some filaments do not break.

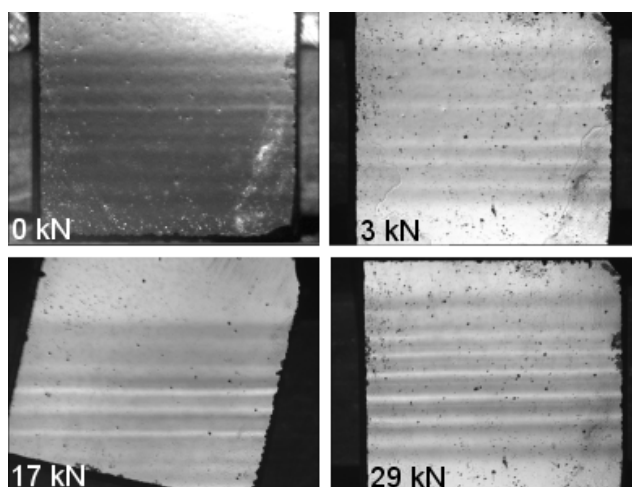


Fig. 1. Magneto-optical images (zero field cooled, 90mT, 10K). Intermediate loads were top left: 0 kN, top right: 3 kN, bottom left: 17 kN, bottom right: 29 kN. Top left image has been subjected to more contrast enhancement than the rest of the images.



Fig. 2. Pieces of filaments after 1 min of ultrasonic vibration. Intermediate load from left to right: 0 kN, 3 kN, 17 kN, 29 kN.

2.3.18. Magneto-optical investigations as a tool to improve quality of (Pb,Bi)-2223 tapes

M. R. Koblichka, *Nordic Superconductor Technologies A/S, Brøndby, Denmark* and Condensed Matter Physics and Chemistry Department, Risø National Laboratory, Denmark, W. G. Wang, B. Seifi, P. Skov-Hansen, P. Vase, *Nordic Superconductor Technologies A/S, Brøndby, Denmark*, N. H. Andersen, *Condensed Matter Physics and Chemistry Department, Risø National Laboratory, Denmark*

e-mail: michael.koblichka@risoe.dk

The study of the current-carrying capacity of individual filaments from a multifilamentary Bi-2223 tape is an essential issue for the further improvement of the critical current density, j_c , and the engineering current density, j_e . As sensitive tool to achieve this goal, we employ magneto-optic (MO) imaging, which provides a spatial resolution of about 2 μm . Magneto-optical visualisation of flux distributions is very sensitive to any kind of structural defects in superconducting samples and can reveal differences in critical current densities even within the filaments. Here, we report on MO flux patterns of cross sections of tapes. To our knowledge we have for the first time applied the field perpendicular to a cross section of an intact tape, i.e. the external field is aligned along the individual filaments. This enables the direct study of filament quality as function of position within the tape, and to obtain information about the filament coupling in an intact tape. This geometry is, therefore, extremely important for the further development of Bi-2223 tapes.

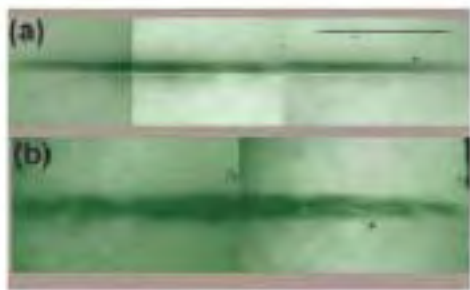


Fig.1 Cross section MO image of a monofilament tape and a multifilamentary production tape (37 filaments). The field of 80 mT is applied parallel to the filaments; T=10K.

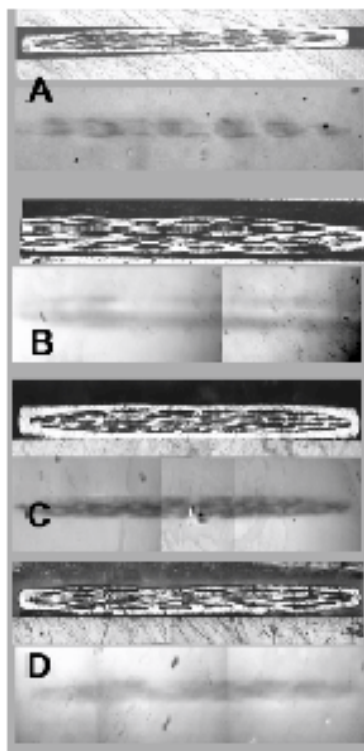


Fig. 2. Flux patterns of cross-sections taken at T=10 K, $\mu H_a = 80$ mT, together with the polarization images. (A) tape A, (B) tape B, (C) tape C, and (D) tape D. All images are scaled in order to fit the figure frame; the tape dimensions are 3.92 x 0.22 mm². Tape A with a low fill factor shows separated stacks of filaments; the filaments along the outer rim are found to be well shielding. Flux enters easily into the thin, inner filaments. Tape B reveals a strong coupling between the filaments (the filaments appear as a dark, continuous line); therefore the shielding currents are flowing on a wide area. Note that the upper part of the tape is not of the same quality. The centre of the tape contains mainly filaments of low quality, as can also be seen from the polarisation image. Tape C is found to be a very homogeneous tape; even at the tape edges, the filaments are well shielding. Note that the filament size distribution is also very homogeneous. Tape D is found to be similar to tape A, except the higher fill factor.

2.4. Structures and defects

2.4.1. A perdeuterated cryoprotectant for neutron studies and a demonstration of its use for neutron powder diffraction on L(-)-ephedrine hemihydrate

F. C. Krebs, M. Jørgensen, B. Lebech *Condensed Matter Physics and Chemistry Department, Risø National Laboratory, Denmark*, K. Frydenvang *Department of Medicinal Chemistry, The Royal Danish School of Pharmacy, Denmark*

e-mail: frederik.krebs@risoe.dk

The use of perdeuteropolyethylpropylene (d-PEP)¹ as a cryoprotectant for neutron studies of molecular organic solids is demonstrated by structure solution of L(-)-ephedrine hemihydrate from neutron powder diffraction data on a sample containing 20% w/w d-PEP. It is demonstrated that no contribution from d-PEP to the scattering is observed. The neutron diffraction studies of solvent containing molecular crystals that requires a perdeuterated cryoprotectant oil is thus possible².

In recent years the complexity of the structural problems that have been addressed using X-ray diffraction has increased. There are many reasons for this but for molecular organic systems the main reason is the advent of fast area detector based data acquisition techniques. This has moved the threshold of the structural problems that crystallographers will engage in and this is further reflected in the increased number of scientific reports where the size of the asymmetric unit is larger and more complex. Examples of these structural problems are molecular crystals and macromolecular crystals that include solvent molecules. Often such solvent containing crystals or clathrates show very limited stability when removed from the mother liquor. The solution to the problem is low temperature data collections or data collections on crystals fixed in a capillary containing the mother liquor. The use of cryoprotectants is sometimes imperative if data collection is to be successful. Many different approaches to this have been reported but generally two categories exist. Either a co-solvent that prevents crystallisation of solvent is carefully included or a cryoprotectant typically in the form of an oil that does not crystallise is used to completely coat and protect the crystal while handling. While this is a well proven technique in single crystal X-ray diffraction experiments and to a lesser extent X-ray powder diffraction experiments one quickly realises that the similar neutron experiment is not feasible as all available oils contain vast amounts of hydrogen. Thus to perform the equivalent neutron experiment one would require a perdeuterated oil to reduce the amount of incoherent scattering from the cryoprotectant and no such perdeuterated oil is available naturally or commercially.

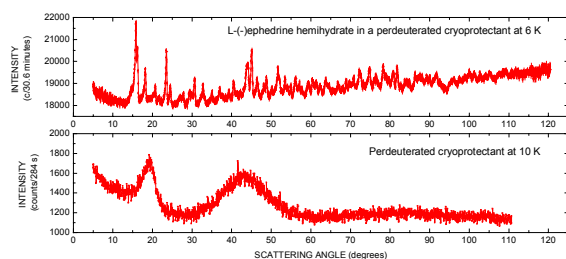


Fig. 1. The neutron powder diffractogram of L(-)-ephedrine hemihydrate (above) and of d-PEP (below, as taken from ref. 1). It is noticeable that negligible or no contribution from the d-PEP cryoprotectant oil is observed (incident wavelength 1.5418Å and 1.55Å respectively).

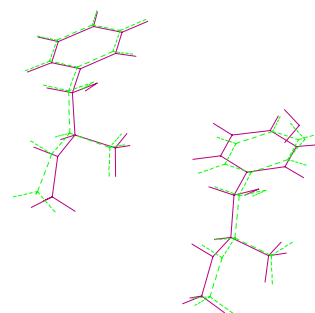


Fig. 2. An overlay of the structural model as obtained from the refinement of the neutron data (dotted) and a structural model obtained from a similar X-ray study (solid). The structures are very similar.

In conclusion this work has made neutron studies of materials that require a cryoprotectant possible.

¹ F. C. Krebs, M. Jørgensen, B. Lebech, K. Almdal and W. B. Pedersen, *Pol. Bull.* **43**, 485 (2000).

² F. C. Krebs, M. Jørgensen, B. Lebech and K. Frydenvang, *J. Appl. Cryst.*, A perdeuterated cryoprotectant for neutron studies and a demonstration of its use for neutron powder diffraction on L(-)-ephedrine hemihydrate, in press.

2.4.2. Synthesis and crystal structure analysis of ZnAPO–35 and $\text{Zn}_2(\text{OH})_{0.14}\text{F}_{0.86}\text{PO}_4$ based on x-ray and neutron powder diffraction data

K.-I. Taasti, A. N. Christensen, *Department of Inorganic Chemistry, University of Aarhus, Denmark*, P. Norby, *Department of Chemistry, Oslo University, Norway*, J. C. Hanson, *Chemistry Department, Brookhaven National Laboratory, Upton, New York, U.S.A.*, B. Lebech, *Condensed Matter and Chemistry Department, Risø National Laboratory, Denmark*, H. J. Jakobsen and J. Skibsted, *Instrument Centre for Solid-State NMR Spectroscopy, Chemistry Department, University of Aarhus, Denmark*

e-mail: bente.lebech@risoe.dk

Microporous compounds with open framework structures as zeolites and aluminophosphates are often made in hydrothermal or organothermal synthesis. In many cases only powders are obtained, but investigations have shown that Al^{3+} in the AlPO_4 -framework can be substituted by Me^{2+} -ions. Recent investigations of the synthesis of Zn^{2+} - and Co^{2+} -substituted aluminophosphates were reported using hydrofluoric acid as a mineraliser¹. With the use of this mineraliser it is possible to synthesise large crystals of microporous compounds² and large crystals of ZnAPO–35. The Zn^{2+} -substituted aluminophosphate $(\text{Zn},\text{Al})\text{PO}_4 \cdot 0.5\text{C}_2\text{H}_{10}\text{N}_2$ was made in hydrothermal as well as in organothermal synthesis. It turned out that the compound $\text{ZnPO}_4 \cdot 0.5\text{C}_2\text{H}_{10}\text{N}_2$ with a powder pattern similar to that of the compound $(\text{Zn},\text{Al})\text{PO}_4 \cdot 0.5\text{C}_2\text{H}_{10}\text{N}_2$ could be made when aluminium was excluded from the reaction mixture. The structure-directing template in these syntheses was ethylenediamine. Using the template 1,4-diazabicyclo[2.2.2] octane, $\text{N}_2\text{C}_6\text{H}_{12}$ (DABCO) and hydrofluoric acid as mineraliser, we were able to synthesise the Zn^{2+} -substituted aluminophosphate ZnAPO–35 with the LEV-type structure.

Single crystal x-ray diffraction data for Zn_2FPO_4 were measured at the beam line X7B at the National Synchrotron Light Source at Brookhaven National Laboratory using a MAR-detector. The synthesis of ZnAPO–35 did not result in single crystals large enough for traditional single crystal x-ray diffraction. Hence, neutron diffraction powder pattern of a calcined ZnAPO–35 sample and a Zn_2FPO_4 sample were measured using the multi-detector TAS3/POW at Risø National Laboratory. The magnitude of the Zn-substitution ($\text{Zn}^{2+}/\text{Al}^{3+}$) in the APO–35 structure was determined from the x-ray fluorescence analysis and from the analysis of the neutron diffraction powder pattern of the calcined ZnAPO–35 sample to be 0.13/0.87 and 0.14/0.86, respectively. However, the profile refinement³ of the neutron diffraction data observed for the calcined ZnAPO–35 revealed that the crystal structure of the calcined sample is not LEV-type, but a mixture of AlPO_4 and α - and γ - $\text{Zn}_3(\text{PO}_4)_2$.

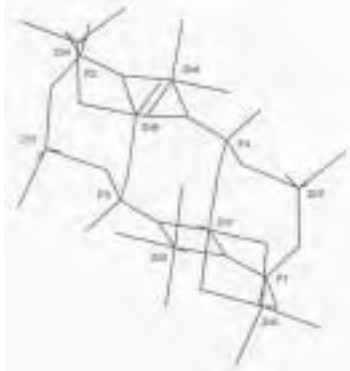


Fig. 1. The asymmetric unit of the crystal structure of $\text{Zn}_2(\text{OH})_{0.14}\text{F}_{0.86}\text{PO}_4$.

The neutron diffraction powder pattern of the Zn_2FPO_4 sample was used to test for a possible OD^-/F^- substitution in the sample. An ordered model structure, where four F-atoms (F_I) had occupancy 1 and the remaining four F-atoms (F_{II}) had occupancy 0, was compared to several disordered model structures (see Taasti et al.⁴ for details), but the GSAS profile refinement did not indicate OD^-/F^- substitution. However, ^1H MAS (Magic Angle Spinning) and $^{31}\text{P}\{^1\text{H}\}$ CP/MAS (Cross Polarisation/Magic Angle Spinning) NMR investigations demonstrated the presence of OH-groups and led us to conclude that the composition of the sample investigated is $\text{Zn}_2(\text{OH})_{0.14}\text{F}_{0.86}\text{PO}_4$.

¹ A. N. Christensen and R. G. Hazell, *Acta. Chem. Scand.* 53, 403 (1999).

² A. Kupermann, S. Nadimi, S. Oliver, G. A. Ozin, J. M. Garcés and M. M. Olken, *Nature (London)* 365, 239 (1993).

³ A. C. Larson and R.B. von Dreele, GSAS, General Structure Analysis System. *Lansce*, MS-H805, Los Alamos National Laboratory, (1994).

⁴ K.-I. Taasti, A. N. Christensen, P. Norby, J. C. Hanson, B. Lebech, H. J. Jakobsen and J. Skibsted, Hydrothermal synthesis of ZnAPO –35 and $\text{Zn}_2(\text{OH})_{0.14}\text{F}_{0.86}\text{PO}_4$. A single crystal structure analysis of $\text{Zn}_2(\text{OH})_{0.14}\text{F}_{0.86}\text{PO}_4$. Submitted for publication.

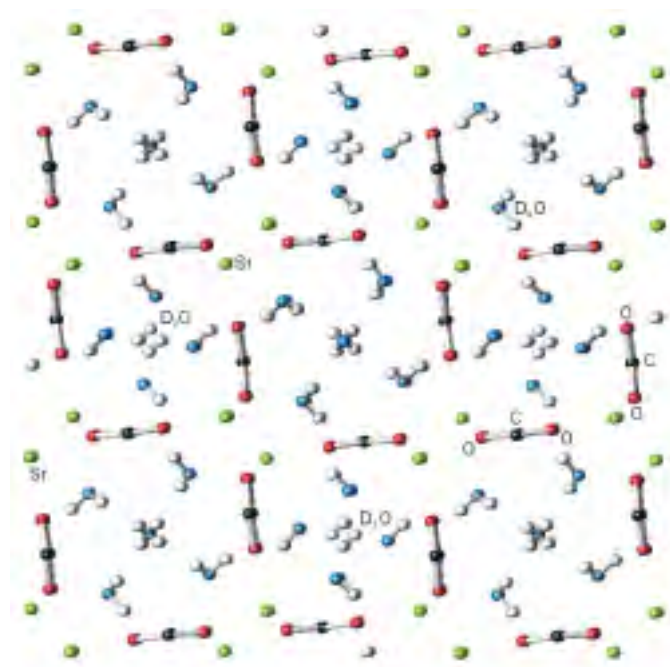
2.4.3. A neutron powder diffraction study Strontium Oxalate Hydrate, $\text{SrC}_2\text{O}_4 \cdot 2\text{D}_2\text{O}$

R. K. Birkedal Nielsen, A. N. Christensen, K.-I. Taasti, *Department of Inorganic Chemistry, University of Aarhus, Denmark*, and B. Lebech, *Condensed Matter and Chemistry Department, Risø National Laboratory, Denmark*

Bente.lebech@risoe.dk

Strontium oxalate can be made as a monohydrate, $\text{SrC}_2\text{O}_4 \cdot \text{H}_2\text{O}$, and as a dihydrate, $\text{SrC}_2\text{O}_4 \cdot 2\text{H}_2\text{O}$. In addition, it is also known as an anhydrous compound, SrC_2O_4 . The dihydrate may contain additional water so that the formula should be $\text{SrC}_2\text{O}_4 \cdot (2+x)\text{H}_2\text{O}$. Thermogravimetric investigation of the dehydration of strontium oxalate hydrates indicates that dehydration is complete at 300°C and that decomposition to strontium carbonate takes place at 485°C ¹. An *in-situ* investigation by neutron powder diffraction of the dehydration of strontium oxalate hydrates has been attempted in the temperature range $50\text{--}350^\circ\text{C}$ ². The idea was to study the water molecules during heating and dehydration. However, because of problems with the temperature stability a neutron diffraction powder pattern of $\text{SrC}_2\text{O}_4 \cdot x\text{D}_2\text{O}$ at 25°C was measured at TAS3/POW in order to get an accurate determination of the water content of the sample at ambient temperature.

The structure of $\text{SrC}_2\text{O}_4 \cdot 2\text{D}_2\text{O}$ was known¹ although the water molecule had an unexpected shape. With other techniques it would only have been possible to study the O-atom in the water molecule, but by using powder neutron diffraction and substituting D for H, it was possible to study the behaviour of the entire water molecule in a sample with low incoherent background. Originally, the idea was to refine the values of the unit cell, atomic positions and the population of the water molecules by the means of the GSAS profile refinement programme³ while constraining the water molecule to a sensible shape during the refinement (Rigid Body). Unfortunately, the sample contained $\text{SrC}_2\text{O}_4 \cdot 2\text{D}_2\text{O}$ as well as $\text{SrC}_2\text{O}_4 \cdot \text{D}_2\text{O}$ and the H:D ratio was 3:2 which in conjunction with the relatively poor signal-to-noise ratio of the data, made it impossible to refine the population and position of the water molecules.



The results of the refinement are as follows: (a) With Rigid Body: $R_p = 3,73\%$, $wR_p = 2,91\%$ and $R_f^2 = 17,6\%$ and (b) without Rigid Body: $R_p = 3,46\%$, $wR_p = 2,68\%$ and $R_f^2 = 16,0\%$. All in all the known structure of $\text{SrC}_2\text{O}_4 \cdot 2\text{D}_2\text{O}$ was confirmed, even though the position of the D-atoms in the water could not be confirmed.

The figure shows the projection on the (a,b) -plane of the crystal structure of $\text{SrC}_2\text{O}_4 \cdot 2\text{D}_2\text{O}$ ⁴ according to the present Rigid Body refinement. Colour code: Sr is green, D and/or H is white, C is black, O connected to C is red and O in water molecules is blue.

¹ A. N. Christensen and R. G. Hazell. *Acta Chem. Scand.* **52**, 508 (1998).

² R. B. Nielsen, P. Norby and A. N. Christensen. Experimental Report HMI (1999).

³ A. C. Larson and R.B. von Dreele, GSAS, General Structure Analysis System. Lancee, MS-H805, Los Alamos National Laboratory, (1994).

2.5. Structures and interfaces

2.5.1 Stabilization of the Si(111)- $\begin{pmatrix} 3 & 2 \\ -1 & 1 \end{pmatrix}$ -Pb low temperature phase at room temperature

C. Kumpf, M. Nielsen, R. Feidenhans'l, *Condensed Matter Physics and Chemistry Department, Risø National Laboratory, Denmark*, Y. Su and R. L. Johnson, *II. Institut für Experimentalphysik, Universität Hamburg, Germany*
e-mail: christian.kumpf@risoe.dk

In recent there has been a focus on low temperature (LT) phases of adsorbate induced surface reconstructions of semiconductors due to their interesting electronic properties. One example is the hexagonal incommensurate (HIC) phase formed by $4/3$ monolayer (ML) of lead on silicon(111), which transforms to a $\begin{pmatrix} 3 & 2 \\ -1 & 1 \end{pmatrix}$ phase – often denoted as $\sqrt{7} \times \sqrt{3}$ – upon cooling¹. The detailed structure of this LT phase has been solved recently². It can be stabilized at room temperature (RT) by alloying the lead overlayer with tin. Here we present the results of our RT surface x-ray diffraction study on an overlayer containing about 33% tin and 67% lead.

RHEED and LEED techniques were used to monitor the Pb and Sn deposition during preparation of the sample under UHV conditions. Afterwards the sample was transferred into a UHV-LT chamber mounted at the surface diffractometer at the BW2 beamline at HASYLAB. The surface consisted partly of the HIC phase and partly of the $\sqrt{7} \times \sqrt{3}$ phase, but since the fractional order reflections of these reconstructions do not overlap, a pure $\sqrt{7} \times \sqrt{3}$ -data set could be measured. From the intensities of symmetry equivalent reflections the populations of all three surface domains could be determined to 23%, 33% and 44%, respectively. The reflections were rescaled and mapped on one domain.

Fig. 1a shows the measured and calculated in-plane intensities of our best fit ($\chi^2 = 1.78$), the corresponding model is depicted in Fig. 1b. Atomic positions (restricted to the mirror line), occupations for the lead- and tin-atoms and Debye-Waller factors were refined. The Si(111)- $\sqrt{7} \times \sqrt{3}$ -Pb model from Ref. [2] was used as a starting model for the refinement. It consists of six Pb atoms per unit cell (#1,2,3,3',4 and 4'), whereby atoms 3 and 3' as well as 4 and 4' are symmetrically equivalent, so there are four atomic sites. Site #1 differs from the others by its lack of bonds to the silicon substrate and by exhibiting only *covalent* bonds to the other Pb atoms. It was speculated that this site is preferably occupied by tin. But several tests performed during the refinement of the Si(111)-Sn+Pb model ensured that the neighboring sites (#2,3 and 3') – those with covalent bonds to the central atom – are occupied by the same percentage of tin as the central atom itself. In such a way groups of four atoms arise which – in our case – exhibit an occupation of 50% tin and 50% lead. Since the two other Pb atoms (#4 and 4') in the unit cell do not mix with tin the total coverage is 0.4 ML Sn and 0.8 ML Pb.

This work was supported by the Danish Research Council (Dansync), the BMBF (05 SE8 GUA6) and the European Commission (IHP progr. "Access to Research Infrastructures", HPRI-CT-1999-00040).

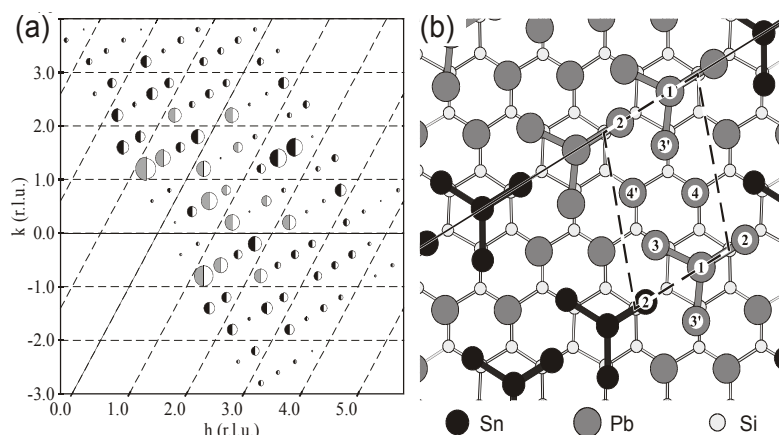


Fig. 1a. Inplane data set. The area of the filled and open semicircles represent measured and calculated intensities. Grey/ white circles have been scaled with 0.5.

Fig. 1b. Model of the Si(111)-Sn+Pb reconstruction. Tin, lead and silicon atoms are shown as grey, black and open circles, respectively. The solid line represents the mirror line.

¹ K. Horikoshi, X. Tong, T. Nagao and S. Hasegawa, *Phys. Rev.* **B60**, 13287 (1999).

² C. Kumpf, O. Bunk, J. H. Zeysing, M. M. Nielsen, M. Nielsen, R. L. Johnson and R. Feidenhans'l, *Surf. Sci.* **448**, L213 (2000).

2.5.2. Structural investigation of Si(111)- $\sqrt{3}\times\sqrt{3}$ -Ag surface at low temperature

Y. Su, R. L. Johnson, II. *Institut für Experimentalphysik, Universität Hamburg, Germany*, C. Kumpf, M. Nielsen and R. Feidenhans'l, *Condensed Matter Physics and Chemistry Department, Risø National Laboratory, Denmark*

e-mail: christian.kumpf@risoe.dk

Si(111)- $\sqrt{3}\times\sqrt{3}$ -Ag surface is one of the most popular and long-standing targets in surface science. After a long controversy on its atomic arrangement, the Honeycomb-Chained-Triangle (HCT) model, first proposed by Takahashi et al.¹, is now widely accepted to be consistent with most of previously reported experimental and theoretical results². The HCT model, as shown in Fig. 1, has $p31m$ symmetry. In the top layer, Ag adsorbates form chained triangles that are arranged in a honeycomb pattern, which can be revealed in STM images. Due to a mirror plane as shown in Fig. 1, these Ag triangles are equivalent and have same size. Si trimers in the second layer are centered around T_4 sites.

But, very recently, Aizawa et al.³ performed first-principles calculations with a structural optimisation upon the $\sqrt{3}\times\sqrt{3}$ -Ag structure again, and found that the HCT is not the ground-state structure. So-called Inequivalent Triangle (IET) structure having $p3$ symmetry, in which a mirror symmetry in the HCT structure is broken, is found to be more energetically favourable. This prediction is confirmed by STM observations at 62 K^{3,4}. The IET structure is characterised by twisted Si trimers and different-sized Ag triangles. The different size of the two Ag triangles in the unit cell makes a difference in the empty-state STM images. Therefore a honeycomb pattern of the HCT structure at room temperature (RT) becomes a hexagonal-lattice pattern which was actually observed by STM at low temperature (LT)^{3,4}. The HCT structure is expected stable around RT and above, a phase transition from the HCT to the IET structure should proceed at LT, however, the nature of this transition is still unclear.

To determine the atomic structure of the IET $\sqrt{3}\times\sqrt{3}$ -Ag surface and establish the nature of the phase transition at LT, we have investigated this surface both at RT and LT using surface x-ray diffraction. After preparation in an ultra-high-vacuum (UHV) system the sample possess a very sharp $\sqrt{3}\times\sqrt{3}$ LEED pattern. The data sets were measured at the BW2 beamline at HASYLAB. By averaging equivalent reflections ($3m$ symmetry) systematic errors of 8.6% (at RT) and 5.5% (at LT) in $|F|^2$ were determined for the in-plane data sets. Some initial structure refinement has been done on this system. As shown in Fig. 2, the HCT model gave a reasonable approach for the in-plane data set measured at RT, but not good for the LT in-plane data ($\chi^2 \geq 30$). The CTRs measured both at RT and LT can be fitted very well using the HCT model, but the in-plane atom positions in the IET model need to be further adjusted. The structural refinement and further investigation are being carried out. This work was supported by the BMBF (05 SE8GUA6), the Danish Research Council (Dansync) and the European Commission IHP programme "Access to Research Infrastructures" (HPRI-CT-1999-00040).

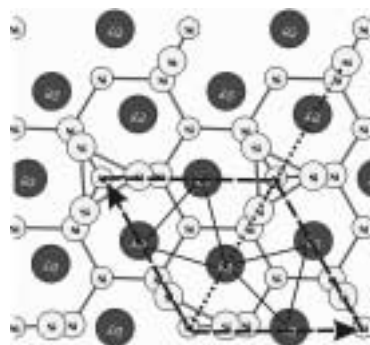
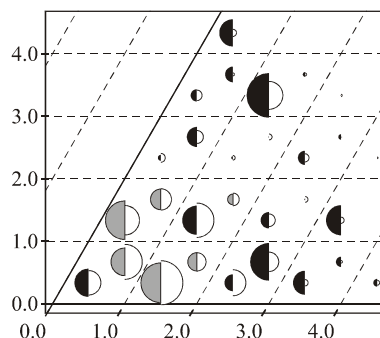


Fig. 1 (left): HCT model. The unit cell is indicated by dashed lines, the mirror line by dotted lines. Two Ag triangles are shown as well.

Fig. 2 (right): The initial fitting of the in-plane data measured at RT. The filled and open semicircles represent measured and calculated intensities. Grey/White circles have been scaled with a factor of 0.1.



¹ T. Takahashi, S. Nakatani, N. Okamoto, T. Ishikawa, S. Kikuta, *Jpn. J. Appl. Phys.* **27**, L753 (1988); *Surf. Sci.* **242**, 54 (1991); T. Takahashi, S. Nakatani, *Surf. Sci.* **282**, 17 (1993).

² V. G. Lifshits, A. A. Saranin, A. V. Zotov, *Surface Phases on Silicon*, Wiley, Chichester (1994).

³ H. Aizawa, A.A. Sarin and A.V. Zotov, *Surf. Sci.* **282**, 17 (1993).

⁴ N. Sato, T. Nago and S. Hasegawa, *Surf. Sci.* **442**, 65 (1999).

2.5.3. Low-temperature structure of indium quantum chains on silicon

C. Kumpf, M. Nielsen, R. Feidenhans'l, K. Bechgaard, *Condensed Matter Physics and Chemistry Department, Risø National Laboratory, Denmark*, O. Bunk, J. H. Zeysing, Y. Su and R. L. Johnson, *II. Institut für Experimentalphysik, Universität Hamburg, Germany*
e-mail: christian.kumpf@risoe.dk

Adsorption of indium on Si(111) produces a variety of surface reconstructions that are semiconducting for coverages below one monolayer and metallic at larger coverages. At the borderline between the two regions a (4×1) phase occurs. Although this phase has been investigated with a variety of techniques over the last thirty years the definitive structural model was only established recently, using surface x-ray diffraction¹. The surface structure consists of quasi one-dimensional indium chains, separated from each other by chains of silicon atoms. It was reported that the system undergoes a reversible phase transition accompanied by a one dimensional charge density wave (1D CDW) along the indium chains at approximately 100 K². Reflection high-energy electron diffraction experiments revealed that – due to the phase transition – the periodicity of the surface reconstruction doubles along the chains with little correlation between the chains. Since half-order streaks rather than peaks were observed in the direction along the chains the new phase was called a (4×"2") reconstruction and it was speculated that the true LT ground state might be a well-ordered (8×2) phase with the CDWs locked in phase².

To establish the nature of the phase transition and determine the geometrical structure of the ground state we have investigated the LT phase using surface x-ray diffraction. The results are published in Ref.³. The sample was prepared using standard procedures in an ultra high vacuum (UHV) system equipped with extensive sample characterization facilities. It was transferred to a UHV-cryostat and after cooling to 20 K an extended data set (230 non-equivalent in-plane reflections, two crystal truncation rods, eight fractional-order rods) was measured at the BW2 beamline. The half-order reflections in the *k*-direction were never sharp, even at low temperatures, but only streaks as in Ref.². Strong eighth-order peaks were observed along the *h*-direction so the measured data set had an (8×1) symmetry.

We used the room temperature reconstruction as a starting model. Refining the positions of the top layer In and Si atoms and two double-layers of the substrate as well as the Debye-Waller (DW) factors of the indium atoms results $\chi^2 = 2.87$. The corresponding structural model is shown in Fig. 1. The final atomic positions of the LT reconstruction (red and blue circles) are shown as well as the positions in the RT model (open circles). It can be seen that the phase transition consists mainly of a pairing effect of the In atoms labelled 1,2 and 7,8. This causes a formation of indium trimers (atoms 1-3 and 6-8) and a doubling of the unit cell in *b*-direction along the chains. The atomic distances within these trimers are between 2.8 Å and 3.1 Å, close to the indium covalent bond length of 2.9 Å. The other two indium atoms 4 and 5 are located very close to T1 on-top positions above the uppermost silicon bulk atoms. The silicon atoms in the top layer (light blue circles) show no discernible in-plane displacements from their RT positions, but a perceptible out-of-plane buckling. The (8×2) unit cell can be subdivided in two (4×2)-subcells containing the indium atoms 1-8 and 1'-8', respectively, as shown in Fig. 1. The doubling of the (4×1) RT unit cell in *a*-direction (perpendicular to the chains) is caused by the appearance of a glide line which maps one subcell (atoms 1-8) on the other (atoms 1'-8'). Sharp eighth-order peaks indicate a strong inter-chain coupling of the displacements between the neighboring chains in this direction. A correlation length of ≈ 240 Å can be derived for this transverse inter-chain coupling from the peak width of the eighth-order reflections.

¹ O. Bunk, G. Falkenberg, J. H. Zeysing, L. Lottermoser, R. L. Johnson, M. Nielsen, F. Berg-Rasmussen, J. Baker, and R. Feidenhans'l, *Phys. Rev.* **B59**, 12228 (1999).

² H. W. Yeom, S. Takeda, E. Rotenberg, I. Matsuda, K. Horikoshi, J. Schaefer, C. M. Lee, S. D. Kevan, T. Ohta, T. Nagano, and S. Hasegawa, *Phys. Rev. Lett.* **82**, 4898 (1999).

³ C. Kumpf, O. Bunk, J. H. Zeysing, Y. Su, M. Nielsen, R. L. Johnson, R. Feidenhans'l and K. Bechgaard, *Phys. Rev. Lett.* **85**, 4916 (2000).

The structural features seen in the adlayer at LT have been suggested to be the result of a CDW condensation related to a Peierls instability of the quasi-1D indium chains². Now we proceed to analyze such a model. A priori it is expected that 1D fluctuations will give rise to diffuse lines related to twice the Fermi wave vector $2k_f$ at temperatures well above the transition, indicating a change of the translation period (e.g. a doubling of the unit cell) in the chain direction. At lower temperature close to the transition, 2D (or 3D) correlations with arbitrary wave vectors are expected to break up the diffuse lines, which then condense into (isotropic) spots indicating the formation of a fully-developed superstructure. The diffuse lines observed at high temperature normally have correlation lengths similar to that of the underlying surface lattice (i.e. widths similar to the fractional-order spots). For the phase transition under study a different behaviour is observed. Around 20 K a good transverse correlation has developed giving rise to a doubling of the unit cell in the direction perpendicular to the chains. But even at 20 K along the chains streaks are observed with a scattering vector of $k = \frac{1}{2}$ indicating that the (8×2) superstructure is not fully developed and that the charge density fluctuations have not condensed. An analysis of the band structure indicates that a gap or pseudo-gap with that wave vector does exist². The diffraction results are not compatible with a 1D CDW condensation, but the simple Peierls picture could be modified by the fact that three Fermi vectors are needed to describe this system.

Financial support from the Danish Research Council through Dansync, the BMBF (project 05 SE8 GUA6), the Volkswagen Stiftung and the IHP programme "Access to Research Infrastructures" of the European Commission (HPRI-CT-1999-00040) is gratefully acknowledged.

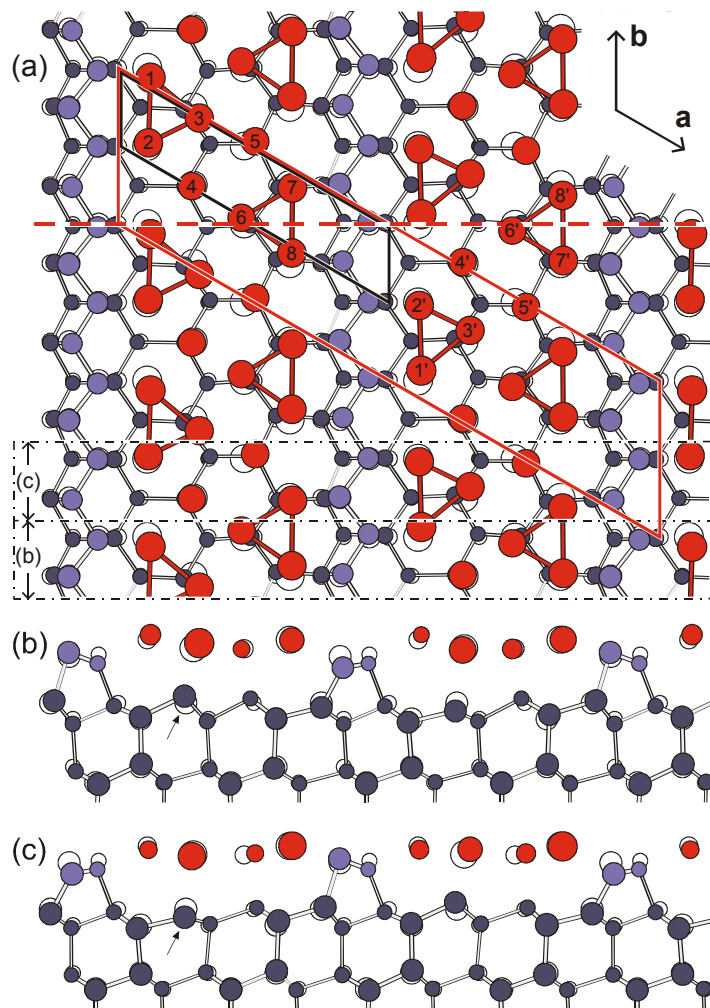


Fig. 1. Model of the Si(111)-(8x2)-In low temperature reconstruction.

(a) top and (b, c) side views. Indium, silicon bulk and silicon top layer atoms are shown as red, dark blue and light blue circles, respectively. Open circles mark the atomic positions of the room temperature (4×1) structure. The (4×1) and (8×2) unit cells are indicated by red and black solid lines. The dashed line indicates the glide line. The regions corresponding to the side views (b,c) are indicated by dash-dotted lines.

2.5.4. Thin bonded Silicon wafers with penetrating strain fields

M. Nielsen, R. Feidenhans'l, C. Kumpf, *Condensed Matter Physics and Chemistry Department, Risø National Laboratory, Denmark*, P. B. Howes, *Department of Physics and Astronomy, University of Leicester, Leicester, England*, F. Grey, M. Poulsen, *Mikroelektronik Centret, Technical University of Denmark, Denmark* and J. Vedde, *Topsil Semiconductor Materials A/S, Denmark*
e-mil: christian.kumpf@risoe.dk

We have studied the interface of thin SOI Si(100) wafers, fusion-bonded to Si(100) substrate wafers. By x-ray diffraction strain fields arising from the misfit dislocations were measured for small twist angles with special emphasis on how this strain penetrates the thin top crystal all the way to the top surface.

For a given twist angle the interface strain field arises from a square net of screw dislocations giving rise to a diffraction signal in the form of satellites around the Bragg points of both crystals. For top crystals, whose thickness is comparable to the period of the dislocation net, the strain is affected by mirror dislocations above the outer surface. Such effects are detected by measuring the line shape of satellite reflections in the direction normal to the surface and this is illustrated in the left panel figure below.

Although the bonded Si(100) wafers ideally have an interface characterized by one extended net of screw dislocations the real samples in addition have a few edge dislocations due to finite miscut angles or finite curvature of bonding surfaces. Such edge dislocations break the lattice of the screw dislocation and neighbouring terraces have a phase shift of π . In samples with small miscut the edge dislocations and thus the terraces will constitute a disordered system. These properties are directly observed in the diffraction results where half of the satellite reflections have destructive interference from neighbouring terraces and half-constructive, and this is illustrated in the right panel of Fig. 1.

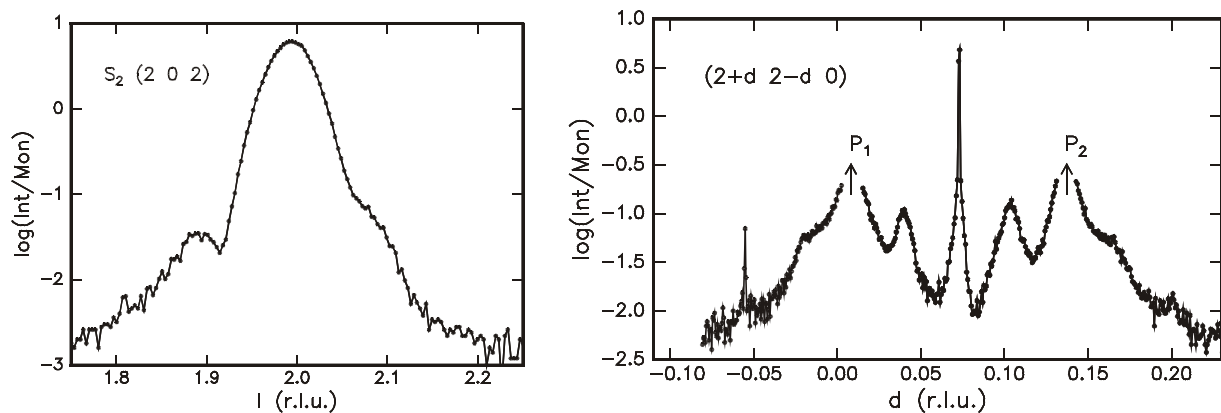


Fig. 1. Left panel: Satellite diffraction profile next to the (2 0 2) Bragg peak of the top crystal. The intensity in the wings, most visible in left wing, is due to strain field penetrating entire top crystal, 50 Å thick. Right panel: Lateral scan through (2 2 0) reflections from both crystals, (P_1 and P_2), with three satellite reflections in between. The central satellite reflects constructive the two other destructive interference of scattering from neighbouring terraces.

2.5.5. Growth of Si cluster on CaF₂ films

J. Wollschläger, M. Bierkandt, C. Deiter, M. Grimsehl, A. Klust, *Institut für Festkörperphysik, Universität Hannover, Germany*, Th. Schmidt, J. Falta, *Institut für Festkörperphysik, Universität Bremen, Germany*, Y. Su, *II. Institut für Experimentalphysik, Universität Hamburg, Germany*, C. Kumpf and R. Feidenhans'l, *Condensed Matter Physics and Chemistry Department, Risø National Laboratory, Denmark*
 e-mail: christian.kumpf@risoe.dk

Insulated nanocrystalline semiconductor films offer an enormous potential in nanoelectronics due to quantum effects. For instance, it has been demonstrated that Si clusters embedded in CaF₂ films show electroluminescence¹. Furthermore, it has been shown for nanocrystalline Si/CaF₂ multilayers that the photoluminescence signal has a blue shift with decreasing Si film thickness². These effects have been discussed in the context of a possible transition from the indirect band gap for bulk Si to a quasi-direct band gap for small Si clusters³. We investigated the Si clusters grown by MBE of Si on smooth CaF₂ films of 1.5nm (5TL=triple layer) thickness at 500°C. The Si film thickness ranges from 3nm (10BL=bi layer) to 12nm (36BL). The double layer structures were grown in a MBE chamber at HASYLAB and immediately transferred to the diffractometer at BW2 for the SXRD experiments.

Figure 1 shows the reflectivity and the specular intensity of the (00) rod close to the first Bragg condition for the 36BL thick Si film. Obviously, strong oscillations are observed demonstrating that the height of the different nanocrystallites is very similar so that the film has little roughness. Furthermore the strong oscillations of the (00) rod close to the first Bragg peak ($l=1$) demonstrate the crystallinity of the Si clusters. In addition, we measured the CTR intensities of the (01), (10) and (11) rod (not shown). From these experiments we conclude that Si clusters grow with A-orientation with respect to the CaF₂ lattice while the CaF₂ film is grown with B-orientation on the Si(111) substrate.

Profiles of the (11) rod for different in-plane conditions ($l=0.04 \dots 0.10$) are presented in Fig. 2. Under these scattering conditions diffuse scattering coming from the Si clusters can be distinguished easily from a strong component caused by the Si(111) substrate. They have the same (lateral) lattice constant as the Si bulk as demonstrated by the identical peak positions. We attribute this effect to the small CaF₂ film thickness provoking that CaF₂ is grown pseudomorphically. The halfwidth of the diffuse scattering can be analysed with respect to the average cluster size, resulting in 18nm for the film presented here. We observed larger clusters for higher deposition temperatures. This study shows that detailed information about the morphology of nanocrystalline Si films can be obtained using SXRD.

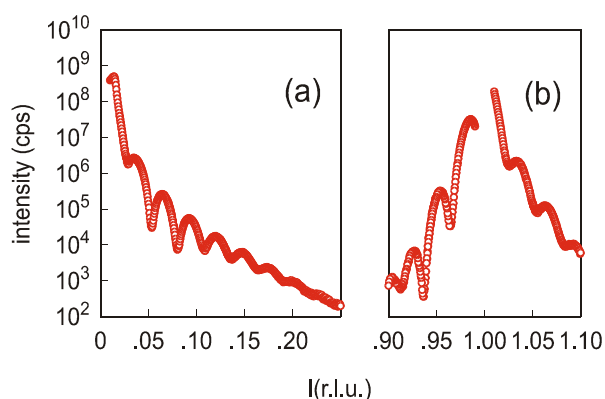


Fig. 1. Intensity of the (00) rod for 36BL Si film grown at 500°C on 5TL CaF₂ films deposited previously at the same temperature: (a) reflectivity, (b) CTR close to first Bragg condition.

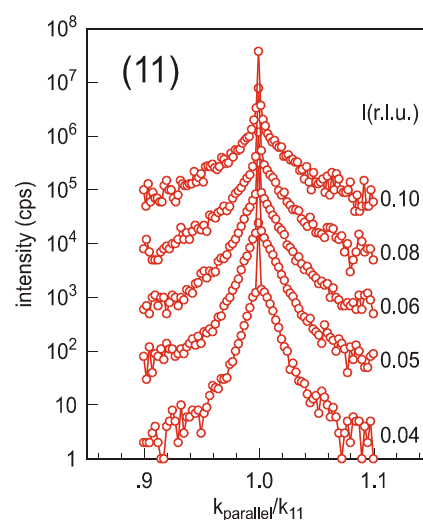


Fig. 2 . In-plane profiles of the (11) rod for the same film.

¹ M. Watanabe, T. Matsunuma, T. Maruyama and Y. Maeda, *Jpn. J. Appl. Phys.* **37**, L591 (1998).

² A.B. Filonov, A.N. Kholod, V.A. Novikov, V.E. Borisko, L. Vervoort, F. Bassani, A. Saul and F. Arnaud d'Avitaya, *Appl. Phys. Lett.* **70**, 744 (1996).

³ S. Ossicini, A. Fasolino, and F. Bernardini, *Phys. Rev. Lett.* **73**, 1044 (1994).

2.5.6. Structure of CaF₂ films on Si(111) examined by SXRD

J. Wollschläger, M. Bierkandt, C. Deiter, M. Grimsehl, A. Klust, *Institut für Festkörperphysik, Universität Hannover, Germany*, Th. Schmidt, J. Falta, *Institut für Festkörperphysik, Universität Bremen, Germany*, Y. Su, *II. Institut für Experimentalphysik, Universität Hamburg, Germany*, C. Kumpf and R. Feidenhans'l, *Condensed Matter Physics and Chemistry Department, Risø National Laboratory, Denmark*
e-mail: christian.kumpf@risoe.dk

One important ingredients for building nanoelectronic devices are ultrathin insulating films which may serve as tunneling barriers, e.g. for Resonant Tunneling devices¹. For this purpose insulating films have to have a homogeneous thickness of 1-2nm on a lateral scale of several μm . One well-suited material fulfilling these demands is CaF₂ due to its small lattice mismatch of less than 0.5% with respect to Si at room temperature. Therefore, we performed Surface X-Ray Diffraction (SXRD) experiments on CaF₂ films in the thickness range 3-12TL where 1TL denotes one molecular CaF₂ layer consisting of one Ca layer embedded in 2 F layers. The films were deposited at 500°C where the films grow in the layer-by-layer growth mode as we proved before by UHV atomic force microscopy (AFM)^{2, 3}. For this study, the CaF₂ films were grown on Si(111) samples in the MBE chamber at HASYLAB and transferred in a baby chamber under UHV condition to the beamline BW2 at HASYLAB where the SXRD experiments were performed on different crystal truncation rods (CTR).

Previous SXRD experiments on thicker CaF₂ films grown at higher temperature were performed by other groups. Analysing the (00)-CTR Lucas *et al.* reported different interface spacing between the CaF₂ film and the Si(111) substrate depending on the film preparation⁴. Later the same group showed that the increasing interface spacing is caused by ageing effects probably due to modifications by ambient air although the films were capped by amorphous Si⁵. Therefore we carried out our experiments immediately after film preparation. Occasionally we controlled the (01)-CTR after one day of experiments and did not find any changes with respect to the same CTR measured before.

Fig. 1 presents (10)-CTRs from 5TL and 12TL thick films. The CTR data are obtained from background subtracted profile measurements (ω -scans) of the CTRs. The CTR intensities show Bragg peaks of the CaF₂ films in addition to the x-ray signal from the Si substrate (arrows). The positions of the CaF₂ Bragg peaks marked by B yield that the films are grown in B-orientation (film structure rotated by 180°C with respect to the Si substrate). Especially the 5TL film has well pronounced fringes due to the finite film thickness demonstrating that the films are very smooth with only little thickness variation.

Analysing the profile of the (11)-rod of the 5TL thick CaF₂ film for in-plane conditions shown in Fig.2 we observe three contributions to the diffracted x-ray beam which are attributed on one hand to large terraces and small step bunches of the Si substrate and on the other hand to the slightly relaxed CaF₂ film. We conclude typical island sizes of more than 100nm in agreement with our previous AFM experiments^{2, 3}. In addition, these scans demonstrate that the films are almost perfect pseudomorphically grown. The lateral relaxation is less than 0.05% compared to the lattice mismatch of 0.5% at room temperature for the bulk structure. In addition, we analysed the spacing between the B-orientation Bragg peaks of the CaF₂ film (cf. the peaks marked by B in Fig. 1). The distance depends on the film thickness. Thinner films have increased molecular layer spacing which approach asymptotically the bulk value.

Finally, an additional feature of the 12TL film (in comparison with thinner films) is the strong intensity maximum at $l=2/3$ (cf. arrow marked by A in Fig. 1). We attribute this feature to CaF₂ domains with A-orientation. The half width of this feature is larger than the half width of the Bragg

¹ T. Suemasu, M. Watanabe, J. Suzuki, Y. Kohno, M. Asada, and M. Suzuki, *Jpn. J. Appl. Phys.* **33**, 57 (1994).

² J. Wollschläger, H. Pietsch, and A. Klust, *Appl. Surf. Phys.* **130-132**, 29 (1998).

³ R. Kayser, Diploma thesis, Universität Hannover (1999).

⁴ G. A. Lucas, G. C. L. Wang, and D. Loretto, *Phys. Rev. Lett.* **70**, 1826 (1993).

⁵ G. A. Lucas, D. Loretto, and G. C. L. Wang, *Phys. Rev.* **B50**, 14340 (1994).

peaks due to B-orientation. Therefore we conclude that the A (nano-)crystallites are thinner than the film in average. Analysing the low intensity of the A-Bragg peaks by kinematic diffraction calculations we conclude that less than 10% of the film have A orientation. This result is in good agreement with previous XSW experiments we performed at HAYLAB. Probably the A-crystallites are formed at the interface and overgrown in later growth stages. The complete CTR analysis to determine relaxation effects, interface spacings etc. are still under work.

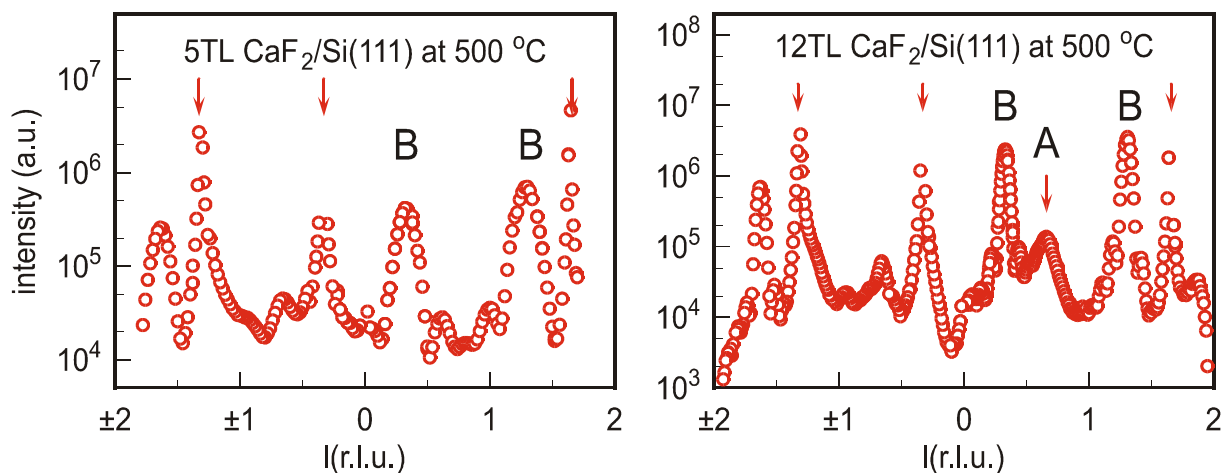


Fig. 1. (10)-CTRs of two CaF_2 films grown at 500°C . The arrows mark the Si Bragg peaks. The additional structure is due to the CaF_2 films. The peaks marked by B are the Bragg peaks of the B-oriented CaF_2 film. The A marked arrow points to an additional structure for the 12TL film which is not resolved for the 5TL film. This structure is attributed to the A-orientation of small parts of the CaF_2 film.

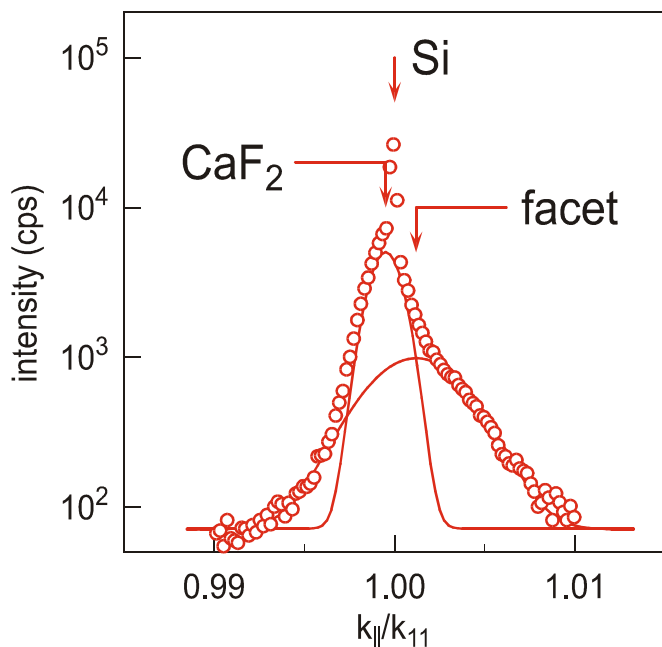


Fig. 2. Radial profile of the (11)-rod at $l=0.14$. The profile has three contributions. The narrow peak at the left (marked by CaF_2) is attributed to the slightly relaxed CaF_2 film. The peak at the centre (marked by Si) is due to the Si substrate. The broad peak at the right (marked by facet) is due to step bunches produced during the preparation of the Si substrate.

2.5.7. Subsurface dimerization in III-V compound semiconductor (001)-surfaces

C. Kumpf, D. Smilgies, E. Landemark, M. Nielsen, R. Feidenhans'l, *Condensed Matter Physics and Chemistry Department, Risø National Laboratory, Denmark*, O. Bunk, J. H. Zeysing, Y. Su, R. L. Johnson, *II. Institut für Experimentalphysik, Universität Hamburg, Germany*, J. Zegenhagen, *European Synchrotron Radiation Facility, France*, L. D. Marks, *Department of Material Science and Engineering, Northwestern University, USA* and D. Ellis, *Department of Chemistry, Northwestern University, USA*

e-mail: christian.kumpf@risoe.dk

The (001)-surfaces of III-V compound semiconductors show a wealth of surface reconstructions that play an important role in both homo and heteroepitaxial growth. It is generally believed that the basic building blocks in these reconstructions consist of group III or group V dimers. For the group V rich surfaces, group V dimers have been clearly identified by scanning tunnelling microscopy (STM). Since the first STM study on the GaAs(001)-c(8×2) surface¹, group III dimers have been assumed to be the primary structural element on group III rich (001) surfaces. However, in STM it has not been possible to uniquely identify the features attributed to dimers as really being made up of two atoms. We show that dimers at the surface are *not* the central element of the group III rich surfaces but sub-surface dimerization in the second bilayer, accompanied by linear arrangement of group III atoms in the top layer^{2, 3}. Therefore a substantial rethinking of the physics of III-V compound semiconductor surfaces is required.

Surface x-ray diffraction data sets (in-plane and out-of-plane) have been measured through the years at beamline BW2 at HASYLAB on three sample types, GaAs, InAs and InSb. By averaging equivalent reflections using a *c*2mm symmetry systematic errors in $|F|^2$ of 7.2% (GaAs), 7.8% (InSb) and 10.2% (InAs) were determined for the in-plane data. The InAs in-plane data set consisted of (4×1) subcell reflections only: eighth-order reflections belonging to the c(8×2) cell were smeared out so that their integrated intensities could not be evaluated. The map of the interatomic vectors, the so-called Patterson function, did not show any sign of group III dimers oriented along the '2' axis³.

A starting model for the refinement was found using direct methods in both two dimensions and in three. Contrary to prior models for the structure, which contain indium dimers in the top layer, we found an indium dimer in the second bilayer and rows of In atoms along $[110]_{\text{bulk}}$. Only with a reduced occupation an indium dimer (site In2d, see Fig. 1) occurs within the In row. For GaAs and InSb the result of the least-squares refinements were close to the starting model, i.e. to the direct methods result. Both data sets were fitted with the same basic model with different (isotropic) DW factors and occupations for some atomic sites. Although the starting model was derived by direct methods using only fractional-order reflections, the model was able to fit the CTR's, further evidence for the correctness of the model. Values for χ^2 of 2.2 and 2.4 were obtained for GaAs and InSb, respectively. Fig. 1 shows the topmost layers of the full InSb structure after refinement. The InAs data set did not behave as smoothly in the refinement, but showed some ambiguity in the position of the In1 site indicated by large DW factors. Using anisotropic DW factors for this site revealed a strong in-plane disorder which explains the diffuse eighth-order reflections found for this sample. More details on all three models will be published in ref. 3.

This new model contains several original features and differs significantly from all other models proposed for this system to date. To our knowledge it is the first time that one unique model has been found for three types of the group-III rich (001) surface of the III-V compound semiconductors. The most significant new feature is the sub-surface dimerization of the In (Ga) atoms (labelled 6 in Fig. 1) in the second bilayer with an In-In distance of 2.89 Å (2.64 Å for GaAs) which – recently and

¹ D. K. Biegelsen, R. D. Bringans, J. E. Northrup and L.-E. Swartz, *Phys. Rev. B* **41**, 5701 (1990).

² C. Kumpf, L. D. Marks, D. Ellis, D. Smilgies, E. Landemark, M. Nielsen, R. Feidenhans'l, J. Zegenhagen, O. Bunk, J. H. Zeysing, Y. Su and R. L. Johnson, *Phys. Rev. Lett.*, Subsurface dimerization in III-V compound semiconductor (001)-surfaces, *Phys. Rev. Lett.*, in print.

³ C. Kumpf, D. Smilgies, E. Landemark, M. Nielsen, R. Feidenhans'l, O. Bunk, J. H. Zeysing, Y. Su, R. L. Johnson, L. Cao, J. Zegenhagen, B. O. Fimland, L. D. Marks and D. Ellis, Subsurface dimerization in III-V compound semiconductor (001)-surfaces, in preparation.

independently from us – has been reported by Lee *et al.*¹ as well. Note that it is the ordering of these dimers that makes up the $c(8 \times 2)$ unit cell. This explains why the $c(8 \times 2)$ ordering has been so difficult to visualize by STM while it was easily recognized in LEED. Furthermore two different group III-chains along the $[110]$ direction occur (In2-In3 and In1-In1), which are shifted by $(0,0.5)_{\text{LEED}}$ relative to each other and hence have a different registry to the substrate. A small buckling (i.e. a different z -coordinate) of 0.1 \AA of the sites In2 and In3 occurs within these chains. This is the only effect in the top layer contributing to the $c(8 \times 2)$ structure. The additional defect site In2d appeared in some of the direct methods maps and was statistically significant albeit of minor importance in the InSb model. In the GaAs structure, where the sites Ga2 and Ga3 (equivalent to In2 and In3 in InSb) are absent, this dimer plays a more pronounced role and occurs with an occupancy of 63%. The second Ga chain (In1 site) exhibits a smaller occupancy compared to the InSb structure but otherwise appears unchanged. This leads to the conclusion that group-III dimerization in the top layer is favored in GaAs.

This work was supported by the Danish Research Council through Dansync, the BMBF (project 05 SE8 GUA6), the Volkswagen Stiftung and the IHP programme "Access to Research Infrastructures" of the European Commission (HPRI-CT-1999-00040).

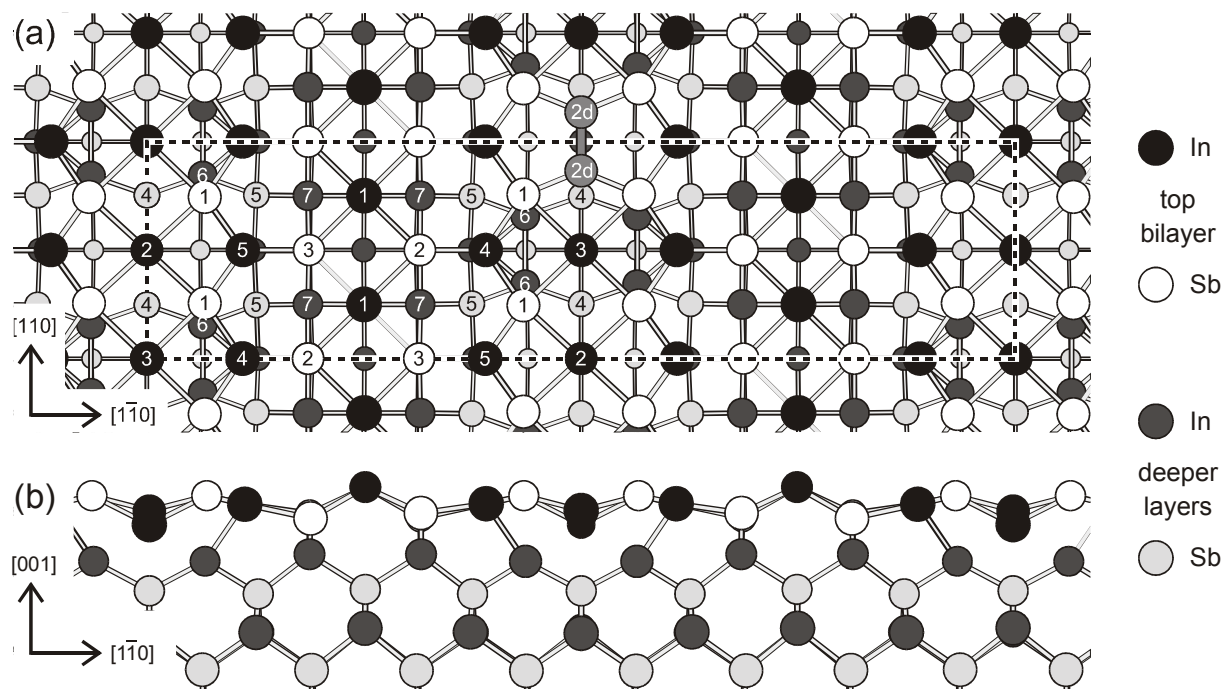


Fig. 1. The structural model viewed from above (a) and from the side (b). Top layer In and Sb atoms are shown as filled and open circles, those in deeper layers are dark- and light-grey. The main atoms in the structure are labeled and the dimer site In2d is shown at one location. Bonds are indicated to assist viewing rather than to denote "true" chemical bonds.

¹ S.-H. Lee, W. Moritz and M. Scheffler, Phys. Rev. Lett. **85**, 3890 (2000).

2.5.8. Ordering of regio-irregular polyalkylthiophenes by doping in solution prior to film formation

M. M. Nielsen, K. Bechgaard, C. Kumpf, R. Feidenhans'l, M. Nielsen, *Condensed Matter Physics and Chemistry Department, Risø National Laboratory, Denmark*, J. J. Apperloo and R. A. J. Janssen, *Laboratory of Macromolecular and Organic Chemistry, University of Technology, Eindhoven, The Netherlands*

e-mail: martin.m.nielsen@risoe.dk

Many applications of conjugated polymers, such as light-emitting diodes, field-effect transistors, or photovoltaic cells, require that charges are transported through a polymer layer. The charge-carrier mobility of solution-processed conjugated polymers is generally limited by the hopping process between polymer chains in disordered regions of the material. For an efficient charge transport, it is therefore desirable both that the polymer backbones possess a high degree of intrachain order and that different chains are favourably aligned to achieve a large overlap of the π -orbitals on adjacent chains. Recently, it was shown that a high degree of regioregularity, (*i.e.*, the percentage of stereoregular head-to-tail (HT) attachment of the alkyl side chains to the 3-position of the thiophene rings in the substitution pattern of poly(3-alkylthiophenes)), leads to more ordered microstructures due to supramolecular self-organization and to higher field-effect mobilities^{1,2,3}.

Here, we describe how high molecular weight regio-irregular poly(3-alkylthiophene)s, which lack an intrinsic tendency to form supramolecular well-ordered structures, due to an unfavourable substitution pattern, can attain a favourable alignment in a film simply by oxidation in solution prior to film formation. Oxidation of the polymers in solution was accomplished by adding solutions of thianthrenium perchlorate or nitrosonium tetrafluoroborate (NOBF₄) from a gas-tight syringe. Films containing neutral polymers were spin-cast from ~2 mg/ml polymer in dichloromethane. Films containing oxidised polymers were spin-cast under inert atmosphere from equally concentrated solutions, to which very small amounts of a saturated solution of NOBF₄ in acetonitrile were added. The thin polymer films were dedoped by exposing them for about 30 s to hydrazine vapour, and subsequently washed with acetonitrile to remove any salts present. UV-vis/near-IR spectra were recorded using a Perkin Elmer Lambda 900 spectrophotometer equipped with an Oxford Optistat cryostat for variable temperature experiments. The temperature was kept constant within ± 0.3 K and spectra were corrected for volume changes.

In order to directly address the self assembled regions of the film, synchrotron X-ray diffraction measurements were performed at the BW2 beam line in HASYLAB at DESY in Hamburg, on films spin-cast from a solution containing neutral P3HT (poly(3-hexylthiophene), $M_w = 175$ kg/mol, $D = 2.5$, regioregularity ≈ 81 %) as well as a film cast from a solution of oxidised P3HT, which was then reduced with hydrazine. The samples were mounted on the diffractometer in a capton chamber, which was flushed with He to minimise air scattering and beam-damage during measurements in the highly intense synchrotron beam. Figure 1 shows the obtained diffraction patterns for (pseudo)-out-of-plane (a) and in-plane (b) scattering geometries, respectively, and the inset of Fig. 2b shows the UV absorption spectra of the corresponding films. The diffraction spectra are corrected for polarisation and geometric effects. Using a fixed, grazing incidence angle of 0.17° , above the angle for total reflection from the film, but below the critical angle for the substrate, the scattering from the substrate is reduced relative to the scattering of the film. (Note that the increase around a scattering vector of 1.5 \AA^{-1} and above is partly due to scattering from the glass substrate). In these experiments, the (100) reflection corresponds to the lamella layer structure (16.5 \AA) and the (010) reflection to the π - π stacking distance (3.85 \AA)⁴. As demonstrated in Fig. 1a, the crystallinity of the oxidised-reduced P3HT film is much higher than of the film cast from a neutral P3HT solution: The (100) reflection is more intense and pronounced (200) and (300) higher order reflections can be observed. Interestingly, the oxidised-reduced film also shows a pronounced degree of preferential orientation as evident from the

¹ Z. Bao, A. Dodabalapur and A. Lovinger, *Appl. Phys. Lett.*, **69**, 4108 (1996).

² H. Sirringhaus, N. Tessler and R. H. Friend, *Science*, **280**, 1741 (1998).

³ H. Sirringhaus, P. J. Braun, R. H. Friend, M. M. Nielsen, K. Bechgaard and B. M. W. Langeveld-Voss, A. J. H. Spiering, R. A. J. Janssen, E. W. Meijer, P. Herwig and D. M. de Leeuw, *Nature*, **401**, 685 (1999).

⁴ E. J. Samuelsen and J. Mårdalen, in *Handbook of Organic Conductive Molecules and Polymers*, **3** (Ed: H. S. Nalwa), Wiley, Chichester (1997).

relatively large in-plane component of the (010) peak (Fig. 1b) and correspondingly large (pseudo)-out-of-plane (100) peak (Fig. 1a). This means that the number of self-organised domains having an orientation where the (010) axis (the π - π stacking distance) is along the sample surface, is much larger than the number of self-organised domains having a random orientation of the (010) axis. Furthermore, the width of the diffraction features, yields estimated sizes of the self-organised domains of approximately 100 Å. These findings confirm the observation of increased structural order, inferred from UV-vis spectra, on poly(3-octylthiophenes) films prepared via the doping-dedoping procedure¹[5].

Recently, an orientation of the π - π bond along the film surface, like the orientation induced by the doping-dedoping procedure was shown to be favourable for obtaining high mobilities in FET devices [3]. To test the transport properties, we measured the charge-carrier mobility of P3HT in FETs prepared with the doping±casting±dedoping procedure. Although good FET characteristics (high on/off ratio, no ionic conductivity) were obtained, and the procedure is compatible with device preparation, the mobility ($\mu_{\text{sat}} = 1\pm 3 \times 10^{-4} \text{ cm}^2 \text{ V}^{-1} \text{ s}^{-1}$) did not improve significantly.

The authors thank Dr. Bea Langeveld-Voss and Ms. Jolanda Spiering for providing the poly(3-alkylthiophene) samples and Mr. Kornel Hoekerd(TNO Industries) for mobility measurements. Financial support from the European Commission (Esprit 24793) and the Training and Mobility of Researchers program is acknowledged.

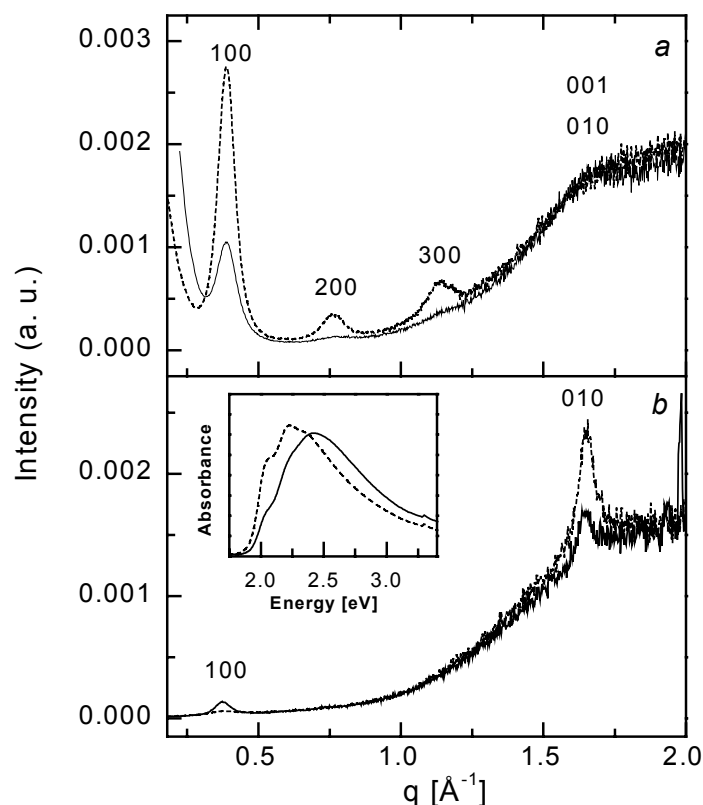


Fig. 1. Pseudo-out-of-plane (a) and in-plane (b) X-ray scattering intensities as a function of the scattering vector q for films spin-cast from neutral P3HT solutions (solid) and from slightly doped P3HT solutions after dedoping (dotted). Absorption spectra of the same films are shown in the inset. The spectra are corrected for geometric and polarisation factors.

¹ J. J. Apperloo, R. A. J. Janssen, M. M. Nielsen and K. Bechgaard, *Adv. Mat.* **12**, 1594 (2000).

2.5.9. Structure of poly-dodecyl-bithiophene films: polymer electronics materials with increased oxidation potential

M. M. Nielsen, C. Kumpf, M. Nielsen, R. Feidenhans'l, K. Bechgaard, *Condensed Matter Physics and Chemistry Department, Risø National Laboratory, Denmark*, D. R. Greve, R. A. J. Janssen, *Laboratory of Macromolecular and Organic Chemistry, University of Technology, Eindhoven, The Netherlands* and M. Shkunov, *Cavendish Laboratory, University of Cambridge, Cambridge, UK*
e-mail: martin.m.nielsen@risoe.dk

The long-term stability of electronic devices based on poly(3-alkylthiophene)s, such as light-emitting diodes, or Field Effect Transistors (FETs), is strongly influenced by ambient oxygen and light. Hence by creating polymers with a higher oxidation potential, one could hope to obtain a candidate material for more stable electronic devices.

The conjugated polymer poly(4-dodecyl-[2,2']bithiophene) PDBT was prepared as outlined in Fig. 1. The synthesis starts with a selective α metallation of 3-dodecylthiophene which is transmetallated *in situ* to 4-dodecyl-2-zinciothiophene. This intermediate is cross-coupled with 2-iodothiophene using Ni(dppp)Cl₂ as the catalyst, to give 4-dodecyl-[2,2']bithiophene. Selective bromination with NBS in THF results in the monomer 5-bromo-4-dodecyl-[2,2']bithiophene. Polymerization of this monomer was achieved by the McCullough method. The polymer was purified by a series of Soxhlet extractions (methanol, hexane, dichloromethane and chloroform). The chloroform fraction was used for the investigations presented here.

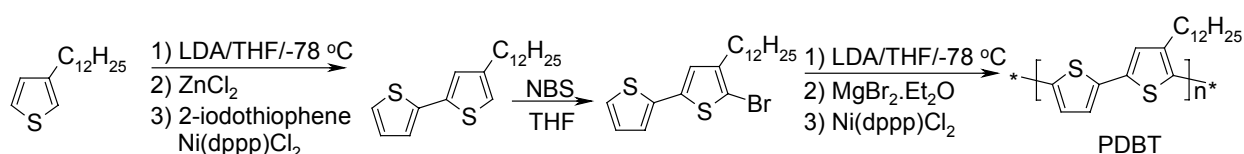


Fig. 1. Synthesis of PDBT.

From ¹H NMR in chlorobenzene (80° C) approximately 95 % Head-Tail couplings could be determined. PDBT strongly aggregates in common organic solvents like chloroform and toluene at room temperature. Variable temperature UV-vis spectra in chloroform are shown in Fig. 2 (left). A transition from aggregated to solvated polythiophene backbones is observed around 40 °C. The UV-vis spectrum at 20 °C highly resembles that of a spin cast film, whereas the spectrum at 55 °C is similar to a solvated poly(3-alkylthiophene) in chloroform at room temperature. The strong aggregation of PDBT excludes SEC analysis. CV measurements on PDBT as a spin cast film on a Pt electrode reveals that the first oxidation wave falls around 0.85 V. This value should be compared to 0.6 V measured for poly(3-octylthiophene) under similar conditions. Hence, the oxidation potential is increased by 0.25 V simply by leaving out every second alkyl chain.

Dropcast and spincoat films were prepared from PDBT in chloroform solution on glass and Si/SiO₂ FET substrates, respectively. In order to directly address the self assembled regions of the film, synchrotron X-ray diffraction measurements were performed at the BW2 beam line in HASYLAB at DESY in Hamburg. The samples were mounted on the diffractometer in a capton chamber, which was flushed with He to minimise air scattering and beam-damage during measurements in the highly intense synchrotron beam. Fig. 3 shows the obtained diffraction patterns for (pseudo)-out-of-plane (a) and in-plane (b) scattering geometries, respectively. The spectra are corrected for polarisation and geometric effects. Using a fixed, grazing incidence angle of 0.1583°, above the angle for total reflection from the film, but below the critical angle for the substrate, the scattering from the substrate is reduced relative to the scattering from the film. The photon energy used was 10,000 eV.

For a *preliminary* analysis, a lamellar packing, as found for the poly(3-alkylthiophenes)¹, is assumed. It is then possible to interpret the diffraction features observed for the pseudo-out-of-plane spincoat film (a) as the (*h*00) reflections, corresponding to a distance between the lamella of ≈25Å, and the corresponding widths give a typical crystallite size of ≈55Å. Remarkably, the corresponding dropcast

¹ E. J. Samuelsen and J. Mårdalen, in Handbook of Organic Conductive Molecules and Polymers, 3 (Ed: H. S. Nalwa), Wiley, Chickerster (1997).

film shows much less structure, and furthermore, the observed (100) distance corresponds to a lamella separation of 33 Å, and a typical crystallite size of 66 Å. The in-plane spectra (b) shows more similarity in that the (100) distance is 29 Å, and 33 Å for the spin-cast and drop-cast films, respectively. The corresponding crystallite sizes are found to be ≈ 66 Å for both films. The spectrum of the spin-cast film shows a hump around $q = 1.5 \text{ \AA}^{-1}$, which is probably due to scattering from the amorphous side chains. A similar feature is seen for the drop-cast films at a slightly lower q -value in both in- and out-of-plane direction. However, there is no clear evidence of a π - π -stacking distance (the (010) reflection, typically found at $q \approx 1.64 \text{ \AA}^{-1}$) in any of the films, indicating a relatively poor chance of obtaining high charge carrier mobilities in the present systems¹. Further work on these systems is currently in progress.

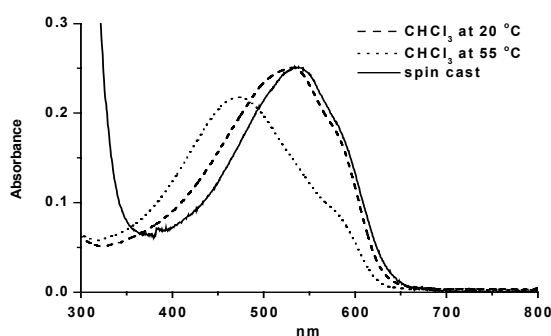


Fig. 2. UV-Vis spectra of PDBT in chl at 20 °C (dashed) at 55 °C (dotted) and as a spin cast film (full).

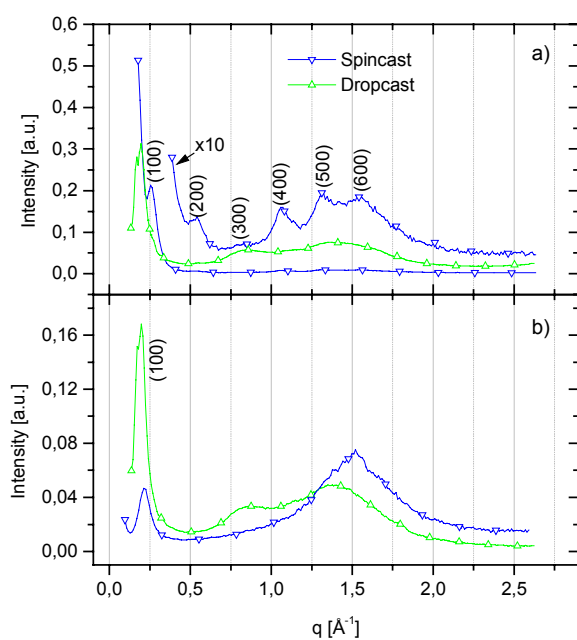


Fig. 3. Pseudo-out-of-plane (a) and in-plane (b) X-ray scattering intensities as a function of the scattering vector q . The spectra are corrected for geometric and polarisation factors. A replica of the curve for spin-cast film with the intensity scaled by a factor 10 is included in (a) for clarity.

¹ H. Sirringhaus, P. J. Braun, R. H. Friend, M. M. Nielsen, K. Bechgaard, B. M. W. Langeveld-Voss, A. J. H. Spiering, R. A. J. Janssen, E. W. Meijer, P. Herwig and D. M. de Leeuw, *Nature*, **401**, 685 (1999).

2.5.10. ASAXS investigations of steam reforming catalysts

F. Berg Rasmussen, A. M. Molenbroek, J. Sehested, H. T. Teunissen, B. S. Clausen, *Haldor Topsøe Research Laboratories, Lyngby, Denmark* and R. Feidenhans'l, *Condensed Matter Physics and Chemistry Department, Risø National Laboratory, Denmark*
e-mail: frb@topoe.dk

Steam reforming of hydrocarbons over nickel catalysts is the most widely used industrial process for producing synthesis gas and hydrogen used in the production of ammonia, methanol, acetic acid, and transportation fuel. It is well known that the nickel crystallite size has influence on important catalyst properties, such as activity and resistance to coke formation¹ but it has proved difficult to obtain information on the size distribution using standard methods in catalysis research.

Anomalous Small Angle X-ray Scattering (ASAXS) allows the measurement of element-specific SAXS on multi-component systems and hence the determination of metal particle size distributions of supported catalysts. We recently reported investigation of a Ni/SiO₂ model catalyst² and have initiated a more general study of nickel catalysts using ASAXS.

A number of Ni catalysts (approximately 10 wt.%) supported on various metal oxides (Al₂O₃, SiO₂, MgO, TiO₂ and ZrO₂) were prepared using different impregnation and precipitation procedures. ASAXS measurements were performed at beamline B1 (JUSIFA) and a typical separated (Ni) SAXS curve of an Ni/MgO catalysts is shown in Fig. 1

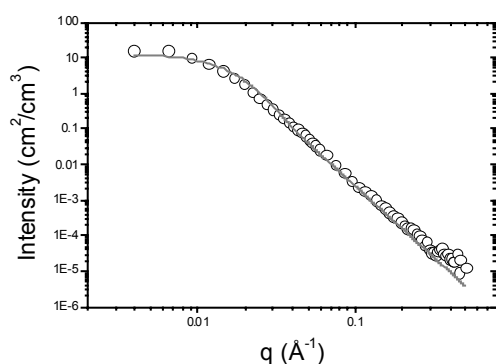


Fig. 1. The figure shows the separated (Ni) SAXS curve (circles) of a Ni/MgO-catalyst as well as the best fit to the data using a log-normal distribution of spherical particles (full line).

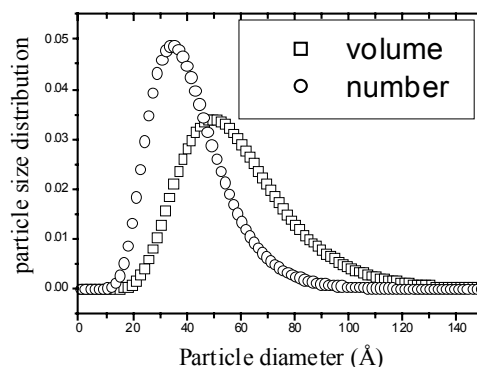


Fig. 2. The figure shows the log-normal number size distribution (circles) obtained by fitting the data of Fig. 1. Also shown is the volume-weighted distribution calculated from the fitted number distribution (squares).

The data of Fig. 1 can be fitted assuming a log-normal distribution of spherical particles. The fitted diameter distribution is shown in Fig. 2 and has a volume weighted mode value of 49 Å. This agrees very well with the volume-average mean size (50 Å) estimated from X-ray powder diffraction experiments on the same sample. Transmission electron micrographs (TEM) were also obtained of the Ni/MgO catalyst revealing Ni-particle sizes ranging from 60 to 120 Å. This is an indication that the Ni-particles observed by TEM consists of several Ni-crystallites.

¹ J. R. Rostrup-Nielsen, *Catalytic Steam Reforming*, Springer-Verlag, Berlin, (1984).

² F. Berg Rasmussen, A. M. Molenbroek, B.S. Clausen and R. Feidenhans'l, *J. Catal.* **190**, 205 (2000).

2.5.11. Different approaches to the analysis of small angle scattering experiments on porous aluminum-hydroxide

F. Berg Rasmussen, *Haldor Topsøe Research Laboratories, Lyngby, Denmark and Condensed Matter Physics and Chemistry Department, Risø National Laboratory, Denmark*
e-mail: fbr@topsoe.dk

Different approaches to the analysis of small angle X-ray scattering (SAXS) data on the porous aluminum-hydroxide pseudo-boehmite were compared¹. Experimental data measured on a number of samples were analysed as scattering from mass fractal aggregates, as scattering of a polydisperse collection of anisotropic particles and using the unified exponential/power-law approach suggested by G. Beaucage². The mass fractal approach used was similar to that used by Posselt *et al*³. whereas the particulate model was the cylinder model used previously by us⁴.

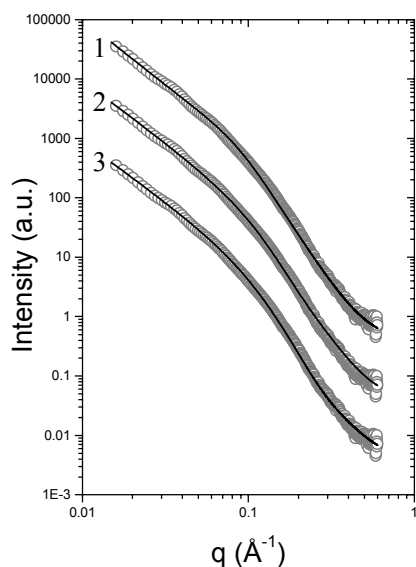


Fig. 1. Best fit to SAXS data of a typical aluminum-hydroxide (circles) using a model of fractal aggregates (1), the unified exponential/power-law approach (2) or a polydisperse model of cylindrical particles (3). The data and fitted curves have been displaced for clarity.

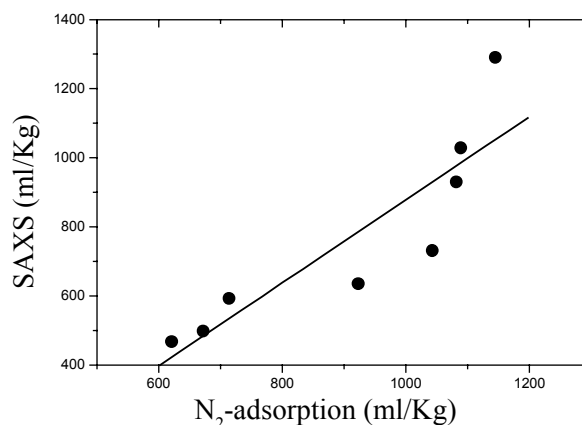


Fig. 2. Specific pore volumes calculated from SAXS and adsorption data as a function of the values measured directly by nitrogen adsorption. The line is drawn to guide the eye. An anisotropic polydisperse cylinder model was used to fit the SAXS data, see ^{1,4}.

Good fits to all the data were obtained using any of the three approaches as shown in Fig. 1. Furthermore, specific surface areas estimated from the fitted parameters of each model provided numerical values in fair agreement with surface areas measured by nitrogen adsorption and correctly predicted the trends in surface areas from sample to sample. However, information on the local porous structure agreeing with transmission electron microscopy images and nitrogen adsorption experiments is only obtained using an approach based on anisotropic particles. This is illustrated in Fig. 2, which shows that trends in the specific pore volume are reproduced if the particulate anisotropic approach is used and the results combined with nitrogen adsorption experiments. On the contrary, using e.g. the mass fractal approach no relation between the fitted parameters and e.g. the specific pore volume is observed. This study clearly demonstrates the importance of combining SAXS with complementary techniques and that the anisotropic nature of aluminum-hydroxide particles is an essential feature to include in any analysis of small angle scattering data of such systems.

¹ F. Berg Rasmussen, Different approaches to the analysis of small angle scattering experiments on porous aluminum-hydroxide, to be published in *Colloids and Surfaces A*.

² G. Beaucage, *J. Appl. Cryst.*, **28**, 717 (1995).

³ D. Posselt, J. S. Pedersen and K. Mortensen, *J. Non-Cryst. Solids*, **145**, 128 (1992).

⁴ F. Berg Rasmussen and J. Jacobsen, Primary particles and porosity in pseudo-boehmite, in preparation.

2.5.12. Particle-particle interaction in aluminum-hydroxides

F. Berg Rasmussen *Haldor Topsøe Research Laboratories, Lyngby, Denmark and Condensed Matter Physics and Chemistry Department, Risø National Laboratory, Denmark* and J. Jacobsen, *Haldor Topsøe Research Laboratories, Lyngby, Denmark*
 e-mail: fbr@topsoe.dk

The structure of aluminum-hydroxides has recently been studied in some detail using small angle X-ray scattering^{1,2}. The data were analysed using a polydisperse model of cylindrical disks neglecting particle-particle interaction. We have studied the effects of particle-particle interaction using a computer simulation method developed previously. The method is based on molecular dynamics of polydisperse plate-shaped rectangular parallelepipeds in a cubic space with periodic boundary conditions².

Fig. 1 shows a result of such a simulation using input parameters (mean half axes and poly-dispersity of the platelets) typical for aluminum-hydroxides. The small angle scattering (SAS) intensity calculated from the simulated aggregated structure is denoted the coherent scattering intensity, whereas, the incoherent intensity corresponds to an incoherent sum over the form factors i.e. neglecting particle-particle interaction. The ratio between the coherent and incoherent intensities defines an effective structure factor. As expected we observe a decrease in the coherent scattering intensity at low q -values due to particle-particle interaction.

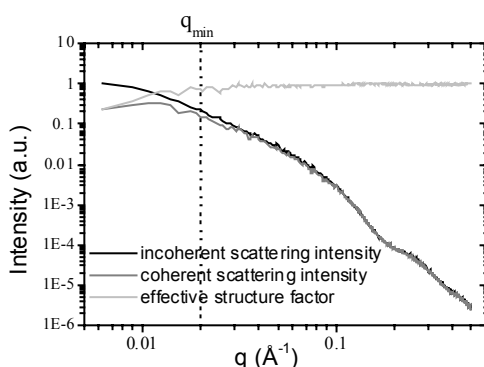


Fig. 1. Simulated scattering curves based on rectangular parallelepipeds with Gaussian distributions in the half axes a , b and c . The mean half axes (standard deviations) were $a_0 = 17$ (3.4) Å, $b_0 = 130$ (52) Å and $c_0 = 130$ (52) Å.

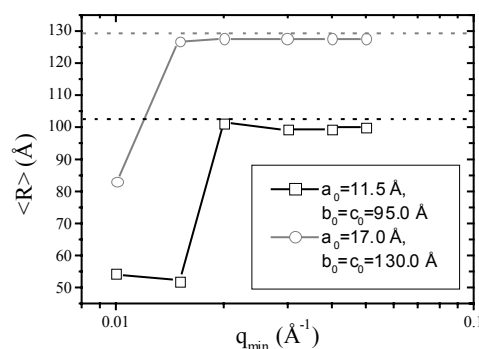


Fig. 2. The mean cylinder radius obtained by fitting a polydisperse cylinder model to simulated coherent SAS curves using different q_{\min} values. The mean values obtained by fitting the incoherent SAS curves are indicated by dotted lines.

Figure 1 suggests that interaction effects may be neglected if only data above a certain minimum q -value (q_{\min}) are analysed. We have investigated the applicability of this procedure fitting simulated data with the cylinder model mentioned above. Fig. 2 shows the fit results of two simulations one with half axes $a_0=11.5$ Å and $b_0=c_0=95$ Å and another with $a_0=17$ Å and $b_0=c_0=130$ Å. It is seen that fits to the incoherent and coherent scattering curves result in the same mean cylinder radii, if a q_{\min} (~ 0.02 Å⁻¹) is introduced in the fit of the coherent data. Fig. 2 also shows that the inputs to the simulation (mean half axes of the parallelepipeds) is nicely reproduced fitting the simulated data assuming cylindrical disks. This illustrates the well-known fact that the precise shape of the particles cannot be deduced from small angle scattering of a very polydisperse system.

¹ F. Berg Rasmussen, Risø-R-1099(EN), 68 (1998).

² F. Berg Rasmussen and J. Jacobsen, Primary particles and porosity in pseudo-boehmite, in preparation.

2.5.13. Adsorption of beta-lactoglobulin on Si investigated by ellipsometry

S. Mentzel, N. B. Larsen, *Condensed Matter Physics and Chemistry Department, Risø National Laboratory, Denmark* and K. Schaumburg, *CISMI, Laboratory for Material Science, Department of Chemistry, Copenhagen University, Denmark*
e-mail: soeren.mentzel@risoe.dk

Ellipsometry is a powerful tool to follow adsorption reactions onto solid planar reflecting samples down to the Ångström regime. However, it cannot determine the chemical character of the adsorbed layer. This study was done to estimate to which degree ellipsometry analysis can be trusted for protein absorption studies by comparison of the ellipsometry results to a chemical specific analysis as XPS. The samples were Si (100) cleaned in a 1:1 ultra pure water (upw) / ethanol solution by ultrasound for 10 min. at 50°C. The samples were immersed in a solution of 2g/L beta-lactoglobulin in PBS-buffer (pH=7.4). Blind samples were also produced by immersion into pure buffer. After the desired reaction time the samples were quickly dipped in upw five times and blow-dried with CO₂. The water dipping were performed to prevent that protein from the remaining solution adhered to the sample during the blow-drying.

Ellipsometry was performed at the Brewster angle and the thickness of the layer was calculated using the refractive indexes of silicon (3.8), silicon oxide (1.5) and protein (1.5). The silicon oxide and the protein layers have the same refractive index, and can consequently be treated as one layer in the calculation. Subsequently, the elemental compositions of the samples were analyzed by XPS. Finally ellipsometry measurements were repeated to see if the ultra high vacuum of the XPS changed the protein layers.

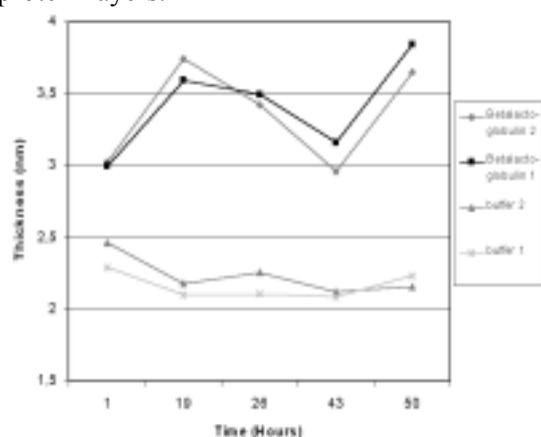


Fig. 1. Ellipsometry analysis. The samples were measured before (1) and after (2) the XPS analysis.

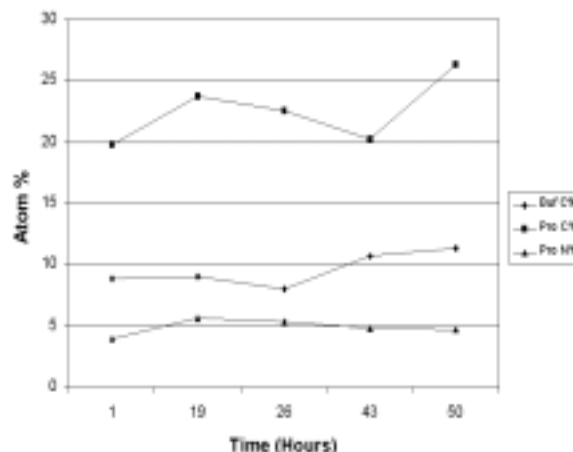


Fig. 2. XPS analysis. The nitrogen level is used as a measure of the amount of protein present on the surface.

Comparison of Figs. 1 and 2 shows that the amount of carbon measured by XPS (protein + organic contamination) follows the same trend as the thickness measured by ellipsometry. The amount of nitrogen measured by XPS is used as a measure of the amount of adsorbed protein. The nitrogen (protein) contents measured by XPS does not follow the same trend as the layer thickness measured by ellipsometry or the carbon content determined by XPS. The surplus adsorbed material must therefore be due to contamination. The blind samples have a silicon oxide/organic contamination layer of a thickness of 2.1-2.4 nm and carbon contents of 8-10 atom % as determined by XPS. This is commonly observed for samples that have not been cleaned immediately before analysis.

This study demonstrates the importance of supporting ellipsometry measurements by chemically specific techniques.

2.5.14. Chain length determination of grafted PEG-silanes by TOF-SIMS

K. Norrman, N. Gadegaard, A. Papra, N.B. Larsen, *Condensed Matter Physics and Chemistry Department, Risø National Laboratory, Denmark* and F. Kamounah, *CISMI, Laboratory for Materials Science, Department of Chemistry, University of Copenhagen, Denmark*
 e-mail: kion.norrman@risoe.dk

Poly(ethylene glycol) (PEG) silanes were grafted on silicon surfaces, Fig. 1, and analyzed with TOF-SIMS (Time Of Flight-Secondary Ion Mass Spectrometry). The ion bombardment of the sample surfaces results in desorption of fragmented pieces of PEG silane and substrate (Si). For larger PEG silane chains, the layer will be thicker, and subsequently the likelihood of observing substrate signals will decrease. In Fig. 2 the intensity of selected positively charged fragment ions are shown for PEG3-40 silanes. The substrate signal (Si^+) is seen, as expected, to decrease for longer PEG silane chains. This is based on the assumption that the grafting density is the same or similar for the PEG3-40 silanes. The desorbed ions with the elemental composition SiCH_3O^+ originates most likely mainly from the silane part of the PEG silanes. However, it can also be formed from the silicon substrate reacting with surrounding organic material. Since the silane group, due to the chemical bond, is in close vicinity of the surface, the SiCH_3O^+ is expected, wherever it originates from, to follow the same qualitative trend as Si^+ . It is evident from Fig. 2 that this is indeed observed. For larger PEG silane chains there will be a greater likelihood for larger fragment pieces to be formed. The larger fragments will after desorption undergo secondary fragmentations, resulting in a contribution to smaller fragments. Furthermore, from the previous discussion it was suggested that larger PEG silane chains results in less substrate signal. All this suggests that the intensity of the fragment ions should increase for larger PEG silane chains. The intensity of the fragment ion $\text{C}_4\text{H}_7\text{O}^+$ is one of the ions, which is, for the conditions in question, most sensitive towards changes in the chain length. In Fig. 3 the logarithm of the normalized intensities *versus* the logarithm of the number of PEG units (chain length) are plotted. It is now possible, using the same conditions, to determine an unknown chain length of a PEG silane from either one of these plots.

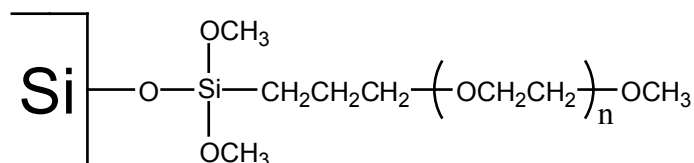


Fig. 1. PEG_n silane grafted on silicon.

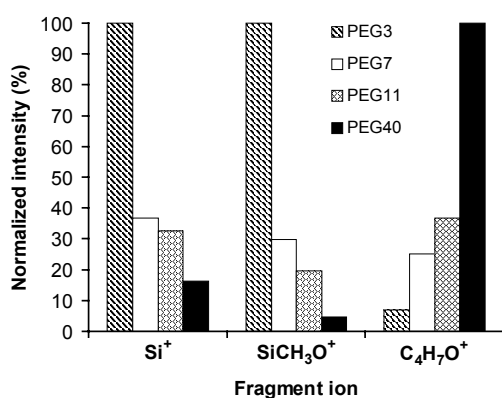


Fig. 2. Selected normalized fragment ion intensities for various chain lengths.

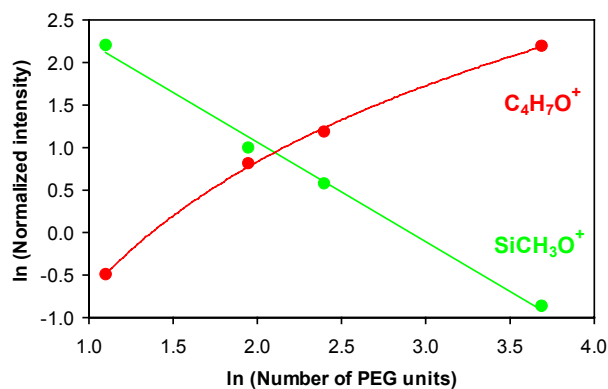


Fig. 3. Selected normalized fragment ion intensities plotted as a function of the number of PEG units.

2.5.15. Poly(ethylene glycol)-silanes – a model system study

N. Gadegaard, A. Papra, K. Norrman and N. B. Larsen, *Condensed Matter Physics and Chemistry Department, Risø National Laboratory, Denmark* and F. Kamounah, *CISMI, University of Copenhagen, Denmark*
e-mail: nikolaj.gadegaard@risoe.dk

It is well documented in the literature that surfaces terminated with poly(ethylene glycol) (PEG) have a pronounced effect on non-specific protein adsorption. We have in recent work¹ developed a method to coat silicon wafers with an ultra thin (1.5 nm) layer of PEG, which has protein repellent properties. The method, based on commercially available PEG-silane, can be used in biomedical sensor systems such as micro fluidic networks² made in Si containing materials, e.g. quartz, silicon or, silicone. The purity of the PEG-silane was determined by GC-MS to have a chain length distribution of 2-7 ethyleneglycol units (95%).

To understand the effect of the polydisperse system, monodisperse PEG-silanes were synthesised and grafted to silicon wafers following the same protocol. The absolute thickness of the films was measured by X-ray reflectometry (XR). This requires ultra flat substrates; thus silicon wafers were used. Fig. 1 clearly shows the expected increase in thickness for larger PEG-silanes. The thicknesses were confirmed by XPS and TOF-SIMS.

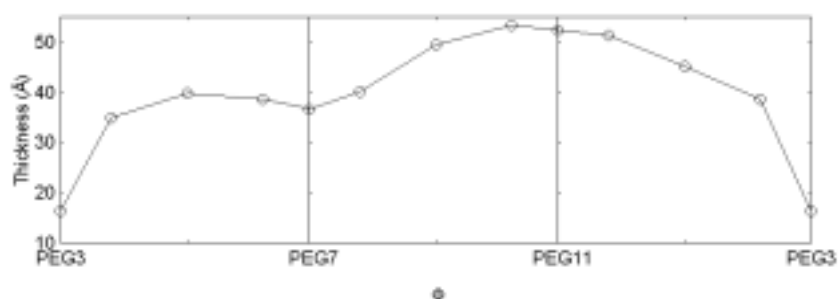


Fig. 1. Thickness of the PEG layer for various binary mixtures of two PEG-silanes of different length. The thicknesses are measured by XR. The thickness of pure 3, 7, and 11 is comparable to the theoretical length of an extended PEG chain.

A combination of equal amounts of 3, 7, and 11 units were mixed and grafted to the surface. This tertiary mixture gives dramatically smoother films than a binary mixture, see Fig. 2. We believe that the polydispersity is important to achieve smooth films due to void filling by smaller PEG-silanes.

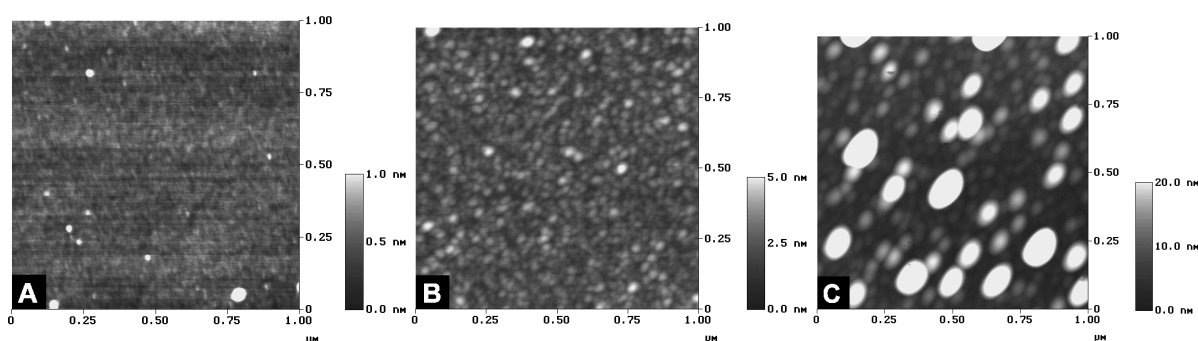


Fig. 2. AFM micrographs of A) commercial PEG-silane, B) 3:7:11 PEG units mixture, C) 3:11 PEG units mixture (1:1 ratio). The RMS roughnesses are 1.5 Å, 5.6 Å, and 78 Å, respectively.

¹ A. Papra, N. Gadegaard, and N. B. Larsen, *Langmuir*, Characterization of ultrathin poly(ethylene glycol) monolayers on silicon substrates, in press.

² A. Papra, A. Bernard, D. Juncker, N. B. Larsen, B. Michel and E. Delamarche, *Microfluidic networks made of polydimethylsiloxane, Si and Au coated with polyethylene glycol for patterning proteins onto surfaces*, submitted to *Langmuir*.

2.5.16. TOF-SIMS investigation of single carbon fibres in a PEEK matrix

K. Norrman, N. B. Larsen, K. Bechgaard, R. Feidenhans¹ and K. West, *Condensed Matter Physics and Chemistry Department, Risø National Laboratory, Denmark*, T. Frello, S. Jensen and H. Jepsen *Danfoss A/S, Nessie™ Water Hydraulics, Denmark*
e-mail: thomas.frello@risoe.dk

The high-performance polymer PEEK (poly-ether-ether-ketone) is often used with reinforcing fibres such as glass fibres or carbon fibres (CF). We have performed corrosion experiments on PEEK/CF samples, and we find that the chemical reactivity of the reinforcing carbon fibres is highly inhomogeneous¹. In basic solutions the core of the fibres is considerably more susceptible to corrosion than the outskirts of the fibres. When a PEEK/CF sample is polished to expose the internal structure of the carbon fibres, the fibre cores appear darker when observed in an optical microscope with linearly polarised light, cf. Fig. 1a). The darker area coincides quite precisely with the corrosive regions of the fibres. It is tempting to ascribe this variation in chemical and optical properties to either inhomogeneity in the chemical composition across the fibre, or a different degree of graphitisation in the fibre core, or both. In order to elucidate this, we have studied a polished sample of PEEK/CF with TOF-SIMS (Time-Of-Flight Secondary-Ion-Mass-Spectrometry). Fig. 1 shows a) carbon fibres seen in an optical microscope with polarised light and b) a TOF-SIMS image of the same fibres analysed using 25-keV Ga⁺. Before acquiring the TOF-SIMS image, the top layer of the surface was sputtered away by 1-keV SF₅⁺ and the intensities of the ions were normalized relative to the total ion intensity. The biggest contrast between the PEEK matrix and the fibres was seen for the Na, Ca and Mg ions. The carbon signals were too weak to be monitored. The intensity of the ions is indicated by a colour code below the figure.

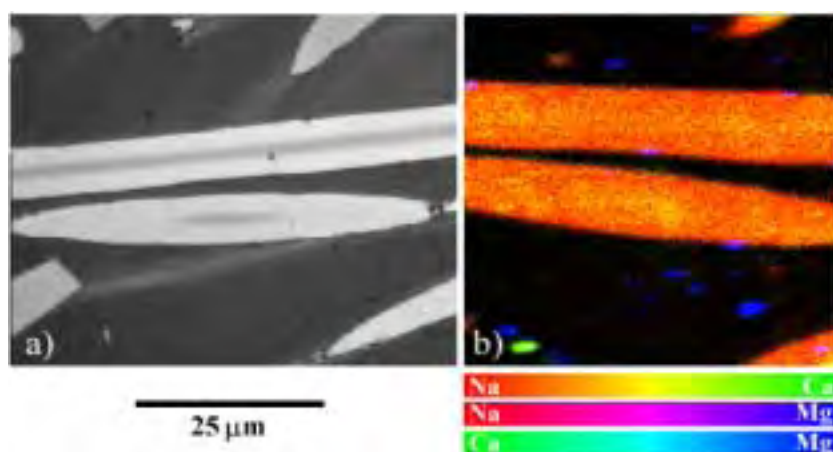


Fig. 1. A polished sample of carbon fibres in a PEEK matrix:
a) Exposed carbon fibres seen with polarised light.
b) TOF-SIMS image of the same fibres. The chemical composition is indicated by the colour code below the image.

Note that picture b) is tilted 10° clockwise with respect to picture a).

While a well-defined boundary is seen between the core and skin region of the fibres in Fig. 1a), only minute variations are seen in the TOF-SIMS image in Fig. 1b). Furthermore these minor variations in the ion signal are not nearly as well defined as the boundary seen in Fig. 1a). The intensity of a monitored ion depends on the conditions of the analysis, on the physical properties of the ion itself, and on the chemical environment. Phase changes within a material will therefore affect the ion intensity of a species. However, only subtle changes can be expected for the monitored ions in question with respect to phase changes in the CF. This is consistent with the observed subtle difference in the relative Na/Ca composition in the core region of the fibres (difficult to see in black and white). From these observations we tentatively conclude that the higher chemical reactivity in the fibre core originates from differences in the degree of graphitisation. The crystal structure of the carbon fibres is essentially graphitic, and it is known that the crystal structure in the fibre core can be considerably less well ordered than the fibre skin². A less perfect graphite structure with more chemically active dangling bonds should be more susceptible to chemical reactions, consistent with our corrosion experiments.

¹ See section 2.5.18 of this report.

² Y. Huang and R. J. Young, *Carbon* **33**, 97(1995).

2.5.17. Polymer tribology - the influence of surface topography on the wear behaviour of carbon fibre reinforced PEEK sliding against stainless steel

T. Frello, S. Jensen, H. Jepsen, *Danfoss A/S, Nessie™ Water Hydraulics, Denmark*, K. Bechgaard, R. Feidenhans¹, K. West, N. B. Larsen and K. Norrman, *Condensed Matter Physics and Chemistry Department, Risø National Laboratory, Denmark*

e-mail: thomas.frello@risoe.dk

A number of series of tribological investigations have been made on carbon fibre reinforced poly-ether-ether-ketone (PEEK/CF) sliding against stainless steel using ordinary water as lubricant. For the experiments a Pin-on-Disc tribometer was used, where a cylindrical PEEK/CF pin of 5 mm diameter is sliding against a polished disc of stainless steel, which is constantly flushed with water. The combination PEEK/CF – steel – water exhibits very low wear at high velocities, where a hydrodynamic film is separating the PEEK/CF pin and the steel disc. At lower velocities, however, there is very little or no hydrodynamic lubrication of the contact area, and the wear can increase dramatically. At low velocities not only the materials properties such as hardness, elasticity and chemical reactivity¹ play an increasing role, but also the topography of the contacting surfaces has a major influence on the friction and wear behaviour. The topography of the worn PEEK/CF surfaces was probed by a Dektak V 200 stylus profilometer, where a sharp tip in contact with the surface registers height variations over a distance of several mm. Fig. 1 shows the topography of two PEEK/CF pins with very different wear rates. The wear rates were determined just before the Pin-on-Disc experiment was terminated. Extreme care was taken to keep all experimental conditions identical for the two tests, but still the pin in Fig. 1a) wears 70 times faster than the pin in Fig. 1b). The conditions were: $P = 10$ Mpa, $V = 0.5$ m/s.

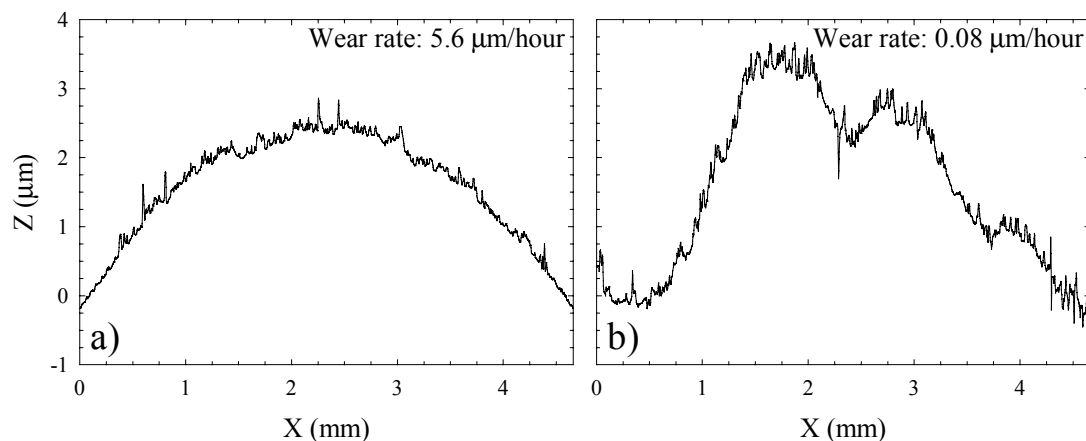


Fig. 1. Topography of two PEEK/CF pins probed perpendicular to the wear direction. The experimental conditions were identical for the two pins, but the wear behaviour was very different with a wear rate of 5.6 $\mu\text{m}/\text{hour}$ for a) and 0.08 $\mu\text{m}/\text{hour}$ for b).

The small features protruding 0.1-0.5 μm from the surface are the reinforcing carbon fibres. Comparing pin a) and pin b) it is evident that the pin with the lowest wear has the most uneven height distribution. When looking at Fig. 1, one must bear in mind that the elastic modulus of PEEK/CF is much lower than that of steel, so the pins are strongly deformed when the load of 10 Mpa is applied. Thus, both pins have been much more flat during the tribological test than after the load has been removed. The large difference in wear rates can be explained by pin a) having poorer lubricating properties than pin b), where the lubricant more easily can be transported in and out of the in the contact region. Water is in many respects a poor lubricant, but it is effective in transporting heat. And since a major wear mechanism is a chemical corrosion of the carbon fibres¹, a more efficient water flow will help cooling the pin, thereby reducing the reaction rate of all chemical reactions taking place in the contact region.

¹ See also section 2.5.18 of this report.

2.5.18. Corrosion of carbon fibres in a PEEK matrix studied by atomic force microscopy

T. Frello, S. Jensen, H. Jepsen, *Danfoss A/S, Nessie™ Water Hydraulics, Denmark*, K. Bechgaard, R. Feidenhans'l, K. West, N.B. Larsen and K. Norrman, *Condensed Matter Physics and Chemistry Department, Risø National Laboratory, Denmark*
e-mail: thomas.frello@risoe.dk

We have studied the tribological properties of carbon fibre reinforced PEEK (poly-ether-ether-ketone) sliding against stainless steel using pure water as lubricant. Atomic Force Microscopy (AFM) studies of worn PEEK/carbon fibre (PEEK/CF) surfaces show that the wear resistance of the fibres is highly anisotropic in an aqueous environment¹: when the fibres are oriented normal to the wear surface they wear faster than when they are oriented parallel to the surface. For PEEK/CF sliding directly against steel without any water present, the wear resistance of the fibres is independent of their orientation. The anisotropic wear in water could be due to a tribochemical corrosion taking place between the carbon fibres and the water, i.e., the high pressures and temperatures generated during the sliding process greatly accelerates chemical reactions that otherwise may be negligible. In order to clarify whether such a chemical process could lead to a corrosion of the carbon fibres, we have performed corrosion experiments in combination with AFM. The samples were polished bricks of injection-moulded PEEK/CF. Corrosion treatments were done using either demineralised water (pH = 7) or a buffer solution (pH = 6 or 8). The aqueous solution containing the sample was heated to 250 °C in an autoclave for 36 hours². Selected areas on the samples were investigated by AFM before and after the corrosion treatment.

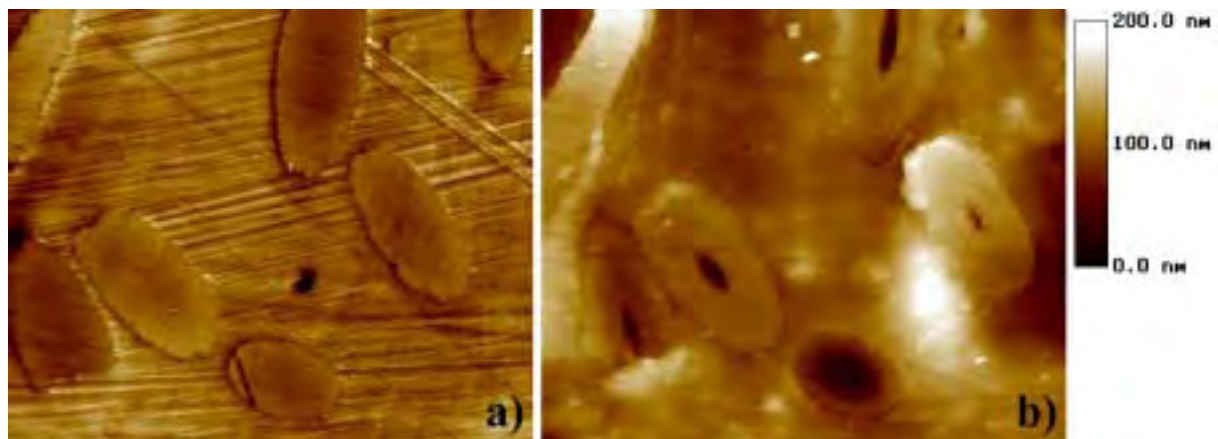


Fig. 1. AFM images ($50 \times 40 \mu\text{m}^2$) of carbon fibre reinforced PEEK a) before and b) after 250 °C corrosion treatment in a basic buffer solution. The sample is polished to expose the carbon fibres, which are seen as elliptic shapes in the figure. After the corrosion treatment the core of the fibres is etched away. The PEEK matrix also changes appearance somewhat because of water absorption.

In demineralised water or acidic solutions there is no detectable effect on the carbon fibres, while in the basic buffer solution the core of the fibres is severely attacked, as shown in Fig. 1. This observation is fully consistent with the wear behaviour of the fibres; when oriented normal to the surface, the fibre core is always exposed rendering it vulnerable to tribochemical corrosion. When oriented parallel to the surface a significant fraction of a fibre must be worn away before the core is exposed. An analysis by TOF-SIMS of the chemical composition of the fibres (mentioned elsewhere in this annual progress report) shows no major spatial variations in the chemical composition of the fibre, and we tentatively conclude that the higher chemical reactivity of the fibre core originates from the core having a lower degree of graphitisation. Work is in progress to verify whether this assumption is correct.

¹ Risø-R-1156(EN), 118 (2000).

² The contact temperature during sliding can exceed 300 °C, see M. Q. Zhang, Z. P. Lu and K. Friedrich, "Thermal analysis of the wear of polyetheretherketone", *Tribology International* **30**, 103 (1997).

2.5.19. High-resolution imaging of cell adhesion to fibrillar collagen-coated substrate

S. Mosler, N. Gadegaard, N. B. Larsen, *Condensed Matter Physics and Chemistry Department, Risø National Laboratory, Denmark* and M. A. Lawson, *Department of Dairy and Food Science, Royal Veterinary and Agricultural University, Denmark*
e-mail: stephan.mosler@risoe.dk

The cultivation of most biological cells depends on adequate adhesion to a solid substrate, substituting the microenvironment of the original tissue. In vivo, extracellular adhesive protein networks trigger the focal assembly of submicron-scaled membran receptor complexes, resulting in a properly developed cytoskeleton. There is growing evidence for a beneficial involvement of substrate nanotopo-graphy¹, calling for further elucidation of possible surface structural cues and their relation to chemical recognition mechanisms. Furthermore, the idea of mass-producible biomimetic polymeric substrates requires a detailed understanding and monitoring of adhesion events at the cell-substrate interface.

The fibrillar collagen network is a mechanically loadable component of the extracellular matrix, displaying distinct width and 65-nm periodicity. Fig. 1 depicts the cell adhesion promoting effect, exerted by a sparse coating of glass with fibrillar collagen, which was deposited after in vitro self-assembled of purified collagen molecules. Confocal micrographs, fluorescently staining for cytoskeletal actin with Texas-Red-coupled phalloidin after 24 hours of cultivation, show increased spreading of the adherent cells. Looking closer, the bioactivity of this substrate coating is also reflected by numerous cellular microprotrusions (examples indicated by arrows), the appearance of which varies with fibril width.

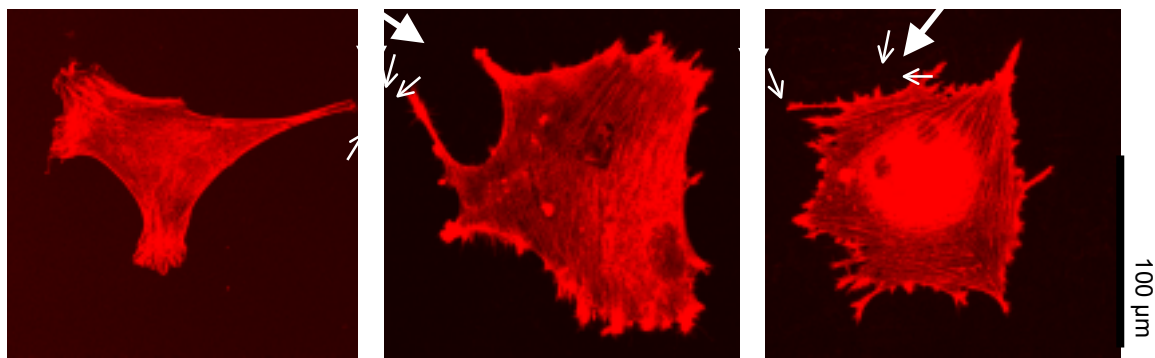


Fig. 1. Cell adhesion to glass (left) vs. fibrillar collagen-coating - coarser (middle) and finer (right).

Atomic force micrographs (Fig. 2) of fixed and dried samples reveal an alignment of the relatively stiff microprocessus tips with single fibrils until these kink (left) or splice into thin filaments (right).

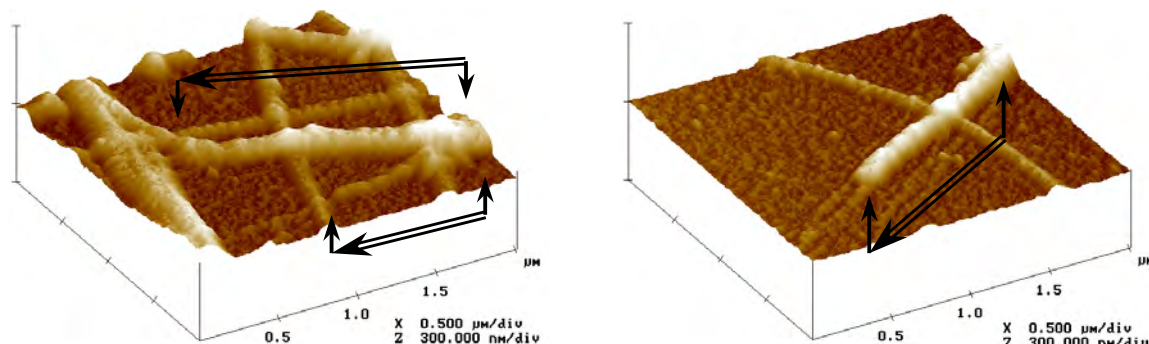


Fig. 2. Adherent cell microprocessi (arrows) aligning with collagen fibrils (banded topography)

¹ A. Curtis and C. Wilkinson, Reaction of cells to topography. *J. Biomater. Sci. Polymer Edn.* **9**, 1313 (1998).

2.5.20. An X-ray reflectivity study of a model biomembrane on solid support

M. C. Gerstenberg, R. Feidenhans¹, C. Kumpf, *Condensed Matter Physics and Chemistry Department, Risø National Laboratory, Denmark*, L. K. Nielsen, *Department of Chemistry, The Technical University of Denmark*, A. V. Hughes and S. Roser, *Department of Chemistry, University of Bath, UK*

e-mail: michael.gerstenberg@risoe.dk

A central feature of biomolecular materials (often termed "biomimetic") is the ability to form self-assembled structures as seen, e.g., in protein folding and phospholipid membranes. The study of the biomimetic materials, thereby understanding their assembly, will lead to design of new and advanced materials of technological importance. Proteins are the essential building blocks in all living cells and detailed knowledge about their function is a prerequisite for understanding the complex behaviour of cells. The multiplicity of functions performed by proteins is delicately linked to their structure. Even though many protein structures have been solved today, only a few of these are related to transmembrane proteins and investigations of biomolecular interactions at membranes still represent a major challenge. This is due to the fact that the processes are surface-related and that membrane-bound proteins in general must remain in a lipid matrix to retain their native structure and activity. Consequently, we have initiated a study of planar solid supported lipid membranes in which we later plan to incorporate transmembrane proteins.

Recently, it has been demonstrated¹ that a double phospholipid bilayer can be fabricated on solid support by the Langmuir-Blodgett (LB) and Langmuir-Schaeffer techniques. The upper 'free' bilayer is separated from the lower bilayer by a hydration layer and is therefore loosely held at the surface. It has been shown that such 'free bilayers' exhibit a similar phase behaviour to real membranes providing their utility as biomimetics. To improve on the transfer ratios of the bilayers at fabrication, we have exchanged the phospholipid layer closest to the supporting surface with a self-assembled monolayer (SAM) of octadecyltrichlorosilane (OTS). Neutron reflection measurements of a double bilayer stack of 3 layers of dimyristoylphosphatidylcholine (DMPC) deposited onto an OTS SAM indicated a high structural integrity of the assembly.² However, neutron reflectometry has a rather limited range of accessible momentum transfers (typically less than 0.2 \AA^{-1}) which results in a coarse 'real space' resolution. Therefore, to achieve better resolution needed for detection of structural changes of membrane components, we have constructed a liquid cell aimed for X-ray reflectometry. Our initial studies have focussed on a single layer of DMPC on the OTS SAM on an oxidised Si(001) surface in aqueous solution. The phospholipid layer was deposited by the LB technique. Using X-rays of 20 keV energy, the reflectivity was measured out to 1.2 \AA^{-1} covering 9.5 orders in dynamic range at the synchrotron beamline BW2, Hasylab, DESY (see Fig. 1), enabling us to probe scattering length density differences on a $\sim 3 \text{ \AA}$ length scale. Model-independent electron density profiles (not depicted) show a striking similarity to profiles of the bilayer structure based on computational and diffraction studies.³ However, the results have shown the necessity for a digress from the conventional box model approach towards an analysis based on distribution functions to map the spatial organisation of the submolecular fragments.⁴

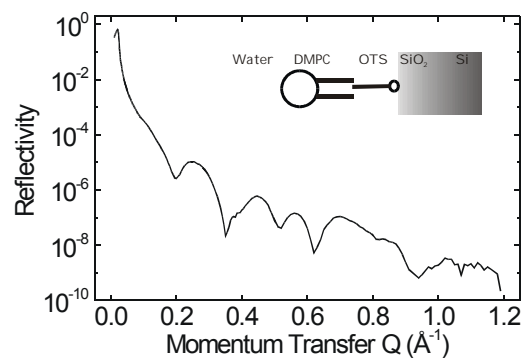


Fig. 1. Reflectivity scan of a single layer of the phospholipid DMPC deposited onto a self-assembled monolayer of OTS on an oxidised Si(001) surface in aqueous solution.

¹ T. Charitat, E. Bellet-Amalric, G. Fragneto, and F. Graner, *Eur. Phys. J.* **B8**, 583 (1999).

² See section 2.5.21. of this report.

³ R. S. Armen, O. D. Uitto and S. E. Feller, *Biophys. J.* **75**, 734 (1998).

⁴ M. Schalke, P. Krüger, M. Weygand, and M. Lösche, *Biochim. Biophys. Acta* **1464**, 113 (2000).

2.5.21. Neutron reflectivity of a model biomembrane

A.V. Hughes, A. Goldar, S. J. Roser, *Department of Chemistry, University of Bath, UK*, M. C. Gerstenberg, *Condensed Matter Physics and Chemistry Department, Risø National Laboratory, Denmark* and J. Bradshaw, *School of Vet. Sciences, University of Edinburgh, Scotland, UK*.
e-mail: a.v.hughes@bath.ac.uk

The phospholipid bilayer is the major component of cell membranes. In the native state, the phospholipid membrane is often difficult to study. Not only are they too complex (in terms of their composition) for the current understanding of lipid bilayer behaviour, but also, cells and vesicles are not in a state whereby they can be easily manipulated for investigation. There is considerable current interest in the development of realistic model biomembranes over which control may be exercised in their composition, and which are localised on a solid support so that they may be easily manipulated and investigated. A number of approaches have been proposed to solve this problem, however, the common flaw in most approaches is that in becoming localised on the solid support, the phospholipid molecules are 'tethered' to the substrate and their freedom within the bilayer is limited. These systems are then unsuitable for investigating all but the simplest of interactions.

Recently, we have developed a novel model system using a combination of Langmuir-Blodgett, Langmuir-Schaeffer and self-assembly techniques. Two layers of phospholipid are transferred vertically onto an octadecyltrichlorosilane SAM on a silicon substrate, and a third layer is then added horizontally by the Langmuir-Schaeffer technique, such that the final assembly is completely submerged in water and fully hydrated¹. In such heavily hydrated systems, it is often possible to form a substantial 'cushioning' layer of water between the layers of lipid, thus limiting the tethering effect of the substrate and forming a far more realistic model membrane system. Due to the "additional resolution" afforded by contrast variation, neutron reflectivity is an ideal technique for evaluating such systems.

Neutron reflectivity data from the model system at three water contrasts is shown in Fig. 1, along with the corresponding scattering length density profiles (Fig. 2). As can be seen, the system is clearly divided into three distinct layers – there are two distinct organic regions, separated by a region of higher SLD which varies with water contrast and must therefore be a hydration layer. This hydration layer is extensive (>30 Å), and insulates the upper phospholipid bilayer from the tethering effect of the substrate, resulting in a system which is far more realistic as a model membrane than other simple deposited systems.

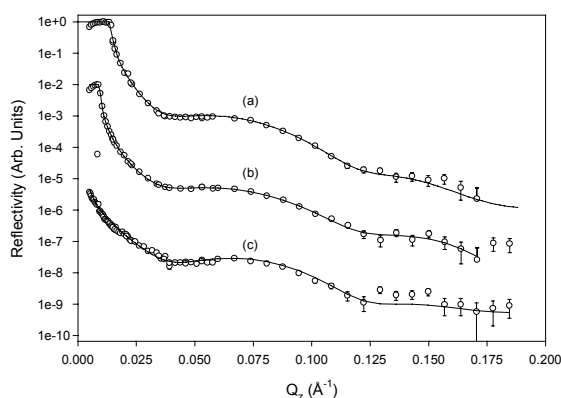


Fig. 1. Neutron reflectometry data at three water contrasts (a: D₂O, b: D₂O/H₂O, c: H₂O). The solid lines are the fits corresponding to the scattering length density profiles shown in Fig. 2.

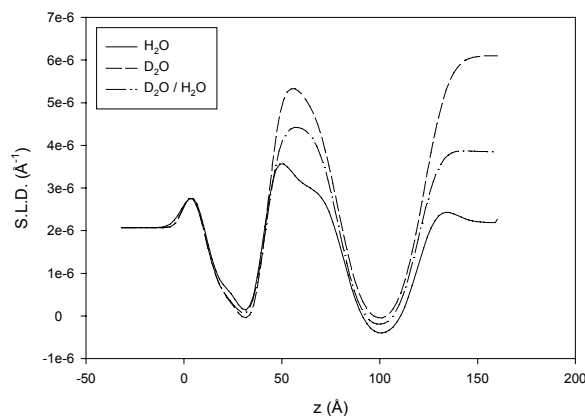


Fig. 2. Scattering length density profiles for the three water contrasts.

¹ A. V. Hughes, A. Goldar, M. C. Gerstenberg, S. J. Roser and J. Bradshaw A hybrid SAM-phospholipid system as a model biomembrane, submitted to Langmuir.

2.5.22. Use of highly n-doped silicon as an electrode for in-situ neutron and X-ray reflection studies of an electrochemical system

A. Goldar, S. J. Roser, A. V. Hughes, *Department of Chemistry, University of Bath, UK* and M. C. Gerstenberg, *Condensed Matter Physics and Chemistry Department, Risø National Laboratory, Denmark*

e-mail: michael.gerstenberg@risoe.dk

Silicon is a potential electrode for *in-situ* neutron (because it reduces the complexity of the interface) and X-ray reflection (because of its low scattering length density compared to more usually used metallic electrodes) from an electrochemical system. There is, however, a major problem with oxidation of silicon surfaces, which we have addressed by the use of n- rather than p-type silicon. The natural oxide layer at the surface of a silicon electrode is known as an especially “blocking” oxide. One of the ways to remove the native silicon oxide is to use the anodic dissolution of silicon in fluoride media. The anodic dissolution takes place under illumination for n-type silicon. Under the cathodic polarisation, hydrogen is incorporated into the silicon lattice.

In order to demonstrate that silicon could be used as an electrode and to understand the surface changes induced by electrochemical etching of silicon surface in 40% NH_4F , we designed a cell to study the in-situ neutron reflection from the silicon/electrolyte interface during the anodic dissolution and the hydrogen evolution. Reflection experiments were carried out on the reflectometer beam line (TAS 8).

Figure 1 shows the variation of the intensity of the reflected beam (at a fixed Q) as a function of time. We relate the variation of the intensity to the restricted diffusion of hydrogen in the case of Fig. 1a in the silicon lattice, and to the diffusion of the fluorine ions toward the surface in the case of Fig. 1b.

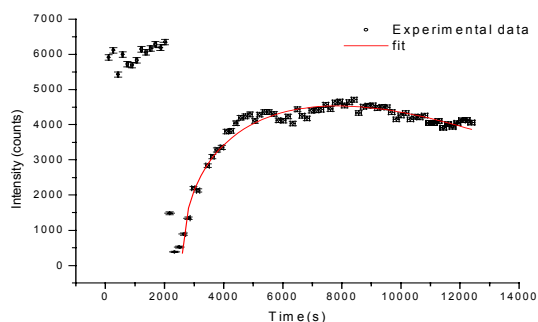


Fig. 1 a. Variation of the reflected intensity during hydrogen evolution.

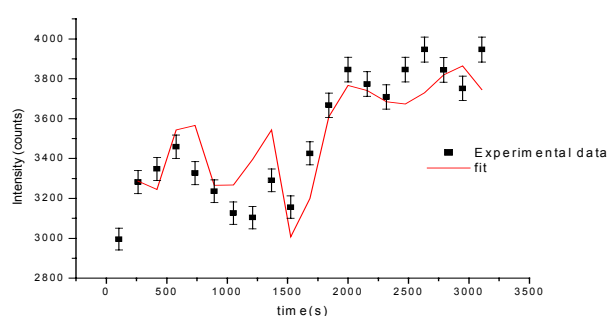


Fig. 1 b. Variation of the reflected intensity during anodic dissolution.

We have developed a mathematical model, based on fluctuation dissipation-like assumptions, in order to fit the data. The red line in Fig. 1 represents the fit of the data by this model.

By analysing the shape of the total reflection feature (Fig. 2), we can conclude that the surface is macroscopically roughened during the hydrogen evolution reaction and in the anodic dissolution the macroscopic surface roughens to a microscopic one.

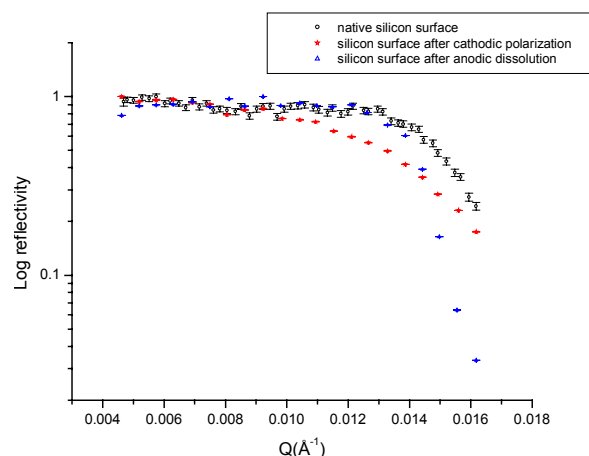


Fig. 2. The shape of the reflectivity profile at the critical angle.

2.6. Langmuir films

2.6.1. Grazing-incidence X-ray diffraction from Langmuir films of alkylthiol passivated gold nanoparticles

M. Brust, *Centre for Nanoscale Science, Department of Chemistry, University of Liverpool*, T .R. Jensen, K. Kjær, *Condensed Matter Physics and Chemistry Department, Risø National Laboratory, Denmark*, K. Nørgaard, N. Reitzel and T. Bjørnholm, *Laboratory for Materials Science, Chemistry Department, University of Copenhagen, Denmark*

e-mail: kristian.kjaer@risoe.dk

Monolayers of thiol-stabilized Au nanoparticles can be prepared at the interface between air and water¹. The in-plane structure of such Langmuir films has been investigated by grazing-incidence X-ray diffraction (GIXD) at beamline BW1. The particles used in this study were expected to have a narrow size distribution, with a diameter around 3 nm. The gold clusters were passivated by coating them with C₁₂H₂₅SH. The narrow diffraction peak (Fig. 1A) indicates that well-ordered hexagonal close-packed films of Au clusters are formed (Fig. 1B), with a center to center distance of 3.2 nm. This result is in good agreement with previous studies of the cluster organization on solid substrates². Between the gold cores the alkyl chains of the thiol passivant are expected to be interdigitated, thus making for a rather rigid monolayer structure. From the FWHM($2\theta_{xy}$) of the diffraction peak the coherence length is estimated as 300 Å.

A broad wide-angle diffraction peak (Fig. 1C) corresponds to a lattice spacing of 2.3 Å, which is close to the (111) spacing of bulk gold. The peak must come from the Au particle core. The coherence length is only 10 Å, indicating that only the central atoms of the gold cluster are well-ordered.

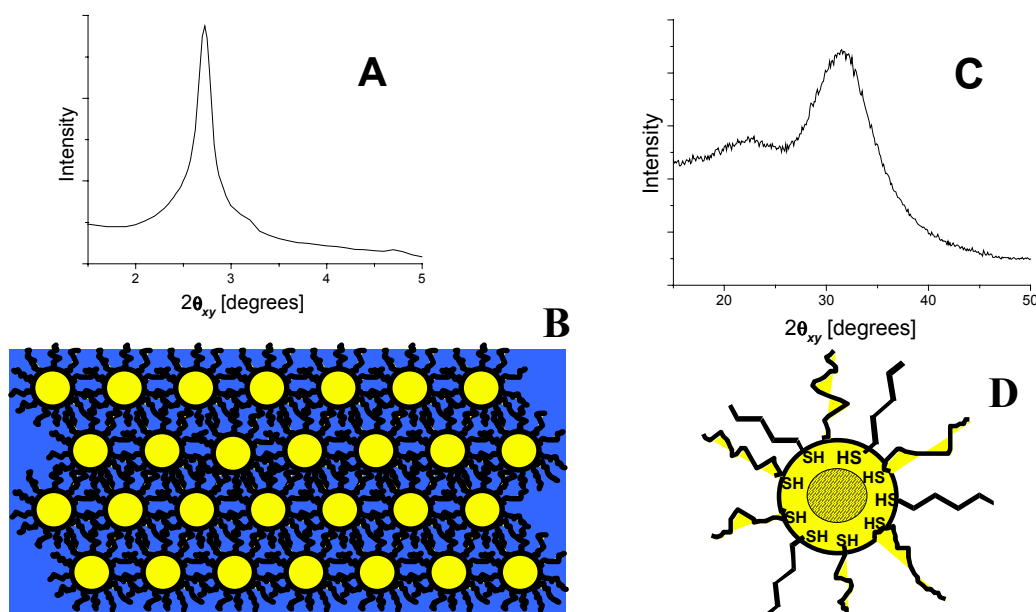


Fig. 1. A: Low-angle diffraction peak (intensity vs. horizontal scattering angle $2\theta_{xy}$, $\lambda=1.30$ Å); B: Artists view of the hexagonal close-packed Langmuir films; C: Wide-angle diffraction peak. D: Illustration of Au particle with well-ordered center.

This work was supported by the DanSync programme of the Danish Natural Science Foundation and by the IHP-Contract HPRI-CT-1999-00040 of the European Community.

¹ J. R. Heath, C. M. Knobler and D. V. Leff, *J. Phys. Chem.* **101**, 189 (1997).

² M. Brust, D. Bethell, D. J. Schiffrin and C. J. Kiely, *Adv. Mater.* **7**, 795 (1995).

2.6.2. Langmuir films of surfactant polythiophene derivatives studied by grazing angle X-ray diffraction and X-ray reflectivity

K. Nørsgaard, N. Reitzel, D. R. Greve, T. Bjørnholm, *Laboratory for Materials Science, Chemistry Dept., University of Copenhagen, Denmark*, P. C. Ewbank, R. D. McCullough, *Department of Chemistry, Carnegie Mellon University, Pittsburgh, USA*, T. R. Jensen and K. Kjær, *Condensed Matter Physics and Chemistry Department, Risø National Laboratory, Denmark*
 e-mail: kristian.kjaer@risoe.dk

A series of surface active polythiophene derivatives have been investigated as self-assembled monolayers at the air-water interface. The in-plane structure of the Langmuir films was studied by grazing-incidence synchrotron X-ray diffraction (GIXD). Specular X-ray reflectivity was used to determine the electron density profile normal to the water surface. The polythiophene derivatives all have the general formula shown in Figure 1, and are highly *regioregular*. Previous studies¹ of the structure of Langmuir films of amphiphilic polythiophenes (**1**, Table 1) have shown that the hydrophilic side-chains are submersed into the water subphase, while the hydrophobic side-chains are pointing away from it (Fig. 2A). The regioregularity ensures that the conjugation along the polymer backbone is maximized. Furthermore, the backbones of adjacent polymers are held together through π - π interactions (Fig 2B) with a π -stacking distance around 3.8 Å. To investigate the effect of the substituents on the packing and orientation of the polymer, the structures of **2** and **3** were elucidated, as well (Table 1). Despite the dramatic changes in the overall amphiphilicity, the molecules **1-3** organize in the same prototype structure. Comparison of **1** and **2** shows that the π -stack becomes tighter when the hydrophobic alkyl substituent is absent. Even replacement of the hydrophobic substituent with another polar substituent (**1**→**3**) does not disrupt the formation of the prototype structure. This indicates that the π -stacking of the polymer backbone is a strong driving force in the packing of surfactant polythiophenes on a water surface. The measured unit cell dimensions and π -stacking distances are shown in Table 1.

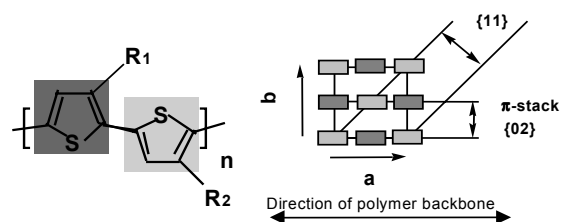


Fig. 1. Structure and unit cell (top view)

| # | R ¹ | R ² | a | π -stack | thickness | L |
|----------|---------------------------------|---------------------------------|----------------------|--------------|-----------|------|
| 1 | C ₁₂ H ₂₅ | MEEM | 7.66 Å | 3.84 Å | 23.9 Å | 50 Å |
| 2 | H | MEEM | n/a | 3.71 Å | 13 Å | 15 Å |
| 3 | MEEM | MEEM | 7.82 Å | 3.81 Å | 15.5 Å | 50 Å |
| 4 | C ₁₂ H ₂₅ | C ₁₂ H ₂₅ | No monolayer formed. | | | |

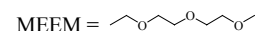


Table 1. Cell dimensions and coherence lengths (L)

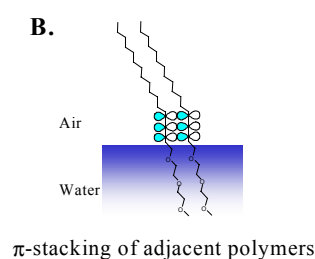
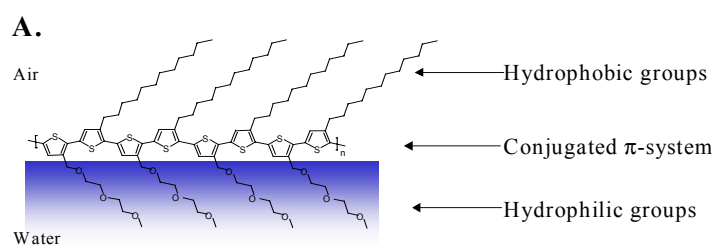


Fig. 2. Packing arrangement at the air-water interface

We are grateful for support by the SNF (DanSync), the IHP contract HPRI-CT-1999-00040 (EC) and for beam time at beam line BW1 at HASYLAB at DESY, Hamburg, Germany.

¹ N. Reitzel, D. R. Greve, K. Kjær, P. B. Howes, M. Jayaraman, S. Savoy, R. D. McCullough, J. T. McDevitt and T. Bjørnholm, *J. Am. Chem. Soc.* **122**, 5788 (2000).

2.6.3. Crystalline β -sheet monolayers - A new class of ordered molecular templates

H. Rapaport, D. A. Tirrell, *Division of Chemistry and Chemical Engineering, California Institute of Technology, Pasadena, USA*, L. Leiserowitz, *Department of Materials and Interfaces, Weizmann Institute of Science, Israel*, T. R. Jensen and K. Kjær, *Condensed Matter Physics and Chemistry Department, Risø National Laboratory, Denmark*
e-mail: kristian.ljaer@risoe.dk

The design and assembly of ordered molecular nanostructures with predictable topologies and functions have become one of the key aims in chemistry and materials sciences. In the search for advanced materials we try to exploit the intriguing architectures of peptides and proteins. We have designed a new class of peptides that form two-dimensional crystalline β -sheet monolayers at interfaces, generating a planar scaffold with regularly spaced functional groups amenable for surface patterning. Grazing-incidence X-ray diffraction measurements on monolayer films of the undecapeptide, Pro-Glu-(Phe-Glu)₄-Pro, on water (pH = 5.3) provide clear evidence for assembly of the peptide into crystalline β -sheet monolayers. The GIXD pattern (Fig. 1a) exhibits four distinct Bragg peaks at $q_{xy} = 0.166, 0.332, 1.007$ and 1.329 \AA^{-1} that can be indexed in accordance with the structural model depicted schematically in Fig. 1b. The Bragg peak at $q_{xy} = 1.329 \text{ \AA}^{-1}$ corresponds to a spacing of 4.7 \AA , which is characteristic of crystalline β -sheet systems. The Bragg peaks at $q_{xy} = 0.166, 0.332$ and 1.007 \AA^{-1} correspond to the first-, second- and sixth-order reflections of a 37.4 \AA spacing. We attribute this spacing to the repeat distance defined by juxtaposition of neighboring molecules along the b axis (Fig. 1b). The full widths at half maxima, $\text{FWHM}(q_z)$, of the Bragg rods (Fig. 1a inset) along q_z indicate a crystalline film $\sim 8 \text{ \AA}$ thick, implying that not only the peptide backbone but also the amino acid side chains are ordered within the crystalline monolayer. The crystalline coherence length L , a measure of the extent of lateral molecular order, as estimated from the $\text{FWHM}(q_{xy})$ of the Bragg peaks, is approximately 400 \AA along both the 4.7 \AA and the 37.4 \AA spacing directions.

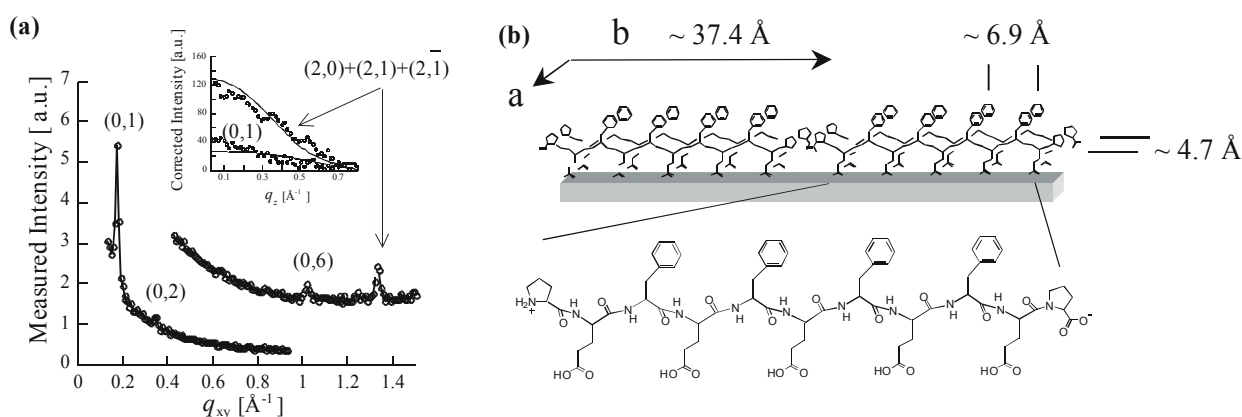


Fig. 1. (a) The observed GIXD pattern $I(q_{xy})$ of the crystalline monolayer Pro-Glu-(Phe-Glu)₄-Pro film on deionized water, uncorrected for Lorenz-polarization and active area (LPA) factors. The two sets of data were collected from the same film with different slit settings in the GIXD set-up. Inset: The observed Bragg rod intensity profiles $I(q_z)$ of the Bragg peaks at $q_{xy} = 0.166$ and 1.329 \AA^{-1} (dots) each corrected for LPA factor and X-ray beam damage effects. The calculated Bragg rod profiles (line) correspond to the molecular model¹. (b) Schematic representation of the peptide Pro-Glu-(Phe-Glu)₄-Pro in the β -pleated conformation and the β -sheet crystalline assembly at the air-water interface (represented by the grey slab).

We are grateful for support by the SNF (DanSync) and the EC (IHP contract HPRI-CT-1999-00040) and for beam time at beam line BW1 in HASYLAB at DESY, Hamburg, Germany.

¹ H. Rapaport, K. Kjær, T. R. Jensen, L. Leiserowitz and D. A. Tirrell, *J. Am. Chem. Soc.* **122**, 12523 (2000).

2.6.4. 2D Mono- and Bi-metal ionic arrays self assembled on different subphases

R. Buller, M. Lahav and L. Leiserowitz, *Materials and Interfaces Department, Weizmann Institute of Science*, T. R. Jensen and K. Kjær, *Condensed Matter Physics and Chemistry Department, Risø National Laboratory, Denmark*
e-mail: kristian.kjaer@risoe.dk

In recent years there has been growing interest in the design of organized hybrid organic/inorganic nano-composites¹. Here we present the spontaneous formation of alternating bimetal ionic arrays, orderly embedded in an organic matrix, by connecting via an aliphatic spacer two different organometallic complexes which are formed exclusively and simultaneously² at the air-solution interface (Fig. 2a). In such a system, the *bola*amphiphilic organic molecules (*d* or (*d,l*)-(HOOC)-C₂₀H₄₀-CONH-C₄H₈-CH(COOH)(NH₂), designated *d* or (*d,l*)-C₂₂Lys (Fig. 3 and section 2.6.5.) are spread at the interface where they associate with the dissolved metal ions (Cu²⁺ and/or Pb²⁺) to form a laterally periodic superstructure of multilayer form. Deposition of the *bola*amphiphiles on pure Pb(Acetate)₂ and on Cu(Acetate)₂ solutions yields crystalline films with *d*₀₁-spacings of 76 Å and 71 Å respectively (Fig. 1b,c), implying metal binding only to the appropriate organic functional group; Cu²⁺ to two amino acids³ and Pb²⁺ to two carboxylic acids⁴. Use of a mixed Cu(Acetate)₂ and Pb(Acetate)₂ subphase results in the self-assembly of a different crystalline film with *d*₀₁ = 73 Å, that incorporates both metallic ions (Fig. 1a). This analysis thus excludes the simultaneous formation, in the mixed Cu-Pb system, of the two monometallic crystalline phases separately. The GIXD patterns from films formed by enantiomerically pure and racemic *bola*amphiphiles spread on the various sub-phases, differ in the relative intensities of their Bragg peaks (even though barely in their *d*-spacings). This distinct difference in Bragg peak intensity excludes the spontaneous separation of the two enantiomers, when using the racemate as a building block for the self-assembled film. This matrix can be transferred to a solid support, reacted or reduced in order to form a nanowire, or a nanocrystalline array of metallic or superconducting character⁴.

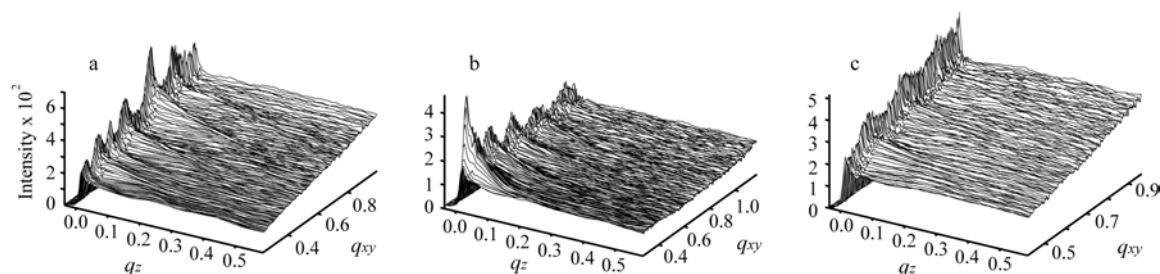


Fig. 1. Surface plot of the scattered intensity $I(q_{xy}, q_z)$ showing the $\{0,k\}$ reflections of (*d,l*)-(HOOC)-C₂₀H₄₀-CONH-C₄H₈-CH(COOH)(NH₂) spread on different subphases: a) mixed Cu(Acetate)₂ and Pb(Acetate)₂, b) pure Pb(Acetate)₂, and c) pure Cu(Acetate)₂.

¹G. A. Ozin, *Adv. Mater.* **4**, 612 (1992); J.-M. Lehn, *Supramolecular Chemistry*, VCH, Weinheim 1995; I. I. Weissbuch, S. Guo, R. Edgar, S. Cohen, P. B. Howes, K. Kjær, J. Als-Nielsen, M. Lahav and L. Leiserowitz, *Adv. Mater.* **10**, 117 (1998); I. Weissbuch, P. W. Baxter, S. Cohen, H. Cohen, K. Kjær, P. B. Howes, J. Als-Nielsen, G. Hanan, U. Schubert, J. -M. Lehn, L. Leiserowitz and M. Lahav, *J. Am. Chem. Soc.* **120**, 4850 (1998); I. Weissbuch, P. N. W. Baxter, I. Kuzmenko, H. Cohen, S. Cohen, K. Kjær, P. B. Howes, J. Als-Nielsen, J.-M. Lehn, L. Leiserowitz and M. Lahav, *Chem. Eur. J.* **6**, 725 (2000).

²The evidence for such a structure arises from X-ray Photoelectron Spectroscopy and the GIXD measurements, serving as complementary methods (manuscript in preparation).

³J. P. Greenstein and M. Winitz, *Chemistry of the amino acids*, John Wiley & Sons 1984; B. A. Fowler, *Environmental Health Perspectives* **106** (1998) 1585.

⁴S. Gou, R. Popovitz-Biro, I. Weissbuch, H. Cohen, G. Hodes and M. Lahav, *Adv. Mater.* **10**, 121 (1998); H. Xiong, M. Cheng, Z. Zhou, X. Zhang and J. Shen, *Adv. Mater.* **10**, 529 (1998).

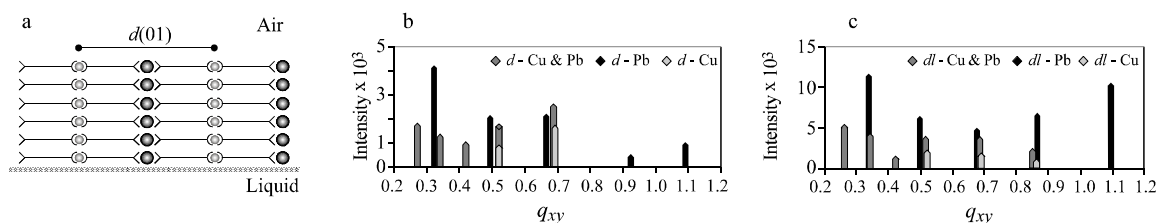


Fig. 2. a) Schematic representation of the packing arrangements of bolaamphiphile molecules connecting two different metal ion types arranged in alternating sheets. b) The positions (along q_{xy}) and intensities of the Bragg peaks, integrated along q_{xy} and q_z measured for d -C₂₂Lys amphiphile spread on different subphase solutions: mixed Cu(Acetate)₂ and Pb(Acetate)₂, pure Pb(Acetate)₂, and pure Cu(Acetate)₂ c) Corresponding results for (d,l) -C₂₂Lys amphiphile spread on the three different subphases.

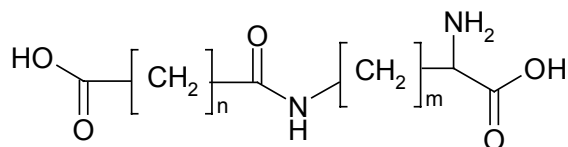


Fig. 3. Bolaamphiphilic series ($n=20,22$ and $m=4,3$) designated as C₂₂Om, C₂₂Lys, and C₂₄Lys.

We are grateful for support by the SNF (DanSync), the IHP contract HPRI-CT-1999-00040 (EC) and for beam time at beam line BW1 at HASYLAB at DESY, Hamburg, Germany.

2.6.5. Self assembled 2D bimetal ionic arrays, with varied organic spacer lengths

R. Buller, M. Lahav and L. Leiserowitz, *Materials and Interfaces Department, Weizmann Institute of Science*, T.R. Jensen and K. Kjær, *Condensed Matter Physics and Chemistry Department, Risø National Laboratory, Denmark*
 e-mail: kristian.kjaer@risoe.dk

When spread on pure deionized water, *bolaamphiphile* (*d,l*)-C₂₂Lys (Fig. 3 in section 2.6.4.) yields a mixture of crystalline films where the molecules lie parallel to the water surface forming a multilayer, and a monolayer where the chains are tilted somewhat from the normal^{1, 2}. On the other hand, these *bolaamphiphiles*, when deposited on mono- or bi-metal ionic subphases, yield crystalline multilayer films where the molecules lie only parallel to the aqueous solution surface, with the appropriate metal cations intercalated within the structure, forming alternating metal ionic films (see Fig. 2a in section 2.6.4.). The observed X-ray diffraction peaks at long spacings could all be assigned Miller indices $\{0, k\}$, yielding a horizontal d_{01} lattice spacing of 70-80 Å, depending upon the length of the molecule in the series. The experimental shape of the multilayer Bragg rods, which peak at $q_z=0 \text{ \AA}^{-1}$, implies an arrangement where the bound metal ions are aligned in sheets perpendicular to the solution surface. The FWHM(q_z) of these Bragg rods provides an estimate of the film thickness $L \sim 40 \pm 10 \text{ \AA}$, which would correspond to about seven layers. The d_{01} spacing corresponds in length to two *bolaamphiphilic* molecules, linked head-to-head and tail-to-tail, via two different ionic complexes, two amino acids with Cu²⁺ and two carboxylic acids with Pb²⁺. Support for this model comes from the observed differences in the d_{01} spacing, which correspond nicely to the differences between the calculated lengths of the molecules in the series [$d_{l\text{-C}22\text{lys}}-d_{l\text{-C}22\text{Orn}}=3.2 \text{ \AA}_{\text{obs}}$, $2.4 \text{ \AA}_{\text{calc}}$, $d_{dl\text{-C}22\text{lys}}-d_{dl\text{-C}22\text{Orn}}=3.4 \text{ \AA}_{\text{obs}}$, $2.4 \text{ \AA}_{\text{calc}}$, $d_{dl\text{-C}24\text{lys}}-d_{dl\text{-C}22\text{Lys}}=4.9 \text{ \AA}_{\text{obs}}$, $4.8 \text{ \AA}_{\text{calc}}$], thus demonstrating the strong dependence of the long spacing on the length of the molecule forming it, in keeping with the model arrangement. It is possible to estimate the angle γ formed between the molecular chain axis and the plane of the metal sheet by comparing the observed d_{01} spacing (between the metal sheets) with the estimated length L of the molecular chain axis. The angle γ is given by $\sin \gamma = d_{01}/L$, resulting in $\gamma = 73.5^\circ$ on average (see Table 1). This type of molecular packing is similar to that formed on monometallic cation subphases by diacid *bolaamphiphiles*¹.

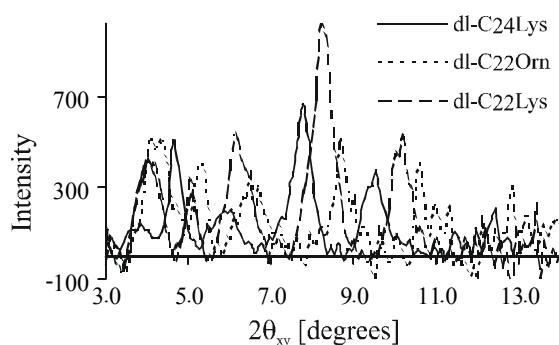


Fig. 1. The positions (along $2\theta_{xy}$) and intensities of the Bragg peaks, integrated along q_z measured for (*d, l*) amphiphile series spread on mixed Cu(Acetate)₂ and Pb(Acetate)₂ subphase.

| Compound | Measured d_{01} spacing (Å) | Calculated axial length (Å) |
|-------------------------------------|-------------------------------|-----------------------------|
| <i>l</i> -C ₂₂ Orn | 69.7 | 73.6 |
| (<i>d, l</i>)-C ₂₂ Orn | 70.2 | 73.6 |
| <i>l</i> -C ₂₂ Lys | 72.9 | 76.0 |
| <i>d</i> -C ₂₂ Lys | 73.4 | 76.0 |
| (<i>d, l</i>)-C ₂₂ Lys | 73.6 | 76.0 |
| (<i>d, l</i>)-C ₂₄ Lys | 78.5 | 80.8 |

Table 1. Long axial spacings of the *bolaamphiphilic* series.

We are grateful for support by the SNF (DanSync), the IHP contract HPRI-CT-1999-00040 (EC) and for beam time at beam line BW1 at HASYLAB at DESY, Hamburg, Germany.

¹ I. Weissbuch, S. Guo, R. Edgar, S. Cohen, P. B. Howes, K. Kjær, J. Als-Nielsen, M. Lahav and L. Leiserowitz, *Adv. Mater.* **10**, 117 (1998); I. Weissbuch, R. Popovitz-Biro, M. Lahav, L. Leiserowitz, J. Als-Nielsen, P. B. Howes and K. Kjær, *Risø-R-1014(EN)* p. 89 (1997).

² R. Popovitz-Biro, R. Edgar, J. Majewski, S. Cohen, L. Margulis, K. Kjær, J. Als-Nielsen, L. Leiserowitz and M. Lahav, *Croat. Chem. Acta.* **69**, 689 (1996).

2.6.6. Self-assembly of interdigitated bilayers of long-chain cholesteryl esters at the air-water interface. Effect of long-chain alcohol and acid additives

C. Alonso, I. Kuzmenko, M. Lahav, L. Leiserowitz, *Materials and Interfaces Department, Weizmann Institute of Science, Israel*, T. R. Jensen and K. Kjær, *Condensed Matter Physics and Chemistry Department, Risø National Laboratory, Denmark*
e-mail: kristian.kjaer@risoe.dk

Interdigitation occurs in three-dimensional (3-D) crystals for the packing of molecules composed of two parts, a hydrocarbon chain of cross-sectional area 18-20 Å² and another moiety with twice the area, as in the 3-D crystals of some long-chain esters of cholesterol¹. Chain interdigitation can also occur in 2D-crystalline bilayers composed of molecules *A* and *B*, exhibiting acid-base complementarity, that form *-A-B-A-B-A-B-* molecular arrays at the air-solution interface, where *A* is a water-insoluble amphiphile bearing a long hydrocarbon chain substituent and *B* is water-soluble without a chain². The interdigitated multilayer can be obtained by compression of such a monolayer film beyond its collapse point. But a mono component bilayer system had not been observed and this is what we have attempted to design, making use of long-chain cholesteryl esters (cholesteryl-O-CO-C_{*n*}-1)H_{2*n*-1}, designated CE-*n*, *n*=13, 16, 18). We have shown by grazing-incidence X-ray diffraction (GIXD) that cholesteryl esters do indeed spontaneously self-assemble on the water surface in order to form interdigitated bilayer films (see Fig. 1). The unit cell parameters of such bilayers at the air-water interface almost match those of the three-dimensional counterpart and thus could provide useful information on the early stages of nucleation of such interdigitated systems.

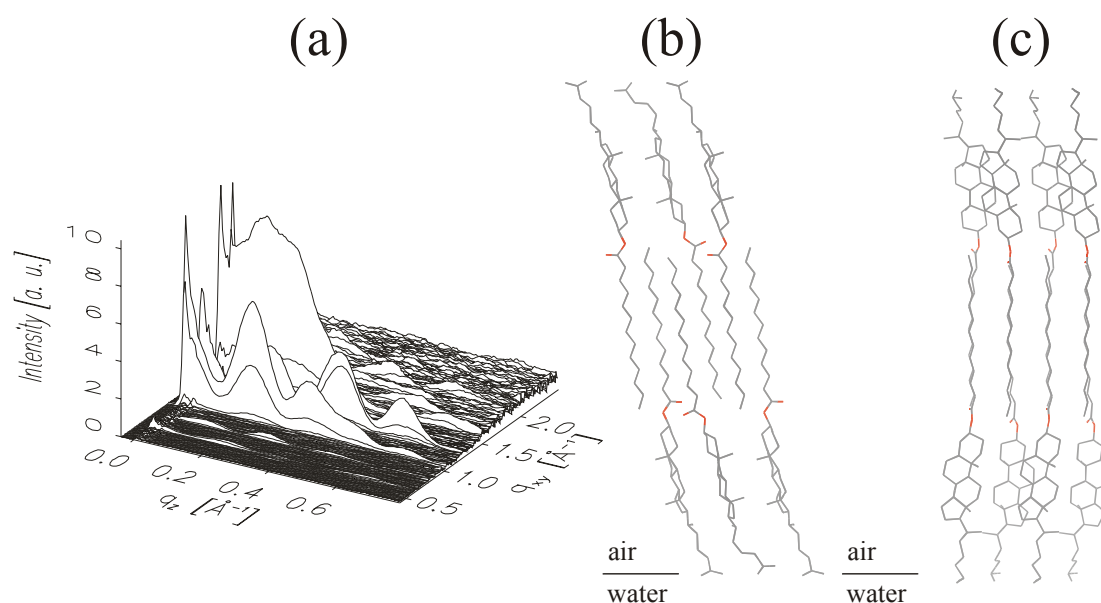


Fig. 1. a) GIXD pattern of a film of CE-13 on water and the corresponding structure. (b, c) views along *b* and *a* axis respectively

We have further considered the possibility of inhibiting the formation of the interdigitated bilayer (Fig. 1b, c, schematic in Fig. 2a) of the long chain cholesteryl esters (CE-*n*, *n*=16,18) by replacing the bottom layer with a long-chain additive molecule such that the system would retain the same chain-chain interactions (Fig. 2b). Successful chain substitution by the foreign molecules would simulate solvent-induced inhibition of the 3D crystal growth of corrugated faces of the 3-D crystals by solvent docking into the grooves of the corrugated surface as has been observed by the effect of water on the α -form of resorcinol, and of methanol and ethanol on the growth of *R,S* alanine and α -glycine³. The

¹ D. M. Small, *The physical chemistry of lipids. Handbook of lipid research* **4**, Plenum Press, New York, (1986); J. A. Barnard and J. E. Lydon, *Mol. Cryst. Liq. Cryst.* **26**, 285 (1974).

² Kuzmenko, R. Buller, W. Bouwman, K. Kjær, J. Als-Nielsen, M. Lahav and L. Leiserowitz, *Science* **274**, 2046 (1996).

³ I. Weissbuch, R. Popovitz-Biro, M. Lahav and L. Leiserowitz, *Acta Cryst.* **B 51**, 115 Part 2 (1995).

additives tried with CE-16 were the long-chain alcohol $C_{15}H_{31}OH$ and acid $C_{14}H_{29}COOH$ and with CE-18, $C_{17}H_{35}OH$ and $C_{17}H_{35}COOH$. As anticipated, the GIXD patterns (Fig. 2c) for 1:1 mixtures of the CE- n and an amphiphilic molecule of the corresponding length indicated formation of the crystalline monolayer on the water surface, instead of the interdigitated bilayer observed for pure CE- n . For each of the four mixtures, five Bragg rods were detected corresponding to a rectangular unit cell of dimensions very close to those observed for the pure CE- n bilayer. But unlike the bilayer, the Bragg rods of the 1:1 mixture exhibit no intensity modulations along q_z and have a FWHM(q_z) compatible with a monolayer (thickness=35 Å). The unit cell contains four molecular units, with the ester and amphiphilic molecules present in the 1:1 ratio.

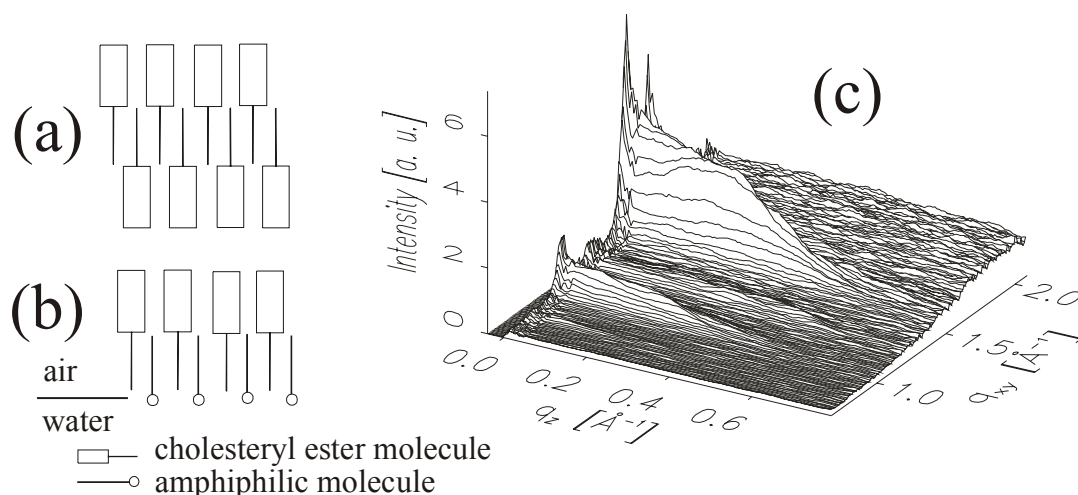


Fig. 2. a) Schematic representation of an interdigitated bilayer, b) schematic representation of the packing of a 1:1 mixture of long chain cholesteryl ester with an amphiphilic molecule, c) diffraction pattern of a 1:1 mixture of CE-18 and $C_{17}H_{35}OH$ yielding a rectangular cell ($a=10.07$ Å and $b=7.54$ Å).

We are grateful for support by the SNF (DanSync) and the EC (IHP contract HPRI-CT-1999-00040) and for beam time at beam line BW1 in HASYLAB at DESY, Hamburg, Germany.

2.6.7. Specific recognition between cholesteryl glutamate and amino acids at the air-liquid interface

C. Alonso, R. Eliash, M. Lahav, L. Leiserowitz, *Materials and Interfaces Department, Weizmann, Institute of Science, Rehovot 76100, Israel*, T.R. Jensen and K. Kjær, *Condensed Matter Physics and Chemistry Department, Risø National Laboratory, 4000 Roskilde, Denmark*
e-mail: kristian.kjaer@risoe.dk

Amino acids being the basic building blocks of proteins, understanding and monitoring their nucleation and crystal growth is an important goal. In order to induce interactions between amino acids and eventually promote their crystallization we have investigated a monolayer, at the water surface, of an amino acid derivative of cholesterol (cholesteryl-*L*-glutamate), designed to give an open structure able to incorporate other amino acids. By grazing-incidence X-ray diffraction we have shown that on water cholesteryl-*L*-glutamate self-assembles in a crystalline monolayer within which the packing is imposed by cholesterol moieties ($a=10.2$ Å, $b=7.6$ Å, $\gamma=92.2^\circ$, Fig. 1), thus effectively yielding voids between the glutamate moieties where a short amino acid can be adsorbed. On spreading cholesteryl-*L*-glutamate on solutions of such short amino acids, we have found that water-soluble hydrophobic amino acids interact with this monolayer by docking into the grooves between the glutamate moieties, yielding lattices ($a=11.8$ Å, $b=9.4$ Å, $\gamma=91.2^\circ$) for *L*-phenylalanine and ($a=11.8$ Å, $b=9.1$ Å, $\gamma=93.7^\circ$) for *L*- and *D*-leucine. Thus the monolayer of cholesteryl-*L*-glutamate specifically recognises hydrophobic amino acids molecules dissolved in the subphase.

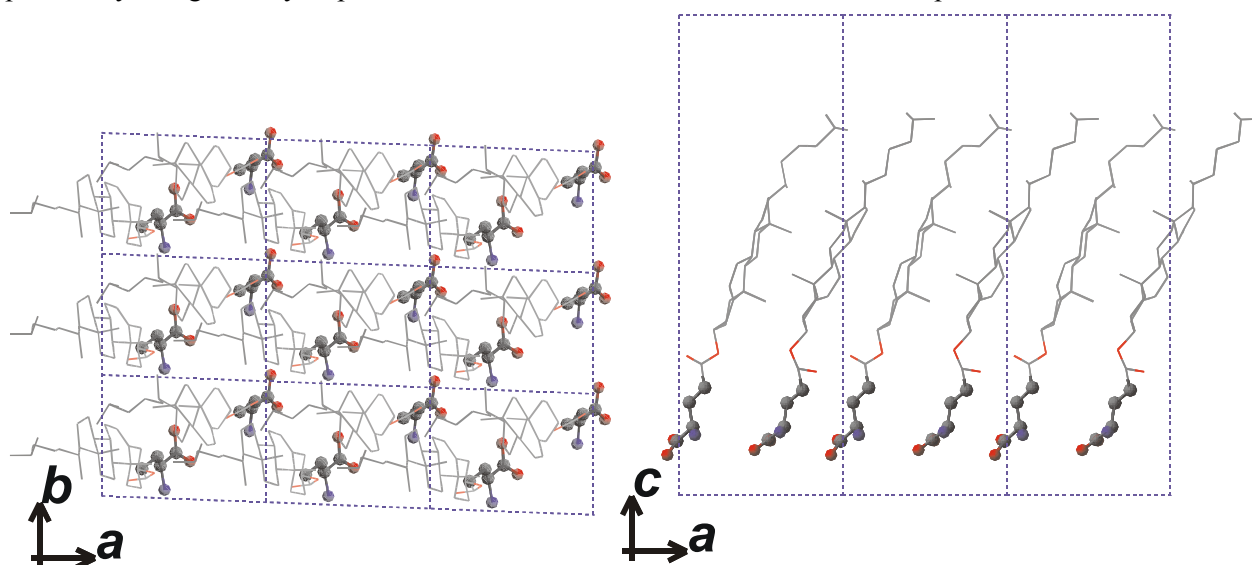


Fig. 1. Packing of a monolayer of cholesteryl-*L*-glutamate.

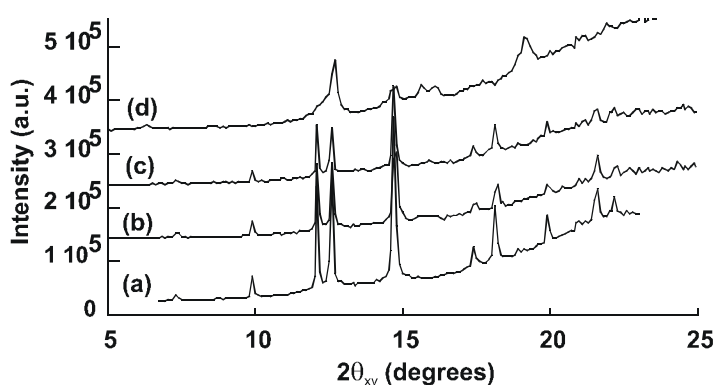


Fig. 2. Diffraction patterns for cholesteryl-*L*-glutamate spread on: (a) water, (b, c, d) on solutions of *L*-asparagine, *L*-glutamine, *L*-leucine respectively.

Moreover, for *L*-leucine (but only *L*-) we also observed crystallisation of a leucine bilayer ($a=9.1 \text{ \AA}$, $b=5.2 \text{ \AA}$, $\gamma=93.7^\circ$), presumably by line epitaxy with the monolayer. This additional phase is not observed in the case of *D*-leucine and no interaction at all was detected with a racemic solution (Fig. 3). These results are not dependent upon concentration.

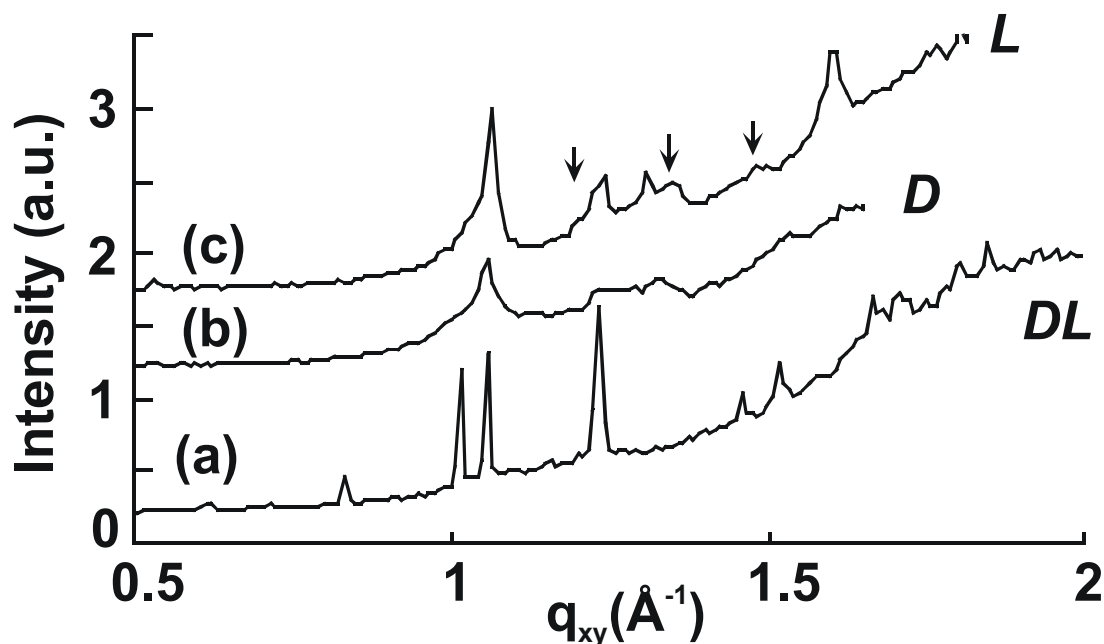


Fig. 3. Comparison of diffraction patterns of a monolayer of cholesteryl-L-glutamate spread on solutions of (a) *DL*-leucine, (b) *D*-leucine, (c) *L*-leucine; the arrows mark Bragg peaks of the leucine bilayer (barely visible in this q_z -integrated view).

This approach may allow us to determine the critical size of nuclei to induce crystal growth of amino acids and to follow the growth.

We are grateful for support by the SNF (DanSync) and the EC (IHP contract HPRI-CT-1999-00040) and for beam time at beam line BW1 in HASYLAB at DESY, Hamburg, Germany.

2.6.8. Mixed films of cholesterol derivatives at the air-solutions interface

R. Eliash, C. Alonso, M. Lahav and L. Leiserowitz, *Department of Materials & Interfaces, Weizmann Institute of Science, Israel*, T. R. Jensen and K. Kjær, *Condensed Matter Physics and Chemistry Department, Risø National Laboratory, Denmark*
e-mail: kristian.kjaer@risoe.dk

Cholesterol and cholesterol derivatives tend to form crystalline 2D films at the air water interface¹. These cholesteryl monolayers and multi-layers have a characteristic rectangular unit cell of $7.5 \times 10 \text{ \AA}^2$. Using this feature we have designed a mixed monolayer of cholesteryl- γ -(L)-glutamate (**1**) and cholesteryl valerate (**2**) expecting that the monolayer will have the typical packing, leaving at the air-water interface empty spaces which would have a size suitable for binding amino acids from solution (Fig 1). We used grazing-incidence X-ray diffraction (GIXD) for the study of the films. GIXD was measured from films of a 1:1 mixture of cholesteryl- γ -(L)-glutamate (**1**) and cholesteryl valerate (**2**) spread on water and on different aqueous solutions of amino acids [(L)-glutamine, (L)-asparagine, (L)-leucine]. The only system that gave diffraction was the mixture on (L)-leucine (Fig 2). After doing the control experiments of each of the amphiphile spread on each of the subphases we discovered that the diffraction for the mixed film is identical to the sum of each film spread separately, so that the expected composite phase has *not* been formed. We plan to continue the investigation, replacing cholesteryl valerate (**2**) by cholesteryl-4-hydroxy-valerate, expecting that a stronger interaction of the amphiphile with the water will facilitate the formation of the mixed monolayer. Cholesteryl- γ -(L)-glutamate (**1**) gave diffraction on all subphases². Cholesteryl valerate (**2**) gave diffraction only on (L)-leucine. The diffraction pattern was indexed using a rectangular cell: $a=9.3 \text{ \AA}$, $b=12.6 \text{ \AA}$. Construction of a model for the structure of this film is now in progress. We have yet to understand why cholesteryl valerate (**2**) forms an ordered monolayer on (L)-leucine but not on water or the hydrophilic amino acids. We plan to perform experiments with different amino acids in order to better understand this phenomenon.

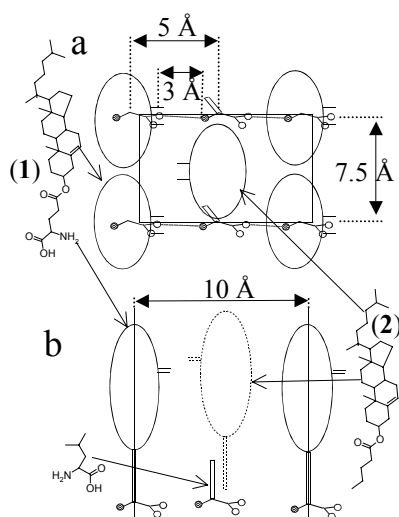


Fig 1. One unit cell of the expected (now disproven) three-component structure. a) Top view. b) Side view.

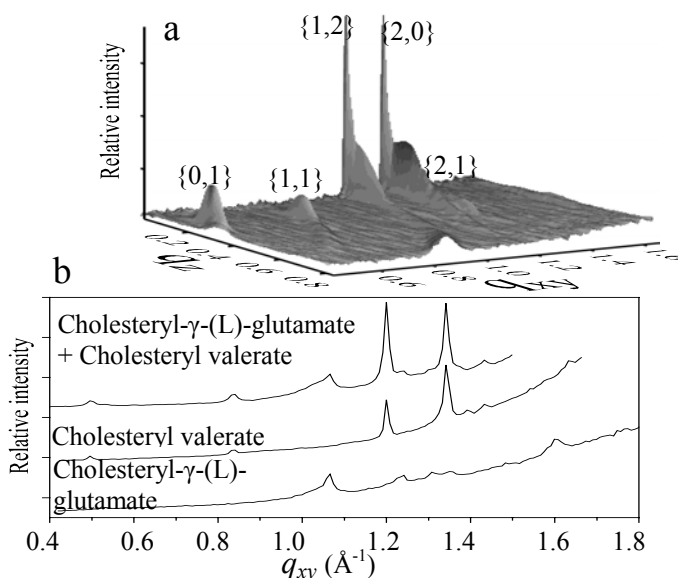


Fig 2. a) GIXD pattern showing surface plot $I(q_{xy}, q_z)$ as measured from cholesteryl valerate on aqueous solution of (L)-leucine. b) Comparison between GIXD patterns of three amphiphiles on aqueous solution of (L)-leucine

We are grateful for support by the SNF (DanSync), the IHP contract HPRI-CT-1999-00040 (EC) and for beam time at beam line BW1 at HASYLAB at DESY, Hamburg, Germany.

¹ S. Lafont, H. Rapaport, G. J. Somjen, A. Renault, P. B. Howes, K. Kjær J. Als-Nielsen, L. Leiserowitz, and M. Lahav, *Journal of Physical Chemistry B* **102** 761 (1998).

² See section 2.6.7 of this report.

2.6.9. Monitoring a polymerization reaction in a self-assembled monolayer at the air-water interface

I. Weissbuch, M. Lahav, L. Leiserowitz, *Materials and Interfaces Department, The Weizmann Institute of Science, Israel*, T. R. Jensen and K. Kjær, *Condensed Matter Physics and Chemistry Department, Risø National Laboratory, Denmark*
e-mail: kristian.kjaer@risoe.dk

The grazing-incidence X-ray diffraction (GIXD) technique has been found very informative in monitoring chemical reactions in monolayers at the air-liquid interface. Within the frame of a project concerning the generation of homochiral oligo-peptides from their racemic monomer precursors in self-assembled two-dimensional (2-D) crystals, we have monitored – by GIXD – the polymerization reaction of an enantiomerically pure N^α -carboxyanhydride derivative of N^ϵ -stearoyl-lysine (NCA- C_{18} -lys) in monolayers at the air-aqueous solution interface. Self-assembled 2-D crystals of stable NCA- C_{18} -lys monomer molecules are formed when they are spread on water at 4°C.¹ However, the GIXD patterns measured from monolayers spread on water at 20°C show, in addition to the major crystalline phase of the NCA- C_{18} -lys, the appearance of weak Bragg peaks that belong to a different phase (Fig. 1a). When an aqueous solution of nickel acetate was injected beneath the film the intensities of these peaks increase with concomitant decrease of those belonging to the major monomer phase. Thus the GIXD pattern clearly shows coexistence of two crystalline phases, one phase of the monomer **1** and the second phase consisting of the oligo-peptide products **2** generated by the catalyzed polymerization reaction (Fig. 1b). Upon injection of a second portion of the catalyst beneath the film, the monomer phase disappears and the GIXD pattern shows only the presence of the oligo-peptide products phase (Fig. 1c). This crystalline phase is very similar to that obtained by spreading the monomer molecules directly on the aqueous solution of the catalyst¹. Moreover, analysis by matrix-assisted laser-desorption ionization-time of flight mass spectrometry of samples taken from the air-liquid interface indicates the formation of a mixture of oligo-peptides up to 12 repeat units long.

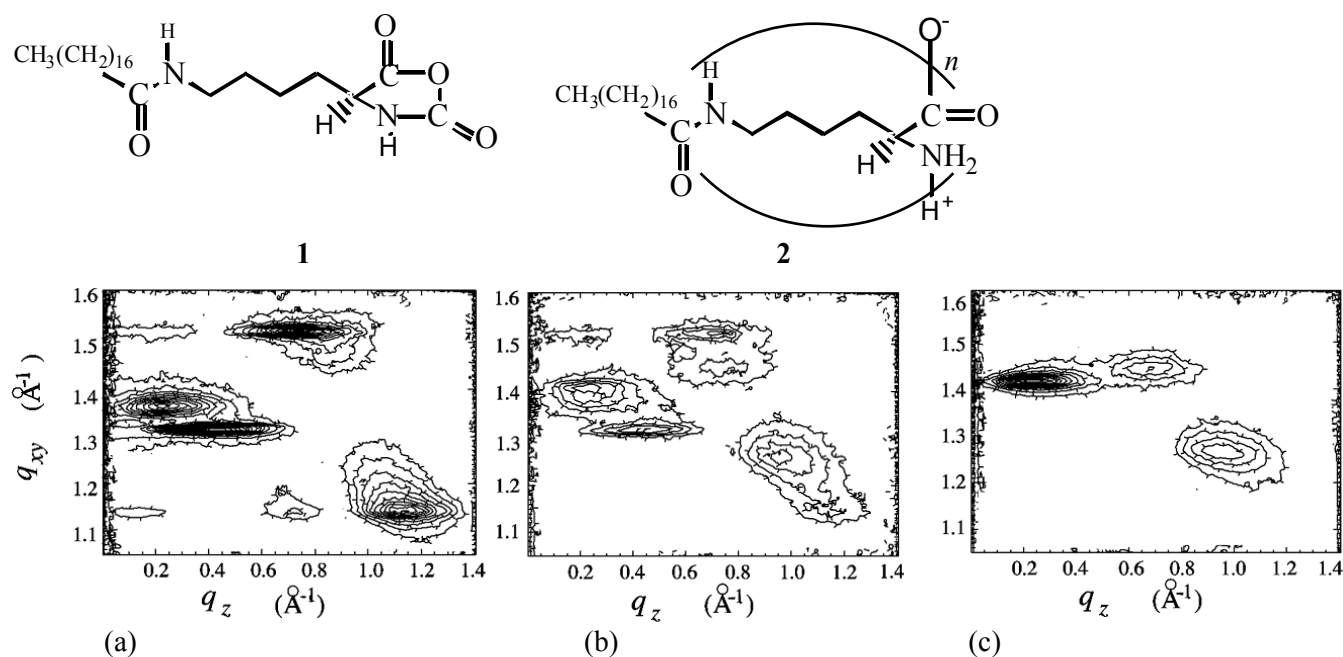


Fig. 1. Monitoring the polymerization reaction by GIXD, shown as contour plots of scattered intensity $I(q_{xy}, q_z)$: (a) monomer molecules spread on water at 20°C and then cooled to 4°C; (b) after injection of the first portion of nickel acetate catalyst beneath the film; (c) after second injection of catalyst.

We are grateful for support by the SNF (DanSync), the IHP contract HPRI-CT-1999-00040 (EC) and for beam time at beam line BW1 at HASYLAB at DESY, Hamburg, Germany.

¹ I. Weissbuch, M. Lahav, L. Leiserowitz, J. Als-Nielsen, T. R. Jensen and K. Kjær, *Risø-R-1156(EN)* 79 (2000).

2.6.10. Homochiral oligo-peptides from racemic precursors

I. Weissbuch, M. Lahav, L. Leiserowitz, *Materials and Interfaces Department, The Weizmann Institute of Science, Israel*, T. R. Jensen and K. Kjær, *Condensed Matter Physics and Chemistry Department, Risø National Laboratory, Denmark*
e-mail: kristian.kjaer@risoe.dk

Recently, we have studied the formation of homochiral peptides via a surface polymerization reaction from racemic N^α -carboxyanhydride derivative of N^ϵ -stearoyl-lysine (NCA- C_{18} -lys) that undergo spontaneous separation into enantiomorphous crystalline domains at the air-water interface¹. The initial self-assembly process into domains containing molecules of single handedness implies molecular packing *via* translation symmetry. This packing arrangement is favored by the presence, within the hydrocarbon chain, of an amide group that promotes $C=O \cdots H-N$ intermolecular hydrogen-bonding along a 5 Å axis. However, racemic NCA- C_{18} -lys amphiphile spread on water surface was found to be too reactive to allow monitoring the spontaneous separation by grazing incidence X-ray diffraction (GIXD). Therefore, new compounds have been considered in our search for an optimized molecule which, on one hand, undergoes spontaneous separation and, on the other hand, is an α -aminoacid reactive derivative that reacts only when a catalyst initiates the polymerization reaction. In this study we focus on the self-assembly behavior of N^ϵ -stearoyl-thio-lysine amphiphiles. The GIXD patterns measured from self-assembled monolayers of enantiomeric and racemic C_{18} -thio-lys on water at 4°C are shown in Fig. 1. The two patterns are very similar, being consistent with a molecular packing in an oblique unit cell of dimensions $a=4.91$ Å, $b=6.41$ Å, $\gamma=123.8^\circ$. This unit cell contains one molecule so the packing arrangement is *via* translation symmetry. The parallel hydrocarbon chains are tilted by 43° from the surface normal and are hydrogen-bonded along the a axis. Such an arrangement is consistent with the spontaneous separation of the racemic amphiphile into enantiomorphous crystalline domains containing molecules of single handedness. In contrast with NCA- C_{18} -lys, racemic C_{18} -thio-lys spread on water surface is a stable monomer molecule that polymerizes only in the presence of the catalyst. The enantiomeric distribution of the oligo-peptide products was determined by mass spectrometrical analysis of (deuterium labelled) samples taken from the water interface.

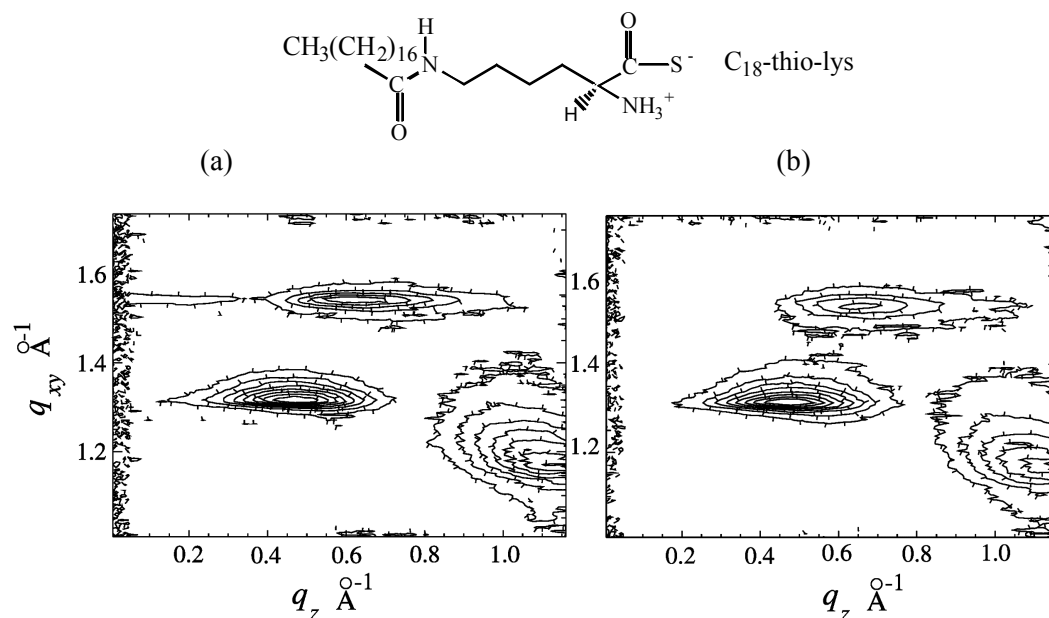


Fig. 1. GIXD patterns, shown as contour plots of scattered intensity $I(q_{xy}, q_z)$, measured from self-assembled monolayers of: (a) enantiomerically pure and (b) racemic stearoyl-thio-lysine on water surface.

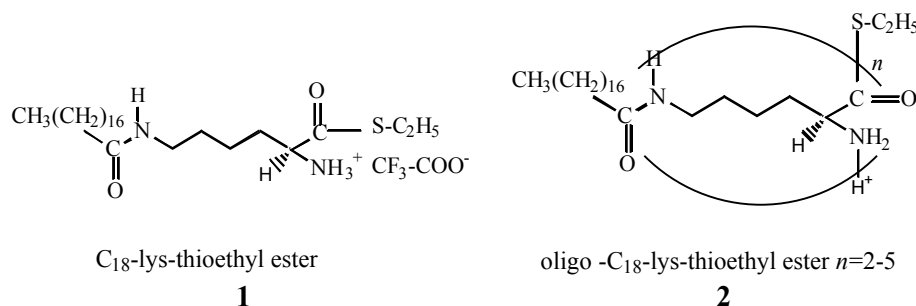
We are grateful for support by the SNF (DanSync), the IHP contract HPRI-CT-1999-00040 (EC) and for beam time at beam line BW1 at HASYLAB at DESY, Hamburg, Germany.

¹ I. Weissbuch, L. Leiserowitz, M. Lahav, J. Als-Nielsen, T. R. Jensen and K. Kjær, *Risø-R-1156(EN)* 79 (2000).

2.6.11. Two-dimensional packing arrangement of enantiomerically pure and racemic stearyl-lysine-thioethyl esters

I. Weissbuch, M. Lahav, L. Leiserowitz, *Materials and Interfaces Department, The Weizmann Institute of Science, Israel*, T. R. Jensen and K. Kjær, *Condensed Matter Physics and Chemistry Department, Risø National Laboratory, Denmark*
 e-mail: kristian.kjaer@risoe.dk

The two-dimensional packing arrangements of enantiomerically pure and racemic mixtures of trifluoro-acetate salts of N^ε-stearyl-lysine-thioethyl esters were determined by grazing incidence X-ray diffraction (GIXD) directly at the air-water interface. Such molecules could be potential candidates for the generation of homochiral oligo-peptides by a catalyzed polymerization reaction, if they would self-assemble into enantiomorphous two-dimensional crystals. The polymerization of such monomers **1** can be initiated by injection of Ag⁺/acetate⁻ catalyst beneath the film, as determined by mass spectrometric analysis of the generated oligo-peptides **2** in samples taken from the liquid surface.



However, the GIXD patterns measured from monolayers of enantiomerically pure and racemic mixtures of the monomers **1**, spread on water at 4 °C, are very different (Fig. 1). The enantiomeric C₁₈-lys-thioethyl ester packs in a pseudo-rectangular unit cell, ($a=5.14$ Å, $b=8.98$ Å, $\gamma=97.3^\circ$) containing two molecules with their chains related by a pseudo-glide parallel to the a axis (a weak $\{0,1\}$ reflection at $q_{xy}=0.7$ Å⁻¹ is not shown). The racemic molecules pack in a pseudo-rectangular unit cell ($a=5.07$ Å, $b=8.79$ Å, $\gamma=86.5^\circ$) (weak $\{1,0\}$ and $\{0,1\}$ reflections at $q_{xy}=1.28$ and $q_{xy}=0.7$ Å⁻¹ are not visible in Fig. 1). The packing arrangement of the enantiomer is significantly different from that of the racemate, indicating that the latter does not spontaneously separate in domains of right- and left-handed molecules. Thus, the racemate packs in a true racemic crystal with one left- and one right-handed molecule in the unit cell so the polymerization products are heterochiral oligo-peptides.

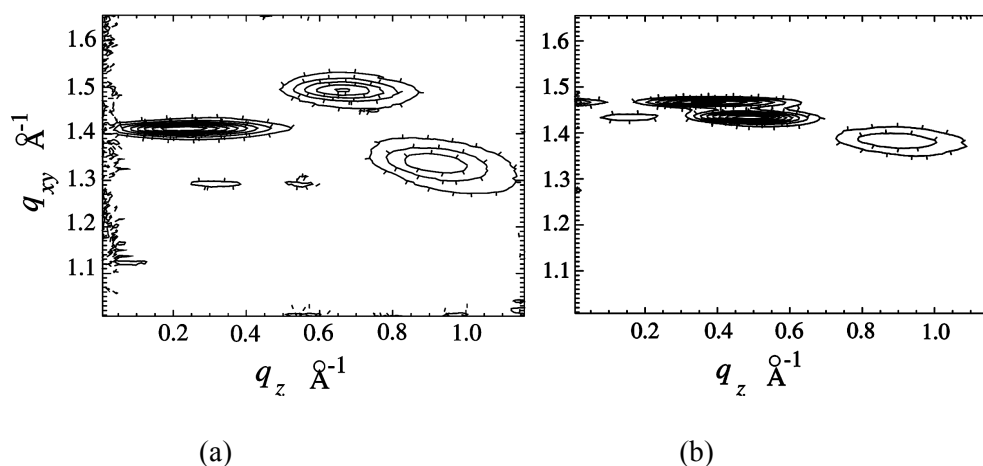


Fig. 1. GIXD patterns, shown as contour plots of scattered intensity $I(q_{xy}, q_z)$, of self-assembled monolayers of: (a) enantiomeric and (b) racemic stearyl-lysine-thioethyl ester **1** on water at 4 °C.

We are grateful for support by the SNF (DanSync) and the EC (IHP contract HPRI-CT-1999-00040) and for beam time at beam line BW1 in HASYLAB at DESY, Hamburg, Germany.

2.6.12. Polystyrene sulfonate at the air-liquid interface

M. Kent, H. Yim, *Sandia National Laboratories, Albuquerque, USA*, J. Majewski, G. S. Smith, *Manuel Lujan Neutron Scattering Center, USA* and K. Kjær, *Condensed Matter Physics and Chemistry Department, Risø National Laboratory, Denmark*
e-mail: kristian.kjaer@risoe.dk

The adsorption of polyelectrolytes onto surfaces is an important factor in stabilization of emulsions in the food, photographic, paint, water purification, flotation separations, enhanced oil recovery, and pharmaceutical industries. Adsorption of biological polyelectrolytes is important for understanding biochemical processes and also for controlling fouling in biotechnological operations. Previously we have used neutron reflectivity to examine the adsorption of the strong polyelectrolyte deuterated polystyrene sulfonate (d-PSS) to the air-liquid interface¹. While the trends of adsorbed amount and layer thickness were in agreement with self-consistent field calculations, the measured bilayer profiles contrasted with the smoothly decaying theoretical profiles². Additionally, the distribution of salt and counter ions was not accessible with neutrons. Work at HASYLAB was performed to address these issues. X-ray reflectivity (XR) was recorded for the high molecular weight sample in dilute concentration as a function of salt concentration. Sample data are shown in Fig. 1. The fitted electron density profiles are shown in Fig. 2. These data revealed that at the air interface an excess of electron density is present, the magnitude of which increases with increasing salt concentration. This elevated electron density is most likely due to a high concentration of counter ions associated with the dense polymer layer at the air surface. This would indicate a very high degree of counter ion condensation. The alternative interpretation, an excess of salt at the air interface, is more difficult to rationalize. Further studies are needed to address the effect of polymer concentration, as the neutron data suggest that the concentration of adsorbed polymer decreases with increasing polymer concentration.

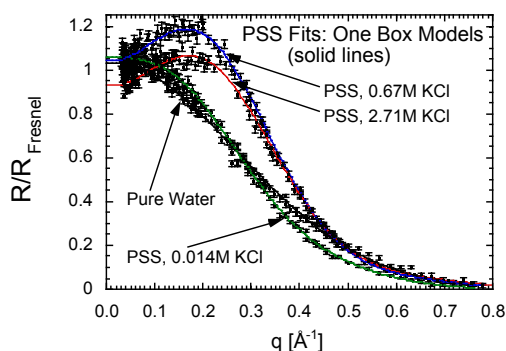


Fig. 1. XR from air interface of a solution of polystyrene sulfonate ($M=1150$ kg/mol) as a function of KCl concentration.

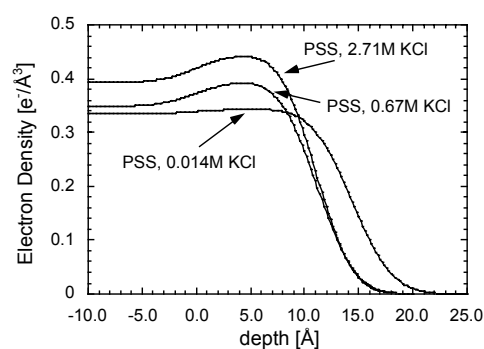


Fig. 2. Fitted electron density profiles showing an excess of electron density within a thin layer (~ 10 Å) at the air interface.

We are grateful for support by the SNF (DanSync) and the EC (IHP contract HPRI-CT-1999-00040) and for beam time at beam line BW1 in HASYLAB at DESY, Hamburg, Germany.

¹ H. Yim, M. Kent, A. Matheson, R. Ivkov, S. Satija, J. Majewski and G. S. Smith, *Macromolecules* **33**, 6126 (1999).

² G. J. Fleer, M. A. Cohen-Stuart, M. J. M. H. M. Scheutjens, T. Cosgrove and B. Vincent, *Polymers at Interfaces*; Chapman and Hall; London (1993).

2.6.13. Mixed ganglioside/phospholipid Langmuir monolayers

J. Majewski, G. S. Smith, *Manuel Lujan Neutron Scattering Center, Los Alamos National Laboratory, USA*, T. L. Kuhl, *Department of Chem. Engineering and Material Science, University of California, USA*, J. N. Israelachvili, *Materials Research Laboratory, University of California, USA* and K. Kjær, *Condensed Matter Physics and Chemistry Department, Risø National Laboratory, Denmark*
 e-mail: kristian.kjaer@risoe.dk

Lipid molecules containing sugar groups are called glycolipids. Glycolipids occur in animal cell plasma membranes and play a role in recognition, adhesion, regulation, and transduction of cells, development of tissues and protection from low pH or degradative enzymes^{1, 2}. They effect the electrical field across the membrane and the concentration of ions at its surface. A common glycolipid is galactosyl-N-acetylgalacto-saminyln(N-acetyl-neuraminyln)galactosylglucosylceramide ganglioside (GM₁, cf. Fig. 1). GM₁ can be incorporated in lipid bilayers to concentrations up to 30 mole %. To understand the role of GM₁ in cellular membranes, it is useful to determine the effect of GM₁ on monolayer structures. Using synchrotron grazing-incidence x-ray diffraction (GIXD) and reflectivity (XR), the in- and out-of-plane structure of mixed ganglioside GM₁ – phospholipid monolayers was investigated at the air–water interface. Mixed monolayers of the phospholipid dipalmitoylphosphatidylethanolamine (DPPE, cf. Fig. 1) and 5, 10, 20, and 100 mole % GM₁ were studied at a surface pressure of 45 mN/m at 23°C.

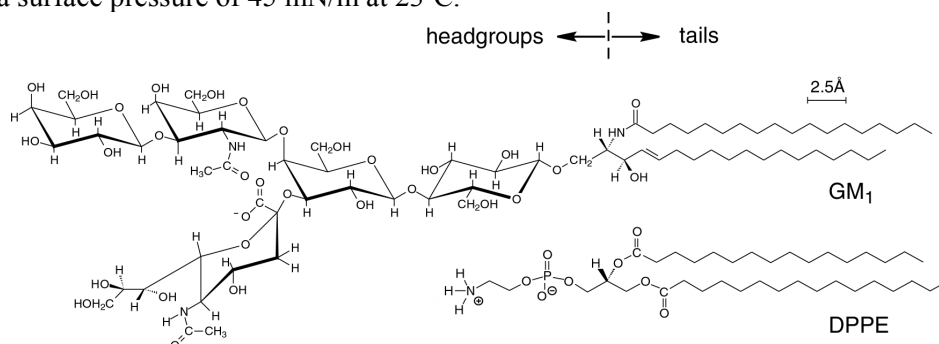


Fig. 1

| Compo- sition | In-Plane Bragg Peaks | | | | | | | Out-of-Plane Bragg Rods | | | |
|-------------------------------|-------------------------------------|---|--|--|------|-------|---------------------------------|-----------------------------------|-------------------|--------------------------|-------------------|
| | Observed d -spacing (Å) | Area per molecule (Å ²) | Projected Area (Å ²) | Primitive Unit Cell a, b, γ (Å, Å, degrees) | | | Coherence Length, L (Å) | Coherence Length, L_c (Å) | tilt angle (°) | tilt direction (°) | σ_z (Å) |
| DPPE | $d_{10} = d_{01} = d_{1-1}$ 4.16 | 39.9 | 39.8 | 4.80 | 4.80 | 120.0 | $L_{10,01,1-1}$ 530 | 18.8 | 3.5 | n/a (*) | 0.5 |
| GM ₁ | $d_{10} = d_{01} = d_{1-1}$ 4.22 | 41.1 | 40.9 | 4.87 | 4.87 | 120.0 | $L_{10,01,1-1}$ 50 | 19.0 | 6.0 | n/a (*) | 0.5 |
| 95:5 DPPE:GM ₁ | $d_{10} = d_{01} = d_{1-1}$ 4.17 | 40.2 | 40.1 | 4.82 | 4.82 | 120.0 | $L_{10,01,1-1}$ 530 | 18.8 | 3.5 | n/a (*) | 0.5 |
| 90:10 DPPE:GM ₁ | $d_{10} = d_{01} = d_{1-1}$ 4.17 | 40.2 | 40.1 | 4.82 | 4.82 | 120.0 | $L_{10,01,1-1}$ 525 | 18.8 | 3.5 | n/a (*) | 0.5 |
| 80:20 DPPE:GM ₁ | $d_{10} = d_{01} = d_{1-1}$ 4.17 | 40.2 | 40.1 | 4.82 | 4.82 | 120.0 | $L_{10,01,1-1}$ 520 | 18.8 | 3.5 | n/a (*) | 0.5 |

(*) The tilt direction is not well-determined for small tilt angles.

Table 1

Over the concentration range studied the increased packing stresses from the large oligosaccharide groups of the GM₁ molecule did not distort the in- and out-of-plane 2-D unit cell of the pure DPPE monolayer (see Table 1). The results suggest that the GM₁ lipids are accommodated within the DPPE unit cell and that staggering of the molecules to reduce lateral interactions does not occur. No diffraction signal from the GM₁ headgroup was detected in the GIXD but it contributes strongly to the

¹ B. Alberts, J. D. Watson, D. Bray, K. Roberts, J. Lewis, M. Raff and R. Adams (eds.), *Molecular Biology of the Cell*, 3rd Edition Garland Publishing Inc. New York, 484 (1994).

² B. Maggio, *Prog. Biophys. Molec. Biol.* **62**, 55 (1994).

monolayer XR profiles (cf. Fig. 2), indicating that the oligosaccharide extends into the water and does not penetrate into the hydrophobic region. Our findings suggest that the monolayer packing is determined by the limiting area of the hydrocarbon tails not the cross-sectional area of the oligosaccharide groups.

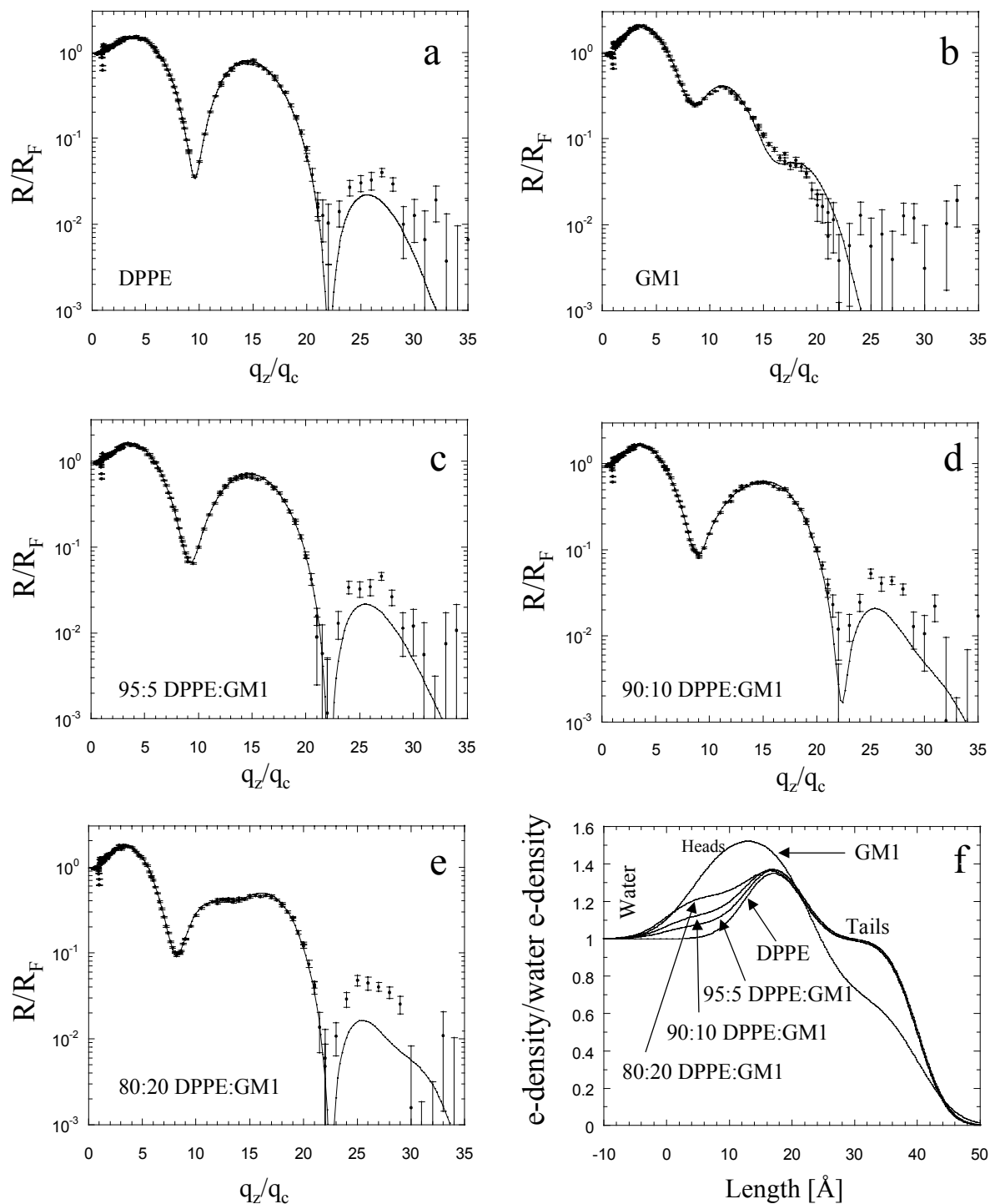


Fig. 2.

We are grateful for support by the SNF (DanSync) and the EC (IHP contract HPRI-CT-1999-00040) and for beam time at beam line BW1 in HASYLAB at DESY, Hamburg, Germany.

2.6.14. Studies on mixed Gramicidin D - lipid monolayers at the air water interface

F. Bringezu, J. A. Zasadzinski, *Department Chem. Engineering, Engineering II, Santa Barbara, USA*, G. Brezesinski, *Max Planck Institute of Colloids and Interfaces, Golm/Potsdam, Germany*, T. R. Jensen and K. Kjær, *Condensed Matter Physics and Chemistry Department, Risø National Laboratory, Denmark*
 e-mail: kristian.kjaer@risoe.dk

The understanding of the molecular basis of interactions between phospholipids and amphiphilic peptides is an important issue in biophysical research. Here we report on our studies of protein-lipid interactions using Grazing Incidence X-ray Diffraction (GIXD) on mixed Gramicidin D (GD) / lipid monolayers at the air water interface. Although extensive studies on GD have revealed information about the structure of the Gramicidin helix under certain conditions, less is known about influences of the peptide adsorption on the phospholipid matrix. Nevertheless, the lipid environment might be of significance for the function of the channel forming model peptide. Therefore, we have studied mixtures of 1,2-dipalmitoyl-glycerophospho-ethanolamine/1,2-dipalmitoyl-glycerophosphatidylserine (DPPE/DPPS) containing GD.

At 20 °C pure DPPE/DPPS (1:3 mol/mol) monolayers show a fully condensed isotherm (Fig. 1). At low lateral pressures, three diffraction peaks indicating an oblique lattice of strongly tilted chains (23° at 5 mN/m) are observed. Increasing lateral pressure decreases the tilt angle, and a phase transition towards a hexagonal phase of upright oriented chains characterized by only one diffraction peak occurs at $\pi_s = (33 \pm 1)$ mN/m. The isotherms of GD and GD/lipid mixtures show a large plateau at approximately 20 mN/m. GIXD measurements of the GD/lipid mixtures revealed three diffraction peaks of the lipid chain lattice as found for the pure lipid film. The analysis of the x-ray data shows that already at low pressures GD-lipid interactions result in lower chain tilt. The comparison of the tilt angles shows that the lipid-peptide interaction leads to a decrease of the phase

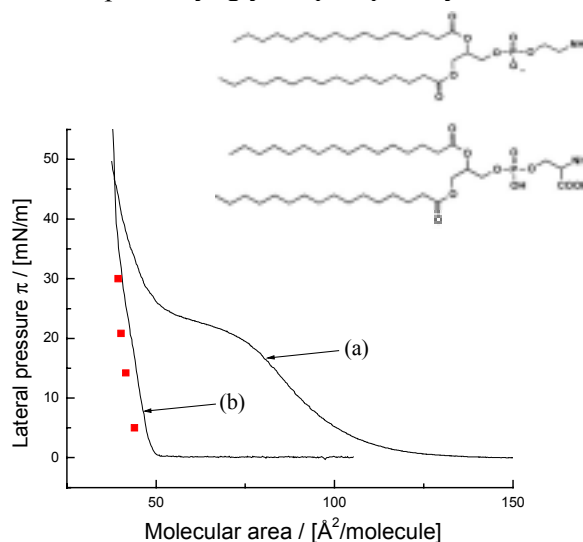


Fig. 1. Pressure area isotherms of: (a) Lipid/GD ($c_{GD} = 10$ mol %) and (b) DPPE(top)/DPPS (bottom) = 1/3 mol/mol monolayers, and A_{xy} -values (■) calculated from the fitted Q_{xy} peak positions.

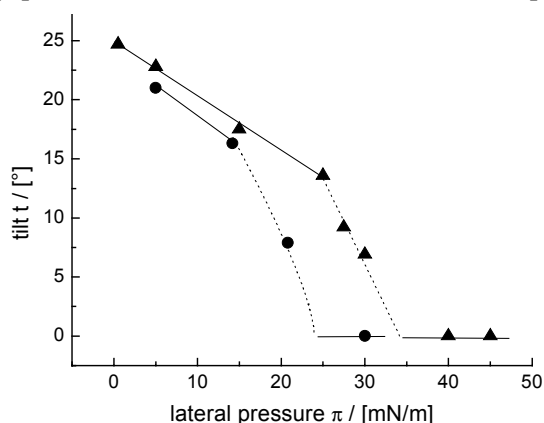


Fig. 2. Lipid chain tilt as a function of the lateral pressure for pure DPPE/DPPS (1/3 mol/mol) (▲) and lipid/GD (10 mol-%) (●) monolayers.

transition pressure (see Fig. 2). While the GD-lipid mixture shows a hexagonal phase at 20 mN/m, the pure lipid film still exhibits a large tilt of approximately 16° at this surface pressure. The lateral density in the pure lipid and GD/lipid films is also different.

Our investigations have clearly demonstrated that the Gramicidin adsorption and incorporation in lipid monolayers shifts the phase transition towards lower pressure values and reduces the space requirements of the lipid chains, leading to a tighter packing in the ordered phases at comparable lateral pressures.

We are grateful for support by the SNF (DanSync), the IHP contract HPRI-CT-1999-00040 (EC) and for beam time at beam line BW1 at HASYLAB at DESY, Hamburg, Germany.

2.6.15. Structure analysis of a metallosupramolecular polyelectrolyte-amphiphile complex at the air-water interface

P. Lehmann, G. Brezesinski, C. Symietz, D. G. Kurth, *Max-Planck-Institute of Colloids and Interfaces, Golm/Potsdam, Germany*, T. R. Jensen and K. Kjær, *Condensed Matter Physics and Chemistry Department, Risø National Laboratory, Denmark*
 e-mail: kristian.kjaer@risoe.dk

The structure of a metallosupramolecular polyelectrolyte-amphiphile complex (PAC) at the air-water interface was investigated using Grazing Incidence X-ray Diffraction (GIXD) performed at the beamline BW1, HASYLAB. The PAC was prepared in solution by metal-ion coordination of Fe(II)acetate and 1,4-bis(2,2':6',2''-terpyridin-4'-yl)benzene followed by self-assembly with the amphiphile dihexadecyl phoshate (DHP)¹. Spreading the preformed PAC at the air-water interface results in a Langmuir film with a stratified architecture, such that DHP forms a monolayer on the water surface, while the metallosupramolecular coordination polyelectrolyte is immersed in the aqueous subphase. This stratified bilayer structure (see Fig. 1. 1 left) was inferred from the measured X-ray reflectivity (XR) of the monolayer. The measured XR data could be fitted with a three-box model (normal to the surface). Box *a* represents the polyelectrolyte immersed in the subphase, box *b* represents the phosphate head groups of the amphiphile and box *c* represents the alkyl chains (see Fig. 1 left). The strong coupling of the polyelectrolyte to the amphiphile monolayer influences the packing of the alkyl chains. Contour plots of the GIXD intensity are shown in Fig. 1 (right). At low surface pressure, pure DHP monolayers form a rectangular lattice with tilted aliphatic chains. Compression of the monolayer above 10.2 mN/m forces the alkyl chains into an untilted orientation. The lattice is hexagonal. The interactions between DHP and the polyelectrolyte lead to a hexagonal monolayer phase with untilted alkyl chains even at low surface pressures. Compression of the monolayer induces a slight distortion of the hexagonal lattice.

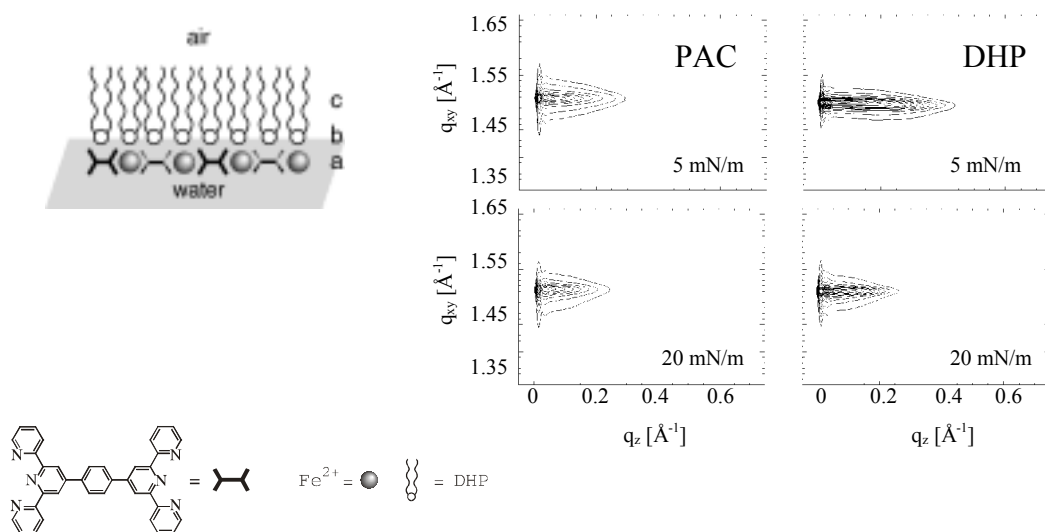


Fig. 1. *Left:* Schematic representation of the architecture of the PAC monolayer at the air-water interface. *Right:* Contour plots of the X-ray diffraction intensities as a function of the scattering vector components of the polyelectrolyte-amphiphile complex (PAC) and dihexadecyl phosphate (DHP). On compression from 5 to 20 mN/m, the single Bragg peak of the PAC monolayer broadens indicating that it is split into two barely resolved peaks located at zero q_z .

We are grateful for support by the SNF (DanSync), the IHP contract HPRI-CT-1999-00040 (EC) and for beam time at beam line BW1 at HASYLAB at DESY, Hamburg, Germany.

¹ D. G. Kurth, P. Lehmann and M. Schütte, *Proc. Natl. Acad. Sci. USA* **97**, 5704 (2000).

2.6.16. Condensation of DNA molecules at cationic lipid monolayers

C. Symietz, G. Brezesinski, H. Möhwald, *Max Planck Institute of Colloids and Interfaces, Golm/Potsdam, Germany*, T. R. Jensen and K. Kjær, *Condensed Matter Physics and Chemistry Department, Risø National Laboratory, Denmark*
e-mail: kristian.kjaer@risoe.dk

Cationic liposomes complexed with DNA are promising nonviral carriers of DNA vectors for gene therapy. The addition of DNA to cationic liposomes resulted in an unexpected topological transition from liposomes to liquid-crystalline condensed globules¹. Alternating stacks of lipid bilayers and DNA monolayers form a multilamellar structure. The DNA chains (average radius of 2 nm) are arranged in a one-dimensional lattice with distinct interhelical distances of between 2.5 and 5.7 nm). DNA molecules adsorbed onto supported cationic lipid membranes are highly condensed². Interhelical distances of 4 nm have been found.

Monolayers of cationic lipids at the air/water interface have the advantage that such parameters like packing density, phase structure or ionic conditions can be easily changed. First experiments to investigate the condensation of DNA at such monolayers were performed at the beamline BW1 using the liquid surface diffractometer.

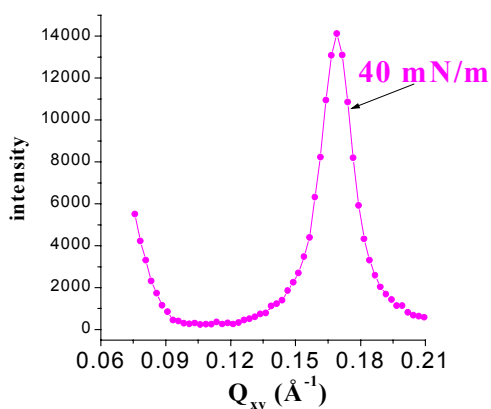
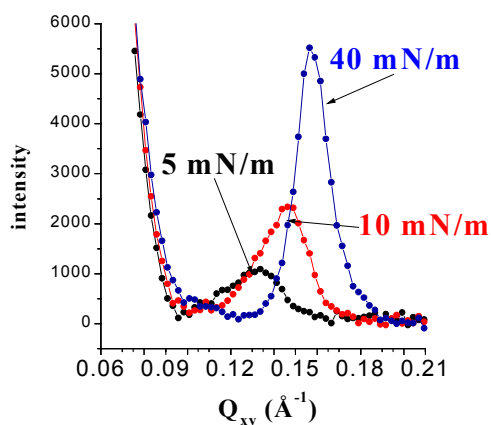


Fig. 2. Bragg peak of DNA adsorbed onto a TODAB monolayer (*top*) or onto a DODAB monolayer (*bottom*) at the air/water interface.

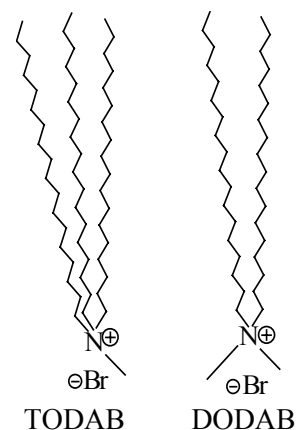


Fig. 1. Molecular structures of lipid molecules used

Dimethyldioctadecyl-ammonium bromide (DODAB) and methyltrioctadecylammonium bromide (TODAB) have been used as lipids (Fig. 1). The lipids form stable monolayers on water. The double-chain DODAB exhibits a liquid-expanded/ condensed transition at 13 mN/m, whereas the triple-chain TODAB forms a condensed phase only above 35 mN/m. DNA (1 mM) was added into the subphase. After an adsorption time of 1 h, the monolayer was compressed to a certain pressure. In the case of the double-chain DODAB, the lipid chain lattice was destroyed due to the DNA adsorption. By contrast, DNA adsorption to a TODAB monolayer leads to the appearance of a condensed lipid phase already at a lower surface pressure as compared to the pure system.

In both systems, a Bragg peak of the DNA ordering can be found in the small-angle region (Fig. 2). The intensity of the diffraction peak increases with increasing pressure and the interhelical distance decreases. The smallest value has been found for DODAB at 40 mN/m (3.7 nm).

We are grateful for support by the SNF (DanSync), the IHP contract HPRI-CT-1999-00040 (EC) and for beam time at beam line BW1 at HASYLAB at DESY, Hamburg, Germany.

¹ J. O. Rädler, I. Koltov, T. Salditt, and C. R. Safinya, *Science* **275**, 810 (1997).

² Y. Fang and J. Yang, *J. Phys. Chem.* **B 101**, 441 (1997).

2.6.17. Langmuir monolayers with fluorinated groups in the hydrophilic head

G. Brezesinski, H. Möhwald, *Max Planck Institute of Colloids and Interfaces, Golm/Potsdam, Germany*, J. G. Petrov, *Institute of Biophysics, Bulgarian Academy of Sciences Sofia, Bulgaria*, T. R. Jensen and K. Kjær, *Condensed Matter Physics and Chemistry Department, Risø National Laboratory, Denmark*
e-mail: kristian.kjaer@risoe.dk

Solutions of fluorinated surfactants and Langmuir monolayers of fluorinated amphiphilic compounds possess unique properties that make them widely used for fundamental studies and practical applications. Such substances strongly decrease the surface energy of liquids and solids, diminish surface friction, and render the surface potential of various interfaces negative when adsorbed or spread on them¹. The effect of fluorination of the hydrophilic head on the behavior of Langmuir monolayers was investigated using the non-ionic amphiphiles trifluoroethyl behenate (TFEB) and ethyl behenate (EB) (see sketch). TFEB forms less stable films than the non-fluorinated EB^{2,3}. Both compounds exhibit compression-expansion hysteresis. At high surface pressure, TFEB molecules occupy a larger area than EB. Based only on surface pressure-area isotherms, different numbers and locations of apparent phase transitions reported in the literature and the identification of the monolayer phases is ambiguous. This necessitates a direct identification of the film structures.

Therefore, the molecular structure of TFEB and EB monolayers at the air-water interface was investigated by Grazing Incidence X-ray Diffraction (GIXD) (Fig. 1).

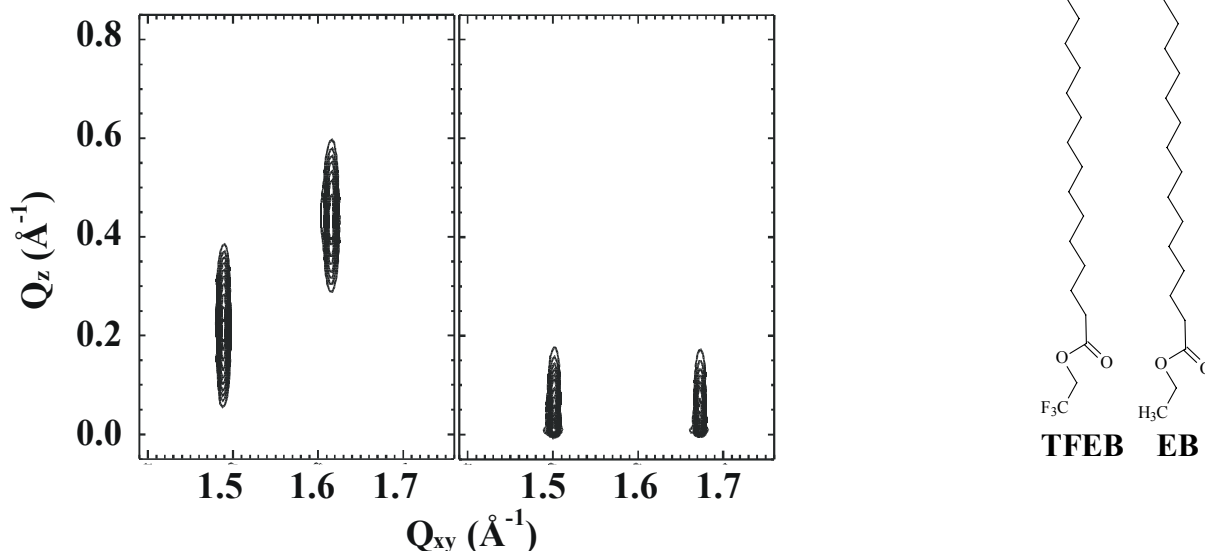


Fig. 1. Contour plots of the corrected X-ray intensities of TFEB (left) and EB (right).

The results obtained show that TFEB forms islands of upright oriented molecules packed in a centered rectangular lattice even at zero surface pressure. Compression of the monolayer only expels the voids between the islands. EB is packed in a centered rectangular lattice and tilted towards next-nearest neighbors (NNN). At high pressures, both monolayers have the same structure and lattice parameters. The cross-sectional area is very small (0.19 nm²). At low surface pressure, the structural difference seems to result from different hydrophilicity of the head groups due to substitution of the CH₃ by a CF₃ group. As registered by BAM, differences in residual voids in TFEB and EB monolayers offer a qualitative explanation for the compression-expansion hysteresis.

We are grateful for support by the SNF (DanSync), the IHP contract HPRI-CT-1999-00040 (EC) and for beam time at beam line BW1 at HASYLAB at DESY, Hamburg, Germany.

¹ Fluorinated Surfactants: Synthesis, Properties, Applications, E. Kiss (ed.), Marcel Dekker, New York (1994).

² J. G. Petrov and H. Möhwald, *J. Phys. Chem.* **100**, 18458 (1996).

³ J. G. Petrov, E. Polymeropoulos and H. Möhwald, *Langmuir*, **16**, 7411 (2000).

2.6.18. A structural study of phosphatidylinositol phosphate monolayers

C. Selle, U. Dietrich, P. Krüger, M. Weygand, B. Kohlstrunk, M. Lösche, *Institute of Experimental Physics I, University of Leipzig, Germany*, T. R. Jensen and K. Kjær, *Condensed Matter Physics and Chemistry Department, Risø National Laboratory, Denmark*
e-mail: kristian.kjaer@risoe.dk

Phosphoinositides (PIs), a minority-component class of biomembrane phospholipids, have been shown to operate as second messengers in cellular and insulin signalling and to be involved in protein binding to plasmamembrane surfaces. In contrast to extensive cell physiological studies and also to physicochemical investigations on neutral phospholipids (PLs) – such as phosphatidylethanolamines and phosphatidylcholines – studies dealing with the biophysical properties of phosphoinositides are still rare. Two reasons may contribute to this situation: The first is the relatively difficult synthesis of structurally uniform PIs. For work on physical model membranes, structurally homogeneous synthetic lipids are preferred over lipid extracts. Secondly, aqueous suspensions of pure PIs do not tend to form bilayer structures, a complication for most structural characterization methods. Therefore, until recently experimental work has been restricted to the use of either PI extracts and/or PIs mixed with other PLs¹².

We have measured the x-ray specular reflectivity (XR) of stereochemically pure dipalmitoyl phosphoinositol-monophosphates (PIPs) in monolayers on water subphases and on physiological buffers at room temperature (20 °C) in dependence on the lateral pressure.

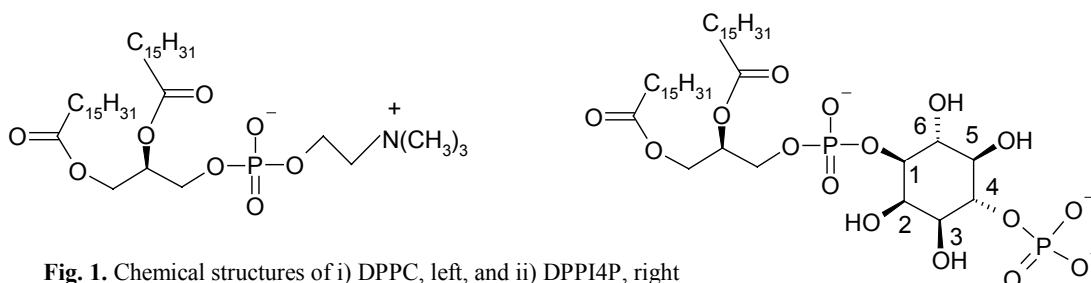


Fig. 1. Chemical structures of i) DPPC, left, and ii) DPPI4P, right

The secondary phosphate group of the compounds under study is located in the 3-, 4- or 5-position of the inositol ring (for short, DPPI3P, DPPI4P, DPPI5P were used).

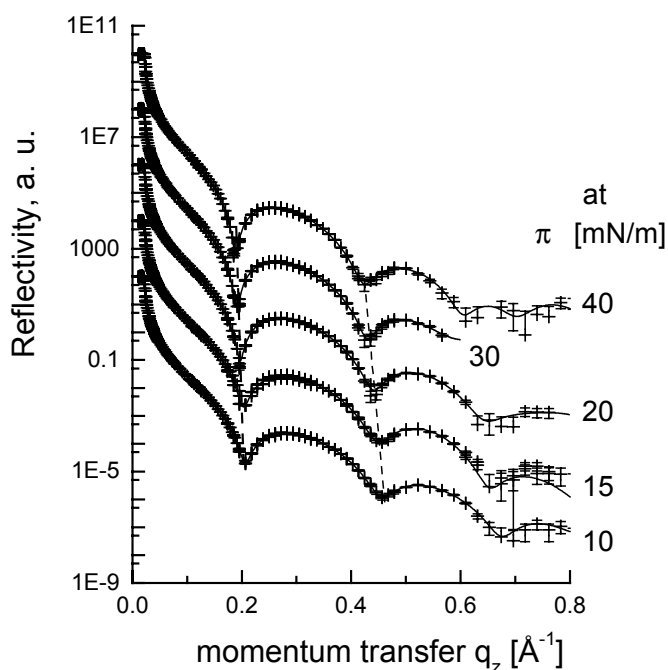


Fig. 2. X-ray reflectivity data of DPPI3P monolayers on water at various lateral pressures (as indicated) measured at DESY. The dashed lines show that with increased pressure, features compact in reciprocal space in a scaling-like manner, corresponding to expanding features in real space, *i. e.*, the monolayer thickness increases. More detailed structural information is obtained by data fits (solid lines) generated by a model independent algorithm³ providing electron density profiles.

¹ J. P. Bradshaw, R. J. Bushby, C. C. D. Giles and M. R. Saunders, *Biochemistry* **38**, 8393 (1999).

² C. DeWolf, S. Leporatti, C. Kirsch, R. Klinger and G. Brezesinski, *Chem. Phys. Lipids* **97**, 129 (1999).

The surface pressure vs. area (π -A) isotherms exhibit large differences between the various isomers. The most condensed monolayers were observed for DPPI3P. For DPPI4P, and even more pronounced for DPPI5P, relatively expanded monolayers were found. Qualitatively, the XR results reflect the large electron densities of the polar headgroups in that the reflectivity observed at high momentum transfer is much larger than for conventional phospholipid monolayers. Also, we noticed that the structure is sensitive to the ionic content of the aqueous subphase: Electron density profiles (fig. 2) – derived using a model-free data inversion technique¹ – if obtained on pure water are significantly different from those on physiological buffer solutions. For example, in DPPI4P monolayers on HEPES (pH 7.4, 100 mM NaCl) at lateral pressures up to 30 mN/m, the electron density peak which is primarily related to the lipid headgroup (i) occurs closer to the surface and (ii) shows a broader distribution across the interface than on water. These differences are most pronounced at low π values and tend to vanish above 40 mN/m.

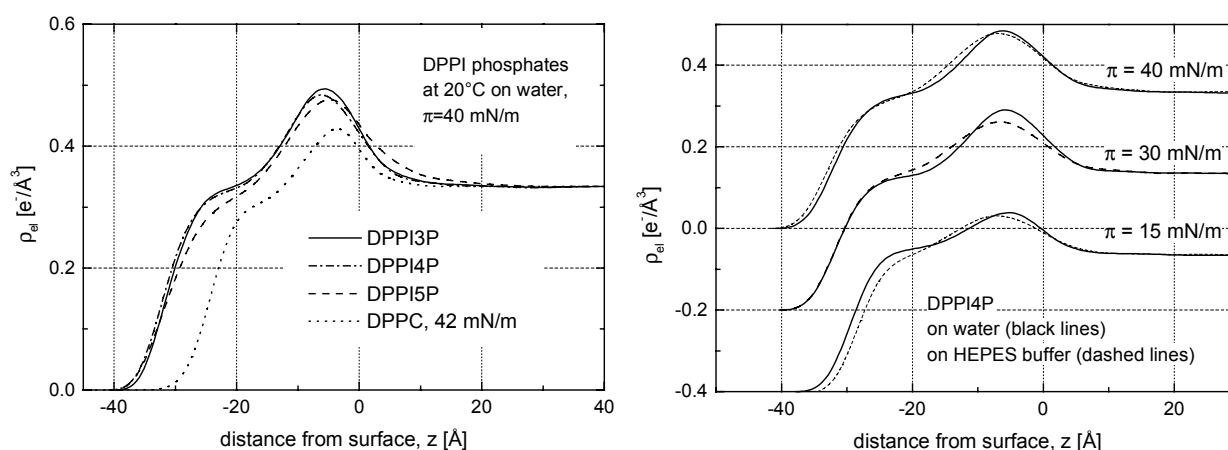


Fig. 3. Electron density profiles obtained by a model independent technique³.

Left: DPPI phosphate monolayers on water at $\pi = 40$ mN/m. Also included is an electron density profile of dipalmitoyl phosphatidylcholine (DPPC). **Right:** Effect of the HEPES buffer at selected lateral pressures on the electron density profile of a DPPI4P monolayer.

To arrive at a more detailed structural characterization of the lipids at the aqueous surface we are currently applying a new data inversion algorithm which uses distribution functions to map the spatial organization of submolecular fragments (*volume-restricted distribution function*, VRDF, model)^{2,3,4}. This technique has been successfully employed to characterize monolayers of the simple phospholipid DMPA (dimyristoyl phosphatidic acid) on the submolecular level [4]. At present, such an extension of the VRDF approach to an evaluation of PIP monolayer data has not yet yielded definite results. Since the PIP molecules are much more complex than simple PLs, rigorous constraints have to be implemented using volumetric data, which we are trying to establish with molecular dynamics simulations. With this approach we expect to obtain a detailed microscopic comprehension of the observed differences in the macroscopic properties of the various PIPs as detected from the π -A isotherms. It is hoped that such a molecular-scale insight in lipid headgroup organization will help understanding the distinct physiological roles of the various PIP isomers.

We are grateful for support by the DFG (SFB 294), SNF (DanSync), the IHP contract HPRI-CT-1999-00040 (EC) and for beam time at beam line BW1 at HASYLAB at DESY, Hamburg, Germany.

¹ J. Skov Pedersen and I. W. Hamley, *J. Appl. Cryst.* **27**, 36 (1994).

² M. Schalke, P. Krüger, M. Weygand and M. Lösche, *Biochim. Biophys. Acta* **1464**, 113 (2000).

³ P. Krüger, M. Schalke, J. Linderholm and M. Lösche, *Rev. Sci. Instrum.*, **72**, 184 (2001).

⁴ M. Schalke and M. Lösche, *Colloid Interf. Sci.* **88**, 243 (2001).

2.7. Microemulsions, surfactants and biological systems

2.7.1. Time evolution of the planar lamellar to the lamellar vesicle phase observed in an ionic surfactant system

K. Mortensen, *Danish Polymer Centre, Condensed Matter Physics and Chemistry Department, Risø National Laboratory, Denmark*, M. Gradzielsky, M. Escalante, H. Hoffmann, *Department of Phys. Chem., University of Bayreuth, Germany*
e-mail: km@polymers.dk

Many aqueous solutions of amphiphilic molecules are known to form lamellar liquid crystalline phases. For instance, such phases may be formed in mixtures of surfactants with n-alcohols. The lamellar phases can be stabilized by long-range repulsive interaction forces resulting from ionic charges or from thermal fluctuations of the membranes, and for instance. Undulation forces dominate when the membranes are flexible, and electrostatic forces are absent or screened out. In general shear flow can have a strong influence on the structure of complex fluids. Samples with lamellar morphology have especially attracted much attention in the past few years. In most experiments the stationary states that are reached for a constant shear rate have been investigated, but so far only little is understood about the kinetics of the structural transitions. We have in an ionically charged system studied the transformation of an L_{α} -phase composed of stacked bilayers to a vesicle phase L_{α}^* under the influence of shear. The ionically charged stacked bilayer phase was prepared by protonation of an L_3 phase from tetradecyldimethylamine oxide hexanol, and water. The protonation was accomplished by a hydrolysis reaction of an ester solubilized in this phase. By the protonation of the bilayers the L_3 phase becomes unstable and, in the absence of shear, is transformed into a classical lamellar phase. This low-viscosity phase was then transformed into the onion phase by shear. The structural changes during this transformation process were monitored by means of both scattering experiments, rheological and conductivity measurements under shear. The transition from stacked lamellae to vesicles is in this system irreversible. The planar lamellar phase is not regained after stopping shear. The formation of multilamellar vesicles requires a total strain of about 2000, for the given surfactant concentration of 100 mM applied in this study. The influence of other parameters on the transformations of the L_{α} phase, such as chain length of the surfactant, chain length of the alcohol, and the total concentration, was studied¹.

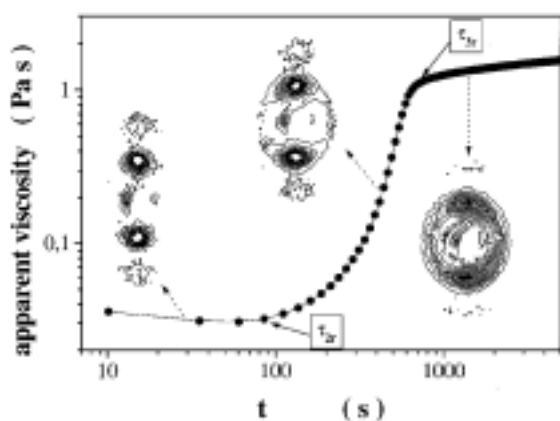


Fig. 1. Viscosity and structural SANS data showing the time-dependent transformation from planar lamellar to lamellar vesicle phase. The figure shows the apparent viscosity after termination of the hydrolysis reaction as a function of time after applying a constant shear rate of 10s^{-1} . Inside are some corresponding curves from the SANS measurements.

¹ J. I. Escalante, M. Gradzielski, H. Hoffmann, K. Mortensen. *Langmuir* **16**, 8653 (2000).

2.7.2. Planar lamellar and lamellar vesicles phases in nonionic surfactant systems

K. Mortensen, *Risø National Laboratory, Condensed Matter Physics and Chemistry, Denmark*, T. D. Le, U. Olsson, *Center for Chem. and Chem. Eng., Lund University, Sweden*, J. Zipfel and W. Richtering, *Institut für Makromolekulare Chemie, Universität Freiburg, Freiburg, Germany*
 e-mail: kell.mortensen@risoe.dk

A significant fraction of the recent microemulsion studies have focused on lamellar systems, both the classical L_α -phase of planar sheets, and systems where the bilayer sheets fold to form closed structures as uni- or multi-layered lamellar vesicles, L_α^* . The latter structure has been given a number of names, such as onions, liposomes, spherulites, or multilamellar vesicles (MLV). We have studied non-ionic $C_{10}E_3$ -water systems in the attempt to investigate the lamellar-to-vesicle transformation in a system with fewest possibly parameters. In the investigation we fixed the shear rate and performed temperature scan experiments passing through a multilamellar vesicle phase L_α^* at low temperature, a lamellar phase L_α at intermediate temperature, and a sponge phase L_3 at high temperature (Fig.1). Small-angle neutron and light scattering *in situ* with shear were used to elucidate the microstructure, to determine the bilayer orientation, and to characterise the size of these structures. The temperature induced topological change from L_α to L_α^* -phase shows remarkable reproducibility, and the fraction of vesicle phases can be evaluated directly from the scattering patterns. The inter-lamellar spacing was observed to be the same in the lamellar as in the MLV phase and the MLV phase exhibited symmetrical scattering in the neutral and flow directions, indicating that the layers in the vesicles are spherical shaped at the selected shear rate ($\dot{\gamma} = 100 \text{ s}^{-1}$). The stability of these bilayer structures formed at a given shear rate can be qualitatively described according to the framework of the elastic curvature energy^{1,2}

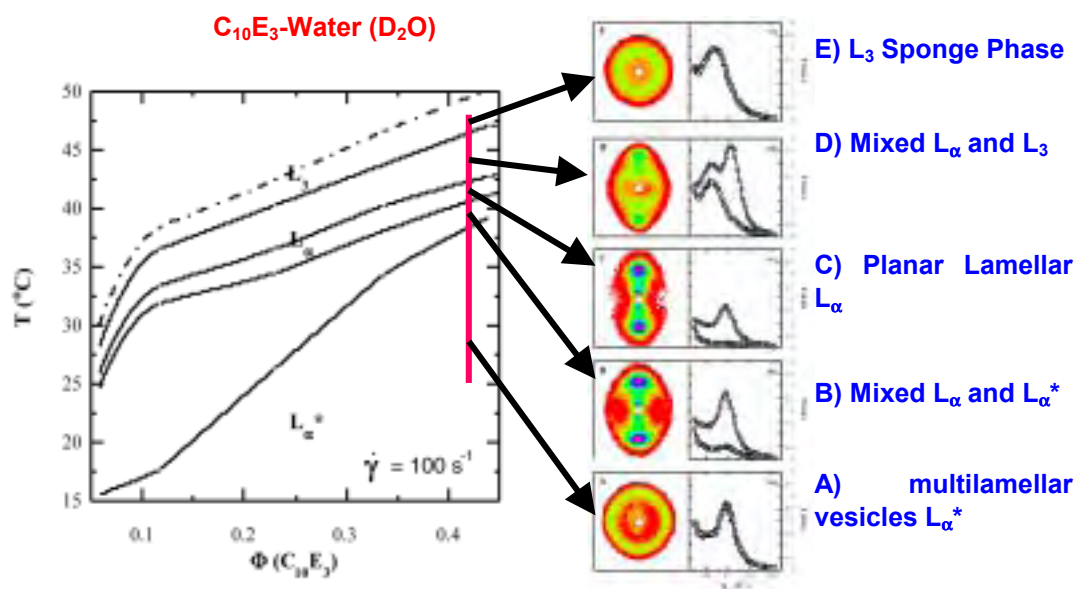


Fig.1 Phase diagram and neutron scattering pattern of $C_{10}E_3$ -water in the MLV L_α^* -, the L_α and the L_3 phases, as obtained at constant shear rate of 100 s^{-1} .

¹ T. D. Le, U. Olsson and K. Mortensen. *Physica B* **276**, 379 (2000).

² T. D. Le, U. Olsson, K. Mortensen, J. Zipfel and W. Richtering *Langmuir*, Nonionic amphiphilic bilayer structure under shear, in press.

2.7.3. Structural characterisation of multi-lamellar di-acyl phosphatidylcholine lipid bilayer by small-angle scattering

T. Ishøy, K. Mortensen, *Condensed Matter Physics and Chemistry Department, Risø National Laboratory, Denmark*, R. Bauer, *Institute for Mathematics and Physics, Royal Veterinary and Agricultural University, Denmark*, O. G. Mouritsen, *Department of Chemistry, Technical University of Denmark, Denmark* and J. S. Pedersen, *Physical Chemistry, Department of Chemistry, University of Aarhus, Denmark*

e-mail: torben.ishoy@risoe.dk

In order to extract as much information on lipid bilayer structures, scattering experiments with both x-ray and neutron have been performed. The data interpretation is, however, made difficult due to lack of perfect order, as related to the flexible nature of the lipid bilayers, and due to a multilamellar vesicle structure rather than a true planar lamellar form.

The analyses of the x-ray or neutron scattering data of such systems can be based on a one-dimensional model of the scattering length density profile, based on, for example, the Caillé¹ or the paracrystalline theory². Different models for the scattering length density, ρ , have been proposed: Lemmich et al.³ introduced a simple Gaussian fluctuating strip model (Fig. 1) combined within paracrystalline theory. The model describes the bilayer as two-head group region with a thickness d_H separate by a hydrophobic region with thickness d_L . The width of the aqueous space between two individual bilayer is denoted d_W . An expansion of the model has been proposed, including a methyl-terminus in the middle of the hydrophobic region (cf. Fig. 1). Another model introduced by Pabst et. al.⁴ describe the profile in terms of two Gaussian functions, one for the head group and one for the methyl-terminus. Pabst et. al. also introduced a term accounting for the diffuse scattering from uncorrelated bilayers.

A thorough comparison of the Caillé and paracrystalline theories in combination with different model profiles have been done by fitting to SAXS data on DMPC and DPPC at a water content of 80%⁵. In general the Caillé theory fits the data best in both the L_{β} , P_{β} and L_{α} phases, even though the physical assumption of Caillé only holds for the liquid crystalline L_{\square} phase. Including the diffused term introduced by Pabst et. al. in the paracrystalline model accounts very well for the diffused scattering observed, for example, between the first and second peak, and reduces the χ^2 -value significantly. A similar term has only minor effect in Caillé theory. The conclusion is that the Caillé theory generally describes the L_{\square} -phase of lipid bilayers best, using either of the two model profiles, the expanded Gaussian strip model or the Gaussian function model (Pabst et al.⁴).

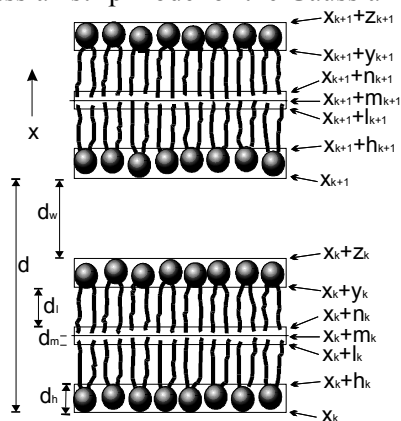


Fig. 1. Schematic illustration of a multilamellar array of lipids bilayers. The repeat distance of the system is d , d_H is the thickness of the head group, d_L is the thickness of the CH_2 and CH part of the lipid acyl chains, d_M is the thickness of the methyl layer, and the water layer between two neighbouring bilayers has the thickness d_W . The repeat distance d is thus equal to $2d_M+2d_L+2d_H+d_W$, the hydrophobic thickness of the bilayer is equal to $2d_M+2d_L$ and the hydrophilic thickness of the bilayer is equal to $2d_H+d_W$.

¹ A. Caillé, C. R. Acad. Sci Ser. B **274**, 891 (1972).

² R. Hossemann and S. N. Bacchi, Direct analyse of Diffraction by Matter (Noth-Holland, Amsterdam) 408 (1962).

³ J. Lemmich, K. Mortensen, J.H. Ipsen, T. Hønger, R. Bauer and O. G. Mouritsen, Phys. Rev. **E53**, 5169 (1996).

⁴ G. Pabst, M. Rappolt, H. Amenitsch and P. Laggner, Phys. Rev. **E62**, 4000 (2000).

⁵ J. Kharkar, J. S. Pedersen, T. Nylander and R. Bauer, private communication.

2.7.4. Simple structural microtubule cap

I. M. Janosi, *Department of Physics of Complex Systems, Eotvos University, Budapest, Hungary*, and H. Flyvbjerg, *Condensed Matter Physics and Chemistry Department, Risø National Laboratory, Denmark*

e-mail: henrik.flyvbjerg@risoe.dk

Microtubules polymerize from GTP-liganded tubulin dimers, but are essentially made of GDP-liganded tubulin. We investigate the tug-of-war resulting from the fact that GDP-liganded tubulin favors a curved configuration, but is forced to remain in a straight one when part of a microtubule. We point out that near the end of a microtubule, the proximity of the end shifts the balance in this tug-of-war, with some protofilament bending as result. This somewhat relaxes the microtubule lattice near its end, resulting in a structural cap. This structural cap thus is a simple mechanical consequence of two well-established facts: protofilaments made of GDP-liganded tubulin have intrinsic curvature, and microtubules are elastic, made from material that can yield to forces, in casu its own intrinsic forces.

We explore possible properties of this structural cap, and demonstrate

- how it allows both polymerization from GTP-liganded tubulin and rapid depolymerization in its absence,
- how a third, meta-stable intermediate state is possible, and can explain some experimental results,
- how the tapered tips observed at polymerizing microtubule ends are stabilized during growth, though they cannot accommodate a lateral cap.

2.7.5. Simple mechanical interpretation of tip shapes observed at growing microtubule ends

I. M. Janosi, *Department of Physics of Complex Systems, Eotvos University, Budapest, Hungary*, D. Chretien, *Cell Biology, Cell Biophysics and Structural Biology Programmes, European Molecular Biology Laboratory, Heidelberg, Germany*, and *Equipe ATIPE, UPRES-A 6026 CNRS, Universite de Rennes, Rennes, France*, S. Leibler, *Departments of Physics and Molecular Biology, Princeton University, Princeton, USA* and H. Flyvbjerg, *Condensed Matter Physics and Chemistry Department, Risø National Laboratory, Denmark*

e-mail: henrik.flyvbjerg@risoe.dk

Cryo-electron microscopy has revealed long, gently curved sheets of tubulin at growing ends of microtubules (D. Chretien, S. D. Fuller, and E. Karsenti. 1995. *J. Cell Biol.* 129:1311-1328). This in-vitro observation was recently repeated in cell extract (I. Arnal, E. Karsenti, and A. A. Hyman. 2000. *J. Cell Biol.* 149:767-764). We have analyzed a large number of micrographs of such sheets, and found that the many shapes observed can be explained by three simple elasto-mechanical properties:

- The protofilaments in the sheets bond laterally in a manner that results in a large intrinsic lateral curvature in the sheets.
- The protofilaments have themselves significant built-in curvature, a curvature away from the microtubule axis. This causes a large intrinsic longitudinal outward curvature in the sheets.
- The sheets are elastic, and yield to the opposing intrinsic forces of the lateral inward curvature and the longitudinal outward curvature.

This scenario describes the sheets observed at ends of microtubules as being made from exactly the same material as the microtubules themselves. The difference in shapes is merely due to different protofilament numbers, especially whether or not the material has closed into a tube. When it has, the intrinsically curved protofilaments are forced into a straight shape, and the sheet's intrinsic longitudinal curvature is unobservable until the tube depolymerizes, at which stage it is observed again, in protofilaments "peeling off" the microtubule. Thus we also demonstrate that the curved state of tubulin-GDP which is observed at depolymerization, is consistent with the curvature observed in sheets at growing microtubule ends, as it must be if the GTP-cap is small, since a small cap implies that these sheets at growing ends are made of tubulin-GDP.

2.7.6. Pulling strings at finite temperature: Another force-extension formula for the worm-like chain model

H. Flyvbjerg, *Condensed Matter Physics and Chemistry Department, Risø National Laboratory, Denmark*

e-mail: henrik.flyvbjerg@risoe.dk

The derivation of Marko and Siggia's interpolation formula for the force-extension relation of the Worm-Like Chain Model (C. Bustamante, J. F. Marko, E. D. Siggia, and S. Smith, *Science* 265, 1599 (1994); J. F. Marko and E. D. Siggia, *Macromolecules* 28, 8759 (1995)) is retraced. Isotropy of space, resulting in rotational invariance of the free energy, is invoked together with analyticity. A new interpolation formula results for the force-extension relationship. It is as simple as the old one, but twice as close to the exact force-extension relationship. Application of the same reasoning to the second-order perturbative result obtained at strong force (J. D. Moroz and P. Nelson, *Proc. Natl. Acad. Sci. USA* 94, 14418 (1997)) results in yet a new interpolation formula, good to 1% at all forces.

2.7.7. Calibrating an optical trap

K. Berg-Sørensen, *Nordita, Copenhagen* and H. Flyvbjerg, *Condensed Matter Physics and Chemistry Department, Risø National Laboratory, Denmark*

e-mail: henrik.flyvbjerg@risoe.dk

The force exerted by an optical trap on a dielectric bead in a liquid is often found from the power spectrum of the stochastic motion of the bead in the trap. This is considered the most reliable calibration procedure. We demonstrate that this procedure may incorporate several systematic errors which sometimes cancel, sometimes do not. We present simple ways to diagnose such errors, and a simple way to avoid them, exponential correlations cause them. We also present a general procedure which works for generic noise. It avoids some common sources of systematic errors of calibration, and squeezes maximal information from data, while providing a check of their consistency.

2.7.8. Automatic differentiation of multichannel EEG signals

B. O. Peters, *John von Neumann Institute for Computing, Forschungszentrum Jülich, Germany*, G. Pfurtscheller, *Institute of Biomedical Engineering, Department of Medical Informatics, Graz University, Austria* and H. Flyvbjerg, *Condensed Matter Physics and Chemistry Department, Risø National Laboratory, Denmark*

e-mail: henrik.flyvbjerg@risoe.dk

Movements of left and right index finger, and right foot are recognised in the electroencephalograms (EEGs) from three subjects. We present a multichannel classification method that uses a "committee" of artificial neural networks to do this. The classification method automatically finds dominant EEG frequency bands and spatial regions on the skull relevant for the classification task. Correct recognition was achieved in 85-98% of trials not seen previously by the committee, on the basis of single EEGs of one-second duration. Additional frequency filtering did not enhance the classification success, i.e., the information relevant for the classification task is encoded in a very wide frequency band. Classification was optimal during the actual movement, but possible also several seconds before and after. Three seconds before the movement, all subjects showed a first peak in the classification success rate¹.

¹ B. O. Peters, G. Pfurtscheller and H. Flyvbjerg, *IEEE Transactions on Biomedical Engineering* **48**, 111 (2001).

2.8. Polymers

2.8.1. Lateral quantification of spin coated polymer films on silicon by TOF-SIMS and AFM

K. Norrman, N. B. Larsen, *Condensed Matter Physics and Chemistry Department, Risø National Laboratory, Denmark*, K.B. Haugshøj, *Surface Analysis, Danish Technological Institute, Denmark*
 e-mail: kion.norrman@risoe.dk

TOF-SIMS (Time Of Flight-Secondary Ion Mass Spectrometry) imaging is not directly quantitative, but needs to be calibrated against a quantitative technique. Polymers were spin coated on silicon wafers using various polymer concentrations, which produced various degrees of surface coverage (sub-monolayers). The degree of surface coverage was determined from AFM (Atomic Force Microscopy) imaging, Fig.1, which was then used to convert relative polymer/substrate signal intensities from TOF-SIMS, Fig. 1, into a degree of surface coverage (lateral quantification). The AFM and TOF-SIMS data were correlated to produce a calibration curve between the degree of surface coverage and relative polymer/substrate signal intensities, Fig. 2.

PMMA (poly methyl methacrylate) and PVC (poly vinyl chloride), Fig. 3, were used as model systems. The hydrophilic PMMA was found, as expected, to be homogeneously distributed on the hydrophilic silicon oxide surface, while the rather hydrophobic PVC is seen preferably to form domains. Sub-monolayer amounts of the homogeneously distributed PMMA could not be quantified by AFM as this requires a topographical difference between covered and uncovered regions. Consequently, calibration of the TOF-SIMS experiments on such systems was not possible.

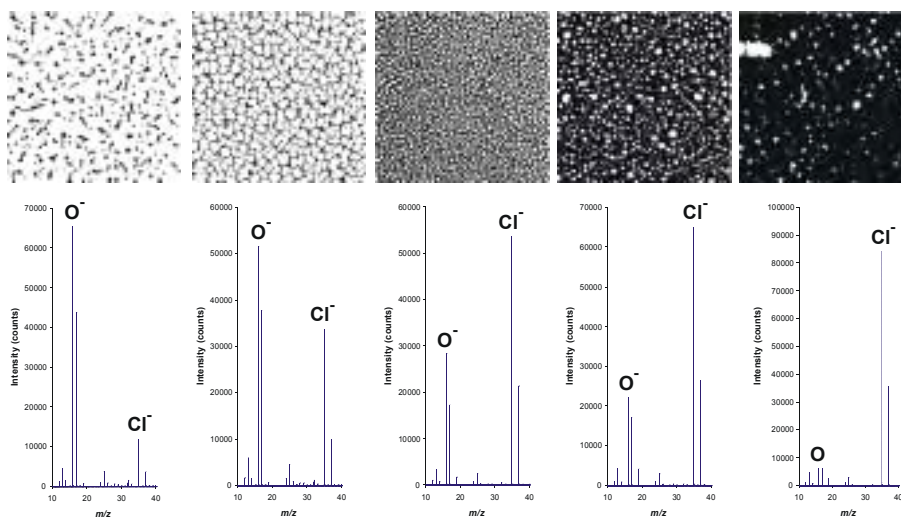


Fig. 1. PVC/Si (black/white) surfaces with corresponding mass spectra

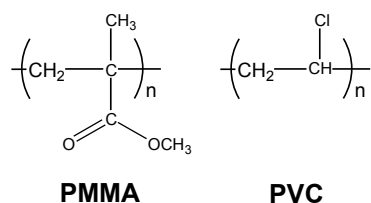


Fig. 3. Repeat units of PMMA and PVC.

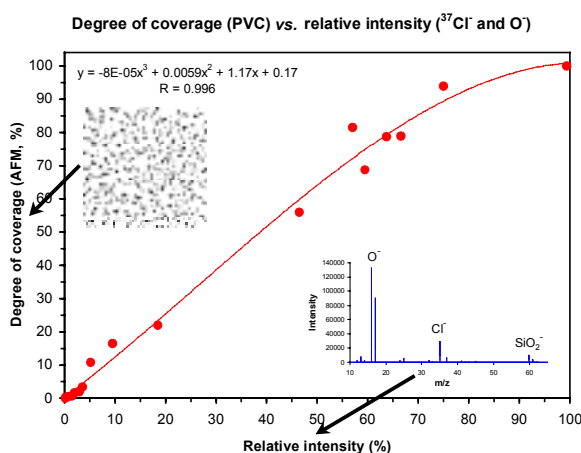


Fig. 2. Calibration curves for PMMA and PVC based on mass spectral data and AFM data.

2.8.2. Vertical quantification of spin coated polymer films on silicon by TOF-SIMS and AFM

K. Norrman, N. B. Larsen, *Condensed Matter Physics and Chemistry Department, Risø National Laboratory, Denmark* and K. B. Haugshøj, *Surface Analysis, Danish Technological Institute, Denmark*

e-mail: kion.norrman@risoe.dk

TOF-SIMS (Time Of Flight-Secondary Ion Mass Spectrometry) depth profiling is not directly quantitative, but needs to be calibrated against a quantitative technique. Polymers were spin coated on silicon wafers using various polymer concentrations, which produced various film thicknesses. The thickness was determined from AFM (Atomic Force Microscopy) profilometry on an applied scratch, which was then used to convert the time scale of a TOF-SIMS depth profile analysis, Fig. 1, into a depth scale (vertical quantification). The AFM and TOF-SIMS data were correlated to produce a calibration curve between the sputter time and the depth, Fig. 2.

PMMA (poly methyl methacrylate) and PVC (poly vinyl chloride), Fig. 3, were used as model systems. These two polymers have different physical properties, PMMA being hydrophilic and PVC being hydrophobic. Because of the difference in physical properties, the two polymers are expected to produce different sputter profiles.

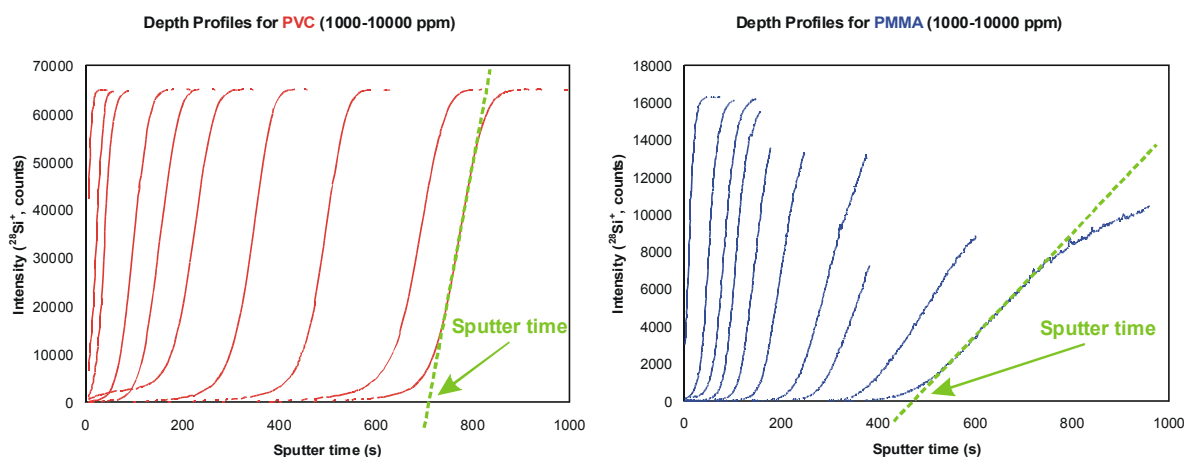


Fig. 1. TOF-SIMS depth profiles for PVC and PMMA. Analysis: 15-keV Ga⁺. Sputter: 1-keV SF₅⁺

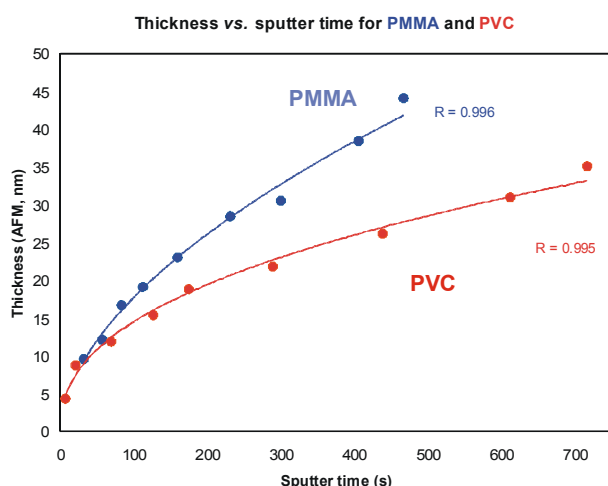


Fig. 2. Calibration curves for PMMA and PVC.

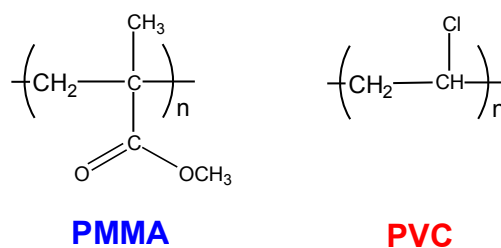


Fig. 3. Repeat units of PMMA and PVC.

2.8.3. The bulk dynamics of a compositionally asymmetric diblock copolymer studied using dynamic light scattering and NMR

C. Papadakis, F. Rittig, G. Fleischer, *Fakultät für Physik und Geowissenschaften, Universität Leipzig, Germany*, K. Almdal, K. Mortensen, *Condensed Matter Physics and Chemistry Department, Risø National Laboratory* and P. Stepánek, *Academy of Sciences of the Czech Republic, Prague*

e-mail: kell.mortensen@risoe.dk

We have studied the bulk dynamics of a compositionally asymmetric poly(ethylene propylene)-poly(dimethylsiloxane) (PEP-PDMS) diblock copolymer both in the ordered and in the disordered states, using dynamic light scattering (DLS) and pulsed field gradient NMR. The sample with volume fraction of the PEP block $f_{\text{PEP}}=0.22$ shows three ordered morphologies, as seen by SANS. In the disordered state, we find that apart from the slow cluster mode a heterogeneity mode related to the self-diffusion of single chains (Figs.1 and 2). The relaxation time τ of this mode reduced by temperature. In the cubic phase right below the ODT temperature, we observe two diffusive processes. We attribute the faster one to the mutual diffusion of micelles and block copolymers not bound to micelles (“free chains”) through the PDMS matrix. The slower mode may either be due to the mutual diffusion of free chains and chains bound to PEP micelles or to the cooperative diffusion of micellar aggregates. In the non-cubic ordered state at intermediate temperatures, an additional weak diffusive mode is observed (Fig.1). The low-temperature ordered state is body-centered cubic, and here, only the mutual diffusion of micelles and free chains lies in our experimental time window¹.

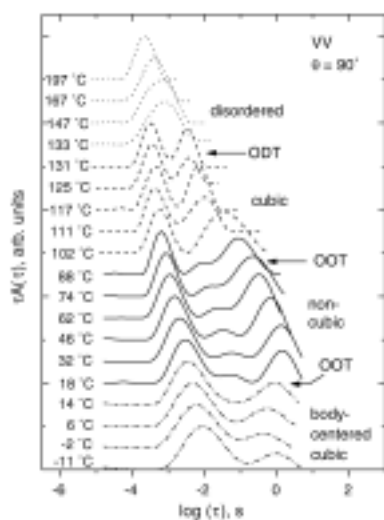


Fig. 1. Distribution functions at different temperatures measured in VV geometry and at $\theta = 90^\circ$. The curves were shifted vertically by 0.5. Different line types indicate different phases.

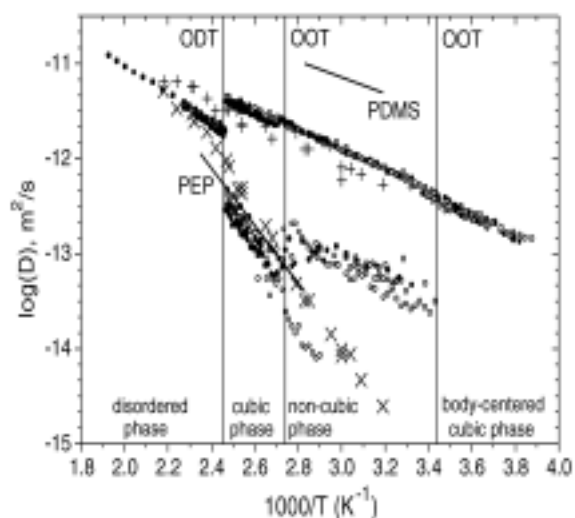


Fig. 2. Diffusion constants of the fast, the middle and the slow mode from DLS: (●) and (●) and from PFG NMR (+) and (×)¹. The lines indicate the self-diffusion constants of ure PEP and PDMS, both for 12 00 g/mol.

¹ C. M. Papadakis, K. Almdal, K. Mortensen, F. Rittig, G. Fleischer and P. Stepanek, *Eur. Phys. J. E* **1**, 275 (2000).

2.8.4. Reversible thermal gelation in soft spheres

K. Mortensen, *Condensed Matter Physics and Chemistry, Risø National Laboratory, Denmark*, M. Kapnistos, D. Vlassopoulos, G. Fytas, *FO.R.T.H., Institute of Electronic Structure and Laser, Heraklion, Crete, Greece*, Fleischer, *Universität Leipzig, Fakultät für Physik und Geowissenschaften, Leipzig, Germany* and J. Roovers, *NRC, Institute for Chemical Process & Environmental Technology, Ottawa, Ontario, Canada*

e-mail: kell.mortensen@risoe.dk

Recently, it has been proposed that soft materials upon heating might undergo a *jamming transition* to a state with solid-like response. We demonstrate such a counterintuitive reversible gelation transition in a system of star polymers suspended in good solvents¹. The studied star-polymers are polybutadienes of nominal functionality $f=128$ and arm molecular weights 28, 56, and 80 kg/mol. As the temperature increases the material behavior changes from viscous liquid ($G'' > G'$) to a weak elastic solid ($G' > G''$). SANS measurements, however, indicate that the liquid like order remains unaffected of the transition (Fig.1). In these systems excluded volume effects represent the only kind of interaction among the polymeric spheres and the solvent is good with improving quality as temperature increases. This suggests the following mechanism of the observed reversible gelation. As the temperature increases, the solvent quality improves and the peripheral blobs of the interacting liquid-ordered soft spheres swell; consequently, due to overall incompressibility of the system, in order to accommodate themselves in the same volume, the spheres increase their arms. Fig.2 shows schematically this behavior, as well as the experimental phase diagram for the star polymers investigated; the excluded volume parameter is related to the temperature and taken as $v=1-\alpha/T$ where the parameter α relates to the theta conditions for the specific system. The effective volume fraction ϕ_{eff} is essentially the volume fraction of the spherical stars by considering their overall dimensions, i.e. as if they were hard spheres. The virtual collapse of the data shown in Fig. 2 for the three different stars (as well as a micellar system¹) is a striking result suggesting a universal behavior for this class of soft materials, which are characterized by significant softness.

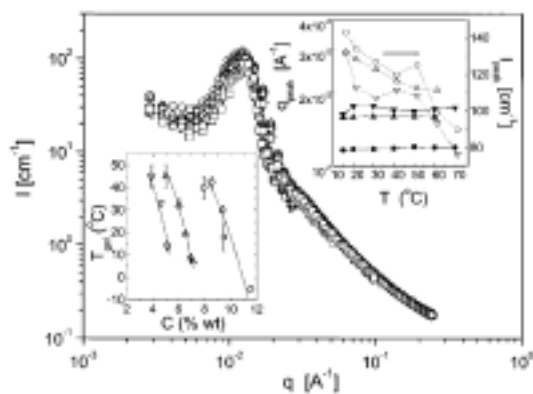


Fig. 1. Scattering function of 128-arm PB star polymers in decane. The upper insert shows $I(q^*)$ - and q^* -value versus temperature. The lower insert shows the gel-transition versus concentration, as obtained from rheology.

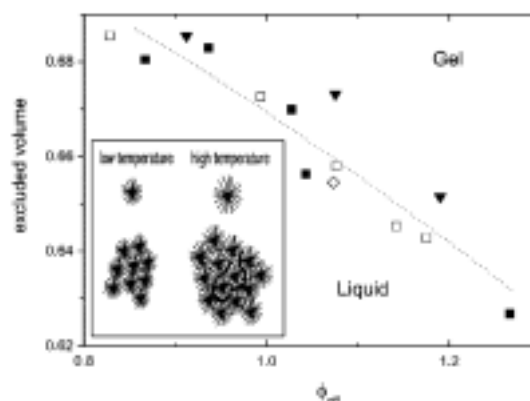


Fig. 2. Jamming phase diagram for ultra soft 128-arm PB star polymers, with arm-molar weight of respectively 28kg/mol (■), 56kg/mol (□) and 80kg/mol (▼). The insert shows schematically the temperature dependent stars.

¹ M. Kapnistos, D. Vlassopoulos, G. Fytas, K. Mortensen, G. Fleischer and J. Roovers, *Phys. Rev. Lett.* **85**, 4072 (2000).

2.8.5. Ordered microphase in Pluronics type block copolymers, PEO-PPO-PEO

K. Mortensen, *Condensed Matter Physics and Chemistry Department, Risø National Laboratory, Denmark*, J. Patric, A Fairclough, A. J. Ryan, *Department of Chemistry, University of Sheffield, UK*, S.-M. Mai, G.-E. Yu and C. Booth, *Department of Chemistry, University of Manchester, UK*
e-mail: km@polymers.dk

Commercial available Pluronics type of block copolymers have triblock architecture, e.g. PEO-PPO-PEO, where PEO represents poly(ethylene oxide) and PPO represent poly(propylene oxide). Given PEO polymerization of about 50 (or more), these copolymers, and their diblock analogous PEO-PPO form semicrystalline solids at ambient temperature, where PEO sheets constitute the crystalline domains. The crystalline structure melts at 50-65°C. Fluctuations due to the partly immisible PEO and PPO can also lead to ordered structures. Such fluctuation induced microphase separation into ordered domains depends not only on the product of the Flory-Huggins interaction parameter and the polymerization, χN , but also on the architecture. According to Leibler, the mean field ordering takes place at $\chi N=10.5$ for symmetric diblock copolymer, whereas the predicted value for corresponding triblock architecture, according to Mayes et al., is $\chi N=18$. In the laboratory in Manchester, partly deuterated Pluronics analogous polymers have been synthesized, with the poly(propylene block) deuterated. Using small-angle neutron scattering experiments, the Flory-Huggins parameter have been evaluated, $\chi=20.2/T+0.0221$ (Fig. 1). This value is quite similar to that obtained for homopolymer blends. SAXS experiments of diblock copolymers of EO_mPO_n show, for symmetric systems with chain-lengths $r=m+1.48n$ larger than 200 clearly a fluctuation induced order-disorder transition in well above the crystallization temperature, in agreement with the predictions. Triblock copolymers of similar molar mass, however, does not show such ordering, supporting the theoretical argument that triblock architecture need larger molar masses to form ordered structures¹.

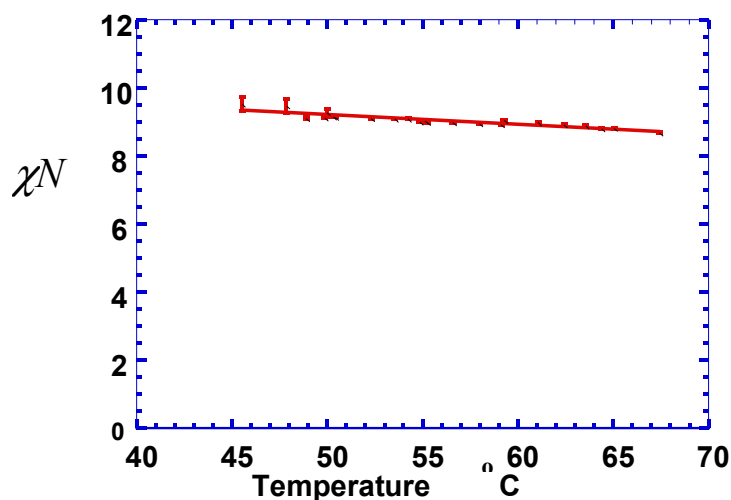


Fig. 1. The Flory-Huggins interaction parameter of PEO-PPO(d)-PEO triblock copolymers.

¹ P. J. A. Fairclough, G. E. Yu, S. M. Mai, M. Crothers, K. Mortensen, A. J. Rya and C. Booth, *Phys. Chem. Chem. Phys.* **2**, 1503 (2000).

2.8.6. Phase behavior near the isotropic critical Lifshitz point of a ternary homopolymer/block copolymer system

K. Mortensen, K. Almdal, H. Frielinghaus, *Danish Polymer Centre, Condensed Matter Physics and Chemistry Department, Risø National Laboratory, Denmark*, D. Schwahn, *IFF, Forschungszentrum Jülich, Germany*. L. Kielhorn, *Bayer AG, Leverkusen, Germany*
 e.mail: km@polymers.dk

The characterization of state of matter remains a fundamental scientific discipline. Each phase belongs to a universality class with a set of unique critical exponents describing the material properties in the vicinity of the phase transitions. Previous studies have included investigation of homopolymer blends, belonging to the 3d-Ising universality class, and diblock copolymers, which belong to the Brazdovski class. A three component mixture of a critical binary homopolymer blend and the corresponding symmetrical diblock copolymer is, according to theory, predicted to constitute one of the few practical realisable examples of the Lifshitz universality class. Using small-angle neutron scattering, we have studied the phase behavior and critical fluctuations of a ternary system of PEE, PDMS and PEE-PDMS. For suitable choices of molar masses, we observe a diagram that beyond the homogeneous disordered phase includes a single ordered phase, a two phase region and a microemulsion channel (fig.1). The mean-field critical Lifshitz point is expected to be near the point where extrapolation of the various phases crosses. The critical exponents observed near this mean-field predicted isotropic Lifshitz critical point are significantly renormalized in relation to both mean-field and Ising numbers, showing the influence of the Lifshitz universality class. In the disordered high- T regime *blend-like* and *diblock-copolymer-like* properties are separated by the Lifshitz Lines (LL). Above the LL the maximum value $S(q^*)$ of the structure factor occurs at finite q -value (fig.2), while below the LL the maximum $S(q^*)$ appear at $q^*=0$ ^{1, 2, 3}.

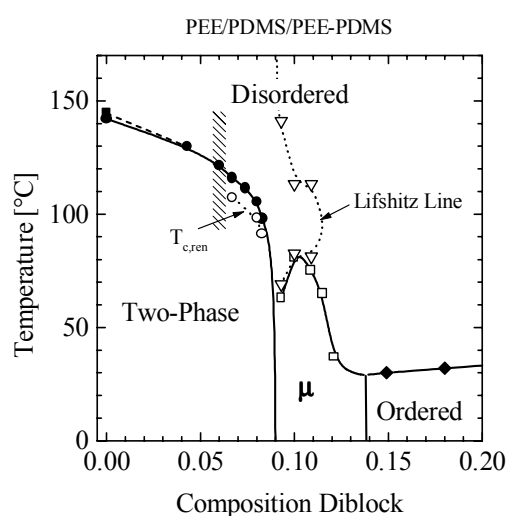


Fig. 1. Experimental phase diagram of the PEE/PDMS/PEE-PDMS ternary system.

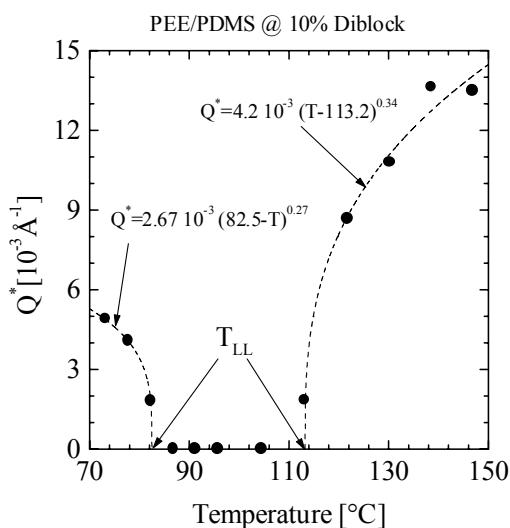


Fig. 2. Q^* values versus temperature for 10% sample of PEE/PDMS/PEE-PDMS. The ranges of diblock and blend character are clearly seen. Near the Lifshitz temperatures Q^* can be fitted by a scaling ansatz.

¹ K. Mortensen, D. Schwahn, H. Frielinghaus and K. Almdal, *J. Appl. Crystallograph.* **33**, 686 (2000).

² D. Schwahn, K. Mortensen, H. Frielinghaus and K. Almdal, *Physica B* **276**, 353-355 (2000).

³ D. Schwahn, K. Mortensen, H. Frielinghaus, K. Almdal and L. Kielhorn, *J. Chem. Phys.* **112**, 5454 (2000).

2.8.7. Composite capable of rapid volume change

P. Sommer-Larsen, I Johanssen, J. Hooker and K. West, *Condensed Matter Physics and Chemistry Department, Risø National Laboratory, Denmark*, E. Smela, *University of Maryland, USA*
e-mail: peter.sommer.larsen@risoe.dk

A patent for a composite capable of rapid volume change, for example for use in an actuator in which the composite is controllable by electrical and/or chemical stimuli was applied for in 1999 and published in 2000¹.

The present invention relates to a composite comprising one conjugated polymer capable of changing oxidation-state upon the onset of an electrical or chemical stimulus, and an ion-sensitive gel capable of changing volume, the polymer and the gel being morphologically interrelated, and wherein the volume change of the gel is in response to the change of the oxidation-state of the conjugated polymer.

The gel composites, shown in Fig.1, shrank and expanded upon addition to acidic and basic solutions, respectively. A film of the composite was spread on a gold-coated piece of Kapton, which functioned as an electrode in an electrochemical experiments. The film bent towards the Kapton site upon reduction and vice versa upon oxidation in acidic solution. The PANi/gel composite showed good electrochemical activity. However, the bending was relatively slow with a bending degree of less than 1.

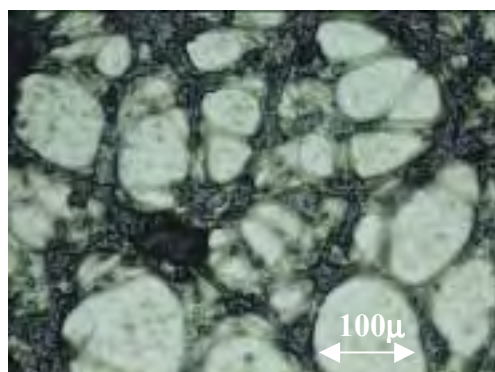


Fig. 1. A composite of polyaniline with a polyvinylalcohol/polyacrylic acid gel. The black PANi constitutes a conducting network surrounding the gel-phase.

PAni, co-doped with polyacrylic acid and HCl, was combined with a blend of polyvinyl alcohol and polyacrylic acid in NMP. Upon addition of glutaraldehyde and heating, a phase separated structure resulted, with a concomitant cross-linking of the PVA and PAA to form a gel composite. Depending on the processing conditions (solution concentrations, pH, etc.) various structures were obtained.

Electro-mechano-chemical activity in conducting polymers normally requires the polymer to be oxidised and reduced in an electrolyte solution with high ionic strength. The ionic strength however also effects the swelling of the gel phase. This is analysed in a simple model based on Flory's treatment of polyelectrolyte gels in which the swelling equilibrium is described through terms in the free energy corresponding to rubber elasticity, Flory-Huggins interaction between water and the polymer and a Donnan type term for the influence of free counterions. 30% linear expansions in the gel-phase is predicted at an ionic strength $s=0.1$ M. A 1:1 composition of PPyDBS and polyelectrolyte shows maximum expansion.

The model results in a minimum prediction for the swelling. Most neglected terms will add to increase the swelling.

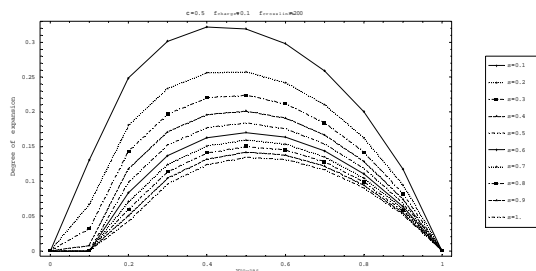


Fig. 2. Degree of swelling as a function of volume fraction of PPyDBS in the composite for various ionic strengths of electrolyte in the polyelectrolyte (PE) phase. The model builds on the assumption that the CP is PPyDBS and that a change of one H^+ per four pyrroles is induced on ox/red.

$\chi_{H_2O-PE}=0.5$. Linear charge density in PE chain is 0.1 and the cross-link density is 1/200.

¹ E. Smela, P. Sommer-Larsen, I. Johansen, J. Hooker and K. West, Eur. Pat. Appl. (2000), 14. EP 1026192 A1 20000809.

2.8.8. Response of a dielectric elastomer actuator

P. Sommer-Larsen, G. Kofod, *Condensed Matter Physics and Chemistry Department, Risø National Laboratory, Denmark* and M. Benslimane, *Danfoss A/S, Denmark*

e-mail: peter.sommer.larsen@risoe.dk

2.8.9. Artificial muscles from 3M VHB 4910 tape

G. Kofod, P. Sommer-Larsen, *Condensed Matter Physics and Chemistry Department, Risø National Laboratory, Denmark*, Roy Kornbluh and R. Pelrine, *Sri International, USA*
e-mail: guggi.kofod@risoe.dk

The artificial muscle of the title is of the type known as a dielectric elastomer actuator. Dielectric in this respect refers to a material, which has a very low conductivity and is polarisable, such that it will enhance an applied electric field. Elastomer is the same as rubber, typically the elastomer consists of cross-linked polymer, with an average chain-length between cross-links of about 100 monomers. Finally, actuator means a transducer that transforms energy to (linear) motion. Well-known actuators are hydraulic and pneumatic actuators.

A dielectric elastomer actuator is basically a capacitor made from a dielectric elastomer with stretchable electrodes. When a voltage is applied to the capacitor, physical plus charges appear on one electrode, and corresponding minus charges appears on the other. A Coulomb force arises between the charges, which will pull the electrodes toward each other. The force per area is described by the formula $p = \epsilon\epsilon_0 E^2$, the pressure generated by the applied electric field is proportional to the dielectric constant, and the square of the electric field. The elastomer is incompressible, thus as the capacitor contracts in thickness it must expand in the plane. These expansions can be very large, and recently a circularly expanding actuator showed an increase in planar extension of 380%¹. This was shown using a particularly well suited elastomer, namely the very high bond double sided tape made by 3M™, VHB™4910. This tape is a polyacrylate elastomer, supplied as a 1mm thick translucent film on a backing. The tape has many useful properties, and is very easy to make well working actuators from. It was shown that the tape may be stretched in the plane to more than 40 times (4000%) the original area, thus reducing the thickness by an equal ratio. A very important factor is the electric field at which the dielectric breaks down, the electric breakdown strength, which is typically 20-100 MV/m for elastomers. It was shown that the electric breakdown strength increases when the polymer is stretched, see Fig. 1.

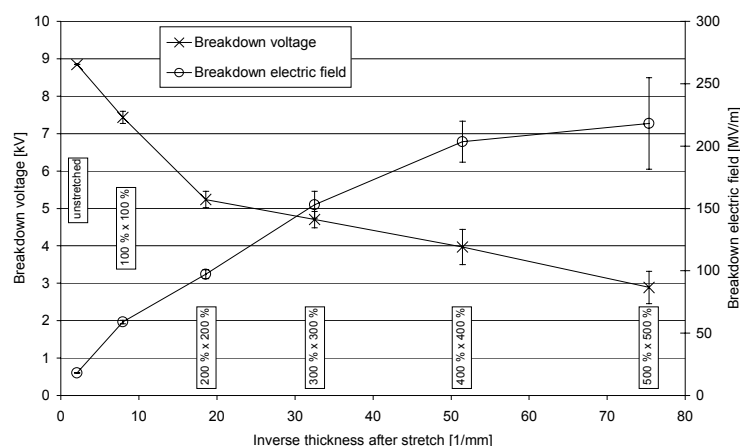


Fig. 1. Electric breakdown strength of isotropically pre-stretched VHB™ 4910. The film with a pre-strain of eg. 300 % x 300 % has increased $(1+300\%)\times(1+300\%)=16$ times in area. As the stretch ratio increases, the electric breakdown strength also increases, from around 20 to 200 MV/m, a huge and important increase.

Using dielectric spectroscopy it was shown, that the dielectric constant of VHB™4910 changes when it is stretched, from 4.7 at no stretch dropping to 3.7 when the area increases 16 times. This phenomenon is known as electrostriction, and is connected to piezo-electric behaviour. Electrostrictive coefficients may be both positive and negative, thus in principle it should be possible to find a material in which the dielectric constant increases upon stretch.

Several actuators were made from VHB™4910. An actuator stretched 36 times in area, with an active area of 200x30 mm, produced a force of 670 g at 5 kV applied voltage. A similar actuator in a rolled-up configuration, with a length of 10 cm and a cross-section of 5x5 mm, weighing just 4 g, was able to lift a 1.5 kg weight 8 mm.

¹ R. Kornbluh, R. Pelrine and Q. Pei, http://ndeeaa.jpl.nasa.gov/nasa-nde/newsltr/WW-EAP_Newsletter2-2.PDF, 10 (2000).

2.8.10. Dielectric elastomer actuators

P. Sommer-Larsen, G. Kofod, J. Hooker, *Condensed Matter Physics and Chemistry Department, Risø National Laboratory, Denmark*, P. Gravesen and M. Benslimane, *Danfoss A/S*
 e-mail: peter.sommer.larsen@risoe.dk

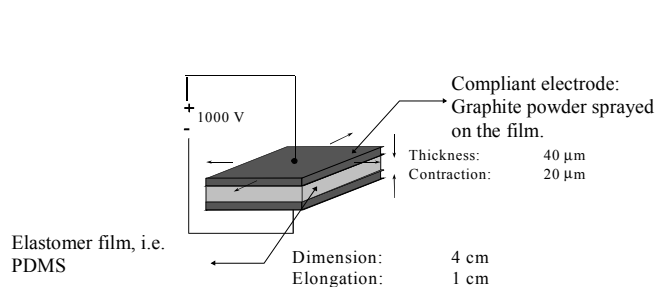


Fig. 1. Basic design for a dielectric elastomer actuator. An elastomer film is sandwiched between two compliant electrodes. When charged, the electrodes attract each other, squeezing the elastomer in the film plane. The concurrent expansion in the plane of the film is utilised in a sheet-actuator or roll-actuator, where the film is rolled up.

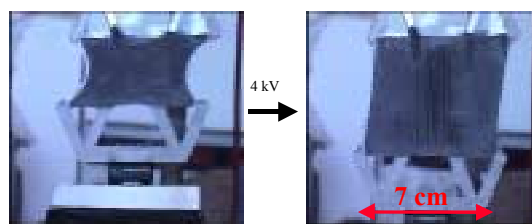


Fig. 2. Sheet-actuator, which expands 67% linearly - 5 Hz response - Lifts 250 g (100 x its own weight). The elastomer is an acrylic adhesive tape from 3M™ (VHB™-4910). Graphite powder containing grease electrode.

Dielectric elastomer actuators are integrated structures combining an elastic film with two electrodes - see Fig. 1. Dielectric elastomer actuators work macroscopically: Actuators expands 100 %, lift more than 100 times their own weight with up to 10 Hz response. An example is shown in Fig. 2. The appearance of an actuator is in the form of an expanding rubber sheet or a rubber band or a strip of several narrow sheets. Figure 3 and 4 pictures two ways to obtain work from the actuator. In both configurations, mechanical work is obtained during the elastic contraction following discharging of the actuator.

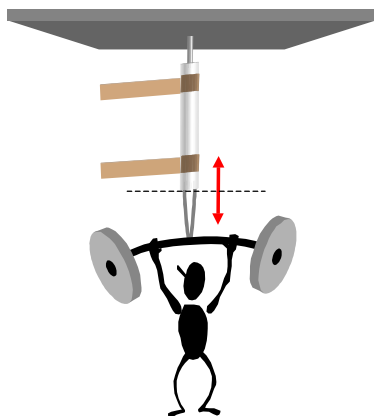


Fig. 3. Roll actuator working in a preloaded configuration. The load stretches the actuator to a certain pre-extension. When activated, the actuator works around this equilibrium state marked by the dashed line, lifting the weight up and down.

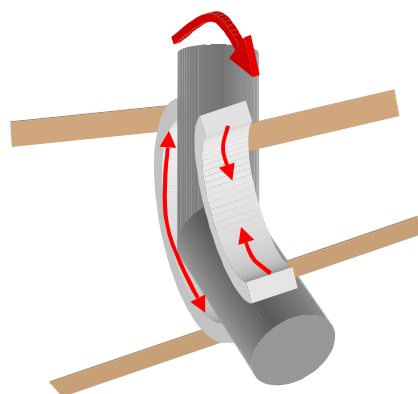


Fig. 4. Strip actuators used in a push-pull configuration to bend an elbow joint. In the equilibrium configuration, both actuators are stretched. Activating one actuator will cause it to expand while the other contracts elastically.

Actuators are produced within the framework of the ARTMUS project: collaboration between Danfoss A/S, Department of chemistry, DTU and the Danish Polymer Centre at Risø.

In 2001 it is the aim of the project to demonstrate a dielectric elastomer actuator consisting of five layers of elastomer sheets and use the actuator to drive a device like a bending arm.

2.8.11. Properties of Polypyrrole doped with alkyl benzene sulfonate

K. West, P. Sommer-Larsen, T. Mazur, O. Jørgensen and H. D. Rasmussen, *Condensed Matter Physics and Chemistry Department, Risø National Laboratory, Denmark*, L. Bay and S. Skaarup, *Department of Chemistry, Technical University of Denmark, Denmark*
e-mail: keld.west@risoe.dk

Many conjugated polymers show an appreciable difference in volume between their oxidised and reduced forms. This property can be utilised in a new type of soft, electrochemically driven actuators, “artificial muscles”. Several geometries have been proposed for the conversion of the volume expansion into useful mechanical work. In a particularly simple geometry, the length change of polymer strips is exploited. The polymer strips are connected to the driving circuit in the end of the strip that is attached to the support of the device. The other end of the strip is connected to the load. The advantage of this set-up is simplicity and that the maximum force generated in the polymer can be transferred directly to the load.

In the ongoing ARTMUS (Artificial Muscles) project, polypyrrole (PPy) doped with alkyl benzene sulfonates have been shown to be particularly useful because of their relative large volume expansions combined with a good chemical stability. The system that has been most studied is PPy doped with dodecyl benzene sulfonate (DBS, an anionic tenside used in household detergents, see figure 1). A chemical analysis of commercial DBS has shown that this is a very impure product containing several isomers and a range of alkyl chain lengths. We synthesised the pure isomers, and showed that the exact nature of the dopant influences the properties of the polymer markedly.

The present work is an investigation of the influence of the length of the alkyl chain on the physical and mechanical properties of the conjugated polymer. We have investigated detergents with alkyl side chains with lengths in the interval from 1 C to 22 C. As most of these are not available commercially, a number of alkyl benzene sulfonates has been synthesised.

Determination of the mechanical properties of these polymers is associated with an appreciable uncertainty. This is mainly because small variations in the synthesis conditions influence the morphology and mechanical properties of the polymer in an erratic way (polymers are disordered materials without the entropic drive for order and regularity known from low-molecular solids).

Figure 2 shows the length changes obtained for a number of polymers under different experimental conditions. The three sets of data differ with respect to the speed of the switching. Despite the scatter of the data, it is clearly seen that maximum elongation is obtained with alkyl benzene sulfonates of intermediate length. Also the stiffness and the electronic conductivity of the polymers vary in a systematic way with the length of the alkyl chain in the dopant.

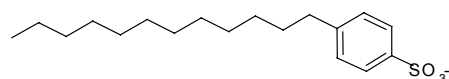


Fig. 1. N-dodecyl benzene sulfonate anion

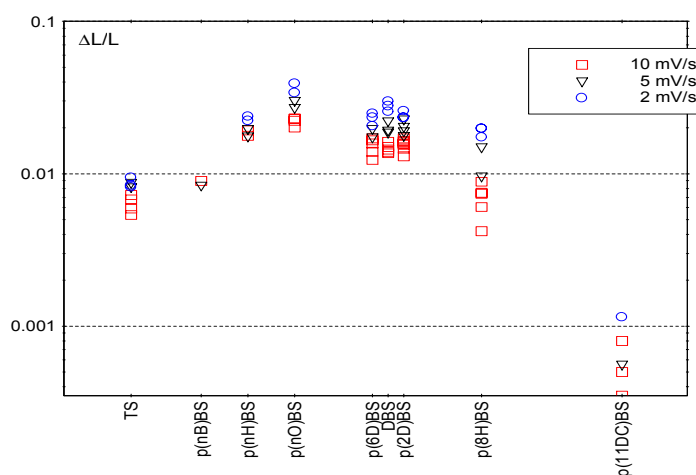


Fig. 2. Relative elongation of PPy strips with different dopants.

2.8.12. Microporous polymer membranes for lithium polymer batteries

A. Munch Elmér, *Polymer Science & Engineering, Lund University, Sweden*, P. Sommer-Larsen and K. West, *Condensed Matter Physics and Chemistry Department, Risø National Laboratory, Denmark*
e-mail: anette.munch_elmer@polymer.lth.se

The electrolyte is one of the most important components in a battery. The fundamental tasks of the polymer electrolyte are to separate the electrodes, conduct ions and at the same time being a bad electron conductor. Among the strategies for improving conductivity for polymer electrolytes the incorporation of low molecular weight plasticizers is one of the more popular, unfortunately this impairs the mechanical stability. Another popular approach for design of polymer electrolyte membranes to avoid mechanical instability is to incorporate a liquid electrolyte solution into a porous polymer membrane. However, these membranes often suffer from leakage of electrolyte.

This project deals with solid polymer electrolyte membranes with semi-IPN structures. The membranes have a morphology of a microporous structure of poly(vinylidene fluoride-co-hexafluoropropylene) (PVDF-co-HFP) incorporated by a continuous network of crosslinked poly(ethylene glycol) (400) monomethyl ether monomethacrylate macromonomers doped with lithium bis(trifluoromethylsulfonyl)imide (LiTFSI). The 3D matrix of PVDF-co-HFP supplies the membranes with mechanical stability while the PEG-phase has conductive properties. These membranes are an interesting step towards polymer gel electrolytes that can combine mechanical stability with ion conductivity without suffering from electrolyte leakage.

The morphology is obtained by ordinary solvent casting of films containing PVDF-co-HFP, macromonomer, LiTFSI, and crosslinker, a short PEG-diacrylate. As PVDF-co-HFP is partly mixable with short PEO chains a microphase separation occurs. The co-continuous structure is locked by UV-irradiation to induce polymerisation of the macromonomer. The pores have a size of $\sim 1\mu\text{m}$, see Fig. 1.

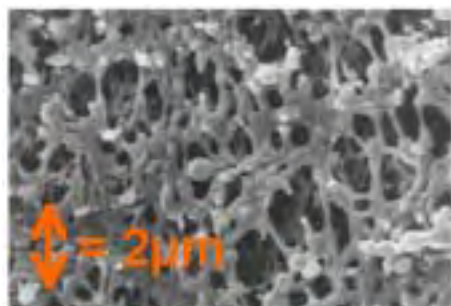


Fig. 1. Scanning electron microscopy picture of the remaining PVDF-co-HFP phase after the PEG phase has been leached out. A co-continuous structure is obtained.

The membranes have a glass transition temperature at $-60\text{ }^{\circ}\text{C}$. Above this temperature the PEO-chains are mobile, which means that the ion conductive properties are visible at higher temperatures. T_g is not affected by the compositions of the blends. The polymer electrolyte membranes are thermo-mechanically stable up to a temperature $135\text{ }^{\circ}\text{C}$ when the PVDF-HFP phase melts.

Electrochemical Impedance Spectroscopy (EIS) is used to measure the ion conductivity of the samples. The results are presented in an Arrhenius plot. The measurements show the conductivity is increased with lower amounts of PVDF-HFP. The conductivity at room temperature ($1000/T(\text{K}) = 3,35$) is still low ($\sim 10^{-5}\text{ S/cm}$) which proves that an eventual incorporation of plasticizer is necessary.

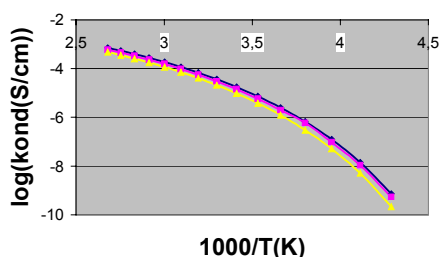


Fig.2. Arrhenius plot of the conductivity data

— 15wt% PVDF-co-HFP
— 20wt% PVDF-co-HFP
— 30wt% PVDF-co-HFP

2.9. Organic chemistry

2.9.1. Easy access to 3,8-diaryl-difurano[2,3-*a*:2',3'-*f*]naphthalenes: A new extended aromatic system

M. Jørgensen, F. C. Krebs and K. Bechgaard, *Condensed Matter Physics and Chemistry Department, Risø National Laboratory, Denmark*
e-mail: mikkel.joergensen@risoe.dk

Extended aromatic systems have gained interest in diverse fields such as organic light emitting diodes¹, two-photon absorption materials², second and higher order non-linear optics and large (supramolecular) structures. New easily prepared building blocks with potential for further elaboration could add stimulus to these research areas.

In a search for new extended π -systems with possible applications in both two photon absorption and electroactive polymers we have developed a synthesis of the hitherto unknown 3,8-diaryl-difurano[2,3-*a*:2',3'-*f*]naphthalene system (see Fig. 1)³. The parent compound difurano[2,3-*a*:2',3'-*f*]naphthalene itself has been described only once in the literature.⁴ Also the 3,8-dimethyl derivative of this compound has been prepared previously from 1,5-dipropyloxy-naphthalene by irradiation⁵. Further removed, but related, are the benzofuranes for which a somewhat similar synthetic strategy has been devised⁶.

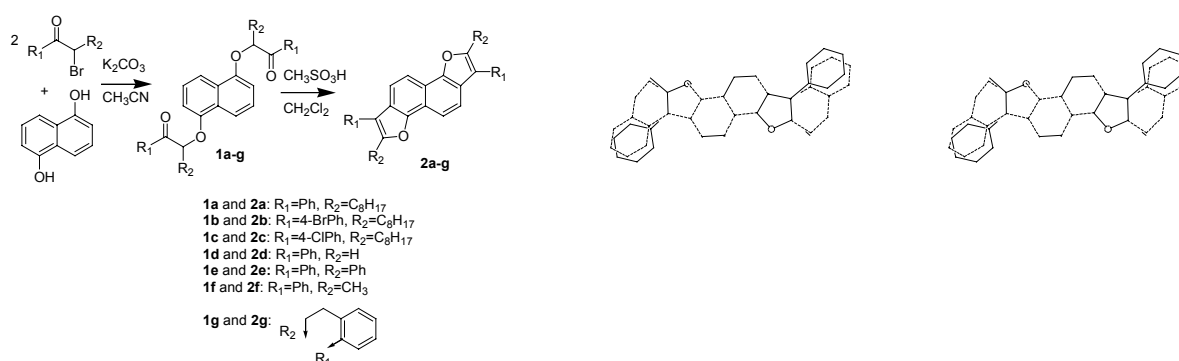


Fig. 1. Synthesis of 3,8-Diaryldifurano-naphthalenes.

Fig. 2. Stereoview of compound **2f** (solid) and **2g** (dotted) overlaid. It is noticeable that the substituents phenyl rings in compound **2g** are more in plane with the central part of the molecule than compound **2f**. This observation also hosts the explanation for the yellow colour of compound **2g** as opposed to the colourless compound **2f**.

¹ a) J. R. Sheats, H. Anthoniadis, M. Hueschen, W. Leonard, J. Miller, R. Moon, D. Roitman and A. Stocking, *Science* **273**, 884 (1996); b) F. Hide, M. A. Diaz-García, B. J. Schwartz and A. J. Heeger, *Acc. Chem. Res.* **30**, 430 (1997).

Habermann, J.; Ley, S. V.; Smits, R. J. *Chem. Soc., Perkin Trans.*, **1**, 2421 (1999).

² M. Albota, D. Beljonne, J.-L. Brédas, J. E. Ehrlich, J.-Y. Fu, A. Heikal, S. E. Hess, T. Kogej, M. D. Levin, S. R. Marder, D. McCord-Maughon, J. W. Perry, H. Röckel, M. Rumi and G. Subramaniam, E. W. Webb, X.L. Wu and C. Xu, *Science* **281**, 1653 (1998).

³ M. Jørgensen, F. C. Krebs and K. Bechgaard, *J. Org. Chem.* **65**, 8783 (2000).

⁴ P. R. Dingankar, T. S. Gore and V. N. Gogte, *Indian J. Chem.* **9**, 24 (1971).

⁵ F. M. Moghaddam, A. Sharifi and M. R. J. Saidi, *J. Chem. Res. Synop.* **7**, 338 (1996).

⁶ J. Habermann, S. V. Ley and R. J. Smits, *Chem. Soc., Perkin Trans.* **1**, 2421 (1999).

2.9.2. On the conformational properties of $[n]$ cyclophanes: A new application of the Ramachandran plot using crystallographic data

F. C. Krebs and M. Jørgensen, *Condensed Matter Physics and Chemistry Department, Risø National Laboratory, Denmark*

e-mail: frederik.krebs@risoe.dk

The Cambridge Crystallographic Database (CSD) was searched for crystallographic information on $[n]$ cyclophanes, namely calix $[n]$ arenes, resorcin $[n]$ arenes and cyclotrimeratrylenes and compared with diphenylmethanes. Particular sets of torsion angles were retrieved and presented in a Ramachandran type plot. Distinct conformers were found to appear in distinct regions of the plot. Furthermore the various macrocycles were found to be distinguishable by using the plot and conformational features were thus highlighted. Of interest here is the considerable number of crystal structures that have been solved for all these molecules thus allowing for a statistical analysis. The most well studied $[n]$ cyclophane (in a crystallographic sense) is by far the calix[4]arenes with more than 313 structures known. Following these the resorcin[4]arenes and the cyclotrimeratrylenes can be found with 50 and 23 structures known respectively. Far less represented are the calix[5], calix[6] and calix[8]arenes. The Ramachandran plot is a very powerful way of correlating the conformational behaviour of molecules provided that the conformation of the individual molecule or parts thereof can be given uniquely by two torsion angles or by sets of two torsion angles. The way the plot is presented is simply by plotting the two distinct torsion angles against each other. In this work we present a conformational analysis of particularly the calix[4]arenes based on the presentation of crystallographic data in a Ramachandran type plot.

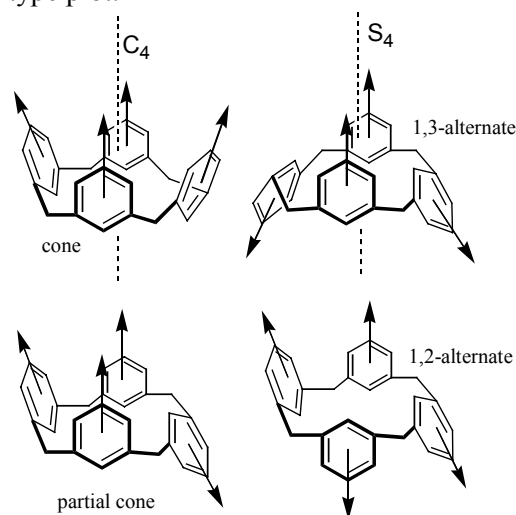


Fig. 1. Structural drawings of the different conformers for the calix[4]arene system. The arrows indicate a directionality of the constituent phenyl rings. The axes denoted C_4 and S_4 represent molecular point group symmetry operators for the cone and the 1,3-alternate conformers respectively.

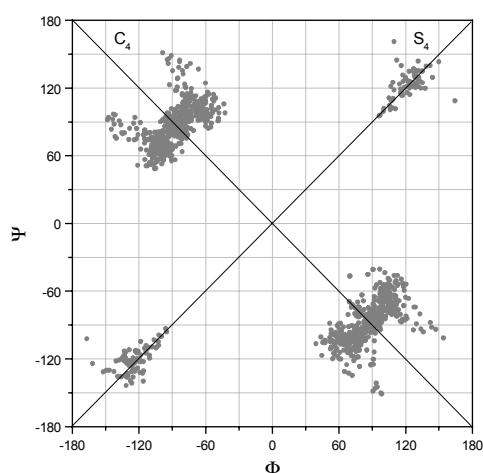


Fig. 2. A Ramachandran plot of all calix[4]arenes. The entire $\Phi\Psi$ -space is shown and the residual symmetry is apparent. The diagonals of the plot are labelled C_4 and S_4 respectively.

The present study¹ has thus shown the use of crystallographic information to compare and contrast the conformational properties of complex macrocyclic molecules.

¹ F. C. Krebs and M. Jørgensen, *J. Org. Chem.* **65**, 3846 (2000).

2.9.3. How the *R*-factor changes as molecules become larger

F. C. Krebs, *Condensed Matter Physics and Chemistry Department, Risø National Laboratory, Denmark*

e-mail: frederik.krebs@risoe.dk

The *R*-factor and the number of independent atoms for the entire set of molecular organic structures contained in CCDC database (CCD) were retrieved and analysed. The average *R*-factor for all the structures containing the same number of independent atoms was plotted against the number of independent atoms. A clear correlation was observed and the plot is suggested to give a graphical overview of how values of the *R*-factor for large molecule structures with 200-1000 independent atoms increase as the number of independent atoms increase. The values of *R*-factors obtained in refinements are expected to depend on the size of the structure because the accurate description of atomic positions, thermal parameters and occupancies requires a large number of observations for every parameter (normally a ratio of 10 to 1). The $R \leq 0.07$ requirement is perfectly valid for small molecule structures ($R = 0.07$ is the upper limit suggested by *Acta Cryst.*). For the very large protein structures *R*-factor values in the range 0.15-0.30 are often considered acceptable (depending on resolution and the amount of solvent included in the crystal (sometimes up to 50%)). What values of *R*-factor should be considered acceptable for structures of intermediate size? This work was undertaken to give a graphical overview of *R*-factors when examining crystallographic data for large molecules. The argument is simply a statistical one based on the vast amount of data that already exists in the CCD (CCD, 1998). It is advantageous to have a graphical overview that is based on the complexity of the system in question (i.e. the number of independent atoms). Figure 1 is such an overview and it gives an indication on the range of values an acceptable *R*-factor should assume for any given system¹.

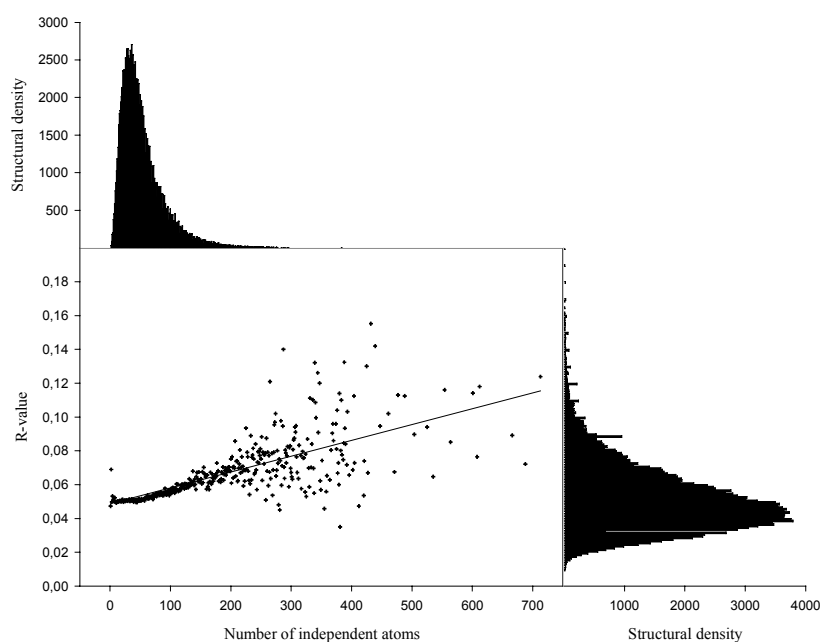


Fig. 1. A plot of the average *R*-factor for all structures with the same number of independent atoms as a function of the number of independent atoms. Below 250 independent atoms the data points represent good averages, between 250 and 300 independent atoms the data points represent averages that are based on 5 –10 structures and above 400 independent atoms the data points do not represent averages but correspond to single structures. All data points are however included for completeness. The line represents a linear fit to all data.

¹ F. C. Krebs, *J. Appl. Cryst.* **33**, 392 (2000).

2.10. Instrumentation

2.10.1. Test of 8.4 Tesla Nb/Ti superconducting magnet

A. B. Abrahamsen, M. Nielsen, B. O. Breiting, F. B. Saxild, A. B. Nørtoft, J. Lebech, B. L. Larsen, N. H. Andersen, *Condensed Matter Physics and Chemistry Department, Risø National Laboratory, Denmark*, N. Hauge, *Danfysik A/S, Jyllinge, Denmark*.

e-mail: asger.abrahamsen@risoe.dk

Two Nb/Ti superconducting magnets were tested for persistent current operation at a field of 8.4 Tesla and $T = 4.2$ K as part of an industrial collaboration with Danfysik A/S.

The magnets consist of two solenoid windings with different Nb/Ti wire thickness and a superconducting switch connected across the terminals of the magnet, whereby the magnet can be operated in persistent current mode. Fig. 1 shows a magnet embedded in a 40 mm iron shielding and the persistent switch (left) mounted outside of the shielding. The electrical connections between the two windings and the switch were made by winding 6 cm of the wires around copper cylinders and soldering them with standard soldering tin.

A liquid helium cryostat was modified to support the 50 kg heavy magnets and an insertion device was constructed for measuring the magnetic field density along the center axis of the magnet using a LakeShore Hall probe.

The purpose of the test was to determine if the epoxy cast of the coils was sufficient mechanically stable to prevent quenching of the superconducting wires during ramping up of the current and to examine the field decay in time when used in persistent current mode. Only minor quenches were observed during the initial ramping of the current to $I = 70$ A and after the initial ramp no further quenches were seen proving that the coil casting was successful. Fig. 2 shows the field decay in the center of the magnet after the persistent switch is closed. The power supply output was maintained at full current during the first 30 minutes and then ramped down to zero during 10 minutes in order to determine the losses in the joint between the coils and in the entire magnet and switch current loop. A field decay of $1.9 \cdot 10^{-5}$ Tesla/min and $6.1 \cdot 10^{-5}$ Tesla/min was obtained, which is equivalent to a resistance of 126 n Ω and 407 n Ω in the coil connection and the magnet loop, respectively. The field decay rate is however a factor of 10 higher than the required by the customer and an improved soldering technique must be developed in the future. A change from a resistive connection between the wires to a superconducting connection will be attempted. Finally in all 4 magnets have to be tested when the superconducting soldering technique is working.



Fig. 1. Superconducting magnet in iron shielding with persistent switch mounted on the side. Dimensions $\text{\O}240\text{mm} \times 280$ mm. Weight = 50 kg.

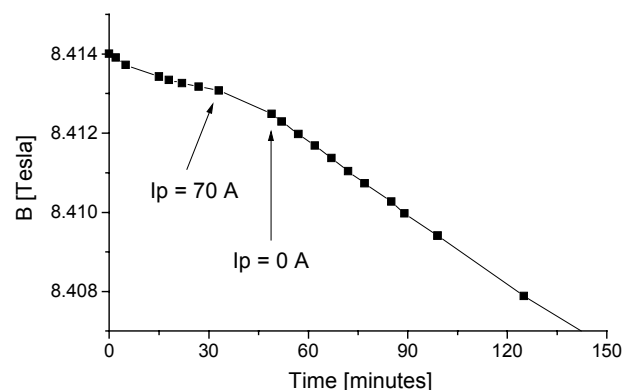



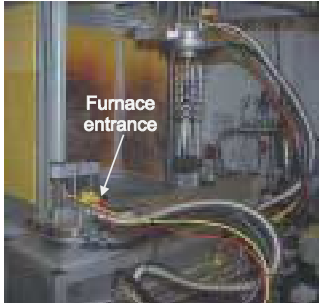







Fig. 2. Magnetic field decay of magnet when operated in persistent current mode. A change in the decay rate is seen as the power supply current (I_p) is ramped down indicating a resistance of 126 n Ω in the joint between the two coils and 407 n Ω in the entire magnet loop. A reduction by a factor 10 is needed.

2.10.2. The facility for plastically deformed germanium single-crystal wafers


B. Lebech, B. Breiting, F. Saxild and K. Theodor, *Condensed Matter Physics and Chemistry Department, Risø National Laboratory, Denmark*
 e-mail: bente.lebech@risoe.dk

The Risø facility¹ for plastically deformed germanium single crystal wafers was inspired by Axe et al.² and motivated by the wish to optimise and improve the neutron flux at the thermal neutron beams at Risø as cost effectively as possible by producing better monochromators. The facility has been in routine operation since June 1996 and has been producing plastically deformed germanium wafers to be used in neutron monochromators for customers since early 1997.


THE FACILITY

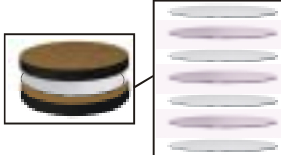
THE PROCESS



Stacks containing four wafers undergoes the following process:
 Heat to 870°C - bend up - cool to 20°C
 Heat to 870°C - flatten - cool to 20°C
 Heat to 870°C - bend down - cool to 20°C
 Heat to 870°C - flatten - cool to 20°C




Heat to 870°C and flatten each wafer between ceramic plates

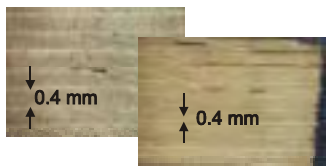


Multi stack of $n+1$ wafers and n tin foils soldered at app. 400°C in helium atmosphere


THE PRODUCT




Perfectly soldered finished composite stacks



Cut through a composite wafer stack




Soldering in vacuum is not a good solution




A bend wafer and a cut composite wafer strip

RISØ design focussing and tilting monochromator holders



LEFT: With 15 pyrolytic graphite crystal strips. Used at TAS7 at Risø for more than 10 years.



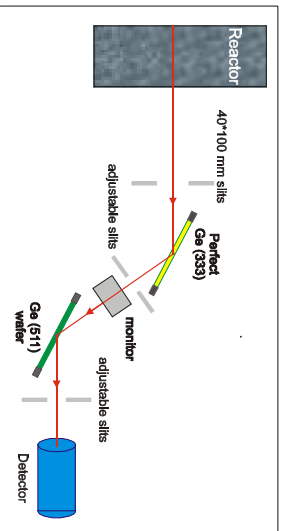
RIGHT: With 19 crystal strips of composite Ge wafer stacks. Delivered to HMI in Berlin 3. October 2000.

¹ B. Lebech, K. Theodor, B. Breiting, P. G. Kealey, B. Hauback, J. Lebech, S. Aa. Sørensen and K. N. Clausen, *Physica B* **241-243**, 204 (1998), Risø-R-1014(EN). Editors: M. Nielsen, K. Bechgaard, K. N. Clausen, R. Feidenhans'l and I. Johansen, pp. 137 and 138 (1998). Risø-R-1099(EN). Editors: K. Bechgaard, K. N. Clausen, R. Feidenhans'l and I. Johansen, 137 (1999), Risø-R-1156(EN). Editor: B. Lebech, 123 (2000).

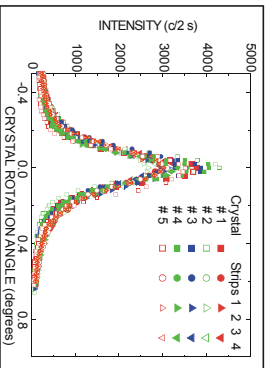
² J. D. Axe, S. Cheung, D.E. Cox, L. Passell, T. Vogt and S. Bar-Ziv, *Neutron Research* **2**, 85 (1994).

SOME FACTS

The Risø facility for plastic deformation of germanium wafers has been in routine operation since early 1996. Until now about 700 wafers have been processed and used to make composite monochromators for neutron scattering instruments at Risø National Laboratory, Denmark, Institute for Energy Technology, Norway, Hahn Meitner Institute, Germany, Oak Ridge National Laboratory, Tennessee and Demokritos Research Centre, Greece. The majority of the processed wafers are cut as (511) slabs, but also several (311) and (111) and a few (711) and (155) wafers have been processed and tested. In a white beam, the Bragg reflected neutrons from the composite monochromators have Gaussian like symmetric line shapes with a full width at half maximum of about 15 to 20 minutes of arc.



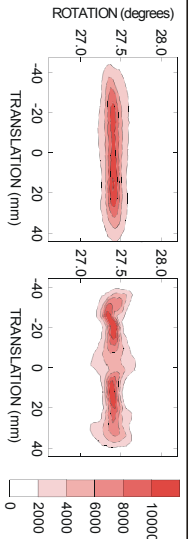
Experimental set-up used to check the $(h\ l\ l)$ germanium wafers and composite monochromator slabs. The (333) reflection from a perfect germanium monochromator with open incident and exit collimation gives perfect focussing for the (511) germanium reflection. Hence, the rocking curve widths shown below measure the mosaicity directly.



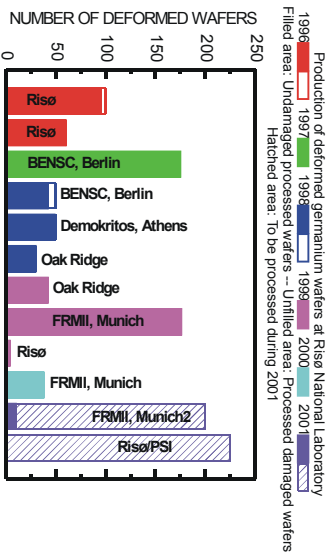
Rocking curves of 20 composite strips. Broad/low intensity and narrow/high intensity peaks are for strips cut from the top and bottom of the slabs, respectively.

Equal intensity contours obtained from rocking curves for different parts of a composite wafer strip. The abscissa is the horizontal position of strip with respect to incident and exit slits. The ordinate is the crystal rotation angle.

LEFT: Slits $h^*v = 20\text{ mm} \times 10\text{ mm}$ - RIGHT: Slits $h^*v = 6\text{ mm} \times 10\text{ mm}$.



About 400 of the processed wafers have been carefully tested by neutron diffraction before being made into composite slabs suitable as a neutron monochromator. Within the experimental accuracy the test results for the individual wafers are consistent and reproducible. The wafers are 75 mm in diameter and 0.4 mm thick. They were delivered cut with the (511) reflection perpendicular to the wafer plane within an accuracy of $\pm 0.05^\circ$. Two minimally composite monochromator crystals by careful alignment of these flats. In the right hand panel, the performance of one of these monochromators is compared to a squashed germanium monochromator.

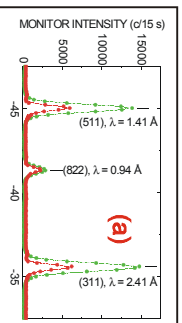


Production of deformed germanium wafers at Risø National Laboratory
 Filled area: Undamaged processed wafers -- Unfilled area: Processed damaged wafers
 Hatched area: To be processed during 2001

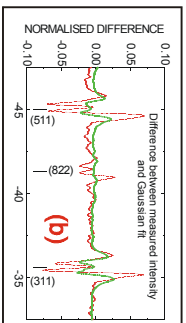
THE PROFIT

NOT MONEY, BUT

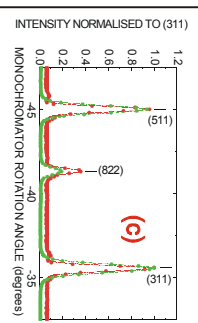
- (a) Higher flux on the sample
- (b) More symmetric peak shape
- (c) Better peak to background ratio
- (d) Accurate data - Better science



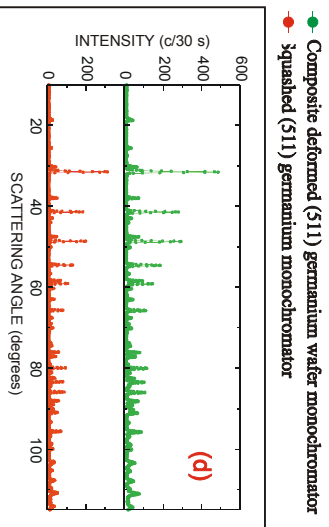
Monitor intensity obtained by rotating the monochromator in the white reactor beam. The solid curves are the results of fits to the sum of three Gaussians.



Difference between the Gaussian fits and the measured data normalised to the peak intensity of (311).



Measured and fitted intensities normalised to the (311) peak intensities.



Composite deformed (511) germanium wafer monochromator
 Squashed (511) germanium monochromator

Powder diffraction pattern obtained for Al_2O_3 using incident neutrons with $l = 1.12\text{ \AA}$ achieved by 90° scattering from the germanium (711) reflection. The total counting time is 1 hour per spectrum with 2000 data points.

TOP: Composite germanium deformed wafer monochromator. Monitor rate 284 c/s.
 BOTTOM: Squashed germanium monochromator. Monitor rate 173 c/s.

2.10.3. McStas developments at Risø

K. Lefmann, P.-O. Åstrand, and K. Nielsen, *Condensed Matter Physics Department, Risø National Laboratory, Denmark*

e-mail: kim.lefmann@risoe.dk

McStas is a program for simulating cold and thermal neutron experiments using ray-tracing Monte Carlo techniques. It consists of a meta-language with compiler, a library of well tested components, a number of example instruments, and a variety of graphical front-ends. McStas is developed and maintained at Risø National Laboratory and both source code and documentation can be obtained freely from our home page neutron.risoe.dk

The year 2000 saw lots of changes for McStas. On the personnel side, K. Nielsen has left the project. K. Nielsen was really to key person in McStas and will be difficult to replace. On the other hand, we found an experienced computer scientist to this hard job: P.-O. Åstrand will from January 2001 take over the responsibility for the McStas kernel, while Kim Lefmann as before is responsible for the component library. On the technical side, the versions 1.2, 1.3, and 1.4 were all launched this year. The main improvements on version 1.1 are:

- The graphical interface for building instruments, compiling simulations and running simulations, *mogui*, has been added to the system. There are, however, problems in some Linux installations, but we believe they will be solved soon.
- More realistic sample components have appeared for single crystal Bragg scattering, even though primary extinction is not included.
- The on-line documentation generator, *mcdoc*, has been added to the system. Mcdoc transforms the comments at the head of component into a manual entry.
- Expressions are now allowed in parameter lists.
- A McStas to Vitess compiler, *mcstas2vitess*, has been produced.
- A tutorial to McStas has been written.

The McStas user group has expanded over the last year, and now counts researchers from almost all neutron sources in Europe, North America, and Australia, and several groups in Asia and Africa. A part of this user community will meet at the 1st McStas Workshop, Risø, January 2001.

In the near future, McStas will be expanded towards realistic experimental set-ups. We will work to include gravity and to make realistic inelastic scattering samples. Further, a suite of components for time-of-flight experiments will be produced. An important test of McStas will be the simulation of the first instrument suite for the European Spallation Source, ESS.

McStas is supported by the European programmes SCANS and Cool Neutron Optimization, and by the Neutron Round Table.

3. Publications, lectures, educational and organisational activities

3.1. International publications

Aasmundtveit, K. E.; Samuelsen, E. J.; Guldstein, M.; Steinsland, C.; Flornes, O.; Fagermo, C.; Seeberg, T. M.; Pettersson, L. A. A.; Ingas, O.; Feidenhans'l, R.; Ferrer, S., Structural anisotropy of poly(alkylthiophene) films. *Macromolecules* (2000) v. 33 p. 3120-3127.

Altankov, G.; Thom, V.; Groth, T.; Jankova, K.; Jonsson, G.; Ulbricht, M., Modulating the biocompatibility of polymer surfaces with poly(ethylene glycol): Effect of fibronectin. *J. Biomed. Mater. Res.* (2000) v. 52 p. 219-230.

Andresen, T. L.; Krebs, F. C.; Thorup, N.; Bechgaard, K., Crystal structures of 2,3,6,7,10,11-oxytriphenylenes. Implications for columnar discotic mesophases. *Chem. Mater.* (2000) v. 12 p. 2428-2433.

Apperloo, J. J.; Janssen, R. A. J.; Nielsen, M. M.; Bechgaard, K., Doping in solution as an order-inducing tool prior to film formation of regio-irregular polyalkylthiophenes. *Adv. Mater.* (2000) v. 12 p. 1594-1597.

Arleth, L.; Pedersen, J. S., Scattering vector dependence of the small-angle scattering from mixtures of hydrogenated and deuterated organic solvents. 11. International conference on small-angle scattering (SAS99), New York, NY (US), 17-20 May 1999. *J. Appl. Cryst.* (2000) v. 33 p. 650-652.

Bailey, L.; Henderson, M. J.; Hillman, A. R.; Gadegaard, N.; Glidle, A., In situ neutron reflectivity studies of poly-o-toluidine films. *Physica B* (2000) v. 276-278 p. 373-374.

Balakrishnan, G.; Keszthelyi, T.; Wilbrandt, R.; Zwier, J. M.; Brouwer, A. M.; Buma, W. J., The radical cation and lowest Rydberg states of 1,4-diaza[2.2.2]bicyclooctane (DABCO). *J. Phys. Chem. A* (2000) v. 104 p. 1834-1841.

Bechgaard, K.; Nielsen, M. M.; Krebs, F.C., (TMTSF) 2X materials and structural implications for low-dimensional polymeric and disordered molecular semiconductors. Organic superconductivity "20. Anniversary", Orsay (FR), 7 Dec 1999. *J. Phys. IV* (2000) v. 10 (no.3) p. 11-17.

Bergström, M.; Pedersen, J. S., A small-angle neutron scattering study of surfactant aggregates formed in aqueous mixtures of sodium dodecyl sulfate and didodecyldimethylammonium bromide. *J. Phys. Chem. B* (2000) v. 104 p. 4155-4163.

Borbely, S.; Pedersen, J. S., Temperature-induced aggregation in aqueous solutions of pluronic F68 triblock copolymer containing small amount of o-xylene. *Physica B* (2000) v. 276-278 p. 363-364.

Brdarski, S.; Åstrand, P.-O.; Karlström, G., The inclusion of electron correlation in intermolecular potentials: Applications to the formamide dimer and liquid formamide. *Theor. Chem. Acc.* (2000) v. 105 p. 7-14.

Brown, W.; Mortensen, K. (eds.), Scattering in polymeric and colloidal systems. (Gordon and Breach Science Publishers, Amsterdam, 2000) 496 p.

Bødker, F.; Hansen, M. F.; Koch, C.B.; Lefmann, K.; Mørup, S., Magnetic properties of hematite nanoparticles. *Phys. Rev. B* (2000) v. 61 p. 6826-6838 Cannavacciuolo, L.; Sommer, C.; Pedersen, J. S.; Schurtenberger, P., Size, flexibility, and scattering functions of semiflexible polyelectrolytes with excluded volume effects: Monte Carlo simulations and neutron scattering experiments. *Phys. Rev. E* (2000) v. 62 p. 5409-5419.

Ceretti, M.; Janssen, S.; McMorro, D. F.; Radaelli, P.; Steigenberger, U., ECNS '99 - Young scientists forum. *Physica B* (2000) v. 276-278 p. 45-51.

Christensen, N. B.; Lefmann, K.; Johannsen, I.; Jørgensen, O., Magnetic Bloch oscillations in the near-Ising antiferromagnet $\text{CoCl}_2 \cdot 2\text{D}_2\text{O}$. *Physica B* (2000) v. 276-278 p. 784-785.

Clausen, K. N.; Bødker, F.; Hansen, M. F.; Kuhn, L. T.; Lefmann, K.; Lindgård, P.-A.; Mørup, S.; Telling, M., Structure and dynamics of magnetic nanoparticles. *Physica B* (2000) v. 276-278 p. 830-832.

Clegg, P. S.; Cowley, R. A.; Goff, J. P.; McMorro, D. F.; Sawicki, M.; Ward, R. C. C.; Wells, M.R., Anomalous magnetic ordering in $\text{Dy}_x\text{Pr}_{1-x}$ alloys. *Physica B* (2000) v. 276-278 p. 698-699.

Coad, S.; Hiess, A.; McMorro, D. F.; Lander, G. H.; Aeppli, G.; Fisk, Z.; Stewart, G. R.; Hayden, S.M.; Mook, H. A., Magnetic response in UBe_{13} . *Physica B* (2000) v. 276-278 p. 764-765.

Daniel, C.; Hamley, I. W.; Mortensen, K., Effect of planar extension on the structure and mechanical properties of polystyrene-poly(ethylene-co-butylene)-polystyrene triblock copolymers. *Polymer* (2000) v. 41 p. 9239-9247.

Edgar, R.; Huang, J. Y.; Popovitz-Biro, R.; Kjær, K.; Bouwman, W. G.; Howes, P. B.; Als-Nielsen, J.; Shen, Y. R.; Lahav, M.; Leiserowitz, L., Absolute orientation of molecules of amphiphilic alcohols in crystalline monolayers at the air-water interface. *J. Phys. Chem. B* (2000) v. 104 p. 6843-6850.

Enderle, M.; Kiefer, K.; Klopperpieper, A.; Albers, J.; McIntyre, G. J.; Lefmann, K.; Schmidt, W.; Kamp, R. van de, Quantum features in the spin dynamics of $S=1/2$ and 1 Heisenberg antiferromagnets in spite of long-range ordered phases. *Physica B* (2000) v. 276-278 p. 782-783.

Enderle, M.; Regnault, L. P.; Broholm, C.; Reich, D.; Zaliznyak, I.; Sieling, M.; Rønnow, H. M.; McMorro, D.F., High-field spin dynamics of antiferromagnetic quantum spin chains. *Physica B* (2000) v. 276-278 p. 560-561.

Engkvist, O.; Åstrand, P.-O.; Karlström, G., Accurate intermolecular potentials obtained from molecular wave functions: Bridging the gap between quantum chemistry and molecular simulations. *Chem. Rev.* (2000) v. 100 p. 4087-4108.

Escalante, J. I.; Gradzielski, M.; Hoffmann, H.; Mortensen, K., Shear-induced transition of originally undisturbed lamellar phase to vesicle phase. *Langmuir* (2000) v. 16 p. 8653-8663.

Eskildsen, M. R.; Fisher, I. R.; Gammel, P. L.; Bishop, D. J.; Andersen, N. H.; Mortensen, K.; Canfield, P.C., Non-locality and the flux line lattice square to hexagonal symmetry transition in the borocarbide superconductors. *Physica C* (2000) v. 332 p. 320-326.

Fairclough, J. P. A.; Yu, G.E.; Mai, S. M.; Crothers, M.; Mortensen, K.; Ryan, A. J.; Booth, C., First observation of an ordered microphase in melts of poly(oxyethylene)-poly(oxypropylene) block copolymers. *Phys. Chem. Chem. Phys.* (2000) v. 2 p. 1503-1507.

Faldt, A.; Krebs, F. C.; Jørgensen, M., Lithium-ion induced conformational change of 5,17-bis(9-fluorenyl)-25,26,27,28-tetrapropoxy calix[4]arene resulting in an egg-shaped dimeric clathrate. *Tetrahedron Lett.* (2000) v. 41 p. 1241-1244.

Fleck, B.; Wenke, L.; Ramanujam, P. S.; Hvilsted, S., Theoretical and experimental investigations on an incoherent optical correlator. *Opt. Commun.* (2000) v. 174 p. 311-315.

Flyvbjerg, H., Book review: Biomathematics. Mathematics of biostructures and biodynamics, edited by S. Andersson, K. Larsson, M. Larsson and M. Jacob, Elsevier, Amsterdam 1999. ISBN 0-444-50273-4. *Chem. Phys. Lipids* (2000) v. 106 p. 191-192.

Frello, T.; Andersen, N. H.; Madsen, J.; Abrahamsen, A. B.; Zimmermann, M. V. von; Niemöller, T.; Schneider, J. R.; Wolf, T., Oxygen-ordering superstructures in NdBa₂Cu₃O_{6.5} single crystals investigated by hard-X-ray diffraction. *Phys. Rev. B* (2000) v. 61 p. R9253-R9256.

Frielinghaus, H.; Mortensen, K.; Almdal, K., Composition fluctuations in homopolymer blends and diblock copolymers. *Physica B* (2000) v. 276-278 p. 375-376.

Frielinghaus, H.; Mortensen, K.; Almdal, K., Differences of interaction parameter of a PS/PEO homopolymer blend and diblock copolymer in comparison to other systems. *Macromol. Symp.* (2000) v. 149 p. 63-67.

Gammel, P. L.; Lopez, D.; Bishop, D. J.; Eskildsen, M. R.; Andersen, N. H.; Mortensen, K.; Fisher, I.R.; Cheon, K.O.; Canfield, P.C., Interwoven magnetic and flux line structures in single crystal (Tm,Er) Ni₂B₂C (invited article). *J. Appl. Phys.* (2000) v. 87 p. 5544-5548.

Garamus, V. M.; Pedersen, J. S.; Kawasaki, H.; Maeda, H., Scattering from polymerlike micelles of TDAO in salt/water solutions at semidilute concentrations. *Langmuir* (2000) v. 16 p. 6431-6437.

Glidle, A.; Swann, M. J.; Gadegaard, N.; Cooper, J. M., Determination of solvation and binding site profile within electropolymerised poly(pyrrole-N-propionic acid). *Physica B* (2000) v. 276-278 p. 359-360.

Goff, J. P.; Hayes, W.; Hull, S.; Hutchings, M. T.; Clausen, K. N., Defect structure of yttria-stabilized zirconia and its influence on the ionic conductivity at elevated temperatures. *Phys. Rev. B* (1999) v. 59 p. 14202-14219.

Goff, J. P.; Sarthour, R. S.; McMorrow, D. F.; Yakhou, F.; Vigliante, A.; Gibbs, D.; Ward, R.C.C.; Wells, M.R., Diffuse magnetic scattering from DHCP Ho_xCe_{1-x} alloys. *Physica B* (2000) v. 276-278 p. 696-697.

Goff, J. P.; Sarthour, R. S.; McMorrow, D. F.; Yakhou, F.; Stunault, A.; Ward, R. C. C.; Wells, M. R., Magnetism in lanthanide superlattices. *Physica B* (2000) v. 283 p. 180-183

Hansen, M. F.; Bødker, F.; Mørup, S.; Lefmann, K.; Clausen, K. N.; Lindgård, P.A., Magnetic dynamics of fine particles studied by inelastic neutron scattering. *J. Magn. Magn. Mater.* (2000) v. 221 p. 10-25.

Hemon, S.; Cowley, R. A.; Ward, R.C.C.; Wells, M. R.; Douysset, L.; Rønnow, H. M., Magnetic structure of Gd, GdH₂ and NdH₂ single crystal films. *J. Phys. Condens. Matter* (2000) v. 12 p. 5011-5020.

Hill, J. P.; McMorrow, D. F.; Boothroyd, A.T.; Stunault, A.; Vettier, C.; Berman, L. E.; Zimmermann, M. von; Wolf, T., X-ray-scattering study of copper magnetism in nonsuperconducting PrBa₂Cu₃O_{6.92}. *Phys. Rev. B* (2000) v. 61 p. 1251-1255.

Holopainen, J. M.; Lemmich, J.; Richter, F.; Mouritsen, O. G.; Rapp, G.; Kinnunen, P. K. J., Dimyristoylphosphatidylcholine/C16: 0-ceramide binary liposomes studied by differential scanning calorimetry and wide- and small-angle X-ray scattering. *Biophys. J.* (2000) v. 78 p. 2459-2469.

Jensen, L.; Schmidt, O. H.; Mikkelsen, K. V.; Åstrand, P.-O., Static and frequency-dependent polarizability tensors for carbon nanotubes. *J. Phys. Chem. B* (2000) v. 104 p. 10462-10466.

Jensen, L.; Åstrand, P.-O.; Sylvester-Hvid, K. O.; Mikkelsen, K. V., Frequency-dependent molecular polarizability calculated within an interaction model. *J. Phys. Chem. A* (2000) v. 104 p. 1563-1569.

Jensen, T. R.; Hazell, R. G.; Vosegaard, T.; Jakobsen, H.J., New rubidium zinc hydrogen phosphate, $\text{Rb}_2\text{Zn}_2(\text{HPO}_4)_3$: Synthesis, crystal structure and ^{31}P single-crystal NMR. *Inorg. Chem.* (2000) v. 39 p. 2026-2032.

Jensen, T. R.; Hazell, R. G., New layered caesium zinc hydrogen phosphate, $\text{CsZn}_{2.5}(\text{HPO}_4)_3 \cdot 2\text{H}_2\text{O}$; synthesis, crystal structure and thermal transformation. *J. Chem. Soc. Dalton Trans.* (2000) v. 16 p. 2831-2835.

Jørgensen, M.; Krebs, F. C., Calix[4]arene-5, 17-dicarboxylic acids and their interactions with aliphatic amines. Part 1. Studies in solution. *J. Chem. Soc. Perkin Trans. 2* (2000) (no.9) p. 1929-1934.

Jørgensen, M.; Krebs, F. C.; Bechgaard, K., Easy access to 3,8-diaryldifurano[2,3- α :2',3'- f]naphthalenes. A new extended aromatic system. *J. Org. Chem.* (2000) v. 65 p. 8783-8785.

Kaminorz, Y.; Smela, E.; Johansson, T.; Brehmer, L.; Andersson, M. R.; Inganas, O., Characteristics of polythiophene surface light emitting diodes. *Synth. Met.* (2000) v. 113 p. 103-114.

Kapnistos, M.; Vlassopoulos, D.; Fytas, G.; Mortensen, K.; Fleischer, G.; Roovers, J., Reversible thermal gelation in soft spheres. *Phys. Rev. Lett.* (2000) v. 85 p. 4072-4075.

Kawano, S.; Lebech, B.; Shigeoka, T.; Iwata, N., Neutron diffraction studies of the magnetic structures of TbRu_2Si_2 . *Physica B* (2000) v. 276-278 p. 572-573.

Keszthelyi, T.; Balakrishnan, G.; Wilbrandt, R.; Yee, W. A.; Negri, F., Evidence of dynamical Jahn-Teller effect on triphenylene radical cation: Resonance Raman spectrum and ab initio quantum-chemical calculations. *J. Phys. Chem. A* (2000) v. 104 p. 9121-9129.

Keszthelyi, T.; Grage, M. M.-L.; Offersgaard, J. F.; Wilbrandt, R.; Svendsen, C.; Mortensen, O. S.; Pedersen, J. K.; Jansen, H. J. A., 2,2'-bithiophene radical cation: An experimental and computational study. *J. Phys. Chem. A* (2000) v. 104 p. 2808-2823.

Knuuttila, T. A.; Tuoriniemi, J. T.; Lefmann, K., Relaxation of polarized nuclei in superconducting rhodium. *Phys. Rev. Lett.* (2000) v. 85 p. 2573-2576.

Koblischka, M. R.; Johansen, T. H.; Baziljevich, M.; Murakami, M.; Wolf, T., SQUID and magneto-optic investigations of flux turbulence. *Physica C* (2000) v. 341-348 p. 1275-1276.

Koblischka, M. R.; Johansen, T. H.; Larsen, B. H.; Andersen, N. H.; Wu, H.; Skov-Hansen, P.; Bentzon, M.; Vase, P., Magneto-optical investigations of multifilamentary Bi-2223 tapes. *Physica C* (2000) v. 341-348 p. 2583-2584.

Koblischka, M. R.; Murakami, M., Second step in the field-cooled magnetization of Bi-2212 single crystals. *Phys. Stat. Sol. B* (2000) v. 218 p. R3-R5.

Krebs, F. C., How the R factor changes as molecules become larger. *J. Appl. Cryst.* (2000) v. 33 p. 392-393.

Krebs, F. C.; Jørgensen, M.; Lebech, B.; Almdal, K.; Pedersen, W. B., Synthesis of small molar mass perdeuterated polyethyl-propylene (d-PEP) as an auxiliary for neutron studies. *Polym. Bull.* (2000) v. 43 p. 485-490.

Krebs, F. C.; Jørgensen, M., On the conformational properties of [n]cyclophanes. A new application of the ramachandran plot using crystallographic data. *J. Org. Chem.* (2000) v. 65 p. 3846-3849.

Krebs, F. C.; Jørgensen, M., Calix[4]arene-5, 17-dicarboxylic acids and their interactions with aliphatic amines. Part 2. A crystal engineering approach. *J. Chem. Soc. Perkin Trans. 2* (2000) (no.9) p. 1935-1941.

Kumpf, C.; Bunk, O.; Zeysing, J. H.; Nielsen, M. M.; Nielsen, M.; Johnson, R. L.; Feidenhans'l, R., Structural study of the commensurate-incommensurate low-temperature phase transition of Pb on Si(111). *Surf. Sci.* (2000) v. 448 p. L213-L219.

Kumpf, C.; Bunk, O.; Zeysing, J.H.; Su, Y.; Nielsen, M.; Johnson, R. L.; Feidenhans'l, R.; Bechgaard, K., Low-temperature structure of indium quantum chains on silicon. *Phys. Rev. Lett.* (2000) v. 85 p. 4916-4919.

Käll, M.; Zimmermann, M. von; Andersen, N. H.; Madsen, J.; Frello, T.; Poulsen, H. F.; Schneider, J.R.; Wolf, T., Anisotropic dynamical scaling in a weakly 3D system: The case of oxygen ordering in YBa₂Cu₃O_{6.5}. *Europhys. Lett.* (2000) v. 51 p. 447-453.

Lauridsen, E. M.; Baker, J.; Nielsen, M.; Feidenhans'l, R.; Falkenberg, G.; Bunk, O.; Zeysing, J. H.; Johnson, R. L., Structure determination of the Si(001)-(2 x 1)-H reconstruction by surface X-ray diffraction: Weakening of the dimer bond by the addition of hydrogen. *Surf. Sci.* (2000) v. 453 p. 18-24.

Laursen, B. W.; Krebs, F. C., Synthesis of a triazatriangulenium salt. *Angew. Chem. Int. Ed.* (2000) v. 39 p. 3432-3434.

Le, T. D.; Olsson, U.; Mortensen, K., Topological transformation of a surfactant bilayer. *Physica B* (2000) v. 276-278 p. 379-380

Leaver, M.; Rajagopalan, V.; Ulf, O.; Mortensen, K., Non-spherical micelles in an oil-in-water cubic phase. *Phys. Chem. Chem. Phys.* (2000) v. 2 p. 2951-2958.

Lederer, K.; Godt, A.; Howes, P. B.; Kjær, K.; Als-Nielsen, J.; Lahav, M.; Wegner, G.; Leiserowitz, L.; Weissbuch, I., Crystalline self-assembly into monolayers of folded oligomers at the air-water interface. *Chemistry. Eur. J.* (2000) v. 6 p. 2173-2183.

Lefmann, K.; Ipsen, J.; Rasmussen, F. B., Thermodynamics of Rh nuclear spins calculated by exact diagonalization. *Physica B* (2000) v. 284-288 p. 1702-1703.

Lefmann, K.; McMorrow, D. F.; Rønnow, H. M.; Nielsen, K.; Clausen, K. N.; Lake, B.; Aeppli, G., Added flexibility in triple axis spectrometers: The two RITAs at Risø. *Physica B* (2000) v. 283 p. 343-354.

Lefmann, K.; Nielsen, K.; Tennant, A.; Lake, B., McStas 1.1: A tool for building neutron Monte Carlo simulations. *Physica B* (2000) v. 276-278 p. 152-153.

Lister, S. J. S.; Boothroyd, A. T.; Andersen, N. H.; Zhokhov, A. A.; Christensen, A. N., Magnetic excitations of single-crystal PrBa₂Cu₃O_{6.2}. *Physica B* (2000) v. 276-278 p. 799-800.

Madsen, G. K. H.; Krebs, F. C.; Lebech, B.; Larsen, F. K., Evaluation of the solid state dipole moment and pyroelectric coefficient of phosphangulene by multipolar modeling of X-ray structure factors. *Chemistry. Eur. J.* (2000) v. 6 p. 1797-1804.

Maeda, H.; Kanakubo, Y.; Miyahara, M.; Kakehashi, R.; Garamus, V.; Pedersen, J. S., Effects of protonation on tetradecyldimethylamine oxide micelles. *J. Phys. Chem. B* (2000) v. 104 p. 6174-6180.

Mays, H.; Mortensen, K.; Brown, W., Microemulsions studied by scattering techniques. In: *Scattering in polymeric and colloidal systems*. Brown, W.; Mortensen, K. (eds.), (Gordon and Breach Science Publishers, Amsterdam, 2000) p. 249-326.

- Mézière, C.; Fourmigué, M.; Canadell, E.; Clérac, R.; Bechgaard, K.; Auban-Senzier, P., Mixed-valence, layered, cation radical salts of the ethane-bridged dimeric tetrathiafulvalene [(EDT-TTF-CH₂)₂•⁺] [X⁻][THF] 0.5, X⁻=FeCl₄⁻, GaCl₄⁻. *Chem. Mater.* (2000) v. 12 p. 2250-2256.
- Michels, A.; Weissmüller, J.; Wiedenmann, A.; Pedersen, J. S.; Barker, J.G., Measuring the exchange-stiffness constant of nanocrystalline solids by elastic small-angle neutron scattering. *Phil. Mag. Lett.* (2000) v. 80 p. 785-792.
- Misaki, Y.; Tani, Y.; Taniguchi, M.; Maitani, T.; Tanaka, K.; Bechgaard, K., Preparation and properties of gold complexes with TTF dithiolato ligands. *Mol. Cryst. Liq. Cryst.* (2000) v. 343 p. 377-382.
- Mortensen, K., Block copolymers studied with small angle neutron scattering. In: *Scattering in polymeric and colloidal systems.* Brown, W.; Mortensen, K. (eds.), (Gordon and Breach Science Publishers, Amsterdam, 2000) p. 413-456.
- Mortensen, K., Small-angle scattering studies of block copolymer micelles, micellar mesophases and networks. In: *Amphiphilic block copolymers. Self-assembly and applications.* Alexandridis, P.; Lindman, B. (eds.), (Elsevier, Amsterdam, 2000) p. 191-220.
- Mortensen, K.; Schwahn, D.; Frielinghaus, H.; Almdal, K., Ternary mixture of homopolymer blend and diblock copolymer studies near the Lifshitz composition by small-angle neutron scattering. 11. International conference on small-angle scattering (SAS99), New York, NY (US), 17-20 May 1999. *J. Appl. Cryst.* (2000) v. 33 p. 686-689.
- Mortensen, N. A.; Rønnow, H. M.; Bruus, H.; Hedegård, P., Magnetic neutron scattering resonance of high-*T_c* superconductors in external magnetic fields: An SO(5) study. *Phys. Rev. B* (2000) v. 62 p. 8703-8706.
- Moser, J.; Cooper, J. R.; Jerome, D.; Alavi, B.; Brown, S. E.; Bechgaard, K., Hall effect in the normal phase of the organic superconductor (TMTSF) 2PF₆. *Phys. Rev. Lett.* (2000) v. 84 p. 2674-2677.
- Müller-Gerking, J.; Pfurtscheller, G.; Flyvbjerg, H., Classification of movement-related EEG in a memorized delay task experiment. *Clin. Neurophysiol.* (2000) v. 111 p. 1353-1365.
- Nielsen, K.; Lefmann, K., Monte Carlo simulations of neutron-scattering instruments using McStas. *Physica B* (2000) v. 283 p. 426-432.
- Nørgaard, K.; Eskildsen, M. R.; Andersen, N. H.; Jensen, J.; Hedegaard, P.; Klausen, S. N.; Canfield, P.C., Interdependence of magnetism and superconductivity in the borocarbide TmNi₂B₂C. *Phys. Rev. Lett.* (2000) v. 84 p. 4982-4985.
- Ohnuma, M.; Hono, K.; Onodera, H.; Ohnuma, S.; Fujimori, H.; Pedersen, J. S., Microstructures and magnetic properties of Co-Al-O granular thin films. *J. Appl. Phys.* (2000) v. 87 p. 817-823.
- Osada, M.; Kakihana, M.; Bäckström, J.; Käll, M.; Börjesson, L.; Frello, T.; Andersen, N. H.; Liang, R.; Dosanjh, P.; Hardy, W.N., Photoinduced metastability in YBa₂Cu₃O_x studied by in situ Raman scattering. *Physica B* (2000) v. 284-288 p. 681-682.
- Paixao, J. A.; Silva, M. R.; Sørensen, S. Å.; Lebech, B.; Lander, G. H.; Brown, P. J.; Langridge, S.; Talik, E.; Goncalves, A.P., Neutron-scattering study of the magnetic structure of DyFe₄Al₈ and HoFe₄Al₈. *Phys. Rev. B* (2000) v. 61 p. 6176-6188
- Paizao, J. A.; Brown, P. J.; Lebech, B.; Lander, G. H., Sublattice interactions in the MFe₄Al₈ compounds. In: Büttner, H. (ed.), *ILL annual report 99.* (2000) 4 p.

- Papadakis, C. M.; Almdal, K.; Mortensen, K.; Rittig, F.; Fleischer, G.; Stepanek, P., The bulk dynamics of a compositionally asymmetric diblock copolymer studied using dynamic light scattering. *Eur. Phys. J. E* (2000) v. 1 p. 275-283.
- Papadakis, C. M.; Mortensen, K.; Posselt, D., Macrophase-separation in binary blends of symmetric polystyrene-polybutadiene diblock copolymers. *Macromol. Symp.* (2000) v. 149 p. 99-105.
- Pedersen, J. S., Form factors of block copolymer micelles with spherical, ellipsoidal and cylindrical cores. 11. International conference on small-angle scattering (SAS99), New York, NY (US), 17-20 May 1999. *J. Appl. Cryst.* (2000) v. 33 p. 637-640.
- Pedersen, J. S.; Hamley, I.W.; Ryu, C. Y.; Lodge, T. P., Contrast variation small-angle neutron scattering study of the structure of block copolymer micelles in a slightly selective solvent at semidilute concentrations. *Macromolecules* (2000) v. 33 p. 542-550.
- Pelrine, R.; Kornbluh, R.; Kofod, G., High-strain actuator materials based on dielectric elastomers. *Adv. Mater.* (2000) v. 12 p. 1223-1225.
- Rapaport, H.; Kjær, K.; Jensen, T. R.; Leiserowitz, L.; Tirrell, D.A., Two-dimensional order in β -sheet peptide monolayers. *J. Am. Chem. Soc.* (2000) v. 122 p. 12523-12529.
- Rapaport, H.; Kuzmenko, I.; Berfeld, M.; Kjær, K.; Als-Nielsen, J.; Popovitz-Biro, R.; Weissbuch, I.; Lahav, M.; Leiserowitz, L., From nucleation to engineering of crystalline architectures at air-liquid interfaces. *J. Phys. Chem. B* (2000) v. 104 p. 1399-1428.
- Rapaport, H.; Kuzmenko, I.; Kjær, K.; Als-Nielsen, J.; Weissbuch, I.; Lahav, M.; Leiserowitz, L., Crystalline architectures at the air-liquid interface: From nucleation to engineering. *Synchrotron Radiat. News* (1999) v. 12 p. 25-33.
- Rasmussen, F. B.; Molenbroek, A. M.; Clausen, B. S.; Feidenhans'l, R., Particle size distribution of an Ni/SiO₂ catalyst determined by ASAXS. *J. Catal.* (2000) v. 190 p. 205-208.
- Reitzel, N.; Greve, D. R.; Kjær, K.; Howes, P. B.; Jayaraman, M.; Savoy, S.; McCullough, R. D.; McDevitt, J. T.; Bjørnholm, T., Self-assembly of conjugated polymers at the air/water interface. Structure and properties of Langmuir and Langmuir-Blodgett films of amphiphilic regioregular polythiophenes. *J. Am. Chem. Soc.* (2000) v. 122 p. 5788-5800.
- Reynisson, J.; Balakrishnan, G.; Wilbrandt, R.; Harrit, N., Vibrational spectroscopic and quantum chemical studies of the trioxatriangulenium carbocation. *J. Mol. Struct.* (2000) v. 520 p. 63-73.
- Ruud, K.; Åstrand, P.-O.; Taylor, P. R., An efficient approach for calculating vibrational wave functions and zero-point vibrational corrections to molecular properties of polyatomic molecules. *J. Chem. Phys.* (2000) v. 112 p. 2668-2683.
- Rønnow, H. M.; Enderle, M.; McMorrow, D. F.; Regnault, L.P.; Dhahlenne, G.; Revcolevschi, A.; Hoser, A.; Vorderwisch, P.; Schneider, H., Neutron scattering study of the incommensurate high-field phase of CuGeO₃. *Physica B* (2000) v. 276-278 p. 678-679.
- Rønnow, H. M.; Enderle, M.; McMorrow, D. F.; Regnault, L. P.; Dhahlenne, G.; Revcolevschi, A.; Hoser, A.; Prokes, K.; Vorderwisch, P.; Schneider, H., Neutron scattering study of the field-induced soliton lattice in CuGeO₃. *Phys. Rev. Lett.* (2000) v. 84 p. 4469-4472.
- Rønnow, H. M.; Wildes, A. R.; Bramwell, S.T., Magnetic correlations in the 2D S=5/2 honeycomb antiferromagnet MnPS₃. *Physica B* (2000) v. 276-278 p. 676-677.

Schindler, W.; Koop, T.; Kazimirov, A.; Scherb, G.; Zegenhagen, J.; Schultz, T.; Feidenhans'l, R.; Kirschner, J., Non-coherent growth patches in pseudomorphic films: Unusual strain relief in electrodeposited Co on Cu(001). *Surf. Sci.* (2000) v. 465 p. L783-L788.

Schneider, D. K.; Chen, S. H.; Capel, M. S.; Hsiao, B.; Kostorz, G.; Pedersen, J. S.; Timmins, P.; Wignall, G.D., 11. International conference on small-angle scattering. *J. Appl. Cryst.* (2000) v. 33 p. U1-U4.

Schwahn, D.; Mortensen, K.; Frielinghaus, H.; Almdal, K.; Kielhorn, L., Thermal composition fluctuations near the isotropic Lifshitz critical point in a ternary mixture of a homopolymer blend and diblock copolymer. *J. Chem. Phys.* (2000) v. 112 p. 5454-5472.

Schwahn, D.; Mortensen, K.; Frielinghaus, H.; Almdal, K., 3D-ising and Lifshitz kritical behavior in a mixture of a polymer blend and a corresponding diblock copolymer. *Physica B* (2000) v. 276-278 p. 353-354.

Schwahn, D.; Mortensen, K.; Brown, W., Thermal composition fluctuations in polymer blends studied with small angle neutron scattering. In: *Scattering in polymeric and colloidal systems*. Brown, W.; Mortensen, K. (eds.), (Gordon and Breach Science Publishers, Amsterdam, 2000) p. 371-412.

Schweitz, K. O.; Böttiger, J.; Chevallier, J.; Feidenhans'l, R.; Nielsen, M. M.; Rasmussen, F. B., Interface stress in Au/Ni multilayers. *J. Appl. Phys.* (2000) v. 88 p. 1401-1406.

Sirringhaus, H.; Brown, P. J.; Friend, R. H.; Nielsen, M. M.; Bechgaard, K.; Langeveld-Voss, B. M. W.; Spiering, A. J. H.; Janssen, R. A. J.; Meijer, E. W., Microstructure-mobility correlation in self-organised, conjugated polymer field-effect transistors. *Synth. Met.* (2000) v. 111-112 p. 129-132.

Stepanek, P.; Morkved, T. L.; Bates, F. S.; Lodge, T. P.; Almdal, K., Dynamic light scattering from ternary polymer blends: Critical behavior and bicontinuous microemulsions. *Macromol. Symp.* (2000) v. 149 p. 107-112.

Svaneborg, C.; Pedersen, J. S., A Monte Carlo study on the effect of excluded volume interactions on the scattering from block copolymer micelles. *J. Chem. Phys.* (2000) v. 112 p. 9661-9670.

Swann, M. J.; Glidle, A.; Gadegaard, N.; Cui, L.; Barker, J. R.; Cooper, J.M., Distribution of adsorbed molecules in electronic nose sensors. *Physica B* (2000) v. 276-278 p. 357-358.

Syljuasen, O. F.; Rønnow, H. M., Quantum renormalization of high-energy excitations in the 2D Heisenberg model. *J. Phys. Condens. Matter* (2000) v. 12 p. L405-L408.

Toftmann, B.; Schou, J.; Larsen, N. B., Ablation from artificial or laser-induced crater surfaces of silver by laser irradiation at 355 nm. *Appl. Phys. A* (1999) v. 69 p. S811-S814.

Travas-Sejdic, J.; Eastal, A.; Knott, R.; Pedersen, J. S., Small-angle neutron scattering from poly(NIPA-co-AMPS) gels. 11. International conference on small-angle scattering (SAS99), New York, NY (US), 17-20 May 1999. *J. Appl. Cryst.* (2000) v. 33 p. 735-739.

Truelsen, J. H.; Kops, J.; Batsberg Pedersen, W., Synthesis by ATRP of triblock copolymers with densely grafted styrenic end blocks from a polyisobutylene macroinitiator. *Macromol. Rapid Commun.* (2000) v. 21 p. 98-102.

Tuoriniemi, J. T.; Knuutila, T. A.; Lefmann, K.; Nummila, K. K.; Yao, W.; Rasmussen, F. B., Double-spin-flip resonance of rhodium nuclei at positive and negative spin temperatures. *Phys. Rev. Lett.* (2000) v. 84 p. 370-373.

Vaqueiro, P.; Powell, A. V.; Lebeck, B., Order-disorder transitions in NiCr₂S₄. *Physica B* (2000) v. 276-278 p. 238-239.

Visser, D.; Monteith, A. R.; Rønnow, H. M.; Maaskant, W. J. A., Acoustic phonons in the hexagonal perovskite CsNiCl₃ around the Gamma-point. *Physica B* (2000) v. 276-278 p. 302-304.

Weichel, S.; Grey, F.; Rasmussen, K.; Nielsen, M.; Feidenhans'l, R.; Howes, P. B.; Vedde, J., Fusion bonding of Si wafers investigated by X-ray diffraction. *Appl. Phys. Lett.* (2000) v. 76 p. 70-72.

Weissbuch, J.; Baxter, P.N.W.; Kuzmenko, I.; Cohen, H.; Cohen, S.; Kjær, K.; Howes, P. B.; Als-Nielsen, J.; Lehn, J. M.; Leiserowitz, L.; Lahav, M., Oriented crystalline monolayers and bilayers of 2 x 2 silver(1) grid architectures at the air-solution interface: Their assembly and crystal structure elucidation. *Chemistry. Eur. J.* (2000) v. 6 p. 725-734.

Weygand, M.; Schalke, M.; Howes, P. B.; Kjær, K.; Friedmann, J.; Wetzer, B.; Pum, D.; Sleytr, U.B.; Lösche, M., Coupling of protein sheet crystals (S-layers) to phospholipid monolayers. *J. Mater. Chem.* (2000) v. 10 p. 141-148.

Wurlitzer, A.; Politsch, E.; Cevc, G.; Gutberlet, T.; Kjær, K.; Lösche, M., Neutron and X-ray reflection from surface monolayers of a lipopolyoxazoline. *Physica B* (2000) v. 276-278 p. 343-344.

Åstrand, P.-O.; Ramanujam, P. S.; Hvilsted, S.; Bak, K.L.; Sauer, S. P. A., Ab initio calculation of the electronic spectrum of azobenzene dyes and its impact on the design of optical data storage materials. *J. Am. Chem. Soc.* (2000) v. 122 p. 3482-3487.

Åstrand, P.-O.; Ruud, K.; Taylor, P. R., Calculation of the vibrational wave function of polyatomic molecules. *J. Chem. Phys.* (2000) v. 112 p. 2655-2667.

Åstrand, P.-O.; Ruud, K.; Sundholm, D., A modified variation-perturbation approach to zero-point vibrational motion. *Theor. Chem. Acc.* (2000) v. 103 p. 365-373.

Åstrand, P.-O.; Sommer-Larsen, P.; Hvilsted, S.; Ramanujam, P. S.; Bak, K. L.; Sauer, S. P. A., Five-membered rings as diazo components in optical data storage devices: An ab initio investigation of the lowest singlet excitation energies. *Chem. Phys. Lett.* (2000) v. 325 p. 115-119.

3.2. Publications for a broader readership, theses and reports

Bechgaard, K., Plastik som leder. Nobelprisen i kemi 2000. *Aktuel Naturvidenskab* (2000) (no.5) p. 14-16.

Eskildsen, M. R.; Andersen, N. H., Eksotiske hvirvler - Fluxliniegitteret i magnetiske superledere. *Kvant* (2000) (no.4) p. 3-11

Faldt, A., Synthesis and structure of functional organic molecules: Calix[4]arenes, trioxatriangulenes and helicenes. *Risø-R-1148(EN)* (2000) 200 p. (ph.d. thesis).

Flyvbjerg, H., The Danish Research Academy's Graduate School of Biophysics: 1999 activity report. (2000) 63 p.

Gadegaard, N., Structural study of symmetric diblock copolymer thin films. *Risø-R-1087(EN)* (2000) 84 p.

Lebeck, B. (ed.), Annual progress report of the Condensed Matter Physics and Chemistry Department 1 January - 31 December 1999. *Risø-R-1156(EN)* (2000) 168 p.

Lindgård, P.-A., Influencing physics in Europe. Divisions, sections, and inter-divisional groups in EPS. *Europhys. News* (2000) v. 31 (no.Sep-Oct) p. 35.

Nielsen, K.; Lefmann, K., User and programmers guide to the neutron ray-tracing package McStas, version 1.2. *Risø-R-1175(EN)* (2000) 175 p.

Reynisson, J., Spectroscopic and photophysical properties of the trioxatriangulenium carbocation and its interactions with supramolecular systems. *Risø-R-1191(EN)* (2000) 135 p. (ph.d. thesis).

West, K.; Bechgaard, K., Nobelprisen i kemi 2000: Ledende polymerer. *Dansk Kemi* (2000) v. 81 (no.12) p. 8-13.

3.3. Conference lectures, published and lectures, inclusive published abstracts

3.3.1. Conference lectures, published

Eskildsen, M. R.; Gammel, P. L.; Bishop, D. J.; Andersen, N. H.; Mortensen, K.; Fisher, I. R.; Canfield, P. C., Flux line lattice symmetries in the borocarbide superconductors. In: *Magnetic and superconducting materials. Vol. 1. First regional conference, Tehran (IR), 27-30 Sep 1999.* Akhavan, M.; Jensen, J.; Kitazawa, K. (eds.), (World Scientific Publishing Co., Singapore, 2000) vp.

Eskildsen, M. R.; Gammel, P. L.; Bishop, D. J.; Andersen, N. H.; Mortensen, K.; Canfield, P.C., Flux line lattice symmetries and magnetism in $TmNi_2B_2C$. In: *Proceedings. HERCULES X Euroconference, Grenoble (FR), 6-9 Apr 2000.* (CNRS, Grenoble, 2000) vp.

Hvilsted, S.; Ramanujam, P. S., Polymer scaffolds bearing azobenzene - A potential for optical information storage. In: *Conference proceedings. International conference on new trends in functional polymers, Huangshan (CN), 8-13 May 2000.* (University of Science and Technology of China, Huangshan, 2000) p. 26-31.

Jensen, T. R.; Kjær, K.; Howes, P. B.; Svendsen, A.; Balashev, K.; Reitzel, N.; Bjørnholm, T., Model systems for biological membranes investigated by grazing-incidence X-ray diffraction and specular reflectivity. In: *Lipases and lipids: Structure, function and biotechnological applications. International conference, Santorini (GR), 6-8 May 1999.* Kokotos, G.; Constantinou-Kokotou, V. (eds.), (Crete University Press, Rethymnon, 2000) p. 127-139.

Kuzmenko, I.; Rapaport, H.; Kjær, K.; Als-Nielsen, J.; Weissbuch, I.; Lahav, M.; Leiserowitz, L., Crystalline architectures at the air-liquid interface: From nucleation to engineering. In: *Soft condensed matter: Configurations, dynamics and functionality. Proceedings. NATO Advanced Study Institute, Geilo (NO), 6-16 Apr 1999.* Skjeltorp, A.T.; Edwards, S.F. (eds.), (Kluwer Academic Publishers, Dordrecht, 2000) (NATO Science Series C: Mathematical and Physical Sciences, v. 552) p. 185-217.

Lee, K. Y.; Majewski, J.; Kuhl, T.; Howes, P. B.; Kjær, K.; Lipp, M. M.; Waring, A. J.; Zasadzinski, J. A.; Smith, G. S., The incorporation of lung surfactant specific protein SP-B into lipid monolayers at the air-fluid interface: A grazing incidence x-ray diffraction study. In: *Applications of synchrotron radiation techniques to materials science 5. MRS 1999 Fall meeting. Symposium R, Boston, MA (US), 29 Nov - 3 Dec 1999.* Stock, S. R.; Perry, D. L.; Mini, S. M. (eds.), (Materials Research Society, Warrendale, PA, 2000) (Materials Research Society Symposium Proceedings, v. 590) p. 177-182.

Nielsen, M.; Feidenhans'l, R.; Howes, P. B.; Grey, F.; Rasmussen, K.; Vedde, J., The interface of directly-bonded Si crystals studied by synchrotron X-ray diffraction. In: *Invited and contributed papers. Advanced Studies Institute on exploration of subsurface phenomena by particle scattering, Monterey, CA (US), 19-23 Oct 1998.* Lam, N. Q.; Melendres, C. A.; Sinha, S. K. (eds.), (IASI Press, North East, MD (US), 2000) (Science and technology series) p. 139-147.

West, K.; Vitins, G.; Koksang, R., LiMnO₂ additives for Li-ion battery electrodes. In: Proceedings. Nordic workshop on materials for electro-chemical energy conversion, Geilo (NO), 8-10 Mar 2000. Åberg, R.J.; Poulsen, F.W.; Norby, T. (eds.), (Nordisk Energiforskningsprogram, [s.l.], 2000) p. 97-102.

3.3.2. Lectures, inclusive published abstracts

Almdal, K., Gels: Swollen physical and chemical networks. MODECS Spring meeting 1999: Gels - Science and technology, Værløse (DK), 27 May 1999. Unpublished.

Almdal, K.; Mortensen, K.; Johannsen, I.; Ivan, B.; Kops, J., Synthesis, characterization, and SANS investigations of poly(ethyl acrylate)-*l*-polyisobutylene bicomponent conetwork. American Physical Society March 2000 Meeting, Minneapolis, MN (US), 20-24 Mar 2000. Unpublished. Abstract available.

Alonso, C.; Kuzmenko, I.; Eliash, R.; Kjær, K.; Jensen, T. R.; Lahav, M.; Leiserowitz, L., Spontaneous self-assembly of interdigitated bilayers at the air/water interface. In: Programme and abstracts. Vol. 1: Oral contributions. 9. International conference on organised molecular films, Potsdam (DE), 28 Aug - 1 Sep 2000. (Potsdam Universitæt, Potsdam, 2000) p. 76 (T 10)

Andersen, T. H.; Almdal, K.; Hubert, L.; Johannsen, I.; Larsen, N. B.; Tougaard, S., Surface morphology of PS-PDMS diblock copolymer films. In: Programme. Abstracts. List of participants. Danish Physical Society annual meeting 2000, Nyborg (DK), 8-9 Jun 2000. (HCØ Tryk, København, 2000) FF05

Bechgaard, K., Magnetic particles for drug targeting. Nanoworkshop on nanomagnetism, Lyngby (DK), 8 May 2000. Unpublished..

Buzin, I.; Godovsky, Y. K.; Makarova, N. N.; Knobler, C.M.; Fang, J.; Jensen, T. R.; Kjær, K.; Ruiz-Garcia, J.; Brezesinski, G.; Möhwald, H., Stepwise collapse of monolayers of liquid crystalline cycloliner poly(organosiloxanes) at the air/water interface. In: Programme and abstracts. Vol. 1: Oral contributions. 9. International conference on organised molecular films, Potsdam (DE), 28 Aug - 1 Sep 2000. (Potsdam Universitæt, Potsdam, 2000) p. 87 (T 22).

Egsgaard, H.; Batsberg Pedersen, W.; Mølgaard, M.; Lessèl, R.; Glastrup, J., Mass spectrometry of polyethylene glycols. 15. International mass spectrometry conference, Barcelona (ES), 27 Aug - 1 Sep 2000. Unpublished. Abstract available.

Eskildsen, J.; Krebs, F. C.; Faldt, A.; Sommer-Larsen, P.; Bechgaard, K., Hydrogen and deuterium containing 7,8-Dioxa[6]helicenes and a possible large structural isotope effect. In: Programme and abstracts. 31. Danske krystallografimøde; Dansync's 3. Årsmøde, København (DK), 30-31 May 2000. (Centre for Crystallographic Studies, Copenhagen, 2000) P 21 (1 p.).

Eskildsen, M. R., Flux line lattice symmetries and the role of non-local effects in the borocarbide superconductors (Invited talk). 18. General conference of the Condensed Matter Division of the European Physical Society, Montreux (CH), 13-17 Mar 2000. Unpublished.

Eskildsen, M. R., Vortex lattice and magnetic properties of TmNi₂B₂C (Invited talk). NATO advanced research workshop: Rare earth transition metal borocarbides (nitrides): Superconducting, magnetic and normal state properties, Dresden (DE), 14-17 Jun 2000. Unpublished.

Faldt, A.; Krebs, F. C.; Jørgensen, M., Lithium-ion induced conformational change of 5,17-Bis(9-fluorenyl)-25,26,27,28-tetrapropoxy calix[4]arene resulting in an egg shaped dimeric clathrate. In: Programme and abstracts. 31. Danske krystallografimøde; Dansync's 3. Årsmøde, København (DK), 30-31 May 2000. (Centre for Crystallographic Studies, Copenhagen, 2000) P 9 (1 p.).

- Feidenhans'l, R., Current trends in surface crystallography. 19. European crystallographic meeting, Nancy (FR), 25-31 Aug 2000. Unpublished.
- Feidenhans'l, R., Low-temperature structure of indium quantum chains on silicon. 19. European Crystallographic meeting, satellite meeting on surface crystallography, Nancy (FR), 31 Aug - 2 Sep 2000. Unpublished.
- Flyvbjerg, H., Modeling microtubule dynamics: Doing molecular biology with the tools of theoretical physics. Seminar in Statistical Physics Department and Particle Theory Department, Jagiellonian University, Cracow (PL), 20 Mar 2000. Unpublished.
- Flyvbjerg, H., Pulling at entropic strings: Simple models for DNA and other polymers. Cross-institutional ph.d.-course on molecular biophysics, Niels Bohr Institute, Copenhagen (DK), 4 Apr 2000. Unpublished.
- Flyvbjerg, H., Modeling microtubule oscillations (Invited talk). Workshop: Biophysics and biochemistry of motor proteins, Banff (CA), 27 Aug - 1 Sep 2000. Unpublished.
- Flyvbjerg, H., Entropic elasticity: The worm-like chain model revisited (Invited talk). Year 2000 Marian Smoluchowski symposium on statistical physics: Fundamentals and applications, Zakopane (PL), 10-17 Sep 2000. Unpublished. Flyvbjerg, H., Mikrotubuli. Forelæsning for Fysiklærerforeningen, Niels Bohr Institutet, København (DK), 16 Nov 2000. Unpublished.
- Flyvbjerg, H., Nucleation-polymerization models for actin and tubulin. MSc course on physics of proteins, Copenhagen (DK), 5 Dec 2000. Unpublished.
- Flyvbjerg, H., Modeling microtubule statics and dynamics: Some examples of physics used to describe form and function of an organelle. Mini-symposium: Exploring the potential for using physics in the study of biological structures, processes, and interactions, Risø (DK), 18 Dec 2000. Unpublished.
- Frello, T.; Bechgaard, K.; Norrman, K.; Larsen, N. B.; Feidenhans'l, R.; Jensen, S.; Jepsen, H., Polymer tribology - water lubricated wear of carbon fibre reinforced PEEK (Poly-ether-ether-ketone) sliding against stainless steel. In: Programme. Abstracts. List of participants. Danish Physical Society annual meeting 2000, Nyborg (DK), 8-9 Jun 2000. (HCØ Tryk, København, 2000) FF34P.
- Frello, T.; Bechgaard, K.; Norrman, K.; Feidenhans'l, R.; Larsen, N. B.; West, K.; Jensen, S.; Jepsen, H., Polymer tribology - tribochemical wear of water lubricated carbon fibre reinforced PEEK (Poly-ether-ether-ketone) sliding against stainless steel. Gordon Research conference: Tribology 2000, Holderness School, NH (US), 2-7 Jul 2000. Unpublished.
- Frielinghaus, H.; Hermsdorf, N.; Almdal, K.; Mortensen, K.; Terrill, N.; Olmsted, P. D.; Hamley, I.W., Characterisation of diblock copolymer blends. American Physical Society March 2000 Meeting, Minneapolis, MN (US), 20-24 Mar 2000. Unpublished. Abstract available.
- Gerstenberg, M. C.; Bracco, G.; Scoles, G., A grazing incidence X-ray diffraction study of 1,10-decanedithiol monolayers on Au(111). ICSFS-10, Princeton (US), 9-13 Jul 2000. Unpublished.
- Gerstenberg, M. C.; Kumpf, C.; Feidenhans'l, R.; Hughes, A.; Roser, S.; Nielsen, L. K., Structural study of biological membranes and their associated proteins. Annual meeting of the Danish Physical Society, Nyborg (DK), 8-9 Jun 2000. Unpublished.
- Gerstenberg, M. C.; Kumpf, C.; Feidenhans'l, R.; Nielsen, L. K.; Hughes, A.; Roser, S., A reflectivity study of biomembranes and solid support. ESRF conference on biological physics and synchrotron radiation, Grenoble (FR), 11-14 Oct 2000. Unpublished.

Gerstenberg, M. C.; Pedersen, J. S.; Smith, G., The surface induced ordering of micelles at the solid-liquid interface. Workshop on recent developments in neutron scattering, Les Houches (FR), 5 May 2000. Unpublished.

Holmelund, E.; Thestrup, B.; Schou, J.; Johnson, E.; Nielsen, M. M., Crystallinity of ITO and AZO thin films produced by laser ablation. In: Programme. Abstracts. List of participants. Danish Physical Society annual meeting 2000, Nyborg (DK), 8-9 Jun 2000. (HCØ Tryk, København, 2000) FF65P.

Hvilsted, S., Polymer and molecular azobenzene materials - the future of optical information storage?. Seminar at Microelektronik Centret, Danmarks Tekniske Universitet, Lyngby (DK), 7 Mar 2000. Unpublished. Abstract available.

Hvilsted, S., Survey of structural implications on polymers for holography. Functional polymers, COST Action 518 WG3 meeting, Milano (IT), 19 Feb 2000. Unpublished. Abstract available.

Hvilsted, S., Molecular and polymer scaffolds for azobenzene - An optical information storage potential. Seminario Grupo de Materiales Moleculares, Departamento de Química Orgánica, Facultad de Ciencias, Universidad Autónoma de Madrid, Madrid (ES), 9 Feb 2000. Unpublished.

Hvilsted, S., Polymer materials for optical storage. Meeting at Department of Polymer Science and Engineering, Lund University, Lund (SE), 28 Mar 2000. Unpublished.

Hvilsted, S., The ordered azobenzene-in-a-matrix puzzle - how polarization FTIR can help. IMAM 2000. Workshop to establish infrared microspectroscopy at MAX-lab, Lund University, Lund (SE), 29 Mar 2000. Unpublished.

Hvilsted, S., New materials for optical storage. Curso doctorado: "Materials opticos no-lineales", Departamento de Fisica de la Material Condensada, Universidad de Zaragoza, Zaragoza (ES), 12 Apr 2000. Unpublished.

Hvilsted, S.; Ramanujam, P. S., Polarized light the landscape gardener of azobenzene polymer films. Nordic polymer days, Helsinki (FI), 24-26 May 2000. Unpublished. Abstract available.

Jacobsen, B. A.; Nielsen, M. M.; Abrahamsen, A. B.; Andersen, N. H.; Wang, W. G., Critical current in high- T_c superconducting BiSCCO-tapes in Ag-clad. In: Programme. Abstracts. List of participants. Danish Physical Society annual meeting 2000, Nyborg (DK), 8-9 Jun 2000. (HCØ Tryk, København, 2000) FF39P.

Jensen, J.; Hedegård, P.; Hansen, T.; Nørgaard, K.; Eskildsen, M. R.; Andersen, N. H., The magnetic RKKY-interaction in the superconducting phase of thulium borocarbide. In: Programme. Abstracts. List of participants. Danish Physical Society annual meeting 2000, Nyborg (DK), 8-9 Jun 2000. (HCØ Tryk, København, 2000) FF12.

Jensen, T. R., Investigation of biological systems using synchrotron X-ray scattering. In: Book of abstracts. 3. Topical meeting on biophysics - biological physics, Copenhagen (DK), 5 Apr 2000. (Niels Bohr Institute, Copenhagen, 2000) 2 p.

Jensen, T. R., Lipid/lipase interactions at the air/water water interface. 8. Meeting of the EU funded lipid lipase project BIO4 CT97 2365, Lund (SE), 26-27 Sep 2000. Unpublished.

Jensen, T. R., Investigation of lipid-lipase interactions using synchrotron X-ray radiation. 7. Meeting of the EU funded lipid lipase project BIO4 CT97 2365, Marseille (FR), 25-27 May 2000. Unpublished.

Jensen, T. R., Lipid/lipase interactions investigated by X-ray reflectivity and grazing incidence diffraction. Baltic subgroup meeting of the EU funded lipid lipase project BIO4 CT97 2365, Bagsværd (DK), 7 Sep 1999. Unpublished.

Jensen, T. R., Materialevidenskab med eksempler fra biofysik og faststofkemi: 2-D biomembraner, lipid-lipase vekselvirkning, nye materialer med åben gitterstruktur, hydrotermal syntese... (Invited lecture). Meeting at University of Southern Denmark, Department of Chemistry, Odense (DK), 8 Mar 1999. Unpublished.

Jensen, T. R., Investigation of pure lipids, mono-oleoylglycerol, di- and tri-palmitoylglycerol using synchrotron X-ray reflectivity and diffraction measurements. Baltic subgroup meeting of the EU funded lipid lipase project BIO4 CT97 2365, Lund (SE), 3 Mar 1999. Unpublished.

Jensen, T. R.; Kjær, K.; Howes, P. B.; Balashev, K.; Reitzel, N.; Jensen, M. Ø.; Peters, G.H.; Svendsen, A.; Bjørnholm, T., Biological systems investigated by synchrotron X-ray scattering. In: Programme and abstracts. 31. Danske krystallografmøde; Dansync's 3. Årsmøde, København (DK), 30-31 May 2000. (Centre for Crystallographic Studies, Copenhagen, 2000) F 5 (1 p.).

Jensen, T. R.; Kjær, K.; Howes, P. B.; Balashev, K.; Reitzel, N.; Jensen, M. Ø.; Peters, G. H.; Svendsen, A.; Bjørnholm, T., Investigation of lipid-lipase interaction by synchrotron X-ray scattering. In: Programme and abstracts. Vol. 1: Oral contributions. 9. International conference on organised molecular films, Potsdam (DE), 28 Aug - 1 Sep 2000. (Potsdam Universität, Potsdam, 2000) p. 251 (T 188).

Jensen, T. R.; Kjær, K.; Howes, P. B.; Jensen, M. Ø.; Peters, G. H.; Balashev, K.; Reitzel, N.; Svendsen, A.; Bjørnholm, T., Synchrotron X-ray scattering: A powerful tool for investigation of lipid lipase interactions. In: Programme and abstracts. European meeting on lipid lipase interaction in the "Øresund" region, Lund (SE), 27-30 Sep 2000. (Lund University, Lund, 2000) p. 19.

Kjær, K., Progress report on X-ray studies of lipid-lipase interaction in Langmuir films. 6. Meeting of the EU funded lipid lipase project BIO4 CT97 2365, Helsinki (FI), 3-4 Feb 2000. Unpublished.

Klausen, S. N., Magnetic fluctuations in maghemite nanoparticles. Nanoworkshop on nanomagnetism, Lyngby (DK), 8 May 2000. Unpublished.

Klausen, S. N.; Lefmann, K.; Clausen, K. N.; Lindgård, P.-A.; Bødker, F.; Mørup, S.; Hansen, M. F., Magnetic fluctuations in maghemite nano-particles. In: Programme. Abstracts. List of participants. Danish Physical Society annual meeting 2000, Nyborg (DK), 8-9 Jun 2000. (HCØ Tryk, København, 2000) FF13.

Klausen, S. N.; Lefmann, K.; Lindgård, P.-A.; Clausen, K. N.; Bødker, F.; Hansen, M. F.; Mørup, S., Ferrimagnetic dynamics of maghemite nanoparticles. In: Abstracts and poster session. 10. International symposium on small particles and inorganic clusters, Atlanta, GA (US), 11-15 Oct 2000. (Georgia Institute of Technology, Atlanta, 2000) 4.29.

Klinke, H. B.; Thomsen, A. B.; Lilholt, H.; Toftegaard, H.; Batsberg Pedersen, W.; Schmidt, A. S., Wood and plant fibre reinforced polypropylene composites. Biomass for energy and industry: 1. World conference and technology exhibition, Sevilla (ES), 5-9 Jun 2000. Unpublished.

Krebs, F. C., How the *R*-factor changes as molecules become larger. In: Programme and abstracts. 31. Danske krystallografmøde; Dansync's 3. Årsmøde, København (DK), 30-31 May 2000. (Centre for Crystallographic Studies, Copenhagen, 2000) P 19 (1 p.).

Krebs, F. C.; Jørgensen, M.; Lebech, B.; Almdal, K.; Batsberg Pedersen, W., Synthesis of small molar mass perdeuterated polyethylpropylene (d-PEP) as an auxiliary for neutron studies. In: Programme and abstracts. 31. Danske krystallografmøde; Dansync's 3. Årsmøde, København (DK), 30-31 May 2000. (Centre for Crystallographic Studies, Copenhagen, 2000) F 14 (1 p.).

Krebs, F. C.; Jørgensen, M.; Lebech, B.; Frydenvang, K., A perdeuterated cryoprotectant for neutron scattering studies and a demonstration of its use in a neutron powder diffraction study on

L-(-)ephedrine hemihydrate. In: Programme and abstracts. 31. Danske krystallografmøde; Dansync's 3. Årsmøde, København (DK), 30-31 May 2000. (Centre for Crystallographic Studies, Copenhagen, 2000) P 7 (1 p.).

Krebs, F. C.; Jørgensen, M., On the conformational properties of [*n*]cyclophanes. A new application of the Ramachandran plot using crystallographic data. In: Programme and abstracts. 31. Danske krystallografmøde; Dansync's 3. Årsmøde, København (DK), 30-31 May 2000. (Centre for Crystallographic Studies, Copenhagen, 2000) P 11 (1 p.).

Krebs, F. C.; Larsen, M.; Jørgensen, M., Disappearing atropisomers. 4,5-Bis(1-naphthyl)-orthoxylylene is only found in the *trans*-conformation in the solid state whereas both forms exist in solution. Further 14,15-dimethylbenzo[*s*]picene does not exhibit atropisomerism. In: Programme and abstracts. 31. Danske krystallografmøde; Dansync's 3. Årsmøde, København (DK), 30-31 May 2000. (Centre for Crystallographic Studies, Copenhagen, 2000) P 23 (1 p.).

Kumpf, C.; Bunk, O.; Zeysing, J. H.; Su, Y.; Nielsen, M.; Johnson, R. L.; Feidenhans'l, R., Low temperature structure of indium quantum chains on silicon. In: Programme and abstracts. 31. Danske krystallografmøde; Dansync's 3. Årsmøde, København (DK), 30-31 May 2000. (Centre for Crystallographic Studies, Copenhagen, 2000) P 20 (1 p.).

Kumpf, C.; Bunk, O.; Zeysing, J. H.; Su, Y.; Nielsen, M.; Johnson, R. L.; Feidenhans'l, R., Nanoscale quasi-one-dimensional quantum structures induced by adsorbates: Structural study of the Si(111)-(8x2)-In low temperature reconstruction. In: Programme. Abstracts. List of participants. Danish Physical Society annual meeting 2000, Nyborg (DK), 8-9 Jun 2000. (HCØ Tryk, København, 2000) FF58P.

Kumpf, C.; Bunk, O.; Zeysing, J. H.; Su, Y.; Nielsen, M.; Johnson, R. L.; Feidenhans'l, R., Low-temperature structure of indium quantum chains on silicon. In: Europhysics conference abstracts. 19. European conference on surface science (ECOSS-19), Madrid (ES), 5-8 Sep 2000. (European Physical Society, Paris, 2000) p. 56.

Kumpf, C.; Bunk, O.; Zeysing, J. H.; Su, Y.; Nielsen, M.; Johnson, R. L.; Feidenhans'l, R., Nanoscale quasi-one-dimensional quantum structures induced by adsorbates: Structural study of the Si(111)-(8x2)-In low temperature reconstruction. In: Programme and abstracts. Surface science 2000: Self-organization at interfaces and in thin films, Grenoble (FR), 11-12 Feb 2000. (European Synchrotron Radiation Facility, Grenoble, 2000) P-12.

Larsen, B. H.; Lister, S. J. S.; Boothroyd, A. T.; Andersen, N. H.; Wildes, A.; Zhokhov, A. A.; Christensen, A. N., Field dependent magnetic ordering and spin waves in PrBa₂Cu₃O_{6+x}. In: Programme. Abstracts. List of participants. Danish Physical Society annual meeting 2000, Nyborg (DK), 8-9 Jun 2000. (HCØ Tryk, København, 2000) FF14.

Larsen, N. B., Biomimetic polymer structures. Symposium: Exploring the potentials for using physics in the study of biological structures, processes and interactions, Risø (DK), 26 Oct 2000. Unpublished.

Larsen, N. B., Surface chemistry and adhesion. Symposium: Bonding and adhesion, Humlebæk (DK), 15 Nov 2000. Unpublished.

Larsen, N. B.; Jannasch, P.; Andersen, T.; Frello, T.; Gadegaard, N., Chemical and topographical surface analysis of multiphase polymer systems. Meeting at Danish Polymer Technical Society, Copenhagen (DK), 25 Oct 2000. Unpublished.

Lebech, B., Closure of the DR3 reactor at Risø. Swedish Neutron Scattering Society annual meeting, Studsvik, 9-10 Nov 2000. Unpublished.

Lebech, B.; Clausen, K. N.; Theodor, K.; Hansen, T. A., Germanium single-crystal wafers for composite neutron monochromators. In: Program and abstracts. 1. International symposium on advanced science research (ASR-2000): Advances in neutron scattering research, Ibaraki (JP), 31 Oct - 2 Nov 2000. (Japan Atomic Energy Research Institute. Advanced Science Research Center, Ibaraki, 2000) p. 93.

Lee, K. Y. C.; Majewski, J.; Nahmen, A. von; Gopal, A.; Howes, P. B.; Kjær, K.; Smith, G. S.; Zsadzinski, J. A., Influence of palmitic acid and hexadecanol on the phase transition temperature and molecular packing of dipalmitoylphosphatidyl-choline monolayers at the air-water interface. 44. Annual meeting of the Biophysical Society, New Orleans, LA (US), 12-16 Feb 2000. *Biophys. J.* (2000) v. 78 p. 1933Pos.

Lefmann, K., Studying nanoparticle magnetism by neutron scattering. Nanoworkshop on nanomagnetism, Lyngby (DK), 8 May 2000. Unpublished.

Lefmann, K.; Knuutila, T. A.; Tuoriniemi, J. T.; Hedegård, P., Spin-lattice relaxation in superconducting rhodium. In: Programme. Abstracts. List of participants. Danish Physical Society annual meeting 2000, Nyborg (DK), 8-9 Jun 2000. (HCØ Tryk, København, 2000) FF37P.

Lindgård, P.-A., Structure and spin-flip of ferro- and antiferro-magnetic nanoparticles. Nanoworkshop on nanomagnetism, Lyngby (DK), 8 May 2000. Unpublished.

Lopez, D.; Gammel, P.; Eskildsen, M. R.; Abrahamsen, A. B.; Mortensen, K.; Canfield, P., Morphology of flux line lattice in the borocarbide superconductors. American Physical Society March 2000 Meeting, Minneapolis, MN (US), 20-24 Mar 2000. Unpublished. Abstract available.

Majewski, J.; Kuhl, T. L.; Kjær, K.; Israelachvili, J. N.; Smith, G. S., Packing of ganglioside - phospholipid monolayers at the air-water interface: An X-ray grazing-incidence diffraction and reflectivity study. In: Programme and abstracts. Vol. 2: Poster contributions. 9. International conference on organised molecular films, Potsdam (DE), 28 Aug - 1 Sep 2000. (Potsdam Universität, Potsdam, 2000) p. 62 (P 42).

Molenbroek, A. M.; Johansen, K.; Rasmussen, F. B.; Clausen, B. S., In situ small and wide angle scattering studies on the dehydration of aluminium hydroxides. In: Programme and abstracts. 31. Danske krystallografmøde; Dansync's 3. Årsmøde, København (DK), 30-31 May 2000. (Centre for Crystallographic Studies, Copenhagen, 2000) F 8 (1 p.).

Mortensen, K., Phosphorlipid bilayer membranes studied by X-ray and neutron scattering. Symposium: Exploring the potentials for using physics in the study of biological structures, processes and interactions, Risø (DK), 26 Oct 2000. Unpublished.

Mortensen, K., Phase behavior of polymer blends and polymer surfactants, as studied by small-angle scattering (Invited talk). European Polymer Federation workshop: Polymeric surfactants, Kollo-Kolle (DK), 24-28 Jun 2000. Unpublished. Abstract available.

Mortensen, K., Structural studies of polymer and surfactant systems under the influence of shear fields (Invited talk). 25. Anniversary of research in the field of colloid and interface science in Bayreuth. Special symposium: Surfactants and water soluble polymers in the bulk phase and at interfaces, Bayreuth (DE), 31 Aug - 2 Sep 2000. Unpublished. Abstract available.

Mortensen, K., Thermoplastics - Structural properties studied by rheology and scattering techniques (Invited talk). Medical plastics 2000, Vienna (AT), 11-14 Sep 2000. Unpublished. Abstract available.

Mortensen, K., Shear induced order-order transition in triblock copolymer gels (Invited talk). Scattering studies of mesoscopic scale structure and dynamics in soft matter, Messina (IT), 22-25 Nov 2000. Unpublished. Abstract available.

Mortensen, K.; Almdal, K.; Kleppinger, R.; Theunissen, L.; Reynaers, H., Block copolymer micellar networks exposed to stretch and shear (Invited talk). 18. General conference of the Condensed Matter Division of the European Physical Society. Colloquium nr. 24: Transient phenomena in complex systems, Montreux (CH), 13-17 Mar 2000. Unpublished. Abstract available.

Mortensen, K.; Schwahn, D.; Frielinghaus, H.; Almdal, K., Anomalous pressure dependence of the critical fluctuations in binary blends and diblock copolymers of PDMS and PEE. American Physical Society March 2000 Meeting, Minneapolis, MN (US), 20-24 Mar 2000. Unpublished. Abstract available.

Mortensen, N. A.; Rønnow, H. M.; Bruus, H.; Hedegård, P., The magnetic neutron scattering resonance of high- T_c superconductors in external magnetic: An SO(5) study. In: Programme. Abstracts. List of participants. Danish Physical Society annual meeting 2000, Nyborg (DK), 8-9 Jun 2000. (HCØ Tryk, København, 2000) FF42P.

Mosler, S.; Gadegaard, N., The role of collagen topography in myoblast morphology, proliferation and differentiation. 40. American Society for Cell Biology annual meeting, San Francisco, CA (US), 9-13 Dec 2000. Unpublished.

Nielsen, M.; Poulsen, M.; Feidenhans'l, R.; Kumpf, C.; Grey, F.; Weichel, S.; Vedde, J.; Howes, P. B., The interface of directly bonded Si crystals studied by synchrotron X-ray diffraction. In: Programme and abstracts. 31. Danske krystallografmøde; Dansync's 3. Årsmøde, København (DK), 30-31 May 2000. (Centre for Crystallographic Studies, Copenhagen, 2000) P 6 (1 p.).

Nielsen, M.; Poulsen, M.; Kumpf, C.; Feidenhans'l, R.; Howes, P. B.; Weichelt, S.; Grey, F., The interface of directly bonded Si crystals studied by synchrotron X-ray diffraction. In: Programme and abstracts. Surface science 2000: Self-organization at interfaces and in thin films, Grenoble (FR), 11-12 Feb 2000. (European Synchrotron Radiation Facility, Grenoble, 2000) P-33.

Nielsen, M. M.; Bechgaard, K.; Siringhaus, H.; Friend, R. H., Building better plastic transistors: Orientation effects of self-organised domains in polymer films. SMARTON 3, Middelfart (DK), 25-28 May 2000. Unpublished.

Nyrup, S. B., X-ray diffraction studies of hair. In: Programme. Abstracts. List of participants. Danish Physical Society annual meeting 2000, Nyborg (DK), 8-9 Jun 2000. (HCØ Tryk, København, 2000) FF55P.

Nyrup, S. B.; Joenson, K.; Feidenhans'l, R.; James, V., X-ray diffraction of hair. In: Programme and abstracts. 31. Danske krystallografmøde; Dansync's 3. Årsmøde, København (DK), 30-31 May 2000. (Centre for Crystallographic Studies, Copenhagen, 2000) P 13 (1 p.).

Nørgaard, K.; Eskildsen, M. R.; Andersen, N. H.; Lefmann, K.; Jensen, J.; Hedegård, P.; Klausen, S.N.; Canfield, P.C., Exotic interplay between magnetism and superconductivity in TmNi₂B₂C. In: Programme. Abstracts. List of participants. Danish Physical Society annual meeting 2000, Nyborg (DK), 8-9 Jun 2000. (HCØ Tryk, København, 2000) FF38P.

Nørgaard, K.; Eskildsen, M. R.; Lefmann, K.; Andersen, N.H., New magnetic phase in the superconducting state of TmNi₂B₂C. 18. General conference of the Condensed Matter Division of the European Physical Society, Montreux (CH), 13-17 Mar 2000. Unpublished. Abstract available.

Poulsen, M.; Nielsen, M.; Feidenhans'l, R.; Kumpf, C.; Grey, F.; Weichel, S.; Vedde, J.; Howes, P. B., The interface of directly bonded Si crystals studied by synchrotron X-ray diffraction. In: Programme. Abstracts. List of participants. Danish Physical Society annual meeting 2000, Nyborg (DK), 8-9 Jun 2000. (HCØ Tryk, København, 2000) FF57P.

Ramzi, A.; Hirschberg, K.; Brunsveld, L.; Sijbesma, R.; Meijer, B.; Mortensen, K., Structural properties of self-assembled polymers with H-bonding in solution. American Physical Society March 2000 Meeting, Minneapolis, MN (US), 20-24 Mar 2000. Unpublished. Abstract available.

Reitzel, N.; Hassenkam, T.; Kjær, K.; Howes, P. B.; Jensen, T. R.; Fechtenkötter, A.; Brand, J. D.; Ito, S.; Müllen, K.; Bjørnholm, T., Structure of Langmuir films of conjugated disk-like molecules studied by synchrotron X-ray diffraction. In: Programme and abstracts. 31. Danske krystallografmøde; Dansync's 3. Årsmøde, København (DK), 30-31 May 2000. (Centre for Crystallographic Studies, Copenhagen, 2000) F 9 (1 p.).

Schwahn, D.; Frielinghaus, H.; Abbas, B.; Willner, L., Temperature- and pressure-dependent composition fluctuations in a d-PB/PS polymer blend and diblock copolymer. American Physical Society March 2000 Meeting, Minneapolis, MN (US), 20-24 Mar 2000. Unpublished. Abstract available.

Selle, C.; Dietrich, U.; Krüger, P.; Weygand, M.; Kohlstrunk, B.; Jensen, T. R.; Lösche, M., Structural studies on phosphatidylinositolphosphate monolayers. In: Programme and abstracts. Vol. 1: Oral contributions. 9. International conference on organised molecular films, Potsdam (DE), 28 Aug - 1 Sep 2000. (Potsdam Universität, Potsdam, 2000) p. 210 (T 146).

Symietz, C.; Brezesinski, G.; Kjær, K.; Jensen, T. R.; Möhwald, H., Coupling of polyelectrolytes to lipid monolayers at the air-water interface. In: Programme and abstracts. Vol. 2: Poster contributions. 9. International conference on organised molecular films, Potsdam (DE), 28 Aug - 1 Sep 2000. (Potsdam Universität, Potsdam, 2000) p. 186 (P 166).

Tranekjær, M.; Thomsen, A. B.; Batsberg Pedersen, W.; Ahring, B.K., Characterization of pretreated wheat straw by size exclusion chromatography. Ethanol from lignocellulosic materials - conference and end of programme seminar, Risø (DK), 11-13 Oct 2000. Unpublished.

Weissbuch, I.; Jensen, T. R.; Kjær, K.; Bolbach, G.; Leiserowitz, L.; Lahav, M., Towards generation of homochiral oligopeptides in Langmuir monolayers of α -amino acid racemates. In: Programme and abstracts. Vol. 1: Oral contributions. 9. International conference on organised molecular films, Potsdam (DE), 28 Aug - 1 Sep 2000. (Potsdam Universität, Potsdam, 2000) p. 212 (T 148).

Wolny, J.; Lebeck, B.; Wnek, A.; Shim, H. S., Magnetic modulation vectors of CeSb - model and experimental results. In: Programme and abstracts. 1. International symposium on advanced science research (ASR-2000): Advances in neutron scattering research, Ibaraki (JP), 31 Oct - 2 Nov 2000. (Japan Atomic Energy Research Institute. Advanced Science Research Center, Ibaraki, 2000) p. 27.

Wurlitzer, A.; Schalke, M.; Politsch, E.; Cevc, G.; Kjær, K.; Lösche, M., Conformation of lipopolyoxazoline as a function of molecular area studied by synchrotron X-ray diffraction. In: Programme and abstracts. Vol. 2: Poster contributions. 9. International conference on organised molecular films, Potsdam (DE), 28 Aug - 1 Sep 2000. (Potsdam Universität, Potsdam, 2000) p. 57 (P 37).

Zrubcová, J.; Kristiak, J.; Batsberg Pedersen, W.; Pedersen, N. J.; Eldrup, M., Light effects on positronium formation in polymers. 12. International conference on positron annihilation, München (DE), 6-11 Aug 2000. Unpublished. Abstract available.

Åstrand, P.-O., Intermolecular interactions. Ph.D. course on computational methods in chemistry, University of Copenhagen, Department of Chemistry, Copenhagen (DK), 26 Jan 2000. Unpublished.

Åstrand, P.-O., Simulations of liquids. Ph.D. course on computational methods in chemistry, University of Copenhagen, Department of Chemistry, Copenhagen (DK), 20 Jan 2000. Unpublished.

3.4. Patent applications

Pedersen, H. C.; Hovarth, R.; Lindvold, L.; Larsen, N. B., Reverse symmetry. UK patentansøgning 0026346.7

3.5. Meetings and Courses

3.5.1. Ph.D. Course on "Magnetism and Magnetic Materials"

15 weeks Ph.D. course at the University of Copenhagen and Technical University of Denmark, Lyngby. Spring semester. Lecturer *Kim Lefmann*, Risø National Laboratory, Roskilde, Denmark.

3.5.2. Topical Meeting on Biophysics – Biological Physics

April 5, 2000, Niels Bohr Institute, Copenhagen

Organising Committee:

H. Flyvbjerg and *K. Mortensen*, Risø National Laboratory

G. Tiana and *M. H. Jensen*, Niels Bohr Institute

O. G. Mouritsen, Technical University of Denmark

This was the third annual meeting for all PhD-students and scientists in biophysics in the Ørestad Region. These meetings provide an opportunity for everyone to introduce themselves and their research in short presentations. 43 participants.

Invited Speakers:

A. Michelsen, University of Southern Denmark, Odense

Biophysics of sound communication

S. B. Pedersen, Aalborg University, Ålborg

Ways of monitoring and perturbing protein structure stability

M. Esman, University of Aarhus, Aarhus

Biophysical methods applied in structure/function studies of membranous Na, K-ATPase

3.5.3. The Danish Physical Society's Annual Meeting

June 8-9, Hotel Nyborg Strand, Nyborg, Denmark

Organising Committee for the Condensed Matter Section:

Henrik Bruus, Niels Bohr Institute

Henrik Flyvbjerg, Risø National Laboratory

Hans C. Fogedby, University of Aarhus

Francois Grey and Jakob Schiøtz, Technical University of Denmark

Ling Miao, University of Southern Denmark, Odense

Dorthe Posselt, Roskilde University

3.5.4. DANSSK- Dansk NeutronSpredningsSelsKab Årsmøde

June 23, 2000 H. H. Koch auditorium, Risø National Laboratory

Main topic:

The future Risø strategy for Danish neutron scattering research will be presented and discussed.

Organising Committee:

Bente Lebech and Anette Liljenström, Risø National Laboratory, Denmark

Programme:

Chairman: *Kim Lefmann, Risø*

Bente Lebech, Risø

Welcome – Present possibilities

Mogens Bagger Hansen, Risø

Status for DR3 per June 23, 2000

Des McMorrow, Risø

The Risø strategy plans for Danish neutron scattering research – Possibilities and perspectives (SNS, ISIS-I, FRMII, PSI)

Uschi Steigenberger, ISIS, UK

ISIS and the ESS Project: Perspectives for neutron scattering in Europe when considering the present plans for ISIS-II and ESS

Discussion chaired by *Martin Vigild, Technical University of Denmark*

Kell Mortensen, Risø and Jens Erik Jørgensen, University of Aarhus

Conclusion and formulation of DANSSK members suggestion and vision for the future of Danish neutron scattering

Other matters

3.5.5. European meeting on "Lipid lipase interaction in the "Øresund" region"

September 27 to 30, Lund, Sweden

Organising Committee:

Allan Svendsen, Enzyme Design, Novo Nordisk A/S, Bagsværd, Denmark

Tommy Nylander, Center for Chemistry and Chemical Engineering, University of Lund, Sweden

Thomas Bjørnholm, University of Copenhagen, Copenhagen, Denmark

Kristian Kjær, Risø National Laboratory, Roskilde, Denmark

Programme Committee:

Steffen Petersen, University of Ålborg, Ålborg, Denmark

Ole Mouritsen, Technical University of Denmark, Lyngby, Denmark

Robert Verger, CNRS, Marseilles, France

Paavo Kinnunen, University of Helsinki, Helsinki, Finland

Karl Hult, KTH, Stockholm, Sweden

Marek Brzozowski, University of York, York, UK

Alsina Alcuncion, Universitat de Barcelona, Barcelona, Spain

Kåre Larsson, Camurus AB, Lund, Sweden

Karl-Erich Jaeger, Ruhr-Universität Bochum, Bochum, Germany

George Kokotos, University of Athens, Athens, Greece

Marina Lotti, Università Milano-Bicocca, Milan, Italy

Approximately 70 participants, 26 lectures and 23 posters.

3.6.6. Inauguration meeting for the ESS-Scandinavia

October 3, Lund, Sweden

Host:

Lund University, Gamla Biskopshuset, Lund, SNNS – Swedish Neutron Scattering Society, DANSSK – Danish Neutron Scattering Society

Organising Committee:

Nils Mårtensson, Lund University, *Lars Börjesson*, SNNS and *Bente Lebech*, DANSSK

Programme:

Chairman: Lars Börjesson, SNNS

Nils Mårtensson, Maxlab, Lund, Sweden

Welcome

Martin E. Vigild, Technical University of Denmark, Denmark

Introduction

Kurt Nørgaard Clausen, ESS Project, c/o Jülich, Germany

Status for ESS

Robert McGreevy, Neutron Scattering Laboratory, Studsvik, Sweden

Spallation Source - The Scientific Case

Chairman: Bente Lebech, DANSSK

Jørgen K. Kjems, Risø National Laboratory, Denmark

ESS in the Öresund/Øresund Region

Lars Börjesson Chalmers Institute of Technology, Göteborg, Sweden

Status of the Swedish Activities

Des McMorro, Risø National Laboratory, Denmark

Status of the Danish Activities

Discussion chaired by *Martin E. Vigild, Technical University of Denmark*

Discussions

Inauguration of ESS-Scandinavia?

Organisation (Executive Committee/Scientific Advisory Board)

Conclusions

3.5.7. Thematic day on “Gluing and adhesion”

November 15, Coloplast A/S, Humlebæk

Organising Committee:

L. H. Christensen and N.-J. Mikkelsen, Danish Technological Institute, Denmark, P. Samuelsen, Coloplast Research, Denmark, *R. Feidenhans'l*, Risø National Laboratory and *J. Garnæs*, Danish Institute of Fundamental Metrology, Denmark

A national symposium organised by the research partners of the Danish Centre for Surface Metrology and Functionality and Coloplast Research, Denmark. The symposium covered a range of aspects of gluing and adhesion. The topics of the presentations included fundamental mechanisms controlling adhesion processes, analytical approaches to establish the type of topography and chemistry present at the adhering surfaces and practical solutions to the gluing of various combinations of materials. Approximately 2/3 of the 90 participants of the thematic day came from industry.

Programme:

| | |
|---|---|
| <i>Ramon Sanchez Morillo</i> , Casco A/S, Denmark | The fundamental mechanisms of gluing of unlike surfaces |
| <i>Peter Sørensen</i> , Danish Technological Institute, Denmark | Surface tension and gluing |
| <i>Lydia Dahl Clausen</i> , Radiometer Medical A/S, Denmark | Surface metrology applied to the joining of a measuring cell |
| <i>Flemming Pedersen</i> , Loctite A/S, Denmark | Modern gluing technology |
| <i>Hanne Everland</i> , Coloplast A/S, Denmark | Development of skin adhesives |
| <i>Claus Erichsen Kudsk</i> , Danish Technological Institute, Denmark | The joining of structures by adhesion technology |
| <i>Niels B. Larsen</i> , Risø National Laboratory, Denmark | Surface chemistry and adhesion |
| <i>B.-G. Rosen</i> , TopoNova AB, Sweden | Topographical characterisation of surfaces |
| <i>Niels Jørgen Mikkelsen</i> , Danish Technological Institute, Denmark | Novel possibilities of improving the adhesiveness of plastics by ion implantation |

3.5.8. Discussion meeting on the “Interaction between Physics and Biology, in Particular in Relation to Teaching Students and Training Young Researchers at the Graduate Level”

December 5, Niels Bohr Institute, University of Copenhagen

Organising Committee:

Henrik Flyvbjerg, Risø National Laboratory, *Mogens H. Jensen*, Niels Bohr Institute and *Ole G. Mouritsen*, Technical University of Denmark

The Graduate School of Biophysics was established in late 1997 under the auspices of the Danish Research Academy to promote the education of PhDs in biological physics/biophysics. It was created as a collaborative effort between institutions in the Copenhagen area. Since early 1998 the school has offered PhD-studentships in biological physics, arranged workshops and PhD-courses, and run an intensive schedule of visiting professors, lecturers, and students.

At the discussion meeting, the achievements of the graduate school were briefly reviewed and the experience obtained so far was summarized. With the help of a number of external contributors and respondents, a structured discussion was arranged addressing the possibility of constructing a more biology-influenced curriculum for the students of the graduate school, as well as for the undergraduate students who wish to qualify for enrolment in this or similar schools.

Contributions to the Discussion:

| | |
|---|---|
| <i>Erik Hviid Larsen</i> , AKI, University of Copenhagen | Physics can influence genetics; can genetics influence physics? |
| <i>Stanley Brown</i> , MB, University of Copenhagen | Physics can influence genetics; can genetics influence physics? |
| <i>Jesper Brahm</i> , Panum Institute, University of Copenhagen | Physics in biology – a tool or a pain? |
| <i>Morten Kielland-Brandt</i> , Carlsberg Research Laboratories | Teach physics students more biology and visa versa. |

Respondents:

Peter Westh and *Dorthe Posselt*, Roskilde University, *Kaj Frank Jensen*, University of Copenhagen, *Iver Jacobsen*, Risø National Laboratory, *Henrik Vibe Scheller*, The Royal Veterinary and Agricultural University, Copenhagen, *Morten Smith*, MSc-student at AKI, University of Copenhagen and *Jesper Donsmark*, MSc-student at The Niels Bohr Institute, Copenhagen

3.6. Memberships of committees and boards

Kristoffer Almdal

Member of MODECS Research Forum

Niels Hessel Andersen

Member of "Fagligt Forum"

Consultant for the Swedish Superconductivity Consortium

Expert evaluator for INTAS, the International Association for the promotion of Co-operation with scientists from the new independent states of the former Soviet Union

Klaus Bechgaard

Board member of "Nationalkomiteen for Kemi"

Board member of "ATV - Akademiet for de Tekniske Videnskaber"

Board member of the Danish Polymer Centre

Member of Advisory Board of Journal of Materials Chemistry

Member of EEC COST D-4 Committee

Member of MODECS Research Forum

Rolf Henrik Berg,

Editorial Board of Journal of Peptide Science

Kurt Nørgaard Clausen,

Chairman of the EURound Table of Neutron Sources

Member of International Union of Pure and Applied Physics, Magnetism Section

Member of ENSA – European Neutron Scattering Association

Member of Editorial board of Journal of Neutron Research

Member of SNS Instrument Oversight Committee

Robert Feidenhans'l

Member of IUCr Commission on Synchrotron Radiation

Danish representative in Nordsync.

Member of the Council of the European Synchrotron Radiation Society

Member of Forschungsberat Synchrotronstrahlung HASYLAB, DESY. Hamburg

Member of MAXLAB, Program Advisory Committee

Board member of "Center for Metrologi og Funktionalitet"

Board member of "Dansk Center for Udnyttelse af Synkrotronstråling"

Chairman of "Den Danske Nationalkomité for Krystallografi"

Henrik Flyvbjerg

Member of Organizing Committee of the International Summer school "Physics of Bio-Molecules and Cells", Les Houches, France (2001)

Member of Advisory Committee on Biophysics, reporting to the Physics

Member of Study Committee of the Faculty of Science at the University of Copenhagen

Member of Reference Panel of the Division of Science and Technology of the Research Council of Norway

Member of Editorial Board of Theory in Biosciences

Søren Hvilsted

Member of "Kontaktudvalg for Dansk Selskab for Termanalyse"
Member of the Management Committee for COST Action 518: Molecular Materials and Functional Polymers for Advanced Devices. Project 5: Polymers for Holography
Member of Organizing Committee of the "12. International Conference on Thermal Analysis and Calorimetry", Copenhagen, Denmark (12-16 August 2000)
Member of the International Advisory Board of the "Conference on New Trends In Functional Polymer", Huangshan, China (8-13 May 2000)
Member of Steering Committee for Experimental and Theoretical Investigation of Complex Polymer Structures (SUPERNET) from 1999 to 2003
Board member of "Polymerteknisk Selskab"
Member of International Union of Pure and Applied Chemistry – Macromolecular Division

Ib Johannsen

Member of the Programme Committee for "Kostbart Udstyr"
Member of "Statens Teknisk-Videnskabelige Forskningsråd"

Bente Lebech

Member of the "Den Danske Nationalkomité for Krystallografi"
Chairman of "DANSSK – DANsk NeutronSpredningsSelsKab"
Member of the ENSA – European Neutron Scattering Association
Member of the NFL Science Advisory Committee at Studsvik Neutron Research Laboratory
Corresponding author of Neutron News

Kim Lefmann

Member of "DANSSK – DANsk NeutronSpredningsSelsKab"
Board member of the ESS - Scandinavia Initiative

Per-Anker Lindgård

Member of the EU TMR Evaluation Panel
Member of Executive Committee of the European Physical Society, including Financial Subcommittee and Editorial Subcommittee for Europhysics News
Member of EPS-Communications and Interdivisional Relation Group

Desmond. F. McMorro

Member of ISIS Scheduling Panel, RAL, UK
Member of the Editorial board of Journal of Physics: Condensed Matter
Member of the European Synchrotron Radiation Facility (ESRF) Review Committees

Kell Mortensen

Board member of the Danish Research Academy's Graduate School of Biophysics
Member of "Danmarks Grundforskningsfond"
Member of the Editorial Board of Journal of Macromolecular Science
Member of "DANSSK – DANsk NeutronSpredningsSelsKab"
Board member of the ESS - Scandinavia Initiative

Jan Skov Pedersen

Co-editor of Journal of Applied Crystallography
Member of the International Advisory Board for the "11. International Conference On Small-Angle Scattering"
Member of the IUCr Commission on Neutron Scattering
Member of the IUCr Commission on Small-Angle Scattering

4. Staff, guests, students, degrees and awards

Scientific staff and consultants

Aeppli, Gabriel (Consultant)
Almdal, Kristoffer
Als-Nielsen, Jens (Consultant)
Andersen, Niels Hessel
Bechgaard, Klaus (Head of Department)
Berg, Rolf H.
Clausen, Kurt N. (From August 1 also Project Director, ESS Project Team, c/o Jülich, Germany)
Feidenhans'l, Robert (Head of Research Programme)
Flyvbjerg, Henrik
Gerstenberg, Michael (From November 1)
Grivel, Jean-Claude (From June 1)
Hvilsted, Søren (Until May 31)
Jensen, Jens (Consultant)
Johannsen, Ib (Head of Research Programme)
Jørgensen, Mikkel
Kingshott, Peter (From October 23)
Kjær, Kristian
Larsen, Niels B.
Lebech, Bente
Lebech, Jens
Lefmann, Kim
Lindgård, Per-Anker
McMorrow, Desmond F.
Mortensen, Kell
Nielsen, Kristian (Until July 31)
Nielsen, Martin Meedon (From November 1)
Nielsen, Mourits
Pedersen, Jan Skov (Until July 31)
Pedersen, Walther Batsberg
Skaarup, Per
Sommer-Larsen, Peter
West, Keld

Post-docs

Frello, Thomas
Gerstenberg, Michael (From February 1 until October 31)
Hermsdorf, Nadja (Until October 31)
Hooker, Jacob (Until August 31)
Jensen, Torben René (Until September 30)
Krebs, Frederik C. (From March 1)
Larsen, Britt Hvolbæk
Mosler, Stephan (From August 1)
Nielsen, Martin Meedom (Until October 31)
Norrman, Kion
Papra, Alexander (Until December 31)
Rasmussen, Frank Berg (Until July 31)

Thom, Volkmar (Until February 29)
Åstrand, Per-Olof

Ph.d. students and other students

Abraham, Asger
Andersen, Sofie Rud (Trainee, until August 31)
Arleth, Lise
Christensen, Niels Bech
Edwards, Henrik (MSc student)
Eskimergen, Rūya
Gadegaard, Nikolaj
Ishøy, Torben
Jacobsen, Birgitte Abery (MSc student)
Klausen, Stine
Kofod, Guggi
Krebs, Frederik C. (Until February 29)
Lausen, Bo Wegge
Mentzel, Søren
Nyrup, Susan Blak (MSc student)
Nørgaard, Katrine
Petterson, Robert (Until August 31)
Poulsen, Mette
Rasmussen, Winnie (Trainee, until August 31)
Spanggaard, Holger
Steenstrup, Frederik
Svaneborg, Carsten
Thomsen, Kristina (MSc student)

Technical staff

Alstrup, Jan
Bang, Steen
Berntsen, Allan Nørtoft
Breiting, Bjarne
Hansen, Thomas Agertoft (Until May 31)
Holm, John Hammer
Hubert, Lene
Jensen, Birgit
Jørgensen, Ole
Kjær, Torben
Larsen, Bent Lykke
Nielsen, Lotte
Rasmussen, Helle D.
Rasmussen, Ove
Saxild, Finn
Stahl, Kim
Sunke, Flemming (Until August 31)
Sørensen, Carsten Gynther
Theodor, Keld (Until May 31)

Secretaries

Frederiksen, Lajla (Until November 30)
Liljenström, Anette M. (Deceased December 13)
Schlichting, Bente O.
Studinski, Ca Thi
Thomsen, Alice

Guest scientists and long time visitors

Bøgelund, Jesper Poder (Until December 31)
Chuai, C.Z.
Enderle, Mechthild (Until November 30)
Koblischa, Michael
Mosler, Stephan (Until July 31)
Paturi, Petriina (From July 1 until December 31)

Short time visitors under the EC-TMR programme

| | |
|-------------------|--|
| Boothroyd, Andrew | University of Oxford, Dept. of Physics (UK) |
| Bradshaw, Jeremy | Univ. of Edinburgh, Dept. of Preclinical Veterinary Sc. (UK) |
| Caruana, Daren | University College London, Dept of Chemistry, (UK) |
| Clegg, Paul | University of Oxford, Dept. of Physics (UK) |
| Cristobal, Galder | Université Bordeaux I, CPMOH (FR) |
| Gardiner, Carol | University of Oxford, Dept. of Physics (UK) |
| Goldar, Arach | University of Bath, Dept. of Chemistry (UK) |
| Hughes, Arwel | University of Bath, Dept. of Chemistry (UK) |
| Karlsson, Annika | Eindhoven Technical University (NL) |
| Kleppinger, Ralf | FOM Inst. f. Atomic Molecular Physics, Amsterdam (NL) |
| Lillywhite, Sarah | University of Birmingham (UK) |
| Panizza, Pascal | Université Bordeaux I, CPMOH (FR) |
| Roser, Steve | University of Bath, Dept. of Chemistry (UK) |
| Stocker, Oliver | University of Bristol, H. H. Wills Lab. (UK) |
| Van Well, Ad A | Delft University of Technology, Dept. of Chemistry (NL) |
| Wagemaker, Marnix | Delft University of Technology, Dept. of Chemistry (NL) |

Short time visitors

| | |
|-----------------------|--|
| Andersen, Trine | Department of Physics, University of Odense (DK) |
| Bergmann, Alexander | Karl Franzens Universität Graz (AT) |
| Bergström, Magnus | Royal Institute of Technology (SE) |
| Brinck, Vibeke | Symbion, University of Copenhagen (DK) |
| Cannavacciuolo, Luigi | Institute for Polymer, ETH - Zürich (CH) |
| Claesson, Per | Institute for Surface Chemistry (SE) |
| Kjellin, Mikael | Institute for Surface Chemistry (SE) |
| Lake, Bella | Oak Ridge National Laboratory (US) |
| Lima, Emmanoel | HMI-Berlin (DE) |
| McEwen, Keith | Univ. College London, Dept of Physics and Astronomi (UK) |
| Nagler, Stephen | Oak Ridge National Laboratory (US) |
| Nedelmann, Lorenz | Weizmann Institute of Science (IL) |
| Radovic, Tamara | University of Copenhagen (DK) |
| Rampling, Richard | Nottingham Trent University (UK) |

| | |
|--------------------|--|
| Rozlosnik, Noemi | Eotvos University , Budapest (HU) |
| Rudershau, Sandra | Partikeltechnologie GmbH, Rostock (DE) |
| Schneider, Harold | Technical University of Munich (DE) |
| Svensson, Birgitta | Physical Chemistry 1, Lund University (SE) |
| Zemb, Thomas | CEA-Saclay (FR) |

Degrees and awards

Martin Meedom Nielsen and Klaus Bechgaard together with researchers at Philips, Holland and the Universities of Cambridge, Eindhoven and Ulm received the EU "René Descartes prize" of 300.000 ECU

Pedersen, Jan Skov, Dr. Scient.

Andersen, Niels Hessel, Appointed Adjoint Professor at University of Copenhagen

Krebs, Frederik Christian, Ph.D. degree

Reynisson, Jóhannes, Ph.D. degree

Rønnow, Henrik Modysson, Ph.D. degree and Allan Mackintosh legat

Christensen, Niels B., MSc degree

Steenstrup, Frederik, MSc degree

Jacobsen, Birgitte Abery, Oticon-scholarship

Nyrup, Susan Blak, Oticon-scholarship

Title and authors

Annual Progress Report of Condensed Matter Physics and Chemistry Department
1 January - 31 December 2000

Edited by Bente Lebech

| | | | |
|---|--------|------------------------|------------|
| ISBN | | ISSN | |
| 87-550-2790-3 | | 0106-2840 | |
| 87-550-2791-1 (Internet) | | 1397-8985 | |
| Department or group | | Date | |
| Condensed Matter Physics and Chemistry Department | | March 2001 | |
| Groups own reg. number(s) | | Project/contract No(s) | |
| Pages | Tables | Illustrations | References |
| 154 | 6 | 160 | 181 |

Abstract (max. 2000 characters)

The Condensed Matter Physics and Chemistry Department is concerned with both fundamental and applied research into the physical and chemical properties of materials. The principal activities in the year 2000 are presented in this progress report.

The research in physics is concentrated on neutron and x-ray scattering measurements and the problems studied include two- and three-dimensional structures, magnetic ordering and spin dynamics, superconductivity, phase transitions and nano-scale structures. The research in chemistry includes chemical synthesis and physico-chemical investigation of small molecules and polymers, with emphasis on polymers with new optical properties, block copolymers, surface-modified polymers, and supramolecular structures. Theoretical work related to these problems is undertaken, including Monte Carlo simulations, computer simulation of molecules and polymers and methods of data analysis.

Descriptors INIS/EDB

CHEMISTRY, COPOLYMERS, SOLID STATE PHYSICS, MAGNETISM, NEUTRON DIFFRACTION, POLYMERS, PROGRESS REPORT, RESEARCH PROGRAMS, RISØE NATIONAL LABORATORY, SUPERCONDUCTIVITY, X-RAY DIFFRACTION

Available on request from Information Service Department, Risø National Laboratory,
(Afdelingen for Informationsservice, Forskningscenter Risø), P.O.Box 49, DK-4000 Roskilde, Denmark.
Telephone +45 46 77 40 04, Telefax +45 46 77 40 13

